



HAL
open science

Elaboration, characterization and modeling of electroactive materials based on polyurethanes and grafted carbon nanotubes

Mohamed Hedi Jomaa

► **To cite this version:**

Mohamed Hedi Jomaa. Elaboration, characterization and modeling of electroactive materials based on polyurethanes and grafted carbon nanotubes. Materials. INSA de Lyon, 2015. English. NNT : 2015ISAL0053 . tel-01339846

HAL Id: tel-01339846

<https://theses.hal.science/tel-01339846>

Submitted on 30 Jun 2016

HAL is a multi-disciplinary open access archive for the deposit and dissemination of scientific research documents, whether they are published or not. The documents may come from teaching and research institutions in France or abroad, or from public or private research centers.

L'archive ouverte pluridisciplinaire **HAL**, est destinée au dépôt et à la diffusion de documents scientifiques de niveau recherche, publiés ou non, émanant des établissements d'enseignement et de recherche français ou étrangers, des laboratoires publics ou privés.

Thèse

**Elaboration, characterization and modeling of
electroactive materials based on polyurethanes
and grafted carbon nanotubes**

Présentée devant
L'institut national des sciences appliquées de Lyon

Pour obtenir
Le grade de docteur

par

Mohamed Hedi Jomaa

Soutenue le 17/06/2015 devant la Commission d'examen

Jury MM.

-Eric BEAUGNON (rapporteur), Prof, CNRS/CRETA, Grenoble

-John Christopher PLUMMER (rapporteur), Prof, EPFL.

-Jean-Yves CAVAILLE (examineur), Prof, MATEIS, INSA-Lyon.

-Jean-François CHATEAUX (examineur), MCF, INL, UCBL.

-Vincent SALLES (examineur), MCF, LMI, UCBL.

-Karine MASENELLI-VARLOT (directrice de thèse), Prof. MATEIS, INSA-Lyon.

-Laurence SEVEYRAT (directrice de thèse), Dr. Ing, LGEF, INSA-Lyon.

INSA Direction de la Recherche - Ecoles Doctorales – Quinquennal 2011-2015

SIGLE	ECOLE DOCTORALE	NOM ET COORDONNEES DU RESPONSABLE
CHIMIE	<p><u>CHIMIE DE LYON</u> http://www.edchimie-lyon.fr Sec : Renée EL MELHEM Bat Blaise Pascal 3e etage 04 72 43 80 46 Insa : R. GOURDON</p>	<p>M. Jean Marc LANCELIN Université de Lyon – Collège Doctoral Bât ESCPE 43 bd du 11 novembre 1918 69622 VILLEURBANNE Cedex Tél : 04.72.43 13 95 directeur@edchimie-lyon.fr</p>
E.E.A.	<p><u>ELECTRONIQUE,</u> <u>ELECTROTECHNIQUE,</u> <u>AUTOMATIQUE</u> http://edeea.ec-lyon.fr Sec : M.C. HAVGOUDOUKIAN eea@ec-lyon.fr</p>	<p>M. Gérard SCORLETTI Ecole Centrale de Lyon 36 avenue Guy de Collongue 69134 ECULLY Tél : 04.72.18 60.97 Fax : 04 78 43 37 17 Gerard.scorletti@ec-lyon.fr</p>
E2M2	<p><u>EVOLUTION, ECOSYSTEME,</u> <u>MICROBIOLOGIE, MODELISATION</u> http://e2m2.universite-lyon.fr Sec : Safia AIT CHALAL Bat Darwin - UCB Lyon 1 04.72.43.28.91 Insa : H. CHARLES Safia.ait-chalal@univ-lyon1.fr</p>	<p>Mme Gudrun BORNETTE CNRS UMR 5023 LEHNA Université Claude Bernard Lyon 1 Bât Forel 43 bd du 11 novembre 1918 69622 VILLEURBANNE Cédex Tél : 06.07.53.89.13 e2m2@univ-lyon1.fr</p>
EDISS	<p><u>INTERDISCIPLINAIRE SCIENCES-</u> <u>SANTE</u> http://www.ediss-lyon.fr Sec : Safia AIT CHALAL Hôpital Louis Pradel - Bron 04 72 68 49 09 Insa : M. LAGARDE Safia.ait-chalal@univ-lyon1.fr</p>	<p>Mme Emmanuelle CANET-SOULAS INSERM U1060, CarMeN lab, Univ. Lyon 1 Bâtiment IMBL 11 avenue Jean Capelle INSA de Lyon 696621 Villeurbanne Tél : 04.72.68.49.09 Fax :04 72 68 49 16 Emmanuelle.canet@univ-lyon1.fr</p>
INFOMATHS	<p><u>INFORMATIQUE ET</u> <u>MATHEMATIQUES</u> http://infomaths.univ-lyon1.fr Sec :Renée EL MELHEM Bat Blaise Pascal 3e etage infomaths@univ-lyon1.fr</p>	<p>Mme Sylvie CALABRETTO LIRIS – INSA de Lyon Bat Blaise Pascal 7 avenue Jean Capelle 69622 VILLEURBANNE Cedex Tél : 04.72. 43. 80. 46 Fax 04 72 43 16 87 Sylvie.calabretto@insa-lyon.fr</p>
Matériaux	<p><u>MATERIAUX DE LYON</u> http://ed34.universite-lyon.fr Sec : M. LABOUNE PM : 71.70 –Fax : 87.12 Bat. Saint Exupéry Ed.materiaux@insa-lyon.fr</p>	<p>M. Jean-Yves BUFFIERE INSA de Lyon MATEIS Bâtiment Saint Exupéry 7 avenue Jean Capelle 69621 VILLEURBANNE Cedex Tél : 04.72.43 71.70 Fax 04 72 43 85 28 Ed.materiaux@insa-lyon.fr</p>
MEGA	<p><u>MECANIQUE, ENERGETIQUE, GENIE</u> <u>CIVIL, ACOUSTIQUE</u> http://mega.universite-lyon.fr Sec : M. LABOUNE PM : 71.70 –Fax : 87.12 Bat. Saint Exupéry mega@insa-lyon.fr</p>	<p>M. Philippe BOISSE INSA de Lyon Laboratoire LAMCOS Bâtiment Jacquard 25 bis avenue Jean Capelle 69621 VILLEURBANNE Cedex Tél : 04.72 .43.71.70 Fax : 04 72 43 72 37 Philippe.boisse@insa-lyon.fr</p>
ScSo	<p><u>ScSo*</u> http://recherche.univ-lyon2.fr/scso/ Sec : Viviane POLSINELLI Brigitte DUBOIS Insa : J.Y. TOUSSAINT viviane.polsinelli@univ-lyon2.fr</p>	<p>Mme Isabelle VON BUELTZINGLOEWEN Université Lyon 2 86 rue Pasteur 69365 LYON Cedex 07 Tél : 04.78.77.23.86 Fax : 04.37.28.04.48</p>

*ScSo : Histoire, Géographie, Aménagement, Urbanisme, Archéologie, Science politique, Sociologie, Anthropologie

Acknowledgements

I would like to thank my supervisor, Professor Karine Masenelli-Varlot for her strong encouragement, support and especially for her teaching along these years. Her guidance, remarks and critical comments on my work have played a crucial role in both the contents and presentation of this thesis. I also would like to thank Professor Karine for the detailed revisions of the manuscripts and brilliant opinions that enrich the project. Moreover, I am deeply thankful to Karine for her generous friendship and professional guidance in all the thesis process.

Also, I would like to express my sincere gratitude and appreciation to my co-supervisor Dr. Ing. Laurence Seveyrat for her elaborated guidance and invaluable discussion that make my research of great achievement and my study life unforgettable. I deeply appreciate the time and effort spent together in discussing the results. I also appreciate all their precious corrections to my papers and thesis, attentive consideration and encouragement to me.

I would like to thank Professor Jean-Yves Cavaille for his scientific advices, enthusiastic encouragement and his help. His warm guidance and complete support improved my scientific attitude and enriched my experience. Especially, his knowledge, interest and commitment to excellence impress me greatly. I really appreciate his taught of enthusiasm by the knowledge, joy of scientific research, and the importance of the hard work. Really, I have the privilege to share with him an invaluable friendship.

In the same manner, I would like to express my sincere gratitude and appreciation to Professor Laurent Lebrun, for his scientific advice, teaching and personal guidance during these years. His motivation and scientific thinking were determinants in the course of my doctoral studies.

I would like to express my thanks to the thesis defence committee: Professor Eric Beaugnon, Professor John Christopher Plummer, Professor Jean-Yves Cavaille, Associate Professor Vincent Salles and Associate Professor Jean-François Chateaux for their insightful, invaluable comments and suggestions that improved the quality of this work.

In addition, the same gratitude goes to Dr. Marie Claire Dib Jawhar, Professor Emmanuel Beyou, Associate Professor Lucian Roiban, PhD-Student Daya Dhungana, and Dr. Diguët Gildas for their kindness help and support, also those who are not mentioned.

Thanks also go to and Mrs. Verinique Perin, Mr. José Ferreira and Mr. Frederic Defromerie for machining the art-like device for my experimental design and measurement.

I also would like to thank the administrative personals of our laboratories MATEIS & LGEF Mrs. Evelyne Dorieux, Mrs. Sandrine Gonnet and Mr. Emmanuel Montero for their help and support.

I want to specially thank to my friends that were adorable and supportive all the time and, if the case, aid me with the inculturation process: Rabia, Mohamed, Fatma, Haifa, Soumaya, Montassar, Issam, Jamil and Amira !,...

My sincere grateful to all the members of my family for the great happiness they bring to my life, and their supportive presence in all of the important facts, as this professional step.

Finally and most importantly, I would like to express all my love and gratitude to my parents Salah and Latifa, for their wonderful presence in my life, their guidance, support, dedication, and incommensurable love in all situations and moments.

شكر ل كل كم جيه عا،

Merci à toutes et à tous,
Thank you to you all,

Mohamed Hedi Jomaa

Abstract

Harvesting systems capable of transforming dusty environmental energy into electrical energy have attracted considerable interest throughout the last decade. Several research efforts have focused on the transformation of the mechanical vibration into electrical energy. Most of these research activities deal with classical piezoelectric ceramic materials, but more recently, a promising new type of materials is represented by electroactive polymers (EAPs). Among the various EAPs, polyurethane (PU) elastomers are of great interest due to the significant electrical-field strains, and due to their attractive and useful properties such as flexibility, light weight, high chemical and abrasion resistance, high mechanical strength and easy processing into various shapes and biocompatibility with blood and tissues. In order to further increase the efficiency of such polymers for energy harvesting and actuation applications, one solution consists in incorporating conductive nanofillers. Due to their interesting intrinsic properties, carbon nanotubes (CNTs) are good candidates.

The key motivation of this work was to use polymer-grafted CNTs to improve the dispersion and interfacial adhesion of CNTs in PU, and understand how this can change the electroactive properties of the PU/CNT nanocomposites. A comprehensive study was first carried out on pure PU, and because the frequency dependence of the response is extremely important, an extensive study of the dielectric and the viscoelastic behaviour has been conducted on three segmented PUs with different fractions of hard and soft segments. They were shown to exhibit 3 mains mechanisms, namely, a secondary or β -relaxation, the main or α -relaxation associated to the glass-rubber transition of the soft phase and their electrical conductivity. Interestingly, the electrostriction retardation time does not depend on mechanical or dielectric relaxations as expected. It seems to be directly linked to space charge diffusion leading to the Maxwell-Wagner-Sillars phenomenon. This study was also used to select the most efficient polyurethane. PU88 appears to be the best candidate for actuation applications among these 3 samples because it exhibits a large electrostriction, low mechanical and dielectric losses in the largest range of frequencies and temperature around room temperature.

The nanostructural properties were studied by DSC, TEM, AFM and SAXS. The diameter of the hard domains (HD) and the HD-HD distance have been determined and introduced in a model taking into account the PU nanostructure. It is found that the model well reproduces the experimental electrostriction properties of these phase-separated PUs. This study allowed the identification of criteria for the optimization of the electromechanical behavior.

In a second part, the incorporation of grafted CNTs in the PU88 matrix was performed. The interfacial adhesion between grafted CNTs and the PU matrix and dispersion state was improved. The CNT dispersion and orientation states in the nanocomposites were quantified using electron tomography through the measurement of the local CNT fraction, the CNT tortuosity, the CNT-CNT distance and the number of contacts.

The dielectric permittivity was largely increased with the introduction of grafted CNT and the percolation threshold was found around 5 vol.%. Measurement of the thickness strain under an applied electrical field demonstrated a twofold increase of the electrostriction coefficient. The energy harvesting properties investigated by monitoring the evolution of the current under a DC electrical field were also enhanced. However, this increase of the electromechanical properties observed with grafted CNT nanofillers can be described as rather limited. The first results obtained from the extension of the model based on the microstructure may bring some explanations.

Résumé

Le besoin de sources d'énergie autonomes connaît un regain d'intérêt de plus en plus important avec la multiplication des équipements portables et le développement des réseaux de capteurs. Au-delà de l'utilisation traditionnelle des batteries, il y a un intérêt évident à générer l'énergie électrique nécessaire au cœur du système lui-même en utilisant le gisement environnemental disponible : gradients thermiques, vibrations mécaniques....Ceci est également rendu possible par la réduction importante de la consommation des composants électroniques observés ces vingt dernières années. Parmi les dispositifs susceptibles d'exploiter le gisement vibratoire, les matériaux électro-actifs occupent une place de choix. Actuellement, on recherche des matériaux légers, pouvant se déposer sur des grandes surfaces et peu coûteux à la réalisation. Ceci ouvre des perspectives séduisantes à l'utilisation de polymères électro-actifs en lieu et place des matériaux céramiques piézoélectriques. Parmi les EAP disponibles, les polyuréthanes (PU) sont des élastomères thermoplastiques d'un grand intérêt pour une vaste gamme d'applications en tant que transducteurs ou actionneurs lorsque l'on considère leur importante déformation sous champ électrique, une énergie spécifique élevée, et leur réponse rapide. De plus, ces matériaux sont légers, très souples, présentent de faibles coûts de fabrication, et peuvent être facilement moulés dans n'importe quelle forme souhaitable. Des travaux récents ont en outre montré que l'énergie récoltée peut être augmentée en incorporant des nanotubes de carbone (NTC) dans une matrice de polyuréthane. Cependant, les nanocomposites peuvent ne pas avoir été optimisées, car il est bien connu que les NTC sont difficilement dispersés dans une matrice polymère et que la force d'adhésion interfaciale est généralement médiocre. Une solution pour améliorer à la fois la dispersion et l'adhésion peut résider dans le greffage de chaînes de polymère sur les surfaces des NTC.

L'objectif principal de cette thèse était de développer des polymères nanocomposites à haute efficacité pour la récupération d'énergie et l'actionnement. La motivation principale était d'utiliser des NTC greffés par un polymère pour améliorer la dispersion et l'adhésion interfaciale dans le PU, et de comprendre comment l'utilisation de tels NTC greffés peut changer les propriétés électroactives des matériaux. En d'autres termes, c'était un projet pluridisciplinaire, comprenant une optimisation du processus d'élaboration, des caractérisations physiques - notamment les comportements de microstructure, électriques et mécaniques dans une large gamme de fréquences et températures - et la détermination des propriétés électroactives. Il s'agissait également de développer une modélisation des lois de comportements en s'aidant de l'analyse de la microstructure par imagerie. Afin de pouvoir identifier le rôle des NTC greffés, une grande partie de cette thèse a été dédiée à l'étude des PU purs, afin de mieux comprendre les relations entre leur microstructure et leurs propriétés électroactives.

Sommaires

ELABORATION, CHARACTERIZATION AND MODELING OF ELECTROACTIVE MATERIALS BASED ON POLYURETHANES AND GRAFTED CARBON NANOTUBES	0
INTRODUCTION	5
PART I: BIBLIOGRAPHIC STUDY	9
CHAPTER 1: BIBLIOGRAPHY STUDY	11
1 ELECTROACTIVE POLYMERS EAP	11
1.1 INTRODUCTION.....	11
1.2 HISTORICAL BACKGROUND	11
1.3 TYPE OF EAP	12
1.3.1 Ionic EAP	12
1.3.2 Electronic EAP.....	15
1.4 COMPARISON OF ELECTRONIC AND IONIC EAPS.....	17
2 ELECTROMECHANICAL PROPERTIES OF PU.....	18
2.1 PHYSICAL PROPERTIES OF PURE PU.....	19
2.1.1 PU microstructure.....	19
2.1.2 Dielectric properties	19
2.1.3 Viscoelastic properties	21
2.2 ELECTROMECHANICAL PROPERTIES.....	22
2.2.1 Electromechanical principles.....	22
2.2.2 Electrostrictive properties of PU	23
2.2.3 Energy harvesting in pseudo piezoelectric behavior.....	24
3 IMPROVEMENT OF THE ELECTROMECHANICAL PROPERTIES	24
3.1 CARBON-BASED FILLERS	25
3.2 IMPROVEMENT OF THE ELECTROMECHANICAL PROPERTIES USING CARBON NANOTUBES	25
3.2.1 Physical properties of polymer/CNT composites	26
3.2.2 Critical issues with polymer CNT composites.....	29
3.2.3 Modification of CNT composites.....	30
4 CONCLUSION.....	31
PART II: MATERIALS AND EXPERIMENTS	39
CHAPTER 2: MATERIALS AND EXPERIMENTS	41
1 MATERIALS	41
1.1 POLYURETHANES MATRIX	41
1.1.1 Generality on thermoplastic elastomers polyurethanes	41
1.1.2 The 3 studied polyurethanes.....	42
1.1.3 Main physical properties of the 3 PU studied.....	42
1.2 CARBON NANOTUBES (CNT).....	43
1.2.1 Characteristics of the raw CNTs.....	43
1.2.2 Grafting of PU chains onto CNTs	44
1.2.3 Control of the grafting process	46

2	FILM ELABORATION:	47
2.1	ELABORATION PROTOCOLE OF PURE PU	47
2.1.1	<i>Elaboration protocol using existing system « open system »</i>	47
2.1.2	<i>Elaboration protocol using « closed system »</i>	48
2.1.3	<i>Optimization of the elaboration process</i>	49
2.2	ELABORATION PROTOCOL OF PU NANOCOMPOSITES	50
2.2.1	<i>Optimization of the grafted CNT dispersion state of in DMF solvent</i>	50
2.2.2	<i>Elaboration protocol of PU nanocomposites</i>	51
3	CHARACTERIZATION TECHNIQUES	52
3.1	MICROSTRUCTURAL	52
3.1.1	<i>Thermal properties characterization</i>	52
3.1.2	<i>Microscopic</i>	53
3.2	ELECTRICAL MEASUREMENT	57
3.3	DYNAMIC MECHANICAL ANALYSIS	60
3.4	ELECTROMECHANICAL	61
3.4.1	<i>Electrostriction</i>	61
3.4.2	<i>Energy harvesting</i>	62
	PART III: STUDY OF PURE POLYURETHANES	65
	INTRODUCTION	67
	CHAPTER 3: DIELECTRIC PROPERTIES OF SEGMENTED POLYURETHANES FOR ELECTROMECHANICAL APPLICATIONS	69
1	INTRODUCTION	69
2	MATERIALS AND METHODS	70
3	RESULTS AND DISCUSSION	72
3.1	MAIN PHYSICAL PROPERTIES OF 3 PU	72
3.2	ELECTROSTRICTION PROPERTIES	72
3.3	DIELECTRIC PROPERTIES OF 3PU	73
3.3.1	<i>Isochronal study</i>	73
3.3.2	<i>Isothermal Study</i>	75
3.3.3	<i>Conductivity</i>	81
4	CONCLUSIONS	83
	REFERENCES	84
	CHAPTER 4: TIME AND FREQUENCY DEPENDENCE OF THE ELECTROMECHANICAL RESPONSE OF SEGMENTED POLYURETHANE-BASED ACTUATORS	87
1	INTRODUCTION	88
2	MATERIALS AND EXPERIMENT	89
3	RESULTS AND DISCUSSION	90
3.1	DENSITY, GLASS TRANSITION TEMPERATURE AND YOUNG MODULUS OF THE 3 PU VERSUS HS CONTENT	90
3.2	VISCOELASTIC PROPERTIES:	91
3.2.1	<i>Isochronal study</i>	91
3.2.2	<i>Isothermal study</i>	92

3.3	ELECTROSTRICTION.....	97
3.4	COMPARISON BETWEEN PU75, PU88 AND PU60	99
4	CONCLUSIONS.....	101
	REFERENCES.....	101
CHAPTER 5: MODELING OF SEGMENTED PURE POLYURETHANE ELECTROSTRICTION BEHAVIORS BASED ON THEIR NANOSTRUCTURAL PROPERTIES		105
1	INTRODUCTION	106
2	MATERIAL AND METHODS	106
3	RESULTS AND DISCUSSION.....	109
3.1	MODELING	109
3.2	EXPERIMENTAL DETERMINATION OF THE MORPHOLOGICAL PARAMETERS	113
3.2.1	<i>Phase separation</i>	113
3.2.2	<i>Diameter distribution of HDs</i>	116
3.2.3	<i>Distance between HDs</i>	119
3.3	ELECTROSTRICTION.....	120
4	CONCLUSIONS.....	122
	REFERENCES.....	122
	CONCLUSION	125
PART IV: PU/ CNT NANOCOMPOSITES.....		127
INTRODUCTION		129
CHAPTER 6: INVESTIGATION OF ELASTIC, ELECTRICAL AND ELECTROMECHANICAL PROPERTIES OF POLYURETHANE/ GRAFTED CARBON NANOTUBES NANOCOMPOSITES..		131
1	INTRODUCTION	132
2	MATERIALS AND METHODS.....	132
3	RESULTS AND DISCUSSION.....	134
3.1	OPTIMIZATION OF ELABORATION PROCESS.....	134
3.1.1	<i>Control of grafting process</i>	134
3.1.2	<i>Optimization of elaboration process</i>	135
3.1.3	<i>Control of dispersion and interfacial adhesion</i>	136
3.2	THERMAL ANALYSIS.....	136
3.3	VISCOELASTIC AND MECHANICAL PROPERTIES OF PU GRAFTED CNT.....	138
3.4	DIELECTRIC PERMITTIVITY, ELECTRICAL CONDUCTIVITY, PERCOLATION THRESHOLD	139
3.5	DIELECTRIC RELAXATION OF PU NANOCOMPOSITES	140
3.6	ELECTROSTRICTION PROPERTIES	144
3.7	HARVESTING ENERGY	145
4	CONCLUSION.....	145
	REFERENCES.....	146
CHAPTER 7: BENEFIT OF CARBON NANOTUBES FOR ENERGY CONVERSION USING POLYMERS		149
1	INTRODUCTION	149
2	MATERIALS AND METHODS	150

2.1	SAMPLE PREPARATION	151
2.2	IMAGE ACQUISITION	151
2.3	VOLUME ANALYSIS	152
3	RESULTS AND DISCUSSION.....	153
3.1	3D RECONSTRUCTION.....	153
3.2	QUANTIFICATION AND CONTROL OF THE CNT DISPERSION STATE.....	154
3.3	ELECTROSTRICTION MODELING	156
4	CONCLUSION.....	159
	REFERENCES.....	159
	CONCLUSION	163
	CONCLUSION	165
	PERSPECTIVES	169

Introduction

EAPs are part of the broad group of smart materials. The use of polymers with electroactive response has only emerged in the last decade with the introduction of new materials which have significant displacement levels. They are now considered as promising alternatives to piezoelectric ceramics in various smart systems. Even though more classical piezoelectric ceramics remain more efficient in terms of energy conversion by weight unit, their stiffness and brittleness limit their use when very small displacements are required. EAP materials are highly attractive for their low-density, large strain capability, superior spectral response, and resilience. In general, the biggest advantages over conventionally used systems in most application fields are the intermittent displacement they can provide, an adaptable stiffness combined with variable sizes and form factors, from micrometers to meters. Among the various EAPs, polyurethane (PU) elastomers are of great interest due to the significant electrical-field strains, and due to their attractive and useful properties such as flexibility, light weight, high chemical and abrasion resistance, high mechanical strength and easy processing to large area films as well as their ability to be molded into various shapes and biocompatibility with blood and tissues. In addition, it has recently been shown that the incorporation into a PU matrix of nanofillers, such as carbon nanotubes (CNTs), can greatly enhance the expected strain, or the harvested energy. This outstanding result seems to be related to the increase of the permittivity when nanofillers are incorporated within the polymers, hence requiring a lower bias electric field for the same effect. Currently, as the electrostriction effect of the obtained composite has to be ensured, the content in volume of fillers is kept low to avoid the percolation phenomenon. However, it is well known that CNTs are hardly dispersed in a polymeric matrix, and the interfacial adhesion strength is generally poor. Furthermore, in all nanocomposites cases, the improvement of the materials performances is limited by the low volume contents of nanocharges, and by impressive conductivities near percolation threshold. An effective method to improve both dispersion and adhesion consists in functionalizing CNTs by grafting polymer chains onto their surfaces.

The main objective of this thesis was to develop high-efficiency polymers nanocomposites for harvesting energy and actuation. The key motivation was to use polymer-grafted CNTs to improve dispersion, interfacial adhesion in PU, and understand how this can change the electroactive properties of the PU/CNT nanocomposites. In other words, it was a pluridisciplinary project including an optimization of the elaboration process, physical characterizations - including microstructural, electrical and mechanical behaviors in a wide range of frequencies and temperatures - and the determination of the electroactive properties. A comprehensive study was then carried out first on pure PU to understand how their electroactive properties depend on their microstructure, and then on the nanocomposites to understand how the incorporation of functionalized CNT can improve the electromechanical properties.

This manuscript is divided in four main parts.

In the first part (chapter 1), we will introduce EAP including their principle, the different types, and their advantages and drawbacks. Then, the main physical and electromechanical properties of Polyurethanes will be reported. Afterwards, we will study, from the literature, the different possible ways to improve the electromechanical properties of EAP using carbon-based nanomaterials, especially using CNT.

The second part (chapter 2) will present the materials and main characterizations tools used. As a first step the main polyurethane matrix is introduced including compositions and physical characteristics. The main properties of CNT, the functionalization steps and the optimization of elaboration process of pure PU and CNT-PU nanocomposites will then be explained. This will be followed by a brief description of the characterization tools, with a short presentation of the relevant information that can be achieved in relation with our objectives.

The third part -will be composed of three chapters- deals with the study of the main matrix (PU). Three different PU with different weight fractions of Hard and Soft Segments (HS and SS) will be studied in order to choose the best one for actuation and harvesting energy applications. The grafted CNTs will be incorporated in a second step in this PU.

In chapter 3, as the electromechanical properties depend both on dielectric and mechanical properties, an extensive study will be carried out on the dielectric and viscoelastic behaviors of the three different PU. A dielectric spectroscopy measurement will be performed in a wide range of temperatures and frequencies. Different dielectric relaxations will be highlighted and discussed depending on the HS content of the 3 PU. Then in chapter 4 we will focus on the viscoelastic and electrostriction properties of the same 3 PU, again as functions of the temperature and the frequency. The relations between the HS fraction and the dielectric, mechanical and electrostrictive properties will be discussed.

In chapter 5, a model, taking into account the PU nanostructure, will be presented to evaluate the electroactive properties. This model is based on several microstructural parameters, such as the HD (domains rich in HS) diameter and weight fractions, the HD-HD distance. In order to validate this model, the three PUs have been characterized using several techniques and their electrostriction properties have been measured.

At the end of this part, the choice of the more suitable PU for electroactive applications will be discussed on the basis of specific requirements for actuation, and in terms of large stability of electrostriction, electrical and mechanical behaviours in a wide range of frequencies and temperatures.

In the fourth part, we will investigate the effect of the incorporation of grafted CNT on the physical properties of PU nanocomposites including microstructural, mechanical, electrical and electromechanical properties.

The chapter 6 will show a multi-scale characterization approach, performed to control the grafting process step-by-step, including the monitoring of the grafted layer thickness and its

compatibility with the PU matrix. The elaboration process of the nanocomposites film will be optimized with the help of TEM observations to avoid any damage in the grafted layer. Thermal analysis will be conducted to study the effect of the CNT on the polymer microstructure. Mechanical and dielectric measurements will be performed in a wide range of frequencies and temperatures in order to study the influence of grafted CNT on the different relaxations processes of the polymer.

Then, in chapter 7, we will report a comprehensive study of the role of grafted CNT on the electroactive properties of PU. The effect of the grafting process onto the CNT dispersion state will be quantified from electron tomography through the measurement of the local CNT fraction, the CNT tortuosity, the CNT-CNT distance and the number of contacts. Finally, a model taking account the experimental microstructural parameter will be used to evaluate the role of CNTs on the improvement of electromechanical properties of Polyurethanes.

At the end a general conclusion will be drawn and perspectives will be proposed.

Note: *The third and fourth parts are presented as scientific articles.*

Part I: Bibliographic study

Chapter 1: Bibliography study

1 Electroactive polymers EAP

1.1 Introduction

Several research efforts have been focused on the transformation of the mechanical vibration into electrical energy. Most of these research activities refer to classical piezoelectric ceramic materials, but more recently promising a new type of materials is represented by electroactive polymers (EAPs) [1]. For the last 20 years, electroactive polymers (EAPs) have devoted much attention since they undergo huge deformations when subjected to external electric fields [2]. Even though more classical piezoelectric ceramics remain more efficient in terms of energy conversion by weight unit, their stiffness and brittleness limit their use. Moreover, the processing of polymeric materials is often easier as it does not require high temperatures, like ceramics [3]. This makes the market potential large - EAPs can be used in various applications including actuators and sensors, biomimetics and robotics, energy harvesting and storage devices etc. Especially in the actuator segment, vast R&D activity can be seen for specialized applications such as medical devices and biomimetic-robotics. Here the features of electroactive polymers are used to enable movement and generate force as well as electrically control surface properties. However, demand in the industry is important, with high performance requirements and also restrictions, especially in the medical field. Today, with touchscreens everywhere it almost seems natural to expand the user experience with better feedback. Implementation of EAPs for haptic feedback, especially for handheld touchscreen devices and peripherals, is the current new market focus [4]. Haptics for consumer portable touch screen devices and peripherals is going to be the next big application and potentially the first large-scale implementation of EAP actuators in general with an expected penetration of 60% for haptic feedback in mobile phones for 2018[5]. One of the biggest challenges at the moment is however the cost of EAP devices in consumer electronics. Already in fairly high production are dielectric elastomer materials commercially available from sources like 3M, and also piezoelectric fluoropolymer (PVDF), that is used in actuators, nanocomposites, capacitors etc. However, the main issue hindering the wide-spread application of dielectric elastomers is the high operating voltage required. New growth needs to come from new innovation - improved materials suitable for less demanding high-volume applications, such as consumer electronics and large-area thin-film sensors.

1.2 Historical background

The field of EAP emerged back in 1880, when Wilhelm Roentgen designed an experiment in which he tested the effect of an electrical current on the mechanical properties of a rubber band [6]. The rubber band was fixed at one end and was attached to a mass at the other. It was then

charged and discharged to study the change in length with the electrical current. Sacerdote followed up on Roentgen's experiment by formulating a theory on strain response to an applied electric field in 1899 [7]. Eguchi discovered the first piezoelectric polymer (electrets) in 1925. In 1969, Kawai [8] was able to demonstrate that polyvinylidene fluoride (PVDF) exhibits a large piezoelectric effect. This sparked research interests in developing other conductive polymers systems that would show a similar effect. In 1977, the conducting polymer of polyacetylene was discovered by Hideki Shirakawa et al [9]. By the late 1980s, a number of other polymers had been shown to exhibit a piezoelectric effect or were demonstrated [10-11]. During the 1990s, focus shifted towards truly EAP, which respond directly to an electric stimulus. Pelrine et al. at SRI International have developed dielectric elastomer actuators which give some handsets percentage of strain level [12]. Besides, Ionic polymer metal composite (IPMC) was shown to have actuator properties in 1992 by Oguro in Osaka, Japan and Shahinpoor [13]. Their co-workers in New Mexico, U.S.A extensively developed the technology. Zhang et al. have developed copolymers of PVDF of which the energy density was significantly increased [14]. Recently, two significant new classes of materials with actuator properties have emerged: carbon nanotube actuators developed by Baughman et al. in 1999 [15]. It is noteworthy that information on many on many research groups, including the ones cited above, can be found on the EAP Web page maintained by Bar-Cohen from the Jet Propulsion Laboratory [16].

1.3 Type of EAP

There are numerous types of EAP but most of them fall into categories which are either ionic (involving mobility or diffusion of ions and their conjugated substances) or electronic (which are driven by electric field or coulomb forces). Bar-Cohen [17] proposed a classification of these polymers, adopted by the scientific community. The classification is reported in Table 1. In the following, the main characteristics of ionic and electronic EAP are reviewed.

Table 1 Main types of EAP, from [17]

Electronic EAP	Ionic EAP
<ul style="list-style-type: none"> ■ Dielectric elastomer EAP <ul style="list-style-type: none"> ■ Acrylics ■ Silicones ■ Polyurethanes (PU) ■ Electrostrictive Graft Elastomers ■ Electrostrictive Paper ■ Electro-Viscoelastic Elastomers ■ Ferroelectric Polymers ■ Liquid Crystal Elastomers (LCE) 	<ul style="list-style-type: none"> ■ Conductive Polymers (CP) ■ ElectroRheological Fluids (ERF) ■ Ionic Polymers Gel (IPG) ■ Ionic Polymer Metallic Composites (IPMC)

1.3.1 Ionic EAP

Their actuation is caused by the displacement of ions inside the polymer. Only a few volts are needed for actuation, but the ionic flow implies a higher electrical power needed for actuation, and energy is needed to keep the actuator at a given position. Example of ionic EAP are listed and briefly introduced here.

1.3.1.1 Ionic Polymer Metallic Composites (IPMC)

Ion-exchange polymer-metal composites (IPMC) are highly active actuators that show very large deformation in the presence of low applied voltage and exhibit low impedance. They operate best in a humid environment and can be made as self-contained encapsulated actuators to operate in dry environments as well. They have been modeled as both capacitive and resistive element actuators that behave like biological muscles and provide an attractive means of actuation as artificial muscles for biomechanics and biomimetics applications [18]. Typical ionic polymers are Nafion® (perfluorosulfonate, made by DuPont) and/or Flemion® (perfluorocarboxylate, made by Asahi Glass, Japan) [19].

Ionic polymer-metal composite (IPMC) consist in a thin ionomeric membrane with noble metal electrodes plated on both surfaces. It also contains cations to balance the charge of the anions fixed to the polymer backbone. A schematic representation is shown in Fig. 1 IPMC work through electrostatic attraction between the cationic counterions and the anode.

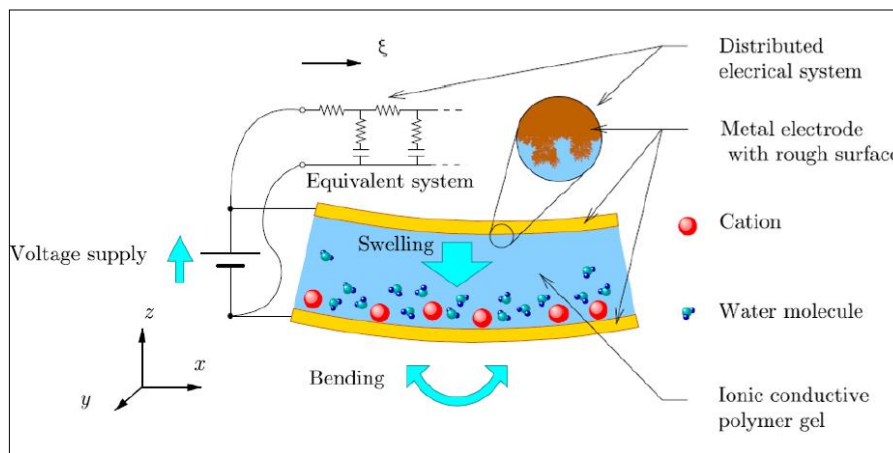


Fig. 1 Physical structure of IPMC

Actuation strains of above 3 % have been reported for IPMCs under applied voltages of 7 V [20]. Fig. 1 shows one example of these cantilever-type actuators. Substantial bending is caused as one side of the material contracts and the other expands. Reported stresses of actuation by IPMC are as high as 30 MPa [21]. The response speed is unfortunately quite limited.

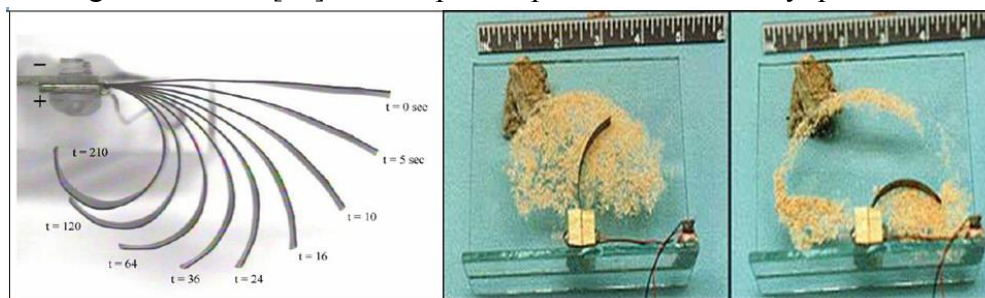


Fig. 2 Actuation of a Flemion-based IPMC strip as a function of time in seconds [21].

An IPMC device was developed for use as a dust wiper in one NASA's missions to address the issue of dust on Mars (see Fig. 2). Its feasibility was demonstrated by removing sawdust from a glass plate. Such a wiper has the potential to serve as a means of cleaning windows and solar cells using low power, light-weight ionomer films [22].

1.3.1.2 Ionic polymer gel (IPG)

Polymer gels are unique materials in the sense that they can be tailored to respond to a lot of different stimuli. In 1970s, the phase transition of a polymer gel, characterized by its abrupt volume change, was found by Tanaka [23]. The stimuli that have been demonstrated to induce abrupt changes in physical properties are diverse, and include temperature, pH, solvent- or ionic composition, electric field, light intensity as well as introduction of specific ions [22]. Fig. 3 shows the shape change of an anionic gel with time under the electric field.

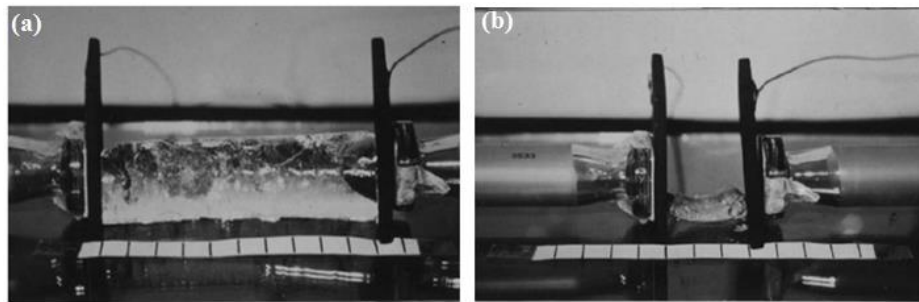


Fig. 3 Pictures of a poly (2-acrylamido-2-methyl-1-propanesulfonic acid) gel before (a) and after (b) imposing an electric field of 15 V for 10 h [24].

Ionic gels show larger changes in the volume change ratio than neutral gels do, because of the existence of ions in the gel network. Some ionic gels can even change their volumes by thousand times. The deformation of such polymer gels is extremely high, compared with other sensor/actuator materials such as piezoelectrics [25].

1.3.1.3 Conductive polymer (CP)

Conductive polymers (CP) are electronically conducting organic materials. Actuation is produced in these polymers due to the electronically change of oxidation state. The flux of ions into and out of the polymer backbones causes deformation. Conducting polymers with appropriate dopants, such as hydrogen chloride or sulphuric acid, exhibit chemically and electrochemically controllable electronic conductivities. Doping induces the presence of ions that can flow across the covalently bound conjugated polymer chains. The bending of a conducting polymer sandwich, composed of two conducting polymer layers separated by an electrolyte, is presented in Fig. 4 [25]. When an electric field is applied, a reversible exchange of ions takes place between the conducting polymer and the electrolyte. Exchange of ions leads to oxidation or reduction reactions in the conducting polymer, which induces significant changes in its volume.

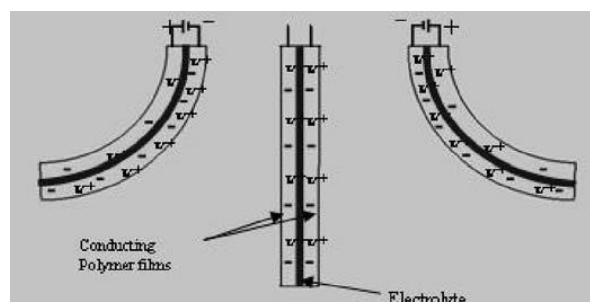


Fig. 4 Schematic representation of three states during the electromechanical cycle of a rocking-chair type of bimorph-conducting polymer actuator [26].

1.3.2 Electronic EAP

In the case of electronic EAP, the actuation is caused by electrostatic forces between two electrodes and/or interaction between dipoles inside the material, squeezing the polymer. One of their main advantages is that they can be manipulated in air. In the following, several types of electronic EAP are reviewed. Electrostrictive polymers and dielectric elastomers are the leading electronic EAP [17].

1.3.2.1 Piezoelectric polymer

A piezoelectric polymer can be defined as a polymer in which the application of an electric field reverses the direction of spontaneous polarization. PVDF and its copolymers are the most promising materials of this class. Kawai et al [8], published the first description of the piezoelectric properties of PVDF in 1969. Many of them have been applied as sensors, transducers, actuators, and underwater acoustic transducers [27]. Their electrostrictive strain is nearly 2 %. It is not large but large enough compared with traditional electro driven sensors/actuators, PZT, which generate an electrostrictive strain around 0.2 % at maximum. PVDF has a high elastic modulus (~1 GPa), and the field-induced strain can operate at frequencies higher than 100 kHz. Large electric fields, around 200 MV/m, are however required, instead of a few hundreds of MV/m for PZT.

1.3.2.2 Dielectric elastomer

Dielectric elastomer actuators consist of a polymer film sandwiched between two compliant electrodes. A schematic model of the dielectric polymer actuator system is presented in Fig. 5. When a voltage difference is placed across the top and bottom electrodes, the polymer is compressed in thickness and stretched in area by the electric field pressure [28].

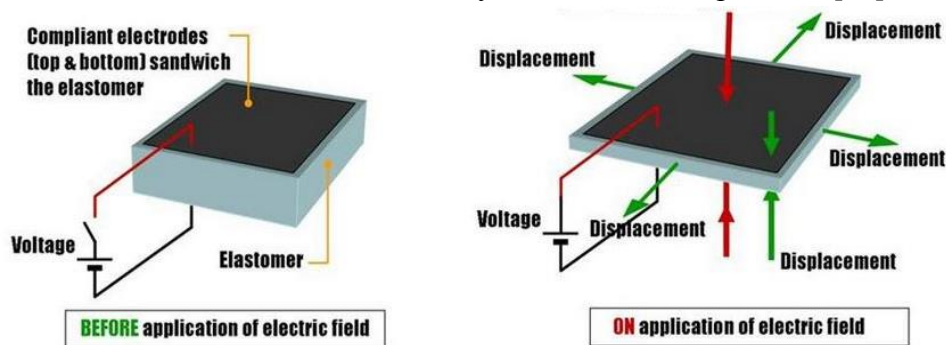


Fig. 5 EAP actuator systems.

The term electrostrictive strain is used here in the generic sense to describe the stress and strain response of a material to an electric field. Many researchers (particularly those investigating ceramic materials) keep the term for the strain response of a material in an electric field that arises from field-induced intermolecular forces. The Maxwell strain in a dielectric polymer with compliant electrodes results from the electrostatic forces generated between free charges on the electrodes, and is proportional to the square of the electric field.

Since the electrostrictive strain results from external electrostatic forces, any elastomeric dielectric material will exhibit electrostrictive strain by this definition, in theory. Thus, it may

be argued that actuators based on this technology are more properly considered to be electrostatic. However, as it will be shown, the dielectric and mechanical properties of the polymer material determine the magnitude of the stress and strain response.

Fig. 6 shows the actuation of a circular dielectric elastomer [29] made of acrylic elastomer. Acrylic and silicon-based elastomers are famous for their extremely large strains. They overcome easily some hundreds of percents, such as 380 %. However this type of polymer typically requires a large actuation voltage to produce high electric fields (hundreds to thousands of Volts).

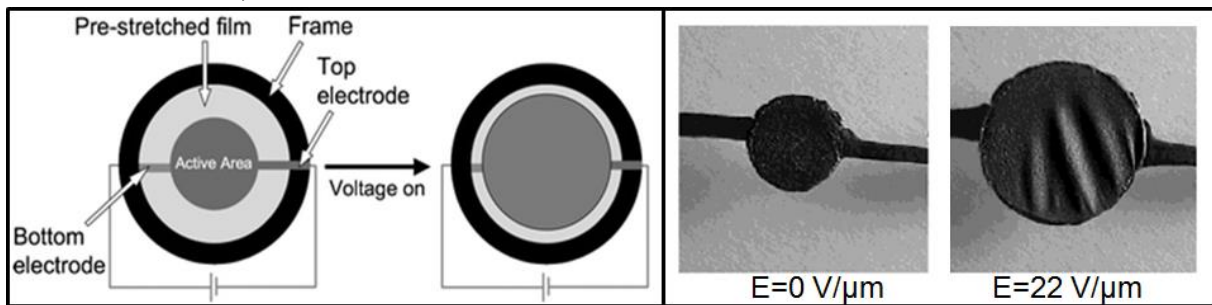


Fig. 6 : Circular strain test and photograph of acrylic dielectric elastomer [29].

Among the various EAPs, polyurethane (PU) elastomers are of great interest due to their significant electrical-field strains [30, 31], and due to their attractive and useful properties such as flexibility, light weight, high chemical and abrasion resistance, high mechanical strength and easy processing to large area films as well as their ability to be molded into various shapes and biocompatibility with blood and tissues [32]. PU can generate a strain above 10% under a moderate electric field. They can therefore be considered as potential actuators [33].

1.3.2.3 Electrostrictive graft elastomer

The electrostrictive graft elastomer is a new type of electroactive polymer developed in the NASA Langley research center in 1999. It was reported that an electrostrictive graft elastomer exhibits large electric field-induced strain (4 %), as shown in Fig. 7 [34]. The 4 % strain are far smaller than the 380% obtained with dielectric elastomers, but much larger than the 0.2 % achieved with PZTs (at maximum). The important thing is that there is no hysteresis in this material. However, its required electrical field is quite high, so that the use is limited.

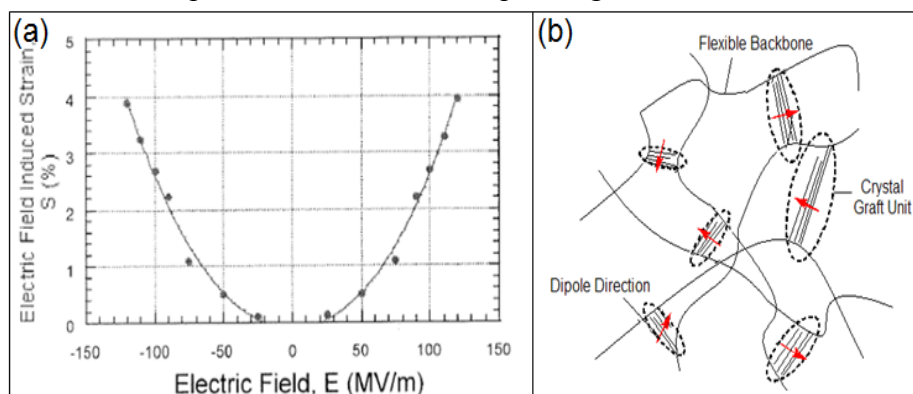


Fig. 7 (a) Electric field dependence of the induced strain on the graft elastomer, (b) Structure of the grafted elastomer

From a microstructural point of view, the graft elastomer consists of two components: flexible backbone chains and side chains attached to the backbone, called grafts [35]. The grafts can crystallize to form physical cross-linking sites for a three-dimensional elastomer network. They generate electric field responsive polar crystal domains. The polar crystal domains are primary contributors to electrostrictive mechanical functionality.

When the materials are under the electrical field, the polar domains rotate to align themselves in the field direction due to the driving force generated by the interaction between the net dipoles and the applied electric field. The rotation of grafts induces the reorientation of backbone chains, leading to deformational change. In the absence of electric field, the polar domains orientations randomize, leading to dimensional recovery. The dimensional change generated demonstrates a quadratic dependence on the applied electric field.

1.4 Comparison of electronic and ionic EAPs

The currently available leading EAP materials are listed in Table 2, with a summary of their advantages and disadvantages, and some applications [4].

Table 2 Advantages and disadvantages of electronic and ionic EAPs, with some applications.

EAP Type	Pros & Cons	Applications
Electronic EAP	Pros <ul style="list-style-type: none"> ■ Rapid response, within milliseconds ■ Can hold strain under DC activation ■ Large actuations forces ■ High mechanical energy density ■ Long operation time 	<ul style="list-style-type: none"> ■ Actuators <ul style="list-style-type: none"> ■ Haptic feedback for portable consumer electronics ■ Overear headphones ■ Sensors (disposable ones, pressure, percolation) ■ Energy harvesting and generation (wave energy)
	Cons <ul style="list-style-type: none"> ■ High voltage requirements (~100 MV/m)- recent R&D~20MV/m in ferroelectric EAP ■ No effect of voltage polarity 	
Ionic EAP	Pros <ul style="list-style-type: none"> ■ Bi-directional actuation depending on voltage polarity ■ Low voltage requirement (1-5V) ■ Bi-stability (in some) 	<ul style="list-style-type: none"> ■ Catheters ■ Automotives devices ■ Prosthetic devices ■ Active noise and vibration ■ Reduction materials ■ Pristaltic pumps
	Cons <ul style="list-style-type: none"> ■ Must be operated in wet state, electrolyte required ■ Encapsulation/barrier layer required ■ Low electrochemical coupling efficiency ■ Do not hold strain under DC voltage ■ Slow response (fraction of a second) ■ Relatively low actuation force (bending EAPs) ■ Electrolysis in aqueous systems at>1.23 V 	

No polymer surpasses another one, each one having their own advantages and drawbacks. Ionic EAP materials (gels, polymer-metal composites, conductive polymers...) are driven by diffusion of ions and they require an electrolyte for the actuation mechanism. Their major advantage is the requirement for drive voltages as low as 1-2 V. One of the constraints of these materials is that they must be operated in a wet state or in solid electrolytes. Ionic EAPs predominantly produce bending actuations that induce relatively lower actuation forces than electronic EAPs. Often, operation in aqueous systems is plagued by water hydrolysis. Moreover, ionic EAPs have slow response characteristics compared to electronic EAPs. In contrast, electronic EAP materials (electrostrictive, electrostatic, piezoelectric and ferroelectric) are driven by electrostatic forces. They are able to have a high mechanical energy density and they can be used in air with no major constraints. However, they require in general a high activation field close to the electrical breakdown level, such as 100 MV/m. The property of these materials to hold the induced displacement, when a DC voltage is applied, makes them potential materials in robotic applications, and these materials can be operated in air without major constraints. Electronic EAPs have high energy densities as well as rapid response times, in the range of milliseconds. In general, these materials have glass transition temperatures inadequate for low temperature actuation applications.

Another way to classify actuators is based on actuation mechanisms. The various mechanisms through which EAPs produce actuation are polarization, mass/ion transportation, molecular shape change, and phase change. Dielectric elastomers and piezoelectric polymers produce actuation through polarization. Conducting polymers and gel polymers produce actuation basically through ions/mass transportation. Liquid crystal elastomers and shape-memory polymers produce actuation by phase change. As can be observed, various stimuli can be actuate active polymers. Development of polymers that can respond to non-contact mode stimuli such as electrical, magnetic, and light can lead to the diversification of the applications of active polymers. Electrical stimulation is considered the most promising, owing to its availability and advances in control systems.

Among the various electronic EAPs, PU elastomers are good candidates for the processing of electromechanical actuators for several reasons: (i) their strong polarity, and (ii) their ability to develop intrinsic electrostriction, in addition to the Maxwell effect. They will be the subject of this PhD thesis.

2 Electromechanical properties of PU

The principle of electrically-driven EAP in actuator mode consists in the application of an electric field perpendicular to the film plane, which results in a contraction of the film in the direction of the electric field and a stretching in the film plane. As with many actuator technologies, electronic EAP are reversible and can be operated in generator mode. In this mode of operation, mechanical work is done against the applied electric field, and electrical energy is produced. Thus, the electronic EAP is acting as an electromechanical generator transducer. Technologically, the generator mode of electronic EAP is potentially as important as the actuator mode. Actuators are indeed pervasive in modern technologies, yet the critical need for new energy systems, such as generators, may be more important than the number of possible applications.

2.1 Physical properties of pure PU

2.1.1 PU microstructure

Polyurethanes are segmented polymers composed of alternating sequences of soft segments (SS) and of hard segments (HS). The structural difference/incompatibility between the SS and the HS leads to a separation into microphases or domains formed from the respective HS and SS. Hard domains (HD) -domains rich in HS- play the role of physical crosslinks and act as high modulus fillers, whereas the soft domains (SD) -domains rich in SS- provide extensibility. In addition, HD exhibit a permittivity larger than soft domains. It has been recently pointed out that the large electric field induced strain in PU results mainly from heterogeneities in contrast to both elastic and dielectric constants and to electric field gradients, which make the soft domains shrink and the whole material compress [36].

Characterization of the PU nanostructural properties, including the diameter distribution of HD and interdistance between domains is primordial in order to have a clear idea about the phase separation and their effect on electrostriction properties. Transmission Electron Microscopy (TEM) is an established technique for the characterization of heterogeneous polymer structures at a high level of resolution. There are some problems associated with the direct investigation of polymers by (TEM), as polymers usually exhibit low contrasts between structural details and are sensitive to the electron beam [37]. The method of heavy-atom staining to enhance the contrast of the specimen in the electron microscope seems to be a good solution to reveal microphase separation [38]. Several structural details (lamellae, amorphous regions, interfaces, regions of different molecular packing densities or different free volumes, several polymer phases, and others) possess different reactivities to the staining agent. Depending on the material, different staining agents may be used (e.g., osmium tetroxide (OsO_4), ruthenium tetroxide (RuO_4), phosphoric-tungsten acid, chlorosulfonic acid (ClSO_3H), Formaldehyde HCHO ...) [39]. The particular choice of the stain used in a given polymer system is largely guided by empirical success.

2.1.2 Dielectric properties

The term dielectric analysis refers to a group of techniques that measure changes in different physical properties of a polar material, such as polarization, permittivity, and conductivity, with temperature or frequency. The reorientation of dipoles and the translational diffusion of charged particles in an oscillating electric field provide the basis of the analysis based on alternating-current (AC) dielectric methods, which principally involve measurements of the complex permittivity ($\epsilon^* = \epsilon' + i\epsilon''$) in the frequency or time domain and at constant or varying temperature. Thus, dielectric spectroscopy is a powerful tool for the electrical characterisation of nonconducting or semiconducting materials in relation to their structure and also of electronic or sensor devices. Fig. 8 presents dielectric relaxation processes in polymers as a function of the frequency.

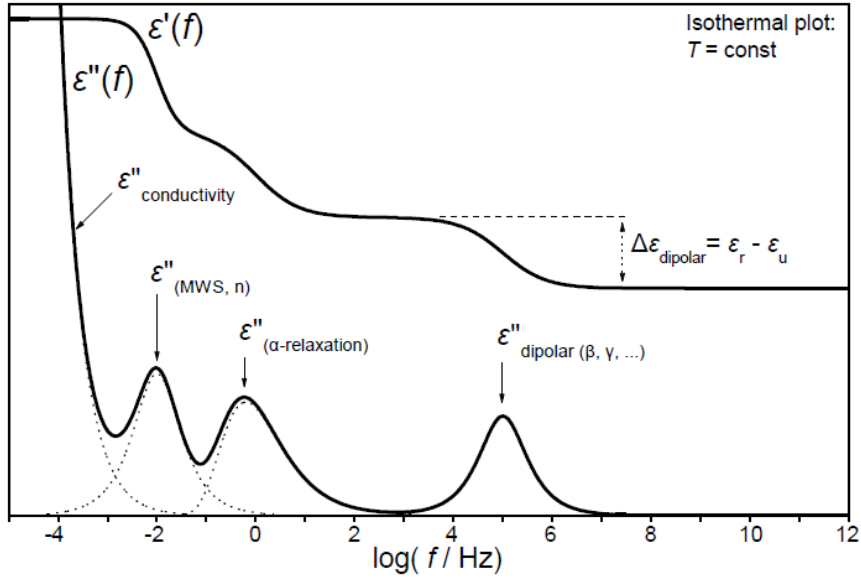


Fig. 8 Schematic presentation of the frequency dependence of ε' and ε'' for typical dielectric relaxation modes in polymers [40].

Polymers are generally characterized by the presence of various dipolar units in different environments. This leads to a broad distribution of relaxation times. The corresponding loss peaks are usually extended over several frequency decades.

Starting from high frequencies the first mechanism is dipolar relaxation which comes from permanent or induced dipoles aligning to an electric field. β and γ secondary relaxations are part of dipolar relaxations. The β relaxation involves local intra-molecular movements such as localized fluctuations of parts of the main chains, conformational changes in cyclic side groups or hindered rotations of side groups [41].

The δ relaxation is due to isolated molecules of impurities. The loss peaks of the two processes are symmetric, and they show an Arrhenius temperature dependence. These are typical features of a non-cooperative process.

$$\tau = \tau_0 \cdot \exp \frac{E}{k_B T} \quad (1)$$

When the frequency decreases the α relaxation is observed: it is related to the glass transition in the amorphous part of the material, that is the onset of segmental movements of the polymer chains. The loss peak of the α relaxation has an asymmetric shape. Its temperature dependence obeys the Vogel-Fulcher-Tammann law (VFT law) which can be derived from the theory of the glass transition:

$$\tau = \tau_0 \cdot \exp \frac{B}{(T - T_0)} \quad (2)$$

Where τ_0 is the pre-exponential time, B is an activation parameter and T_0 is the ideal glass transition temperature (or the Vogel temperature) which is related to the dynamic glass-transition temperature. The asymmetric shape and the VFT behaviour are typical features of a co-operative process. Generally, the α relaxation has the highest strength, therefore it is often called the primary or main relaxation. On the low-frequency end of the spectrum ionic relaxations appear: they comprise ionic conductivity and interfacial and space charge relaxation. The macroscopic motion of space charges comes from the electrodes which create

a large electric dipole. Interfacial polarization or Maxwell-Wagner-Sillars (MWS) polarization [42] is a characteristic bulk phenomenon in polymer systems with a heterogeneous structure with regions having different dielectric permittivity or conductivity. It results in an accumulation of charges at the interfaces. Such relaxations are sometimes or very often for some types of polymers overlaid with dipolar relaxations. The movement of charges between boundaries (electrodes or phase boundaries) is very efficient because it generates a large effective dipole moment due to larger charge displacements than in case of rotating dipoles, and huge losses due to strong internal friction. As the MWS relaxations depend on the morphology of the phase-separated components, dielectric analysis would provide useful informations on the microstructure of the polymer. The charge carrier relaxations exhibit an Arrhenius temperature dependence because they are closely related to the exponential temperature dependence of the conductivity [43].

2.1.3 Viscoelastic properties

Polymers composed of long molecular chains have viscoelastic properties, which combine the characteristics of elastic solids and Newtonian fluids. The solid state deformation of a polymer is time-dependent and nonlinear and gather some combination of elastic and viscous responses. The variation of the elastic part of the Young modulus as a function of temperature, for a given frequency is schematically described in Fig. 9. The same kind of plot can be obtained as a function of the time, for a given temperature. This is a manifestation of viscoelasticity, in which the effect of time, temperature and frequency on a polymer are all closely interrelated. Time-temperature equivalence assumes that the viscoelastic behavior at one temperature can be related to that at another temperature by a change in the time scale only [44]. It's often used by researchers.

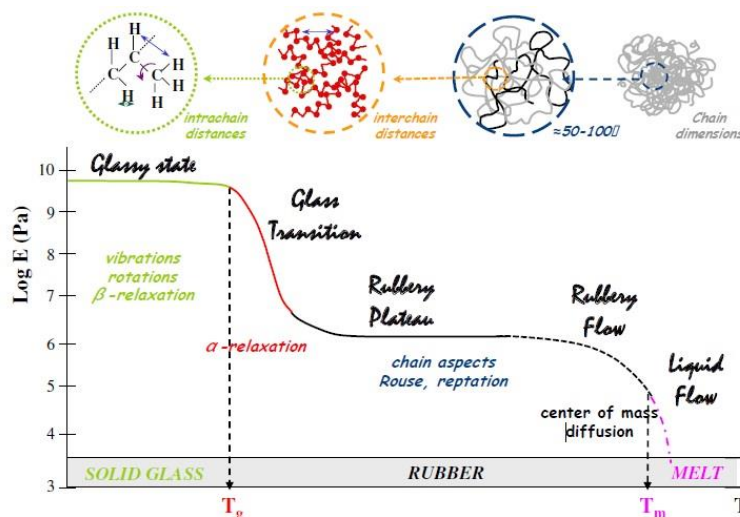


Fig. 9 Variations of the dynamic modulus in a bulk polymer and its molecular origin [45].

At low temperature (or short time), the material is in the glassy state and only small amplitude motions like vibrations, short range rotations or secondary relaxations are possible. The secondary relaxations cause the first characteristics of the dynamic modulus variations of such a polymer system. It's a local process mostly intra-molecular and it has Arrhenius temperature dependence. The glass transition appears when the chains in the amorphous regions begin to coordinate large scale motions. At the glass transition temperature T_g the primary relaxation

(α -relaxation), related to segmental motions of the chain, becomes active, allowing the system to flow. The α -relaxation causes a huge step of typically three orders of magnitude in the dynamic modulus amplitude [46]. Segmental relaxation exhibits non-Arrhenius temperature dependence that is usually approximated by VFT equations. The following rubbery plateau is related to large scale motions within a polymer chain.

When a chain has lost the memory of its initial state, rubbery flow sets in. This is the beginning of the liquid flow, which is characterized by the translational diffusion coefficient of the chain.

2.2 Electromechanical properties

2.2.1 Electromechanical principles

The total deformation of a dielectric material created under an electric field is:

$$S_{ij} = s_{ijkl} \sigma_{kl} + d_{kij} E_k + M_{klj} E_k E_l \quad (3)$$

The first term is the strain generated by an external mechanical stress σ_{kl} and is related to the elastic compliance s_{ijkl} . The second term takes into account the piezoelectric effect and depends on the piezoelectric coefficient d_{kij} . The evolution is linear with the electric field. The third term is the deformation due to electrostriction and / or electrostatic involving an apparent coefficient of deformation M_{klj} . This is a quadratic function of the electric field.

For thermoplastic polyurethanes, contributions have an electrostatic and / or electrostrictive origin. The thickness strain S in direction along which the electric field is applied can be written as a combination of electrostriction *Selectrostriction* and Maxwell strains *SMaxwell*, as shown in Equation (1) [47]:

$$S = S_{electrostriction} + S_{Maxwell} = M_{33}^* E^2 \quad (4)$$

Where M_{33}^* is the apparent electromechanical coefficient, and E the applied electrical field. The Maxwell stress effect comes from electrostatic attractions between the electrodes and can be expressed as:

$$S_{Maxwell} = -\frac{\epsilon'_r \epsilon_0}{Y} E^2 \quad (5)$$

Where ϵ'_r , ϵ_0 , and Y refer to the real part of the relative permittivity, to the vacuum permittivity and to the Young modulus of the polymer, respectively.

The electrostriction is the direct coupling between the polarization and mechanical response in the material:

$$S_{electrostriction} = Q P^2 \quad (6)$$

By assuming a linear relationship between the polarization P and the electrical field E ,

$$P = \epsilon_0 (\epsilon'_r - 1) E \quad (7)$$

Selectrostriction can be expressed by Equation (3):

$$S_{electrostriction} = Q P^2 = Q \epsilon_0^2 (\epsilon'_r - 1)^2 E^2 = M_{33} E^2 \quad (8)$$

Where, Q is the charge-related electrostrictive coefficient and M_{33} the electrical field-related electrostrictive coefficient.

It has been previously published [48] that the M_{33} coefficient of electrostriction varies like

$$(\epsilon_0 (\epsilon_r' - 1)^2) / (\epsilon_r' Y) \quad (9)$$

As seen in these equations, actuation capabilities depend on the dielectric and mechanical properties of the polymer. It is always reported as a compressive effect.

Generally, in the case of electrostriction in soft elastomers, deformation is considered to be rather proportional to the square of the electric field, which is a valid assumption for dielectrics with low permittivities, for which the electric field is proportional to the polarization [49].

2.2.2 Electrostrictive properties of PU

In experimental investigations of the electromechanical response of PUs, it has been found that for more moderate electric fields, a large part of the response is due to causes other than the Maxwell effect [50'51]. At contraction of up to some percents on PU elastomers has been reported and exhibit inherent electrostriction [52'53]. Strains up to 4–5% for electric fields up to 10 MV/m have been reported by Diaconu et al. [54]. Although the reason for the inherent electrostriction in PUs is not yet fully explained, it has been suggested that it is due to space charge impurities in the samples (the interfaces between SS and HS are regions of space-charge trapping which create non uniform electric field across the film thickness, in addition the unfiltered sample showed the largest strain) [52]. Moreover, experimental investigations have shown that the electromechanical response is a thin film effect and that the magnitude of the electrostrictive coupling depends on the thickness of the specimens, where the investigated thicknesses range from some 10 microns to a few millimeters [54'52]. The thickness dependence may also possibly be related to the influence of space charge impurities [49]. Su et al. [53], reported that for thick samples, the local electric field is not very different from the average field and there is no enhancement effect due to the interface space-charge. On the contrary as the thickness is reduced, the local field becomes larger than the average field, which results in an enhanced electromechanical response. From a macroscopic level, Guillot et al [48] found an empirical relationship to predict the values of the electrostrictive coefficients from the dielectric constant and the compliance coefficient of the material. This empirical relationship was already established by Eury et al [55] for a variety of dielectric materials, including glasses, ceramics, single crystals, and polymers.

Diaconu *et al.* reported that the thickness strain decreases when the relaxation time is decreased. Moreover the relaxation time also influences the electrostrictive polymer behavior [56]. Guillot et al. [48] have demonstrated that the electrostriction coefficient of PU should decrease when the frequency is increased. Furthermore, Putson et al. confirmed that an increase of frequency- for example from 0.1 Hz to 1 KHz- induces a decrease by a factor of 100 of the electrostrictive coefficient [57].

The electromechanical properties of this material have not been completely investigated and the fundamental mechanisms responsible for electrostriction are not yet well understood. Indeed, the models proposed in the literature do not take into account their microstructural heterogeneities.

In order to understand and optimize the electrostriction properties of segmented PU, it would be interesting (i) to characterize the microstructural properties of pure PU, in terms of phase separation and diameter and shape of the HD (ii) to understand the variations of physical

behavior, based on the different relaxation processes in a wide range of frequency and temperature.

2.2.3 Energy harvesting in pseudo piezoelectric behavior

A way of harvesting energy using electrostrictive polymers consists of working in the pseudo piezoelectric behavior. For this, the electrostrictive polymer is subjected to a DC biased electric field. As the polymer is not piezoelectric, it is necessary to induce polarization with a DC bias in order to obtain a pseudo piezoelectric behavior [58, 59].

An isotropic electrostrictive polymer film contracts along the thickness direction (the electric field direction) and expands in the film plane when an electric field is applied across the thickness, assuming that only a nonzero stress is applied along the length of the film.

Based on this assumption, it was possible to calculate the harvested current from a polymer film as a function of the strain and the electric field using the following formula [60,61]:

$$I = 2 M_{31} Y E_{dc} A \frac{\partial S_1}{\partial t} \quad (10)$$

Here, I is the harvested current, A is the area of sputtered electrode on the polymer film, Y is the Young modulus of the polymer, E_{dc} the applied electric field, M_{31} electrostriction coefficient, $\frac{\partial S_1}{\partial t}$ are the time derivate of the strain.

By assuming that M_{31} was almost proportional to ϵ_r/Y , it is deduced that the figure of merit for the harvested current is close to the permittivity of the film. Consequently, an improvement of dielectric permittivity leads to increase the energy harvesting of the polymer, however for actuation properties an increase of dielectric permittivity while maintaining a moderate Young modulus is needed.

3 Improvement of the electromechanical properties

The electromechanical properties of the electrostrictive polymers or dielectrics elastomers are inherently governed by the permittivity of the material [62, 63, 64]. This parameter controls the electromechanical deformation in the actuator mode but also the power density recoverable in the generator mode. An increase in permittivity generates substantial increase in performance. In the literature, there are different solutions to increase the permittivity. For example, elaboration of composite by introducing a second dielectric phase with high dielectric constant (ceramic powders or polymer blends for example can be introduced in the polymer matrix) [65]. However, this is generally associated with an increase in rigidity (elastic modulus) of the material [66]. Another way is to synthesize new materials from a mixture of polymers or organic materials with tailored characteristics [67]. New synthetic polymers may be obtained as blends of known polymers or by copolymerisation or by grafting highly polarizable lateral chains to existing molecules [68,69,70]. In a similar way, another method to increase the permittivity is to add a conductive phase, like conductive polymers, metallic powders or carbon-based materials [71]. Many parameters affect the properties of nanocomposites, such as the type and the shape of the fillers, the state of dispersion, and polymer-nanofiller interactions. Carbon-based nanocomposites are good candidates for electroactive nanocomposites. As this PhD deals with the use of carbon nanotubes, we will only describe the use of carbon-based materials, and more specifically carbon nanotubes.

3.1 Carbon-based fillers

The use of conductive carbon-based nanomaterials is an attractive solution to increase the permittivity. Indeed, the dispersion of conductive particles causes an accumulation of charges at the interfaces between both phases (matrix, particles). These free charges present in the polymer do not only contribute to the conduction, but also increase the interfacial polarization, so the permittivity. The experimental study of electrical conduction in a medium composed of conductive inclusions randomly distributed in an insulating matrix shows that below a given concentration of inclusions, the medium is insulating and above this level the medium is conductor.

Carbon can be used in various forms, depending on its crystalline arrangement. In addition to the nanomaterials displayed in Fig. 10, one can cite carbon black (CB) and graphite. One can also distinguish carbon nanotubes which are categorized as single-walled (SWCNT) or multi-walled (MWCNT), depending on the number of graphene layers present in their walls. For any of these particles dispersed within the polymer matrix, an important parameter, influencing the overall properties, is the compatibility between the matrix and the particles, in terms of dispersion and particle-matrix interactions [72,73].

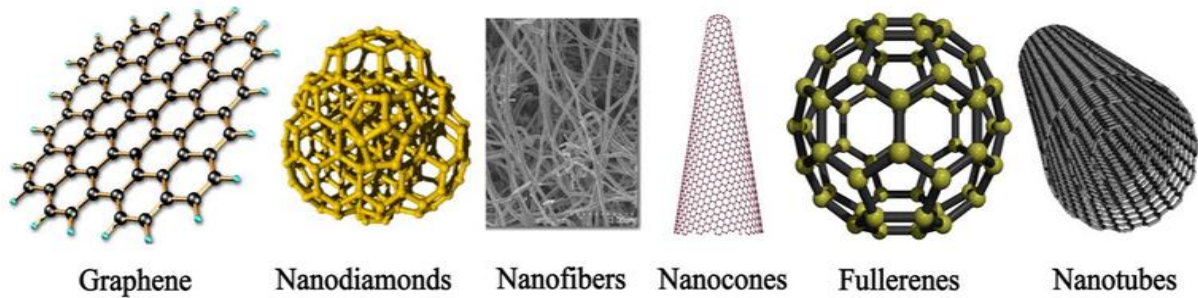


Fig. 10 Carbon-based nanomaterials [74].

3.2 Improvement of the electromechanical properties using carbon nanotubes

CNTs possess outstanding properties, among which extremely high aspect ratios or Young moduli. They have attracted much attention for the design of multifunctional materials that combine structural, electrical, thermal and mechanical properties. As far as their electrical behavior is concerned, CNTs, and particularly MWCNTs, show better electrical conductivities than CB. They may therefore provide a better interfacial polarization and increase the dielectric constant of dielectric polymer-based EAPs [75]. Wongtimnoi et al [76] found an improvement of the electromechanical properties of PU by three orders of magnitude when filled with carboxyl-functionalized multi-walled carbon nanotubes (MWCNT-COOH). However, it is well known that the electromechanical performance is limited by the low volume content of CNTs, and by the impressive conductivity near the percolation threshold [77].

3.2.1 Physical properties of polymer/CNT composites

3.2.1.1 Morphological and microstructural properties

The morphological properties of polymer-CNT composites strongly depend on the materials, processing and their critical processing issues. In the same manner, the morphology characteristics affect the material performance. Therefore, most of all of the reported results in composite production dedicate some effort to describe the morphology of their products before characterize them physically.

The investigation of nanocomposite morphology needs techniques that can provide details down to a subnanometer size scale. Indeed, the geometrical arrangement and sizes of the polymer and nanofillers phases have to be characterized.

3.2.1.2 Microstructural properties of PU nanocomposites

Carbon nanotubes show a strong dependence of their properties (electronic, mechanical and other physical properties) with their geometrical structure often characterized through parameters such as diameter, length Consequently, the structural characterization of carbon nanotubes is very important. Several microscopic techniques have been used to characterize the morphology, structure and composition of the nanosized polymer brushes and polymer-nanocomposites.

Transmission Electron Microscopy (TEM) and Scanning Electron Microscopy (SEM) are commonly used to investigate the microstructure at the sub-micron scale. Moreover, SEM is a very useful tool to observe the fracture surfaces of the composites [78, 79], thus permitting to obtain information related to the adhesion of the fillers within the matrix. Nevertheless, it is very difficult to quantify the CNT dispersion state from either TEM or SEM images and precisely measure several parameters, including the distance between CNTs, the number of contacts, the CNT orientation, the CNT curvature as well as the distance between entanglements. Indeed such parameters can hardly be determined on 2 dimensional images, but need to be measured in 3D for a good accuracy. Electron tomography is undoubtedly the most pertinent technique to obtain a three dimensional view of polymer/ CNT microstructures. Until now, this information is still missing in the literature and all the published studies presenting electron tomography polymer /CNT nano-composites concentrate more on how to obtain a good contrast between polymer matrix and CNT and the most appropriate microscopy for such observation rather than on a quantitative studies on dispersion states with a quantitative parameters [80,81].

3.2.1.3 Thermal properties of CNT composites

The thermal properties of polymer-CNT composites were extensively studied. The addition of functionalized or non-functionalized carbon nanotubes in most polymeric matrices seems to result in a shift on the glass transition temperature (T_g) due to change of molecular weight of the polymer matrix depending on the filler type and content [82].

Furthermore, the crystallization and morphology of semicrystalline polymers can be strongly affected by the addition of carbon nanotubes. Lozano and Barrera [83] showed that the addition of catalytically grown carbon nanofibers can promote nucleation of polypropylene. In general,

the cristallinity of polymer has shown to be increased with the addition of carbon nanotubes [84]. Changes in the crystal structure of polymers can also be induced by nanotubes [85].

3.2.1.4 Electrical properties

Carbon nanotubes exhibit high aspect ratios, excellent electrical properties that make them suitable to use as conductive fillers in polymer composites. Additionally, nanotubes present the tendency to become entangled into a three-dimensional interconnecting network that favors the connectivity and conductivity. In fact, it was reported conductivity at extremely low CNTs contents in a polymer matrix because of the large CNT aspect ratio [86].

It is important to notice that the percolation threshold depends upon the morphology of the conductive network, which again is influenced by the processing route. For instance, aligned carbon nanotubes have lower percolation threshold than entangled carbon nanotubes even though the maximum conductivity is the same.

The use of raw or functionalized nanotubes as conductive fillers remains a challenge. Even though in some cases the functionalization helps their dispersion in the matrix, it sometimes reduces the quality and quantity of electrical contacts between the nanotubes because of adsorbed or covalently attached molecules.

■ *Electrical properties below the percolation threshold*

The introduction of CNT in an insulator matrix results in a local polarization. They can be modeled by a serie-parallel network of capacitances and resistances [87]. Thus, below the percolation threshold, the material conductivity is frequency dependent. The higher the frequency, the higher the conductivity. Moreover, if the quantity (volume fraction) of CNTs is increased, an increase in the quantity of local capacitances is expected, thus the material should be more capacitive. It has been reported that CNT filled polymers near to the percolation threshold reveal a change in the electrical properties [88].

■ *Electric properties above percolation threshold*

The percolation threshold is represented by the existence of a continuous conductive path through the material, with CNTs physically in contact with each other. Because the contact is not perfect, the continuous path should be modeled with series of resistors, where each resistor represents a contact between tubes. Thus, the conducting phenomenon is essentially ohmic, and as a consequence frequency independent [87].

Nevertheless, close to the percolation, dead arms or isolated tubes still remain in the material. These particles act as local nano-capacitors. Thus the behavior observed is the sum of an electrical capacitance and an ohmic electrical transport [87]. As shown in Fig. 11, for a given frequency (namely the critical frequency), the capacitive effect exhibits a higher value than the ohmic effect. For higher filler volume fractions, the resistance of the system dramatically falls and the capacitive transport is dominated by the ohmic conduction.

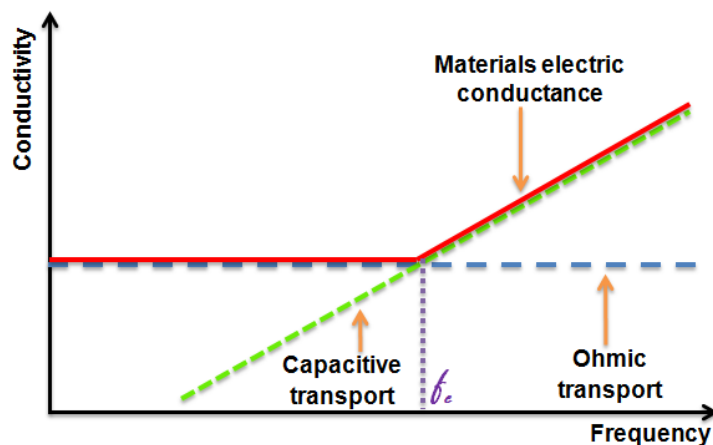


Fig. 11 Electrical conductivity against frequency next to percolation threshold

3.2.1.5 Mechanical properties

As for other applications, carbon nanotubes are excellent reinforcing charges in polymers, due to their high aspect ratios, the specific surface areas and their intrinsic individual mechanical properties (extremely high Young's modulus (1-5 TPa), stiffness and flexibility). Thus, both SWNTs and MWNTs have been used as fillers in polymer systems of thermoset polymers (epoxy, polyimide, and phenolic), as well as thermoplastic polymers (polypropylene, polystyrene, poly (methyl methacrylate), nylon 12, and poly ether ketone (PEEK)). An increment in the filler content also lead to an increase in the viscosity with disadvantages in the processing step. Literature reports numerous studies on the mechanical properties of polymer nanotube composites, most of them considering tension and compression properties [89]. In general, the results revealed that the compression modulus is higher than the tensile modulus, indicating that the load transfer to the nanotubes in the composite is much higher in compression due to interwall sliding [90].

Reported results on mechanical behavior of polymer-CNT composites have shown that the macroscopic behavior of these materials depends on many factors such as the type of nanotubes, dispersion state, interfacial adhesion filler and matrix, the nature of the polymer used (CNT can have a nucleating effect in semicrystalline matrices or can induce a modification in the crosslink network as in epoxy) and the processing method (in situ polymerization, solvent method, or melt mixing) [91]. The Young's modulus enhancement ranges from some percents to 3 orders of magnitude [92]. However, if the interfacial adhesion between the phases is weak, the CNTs can behave as cavities or nanostructured flaws, inducing local stress concentrations, and the benefits of the CNTs properties may be lost [93]. In addition, if the nanotubes are poorly dispersed, the nanotubes will fail by failure of the bundle rather than of the nanotube itself, resulting in a significantly reduced strength [94].

In the cases of non-functionalized nanotubes, no permanent stress transfer was observed when cohesion involves Van der Waals bonds. When chemically functionalized CNTs are concerned, the nanocomposite is found to have an improved shear yield strength. As a consequence, the chemical functionalization or the grafting of polymeric chains on the carbon nanotube surface is expected to be a solution to prevent the aggregation phenomenon as well as to improve the physical interactions between matrix and fillers.

3.2.2 Critical issues with polymer CNT composites

To summarize, there is an increasing interest in the design and production of polymer-CNTs composites due to their potential amazing properties, close to those of carbon nanotubes; however, some difficulties have to be overcome before, like the inherent insolubility and entanglement of carbon nanotubes. Moreover, an optimization of the process conditions is necessary to improve the dispersion, interface adhesion and alignment of the CNTs. In the following section the main critical issues of polymer CNT nanocomposites are presented with more details.

3.2.2.1 Dispersion of CNT within the matrix

The effective use of CNTs in composite applications strongly depends on the ability to disperse them individually and uniformly throughout the matrix, without destroying their structure, or reducing their aspect ratio. Thus, an appropriate dispersion is essential to achieve the required nanocomposite properties and isotropy.

Some of the nanofillers properties that have an impact on their dispersability on the polymer matrix are the specific surface area (SSA) and the aspect ratio. Differences in the specific surface area (SSA) of SWNTs and MWNTs revealed changes in the nanotube dispersability in polymers. Indeed, according to Gogny *et al* [95], the SSA for SWNT causes agglomeration in polymer nanocomposite, whereas the smaller SSA of MWNT had shown better dispersability. Furthermore, Martin *et al* [96] studied the influence of the nanotube aspect ratio in the dispersability and stability of CNT dispersions. They found that while the long nanotubes, i.e. those with high aspect ratios, remained well-dispersed, the shorter ones were found to have formed small agglomerates immediately after stirring was stopped. Even more, the agglomerates formed by the short nanotubes were much bigger than those consisting of long nanotubes.

Different procedures have been developed to efficiently disperse nanotubes in polymer matrices using the processing methods of nanocomposites. Some reported examples are melt-mixing [97], in situ polymerization under sonication, solution process with the aid of ultra-sonication [98], acid treatment, or use of surfactants and processing aids, combination of solution-casting and melt mixing processing methods [99], functionalization of CNT, among others

3.2.2.2 Interaction of CNT with the polymer matrix

As mentioned in the previous section, the filler dispersion is a fundamental issue in the preparation of polymer nanocomposites to obtain isotropic improved materials. However, the properties enhancement is also related to the interaction of the fillers with the polymer matrix at the interface, i.e. interfacial bonding or interfacial adhesion strength. Inherently weak interactions between the nanotubes and polymer result in poor interfacial adhesion, which can lead to nanotube aggregation within the matrix and potentially weaken the composite mechanical performance [100].

Several factors are related to an enhancement of the polymer-matrix interaction. The uniform and individual dispersion of carbon nanotubes in a polymer matrix by itself maximizes their contact surface area with the matrix. Even more, the inherent filler specific surface area

determines the extent of interface for stress-transfer. High aspect ratio increases the filler interactions [95].

Furthermore, the modification of nanotube surfaces by the introduction of vacancies, defective sites, or functional groups on the nanotube surface have proved to enhance their interactions and interfacial adhesion strength. In addition, a tailored functionalization can lead to the formation of covalent bonds and/or additional dipole-dipole interactions between CNTs and the polymeric matrix, resulting in a strengthened interface and an improved wettability of the CNTs [101].

3.2.2.3 Alignment and orientation of CNT within matrix

Dispersion and interfacial adhesion strength are primordial for the macroscopic properties of nanocomposites. In a similar way, nanotube alignment could enhance some nanocomposite properties at the macroscopic level [102]. In fact, in most processing methods, the nanotube alignment was observed to depend strongly on the quality of the initial dispersion and deposition method: well dispersed and separated nanotubes could be aligned, while entangled non-separated nanotubes formed dense aggregates [103]. In general, there still exist a lack of control on the alignment and orientation of nanotubes in a polymer matrix due to the nano-sized scales.

3.2.3 Modification of CNT composites

We have seen that two main problems make the fabrication process of polymer/CNT nanocomposites difficult: (i) the insolubility of carbon nanotubes in most solvents, and (ii) the weak matrix-nanotube interaction, usually ensured only through van der Waals forces, leading poor interfacial adhesion and nanotube aggregation. Chemical functionalization of the carbon nanotube surfaces has been proposed [104] to overcome these problems.

3.2.3.1 Grafting of polymer chains on CNT surface

Grafting of polymers onto a surface can be made by: (a) “grafting to” the surface, in which a polymer chain is attached on the surface. Most reports concerning the “grafting to” method. Carbon nanotubes have been functionalized with acids that react with functional groups in polymers, leading to esterification or amidification reactions. In the review by Liu [105], there is an indication of several polymers and copolymers grafted using the “grafting to” method. (b) “grafting from” the surface, in which the polymerization is initiated from initiating groups (typically free radicals) introduced onto the substrate. “**Grafting from**” is an alternative way to graft polymers on the external layer of MWNTs. In this particular technique, the CNT contains the polymerization reaction initiator grafted on its surface. The reactional groups on the surface will react with monomers. The macromolecules grow-up from the surface through a polymerization reaction. As an example, Liu [105] reports reactions by Atomic Transfer Radical polymerization (ATRP) brushes based on the polymerization of Methyl Methacrylate (MMA) [106] monomer, styrene monomer [107] or Polystyrene-*b*-Poly (acrylic acid) (PS-*b*-PAA).

One can also mention “mixed” methods, involving polymer reactions with functional groups on the surface. In this approach, a polymer exhibiting terminal functional groups reacts with other functional groups that are present on a specific surface [108].

In both “grafting from” and “grafting to” procedures, a broad distribution of molecular weights and compositions of the polymer chains are expected, if the polymerization proceeds by an uncontrolled method [109]. Additionally, polymer reactions with functional groups present on the surface experience low chain polymer attachment due to steric repulsion. Fortunately, the molecular weight, and a well-defined polymer structure can be controlled [110].

In summary, the “grafting from” method is preferred over the other methods, because of its possible advantages, such as a higher degree of functionalization, that could be related to surface coverage, the control of the polymer molecular weight composition.

4 Conclusion

Electroactive polymers (EAPs), whose responses are stimulated by external electrical fields, have drawn tremendous attention in recent years. These EAPs are attractive for a broad range of applications such as high performance sensors, actuators, artificial muscles, microelectro-mechanical systems (MEMS), etc., because they can exhibit high field-induced strain in response to electrical stimulation.

Among the various available EAPs, polyurethane (PU) elastomers are of great interest for a wide range of transducer and actuator applications when considering their significant electrical field-induced strains, high specific energy and small response time. However, their electromechanical properties have not been completely investigated and the fundamental mechanisms responsible for electrostriction are not yet well understood. In particular, the models proposed do not take into account their heterogeneous microstructures.

The electromechanical properties of the electrostrictive polymers or dielectrics elastomers are inherently governed by the permittivity of the material. For actuator mode the deformation is proportional to the ratio of the permittivity to the Young modulus, however for energy harvesting applications, the harvested current is recovered by the permittivity. An increase in permittivity generates substantial increase in performance.

It is important to analyze the energy conversion efficiency by investigating the dielectric and viscoelastic properties over a wide range of frequencies and temperatures.

In a first part of this PhD, we will focus on the role of microstructure of segmented pure PUs on their electrostriction properties. We will consider three different PUs with different weight fractions of hard segments. On these materials, we will characterize the shape and the diameter distribution of the hard domains, as well as the distance between hard domains. Their electrical and mechanical behaviors will be studied over a wide range of frequencies and temperatures in order to localize a large range of utilization with stable mechanical and electrical properties. Relationships between microstructure, electrical, mechanical and electrostrictive properties will be analyzed for the three PUs.

We have also seen that carbon nanotubes may be efficient to increase the permittivity of the films. However, having a good dispersion of the CNTs in the matrix and a strong interfacial

adhesion between CNTs and the matrix remains a challenge. Grafting a compatible polymer onto the CNT surface could overcome these issues. Thus, in a second step, we will investigate how the electromechanical properties of PU films can be improved by the incorporation of grafted CNTs. We will first optimize the film fabrication process to obtain the best dispersion without damaging the CNTs or the grafted layer. The CNT dispersion will be quantified using electron tomography. Then, the nanocomposite electrical, mechanical properties will be characterized. Finally, the impact of the CNTs and of the grafted layer on the actuation properties will be discussed.

References

- [1] L. Lebrun, D. Guyomar, B. Guiffard, P-J: Cottinet, C. Putson. *Sensors and actuators A* 153 (2009) 251-257
- [2] José Oscar Mur Miranda: *Electrostatic Vibration-to-Electric Energy Conversion*. PhD thesis. 2004
- [3] Paolo Colombo. *Polymer-Derived Ceramics: 40 Years of Research and Innovation in Advanced Ceramics*. *J. Am. Ceram. Soc.*, 2010, 93, 1805–1837
- [4] Raghu Das. *Electroactive Polymers and Devices 2013-2018: Forecasts, Technologies, Players* Dielectric elastomers, electronic & ionic EAPs and their applications:
- [5] Cathleen Thiele. *Electroactive Polymers and Devices 2013-2018: Forecasts, Technologies, Players*. 2013
- [6] http://en.wikipedia.org/wiki/Electroactive_polymers
- [7] Sacerdote M. P., *Déformations électriques des diélectriques solides isotropes*. *J. Physics*, 3 Series, 31 1899.
- [8] Heiji Kawai. *Polyvinylidene fluoride (PVDF)*. *Plastics Europe*. 1969
- [9] Shirakawa, Hideki; Louis, Edwin J.; MacDiarmid, Alan G.; Chiang, Chwan K.; Heeger, Alan J. *Synthesis of electrically conducting organic polymers: Halogen derivatives of polyacetylene, (CH) x*. *Journal of the Chemical Society, Chemical Communications*. 1977 16: 578.
- [10] Lovinger, A.J. *Ferroelectric polymers*. *Science*. 1983; 220 1115–1121.
- [11] T. Furukawa. *Ferroelectric Properties of Vinylidene Fluoride Copolymers*. *Phase Transitions: A Multinational Journal*. 1989, Vol. 18, pp. 143-211.
- [12] Q. Pei, R. Pelrine, S. Stanford and R. Kornbluh, Marcus Rosenthal, *Electroelastomer rolls and their application for biomimetic walking robots*, *Synthetic Metals*, 2003, 135-136.
- [13] K. Oguro, Y. Kawami, and H. Takenaka, "Bending of an Ion-Conducting Polymer Film-Electrode Composite by an Electric Stimulus at Low Voltage," *J. of Micromachine Society*, vol. 5, 27-30, 1992.
- [14] Zhang, Q. M., Bharti, V., Kavarnos, G., Schwartz, M. (Ed.), (2002). "Poly (Vinylidene Fluoride) (PVDF) and its Copolymers", *Encyclopedia of Smart Materials*, Volumes 1–2, John Wiley & Sons, 807–825.
- [15] Baughman, null et al. *Carbon nanotube actuators*. *Science* 284, 1340–1344 (1999).
- [16] Y. Bar-Cohen, *Electro-active polymers: current capabilities and challenges*, Paper 4695-02, *Proceedings of the SPIE Smart Structures and Materials Symposium, EAPAD*, 2002.
- [17] Y. Bar-Cohen. *Electroactive polymer (EAP) actuators as artificial muscles : reality, potential, and challenges*. SPIE Press, 2001.
- [18] M. Shahinpoor, Y. Bar-Cohen, T. Xue, J.O. Simps and J. Smith. *Ionic Polymer-Metal Composites (IPMC) As Biomimetic Sensors and Actuators- Artificial Muscles*. *Proceedings of SPIE's 5th Annual International Symposium on Smart Structures and Materials*, 1998.
- [19] T. Hirai, T. Ueki and M. Takasaki, *Electrical Actuation of Textile Polymer Materials*, *Journal of Fiber Bioengineering and Informatics (JFBI)* 1 (2008).
- [20] K. J. Kim and M. Shahinpoor, *A novel method of manufacturing three-dimensional ionic polymer-metal composites (IPMCs) biomimetic sensors, actuators and artificial muscles*, *Polymer*, 43 (2002) 797-802.
- [21] S. Nemat-Nasser, *Micromechanics of actuation of ionic polymer-metal composites*, *J. Appl. Phys.*, 92 (2002) 2899-2915.
- [22] Y. Bar-Cohen, T. Xue, M. Shahinpoor, J. O. Simpson, and J. Smith, *Flexible, lowmass robotic arm actuated by electroactive polymers*, *Proc. of SPIE's 5th Annual Int. Symp. on Smart Structures and Materials*, San Diego, CA. 1998 pp. 1-6.
- [23] H. Tamagawa and M. Taya, *A theoretical prediction of the ions distribution in an amphoteric polymer gel*, *Materials Science and Engineering A*, 285 (2000) 314-325.
- [24] Y. Osada and J.-P. Gong, *Soft and Wet Materials: Polymer Gels*, *Adv. Mater.*, 10; 1998, 827-837.
- [25] R. H. Baughman, *Conducting polymer artificial muscles*, *Synthetic Metals*, 78 (1996) 339-353.
- [26] Kwang J. Kim and Satoshi Tadokoro (Eds.). *Electroactive Polymers for Robotic Applications. Artificial Muscles and Sensors*.
- [27] A. M. Vinogradov, V. H. Schmidt, G. F. Tuthill and G. W. Bohannon, *Damping and electromechanical energy losses in the piezoelectric polymer PVDF*, *Mechanics of Materials*, 36 (2004) 1007-1016.

- [28] R. Pelrine, R. Kornbluh, J. Joseph, R. Heydi, Q. Pei and S. Chiba, High-field deformation of elastomeric dielectrics for actuators, *Materials Science and Engineering C*, 11 (2000) 89-100.
- [29] R. Pelrine, R. Kornbluh and G. Kofod, High-Strain Actuator Materials Based on Dielectric Elastomers, *Adv. Mater.*, 12 (2000) 1223-1225.
- [30] M. Watanabe, T.H., M. Suzuki & Y. Amaike Y, Electric Conduction in Bending Electrostriction of Polyurethanes *Appl. Phys. Lett*, 74 (1999). 2717.
- [31] B. Guiffard, L.S., G. Sebald and D. Guyomar . Enhanced electric field induced strain in non-speculative carbon nanopowder/ polyurethane nanocomposites *J. of Phys. D: Appl.Phys.*, 2006 39, 3053.
- [32] L. Irusta and M. J. Fernandez-Berridi, Photooxidative behaviour of segmented aliphatic polyurethanes , *Polym. Deg. & Stab.*, vol. 63, (1999)p. 113-119.
- [33] Guiffard, B., Guyomar, D., Seveyrat, L., Chowanek, Y., Bechelany, M., Cornu, D., and Miele, P. (2009). Enhanced electroactive properties of polyurethane films loaded with carbon-coated SiC nanowires *Journal of physics. D, Applied physics*. Vol. 42, 0022-3727.
- [34] J. Su, J. S. Harrison, T. L. Clair, Y. Bar-Cohen and S. Leary, Electrostrictive graft elastomers and applications, *MRS Symposium: FF: Electroactive Polymers*, Boston, MS (1999).
- [35] Y. Wang, C. Sun, E. Zhou and J. Su, Deformation mechanisms of electrostrictive graft elastomer, *Smart Mater. Struct.*, 13 (2004) 1407-1413.
- [36] Diguet. G, Bogner. A, Chenal. J-M, Cavaillé. J-Y. Physical modeling of the electromechanical behavior of polar heterogeneous polymers, *Journal of Applied Physics*.2012; 112: 0000. DOI: 10.1063/1.4766280.
- [37] Goerg H. Michler. Electron microscopic investigations of morphology and structure formation of polymers. *Journal of Macromolecular Science, Part B: Physics*, 35,329-355, 1996
- [38] Sigurd Schrader, Xuan Li, Fanxiu Guo, Yong Liu, Jijiang Luo² and Duanfu Xu. Electron microscopy investigations of polyester-polyurethane elastomers stained with ruthenium tetroxide. *Die Makromolekulare Chemie, Rapid Communications*. 19889, 597–601.
- [39] H.G Haubruge, A.M Jonas, R Legra. Staining of poly(ethylene terephthalate) by ruthenium tetroxide. *Polymer*, 44, 2003, 229–3234
- [40] AGLAIA VASSILIKOU-DOVA and IOANNIS M. KALOGERAS. DIELECTRIC ANALYSIS (DEA). *Thermal Analysis of Polymers: Fundamentals and Applications*, Edited by Joseph D. Menczel and R. Bruce Prime ; Copyright © 2009 by John Wiley & Sons, Inc.
- [41] Hedvig 1977 *Dielectric spectroscopy of polymers*
- [42] van Beek, L. K. H. *Dielectric Behavior of Heterogeneous Systems*; Heywood Books: London, 1967; Vol. 7
- [43] Peter Frubing. *Dielectric spectroscopy*. University of Potsdam, Institute of Physics Advanced lab experiments. 2001
- [44] D. Richter, M. Monkenbusch, A. Arbe and J. Colmenero. *Neutron Spin Echo in Polymer Systems* (Springer, Berlin, 2005).
- [45] Clément Riedel. *Dielectric and mechanical properties of polymers at macro and nanoscale*. Physics. Université Montpellier II - Sciences et Techniques du Languedoc, 2010.
- [46] P. G. de Gennes: *Scaling Concepts in Polymer Physics* (Cornell University Press, Ithaca and London, 1979).
- [47] Zhang Q M, Su J, Kim C H. An experimental investigation of electromechanical responses in a polyurethane elastomer. *J. Appl. Phys.* 1997; 81:2770-2776. DOI: 10.1063/1.363981.
- [48] Guillot F M, Balizer E. Electrostrictive effect in polyurethanes. *J. Appl. Polym. Sci.* 2003; 89: 399-404. DOI: 10.1002/app.12096.
- [49] Newnham, R.E., Sundar, V., Yimmirun, R., Su, J., Zhang, Q.M., 1997. Electrostriction: Gd nonlinear [electromechanical coupling in solid dielectrics. *The Journal of Physical Chemistry B* 101, 10141–10150.
- [50] Zhenyi, M., Scheinbeim, J.I., Lee, J.W., Newman, B.A., 1994. High field electrostrictive response of polymers. *Journal of Polymer Science Part B: Polymer Physics* 32, 2721–2731.
- [51] Diaconu, I., Dorohoi, D.O., Topoliceanu, F., 2006. Electrostriction of a polyurethane elastomer-based polyester. *IEEE Sensors Journal* 6, 876– 880.
- [52] Wang, H., Zhang, Q., Cross, L., Ting, R., Coughlin, C., Rittenmyer, K., 1994. The origins of electromechanical response in polyurethane elastomers. In: *Proceedings of the Ninth IEEE International Symposium on Applications of Ferroelectrics, ISAF '94*, 182–185.

- [53] Su, J., Kim, C., Kugel, V., Zhang, Q., Ting, R., Capps, R., 1996. Temperature-frequency dependence of electrostrictive properties of a polyurethane elastomer. In: Proceedings of the Tenth IEEE International Symposium on Applications of Ferroelectrics, ISAF '96, 927–930.
- [54] Diaconu, I., Dorohoi, D.O., Ciobanu, C., 2008. Electromechanical response of polyurethane films with different thicknesses. *Romanian Journal of Physics* 53, 91–97.
- [55] Sylvie Eury, Rattikorn Yimmirun, V Sundar, Paul J Moses, Sei-Joo Jang, Robert E Newnham. Converse electrostriction in polymers and composites *Materials Chemistry and Physics - MATER CHEM PHYS*, 61, 18-23, 1999.
- [56] I. Diaconu, D. Dorohoi. PROPERTIES OF POLYURETHANE THIN FILMS. *Journal of Optoelectronics and Advanced Materials* Vol. 7, No. 2, April 2005, p. 921 - 924.
- [57] Chatchai P. Energy conversion from electroactive materials and Modeling of behaviour on these materials. PhD Thesis, 2010 INSA Lyon, France.
- [58] A. M. Vinogradov, V. H. Schmidt, G. F. Tuthill and G. W. Bohannon, Damping and electromechanical energy losses in the piezoelectric polymer PVDF, *Mechanics of Materials*, 36 (2004) 1007-1016.
- [59] K. Yuse, D. Guyomar, M. Kanda, L. Seveyrat and B. Guiffard, Development of large-strain and low-powered electro-active polymers (EAPs) using conductive fillers, *Sensors and Actuators A*, 165 (2011) 147-154.
- [60] Pierre-Jean Cottinet, Daniel Guyomar, Benoit Guiffard, Laurent Lebrun and Chatchai Putson. Electrostrictive polymers as high-performance electroactive polymers for energy harvesting
- [61] Fouad Belhora, Pierre-Jean Cottinet, Abdelowahed Hajjaji, Daniel Guyomar, M'hammed Mazroui, Laurent Lebrun, Yahia Boughaleb. Mechano-electrical conversion for harvesting energy with hybridization of electrostrictive polymers and electrets. *Sensors and Actuators A* 201, 2013, 58–65
- [62] P.-J. Cottinet, D. Guyomar, B. Guiffard, C. Putson, and L. Lebrun, *IEEE Trans. Ultrason. Ferroelectr. Freq. Control* 57, 774 (2010).
- [63] C. Huang, Q.M. Zhang, Fully functionalized high-dielectric-constant nanophase polymers with high electromechanical response, *Adv. Mater.* 17 (2005) 1153-1158.
- [64] Y. Liu, K.L. Ren, H.F. Hofmann, Q. Zhang, Investigation of electrostrictive polymers for energy harvesting, *IEEE Transactions on Ultrasonics, Ferroelectrics and Frequency Control* 52, 2005, 2411–2417.
- [65] L. K. H. Van Beek, Dielectric behaviour of heterogeneous systems, In *Progress in Dielectrics*, vol. 7, Eds. Birks, J. B. London Heywood Books, New York, 69-114, 1967.
- [66] Y. Bai, Z.-Y. Cheng, V. Bharti, H. S. Xu, and Q. M. Zhang, High-dielectric-constant ceramic powder polymer composites, *Appl. Phys. Lett.*, Vol. 76(25), 3804-3806, 2000.
- [67] Q. M. Zhang, M. Wissler, B. Jaehne. Effect of crosslinking, prestrain and dielectric filler on the electromechanical response of a new silicone and comparison with an acrylic elastomer. *Smart Structures and Materials*, Proc. SPIE, 5385, 78-86, 2004
- [68] J. Su, Z. Ounaies, J. S. Harrison. Electromechanically active polymer blends for actuation. *Smart Structures and Materials*, Proc. SPIE, 3987, 65-72, 2000
- [69] W. Lehmann, H. Skupin, C. Tolksdorf, Giant lateral electrostriction in ferroelectric liquid-crystalline elastomer, *Nature*, 410, 22, 2001
- [70] K. Jung, J. Lee, M. Cho, J. C. Koo, J.-d. Nam, Y. Lee and H. R. Choi, Development of enhanced synthetic elastomer for energy-efficient polymer actuators. *Smart Mater. Struct.* 16, 288-294, 2007
- [71] C. Huand, Q. M. Zhang, G. deBotton, and K. Bhattacharya, All-organic dielectric-percolative three-component composite materials with high electromechanical response, *App. Phys. Lett.*, vol. 84, 22, 2004.
- [72] M. H. Al-Saleh and U. Sundararaj, An innovation method to reduce percolation threshold of carbon black filled immiscible polymer blends, *Composite: Part A*, vol. 39, 284-293, 2008.
- [73] C. Yang, Y. Lin, and C. W. Nan, Modified carbon nanotube composites with high dielectric constant, low dielectric loss and large energy density, *Carbon*, 47, 1096-1101, 2009.
- [74] Bo-Tao Zhang, Xiaoxia Zheng, Hai-Fang Li, and Jin-Ming Lin. Application of carbon-based nanomaterials in sample preparation: A review. *Anal. Chim. Acta*, 2013, 784, 1-17.
- [75] C. Park, J. H. Kang, J. S. Harrison, R. C. Costen, S. E. Lowther, Actuating Single Wall Carbon Nanotube-Polymer Composites: Intrinsic Unimorphs, *Adv. Mater.* 20, 2074-2079, 2008.

- [76] K. Wongtimnoi, B. Guiffard, A. Bogner-Van de Moortèle, L. Seveyrat, J.-Y. Cavaillé. Electrostrictive thermoplastic polyurethane-based nanocomposites filled with carboxyl-functionalized multi-walled carbon nanotubes(MWCNT-COOH):Properties and improvement of electromechanical activity *Composites Science and Technology* 85,2013, 23–28
- [77] J. K. W. Sandler, J. E. Kirk, I. A. Kinloch, M. S. P. Shaffer and A. H. Windle Ultra-low electrical percolation threshold in carbon-nanotube-epoxy composites, *Polymer*, (2003) vol. 44: p. 5893-5899
- [78] N. H. Tai, M. K. Yeh and J. H. Liu Enhancement of the mechanical properties of carbon nanotube/phenolic composites using a carbon nanotube network as the reinforcement, *carbon*, (2004) vol. 42:2735-2777
- [79] R. Czerw, M. Terrones, J.-C. Charlier, W. Blase, B. Foley, R. Kamalakaran, N. Grobert, H. Terrones, D. Tekleab, P. M. Ajayan, W. Blau, M. Ruhle and D. L. Carroll *Nano Lett.*, 2001
- [80] GB Thompson, M Abdalla and D Dean. Tomography of a Polymer/Carbon-Nanotube Matrix Composite. *Microscopy and Microanalysis*, 12 2006, pp 1578-1579
- [81] MH Gass, KKK Koziol, AH Windle, PA Midgley. Four-dimensional spectral tomography of carbonaceous nanocomposites. *Nano letters* 6 (3), 376-379. 2006
- [82] Pham, J.Q., C.A. Mitchell, J.L. Bahr, J.M. Tour, R. Krishnamoorti, and P.F. Green, Glass transition of polymer/single-walled carbon nanotube composite films. *Journal of Polymer Science, Part B: Polymer Physics*, 2003. 41(24): p. 3339-3345.
- [83] Lozano, K. and E.V. Barrera, Nanofiber-Reinforced Thermoplastic Composites. I. Thermoanalytical and Mechanical Analyses. *Journal of Applied Polymer Science*, 2001. 79: p125-131.
- [84] Czerw, R., Z. Guo, P.M. Ajayan, Y.P. Sun, and D.L. Carroll, Organization of Polymers onto Carbon Nanotubes: A Route to Nanoscale Assembly. *Nanoletters*, 2001. 1(8): p. 423- 427.
- [85] Sandler, J., P. Werner, M.S.P. Shaffer, V. Demchuk, V. Altstadt, and A.H. Windle, Carbon nanofiber-reinforced poly(ether ether ketone) composites. *Composites Part A Applied Science and Manufacturing*, 2002. 33: p. 1033-1039.
- [86] Andrews, R., D. Jacques, M. Minot, and T. Rantell, Fabrication of carbon multiwall nanotube/polymer composites by shear mixing. *Macromolecules Materials Engineering*, 2002. 287: 395-403.
- [87] L. Flandin PhD, Etude expérimentale et modélisation microstructurale de l'évolution des propriétés électriques d'un matériau composite, (1992) Université Joseph Fourier.
- [88] Bryning MB, Islam MF, Kikkawa JM, Yodh AG. Very low conductivity threshold in bulk isotropic single-walled carbon nanotube-epoxy composites. *Adv Mater* 2005;17:1186–91
- [89] Qian, D., E.C. Dickey, R. Andrews, and T. Rantell, Load transfer and deformation mechanisms in carbon nanotube-polystyrene composites. *Applied Physics Letters*, 2000. 76. 2868-2870.
- [90] Schadler, L.S., S.C. Giannaris, and P.M. Ajayan, Load transfer in carbon nanotube epoxy composites. *Applied Physics Letters*, 1998. 73(26): p. 3842-3844.
- [91] Dalmas, F., L. Chazeau, C. Gauthier, K. Masenelli-Varlot, R. Dendievel, J.Y. Cavaillé, and L. Forró, Multiwalled carbon nanotube/polymer nanocomposites: processing and properties. *Journal of Polymer Science: Part B: Polymer Physics*, 2005. 43: p. 1186-1197.
- [92] O. Breuer and U. Sundararaj Big returns from small fibers: a review of polymer/carbon nanotube composites, *Polymer composites*, (2004) vol. 25: p. 630-645.
- [93] X. Zhang, T. Liu, T. V. Sreekumar, S. Kumar, X. Hu and K. Smith Gel spinning of PVA/SWNT composites fiber, *Polymer*, (2004) vol. 45: p. 8801-8807.
- [94] G. M. Odegard, T. S. Gates, K. E. Wise, C. Park and E. J. Siochi Constitutive modeling of nanotube-reinforced polymer composites, *Composites Science and Technology*, (2003) vol. 63: p. 1671-1687.
- [95] Gojny, F.H., M.H.G. Wichmann, B. Fiedler, W. Bauhofer, and K. Schulte, Influence of nano-modification on the mechanical and electrical properties of conventional fiber-reinforced composites. *Composites: Part A*, 2005. 36(11): p. 1525-1535.
- [96] Martin, C.A., J.K.W. Sandler, M.S.P. Shaffer, K.B. Schwartz, W. Bauhofer, K. Schulte, and A.H. Windle, Formation of percolating networks in multi-wall carbon-nanotube-epoxy composites. *Composites Science and Technology*, 2004. 64: p. 2309-2316.
- [97] Choi, Y.-J., S.-H. Hwang, Y.S. Hong, J.-Y. Kim, C.-Y. Ok, W. Huh, and S.-W. Lee, Preparation and Characterization of PS/Multi-Walled Carbon Nanotube Nanocomposites. *Polymer Bulletin*, 2005. 53 p. 393-400.
- [98] Safadi, B., R. Andrews, and E.A. Grulke, Multiwalled carbon nanotube polymer composites:

- synthesis and characterization of thin films. *Journal of Applied Science*, 2002. 84: 2660-2669.
- [99] Haggenueller, R., W. Zhou, J.E. Fischer, and K.I. Winey, Production and characterization of polymer nanocomposites with highly aligned single-walled carbon nanotubes. *Journal of Nanoscience and Nanotechnology*, 2003. 3: 105-110.
- [100] N. H. Tai, M. K. Yeh and J. H. Liu. Enhancement of the mechanical properties of carbon nanotube/phenolic composites using a carbon nanotube network as the reinforcement, *carbon*, (2004) vol. 42: p. 2735- 2777
- [101] Frankland, S.J.V., A. Caglar, D.W. Brenner, and M. Griebel, Molecular simulation of the influence of chemical cross-links on the shear strength of carbon nanotube-polymer interfaces. *Journal of Physical Chemistry B*, 2002. 106: p. 3046-3048.
- [102] Thostenson, E.T. and T.-W. Chou, Aligned multi-walled carbon nanotube-reinforced composites: processing and mechanical characterization. *Journal of Physics D: Applied Physics*, 2002. 35(16): p. L77-L80.
- [103] Salalha, W., Y. Dror, R.L. Khalfin, Y. Cohen, A.L. Yarin, and E. Zussman, Single-walled carbon nanotubes embedded in orientes polymeric nanofibers by electrospinning. *Langmuir*, 2004. 20: p. 9852-9855.
- [104] Niyogi, S., M.A. Hamon, H. Hu, B. Zhao, P. Bhowmik, R. Sen, M.E. Itkis, and R.C. Haddon, Chemistry of single-walled carbon nanotubes. *Accounts of Chemical Research*, 2002. 35: p. 1105-1113.
- [105] P. Liu Modifications of carbon nanotubes with polymers, *European Polymer Journal*, (2005) vol. 41: p. 2693-2703.
- [106] H. Kong, C. Gao and Y. Yan Functionalization of multiwalled carbon nanotubes by atom transfer radical polymerization and defunctionalization of the products, *Macrom.*, (2004). 37:4022-4030.
- [107] X. D. Lou, C. Detrembleur, V. Sciannamea, C. Pagnouille and R. Jerome Grafting of alkoxyamine end-capped (co) polymers onto multi-walled carbon nanotubes *Polymer*, (2004) vol. 45: p. 6097-6102.
- [108] Matyjaszewski, K., P.J. Miller, N. Shukla, B. Immaraporn, A. Gelman, B.B. Luokala, T.M. Siclovan, G. Kickelbick, T. Vallant, H. Hoffmann, and T. Pakula. *Macromolecules*, 1999. 32: 8716-8724.
- [109] Adronov, A., C.M. Homenick, Y. Liu, and Z. Yao, Functionalization of single-walled carbon nanotubes with well-defined polymers. *Polymer Preprints*, 2005. 46(1): p. 201-202.
- [110] Hayashi, S., A. Naitoh, S. Machida, M. Okazaki, K. Maruyama, and N. Tsubokawa, Grafting of polymers onto a carbon black surface by the trapping of polymer radicals. *Applied Organometallic Chemistry*, 1998. 12: p. 743-748.

Part II: Materials and experiments

Chapter 2: Materials and experiments

1 Materials

1.1 Polyurethanes matrix

1.1.1 Generality on thermoplastic elastomers polyurethanes

Thermoplastic elastomers (TPEs) are polymers that combine advantages of both thermoplastics and elastomers [1]. In general, their specific properties depend on their morphology. At ambient temperature, physical crosslinks in the amorphous matrix make the material elastomeric, with rubber-like properties. At higher temperatures, these physical crosslinks are broken and the material can be processed easily, which is a characteristic of thermoplastics. In many thermoplastic elastomers, the reversible crosslinks originate from the crystallization of one of the blocks of the segmented copolymer. These 'hard' blocks are generally polyester [2], polyamide, or polyurethane segments [3]. At low temperatures, crystalline domains account for the mechanical stability of the material; however, above the melting point of the hard block, a polymer melt is obtained.

Polyurethanes are a collective term for all polymers comprising urethane, urea, or other isocyanate derived groups, even if they are only a minor part of the total structure [4].

Thermoplastic elastomeric polyurethanes (TPUs) are the most common segmented copolymers. Their structure is schematically shown in Fig. 1. The TPU consists basically of three building blocks [5]:

- a long-chain diol, normally with a polyether or polyester backbone,
- a diisocyanate, mostly an aromatic one,
- a chain extender, such as water, a short-chain diol, or a diamine.

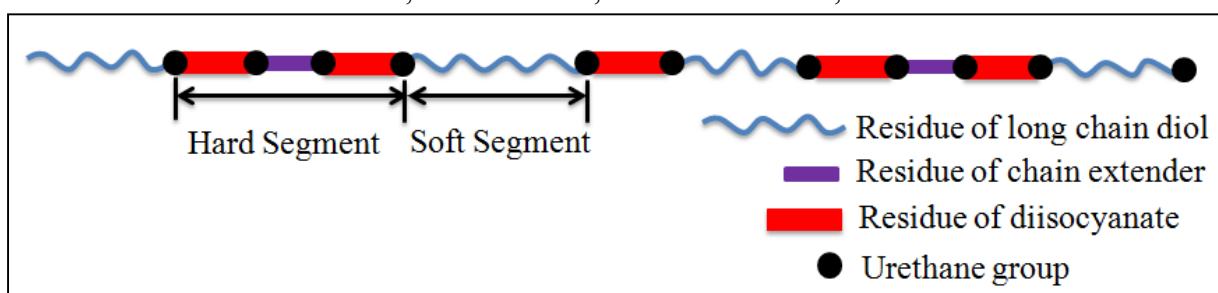


Fig. 1 Schematic representation of TPU and its building blocks.

Linear segmented copolymers consist of alternating hard and soft segments along their backbone. Their ability to develop microphase separation is one of their most defining features because such a morphology imparts many useful properties for practical applications [6]. Under appropriate conditions for microphase separation, and when the relative hard segment (HS) volume or weight fraction of the copolymer is low, the HSs generally are assumed to segregate

into isolated microdomains that are randomly dispersed in the continuous matrix of the soft segment (SS) phase [7]. It seems clear therefore that the physical properties of PU are not only determined by its chemical structure, but also by the degree of phase separation between hard and soft domains, also depending on the thermal and kinetics effects [8].

As the HS content increases, the long range connectivity of the HSs is also expected to increase, which in turn may be expected to promote a percolation of the hard phase through the soft matrix. The hard domains act as physical cross-link sites and reinforce the soft matrix thereby enabling the copolymer to display controlled useful structural properties in its ‘service window’, in which is defined for block and segmented copolymers as the region in the storage modulus (G')–temperature space within which the value of G' is relatively temperature insensitive.

1.1.2 The 3 studied polyurethanes

The studied polyurethane elastomers are polyether-based block copolymer with a complex form as shown in the diagram of Fig. 2, representing the molecular structure of an aromatic PU chain consisting of 4,4-Methylene Diphenyl Diisocyanate (MDI), of Butane Diol (BDO) and Poly (TetraMethylene Oxide) (PTMO). This is an example of one of the 5000 PU conceivable from different compounds, existing in the world market forms.

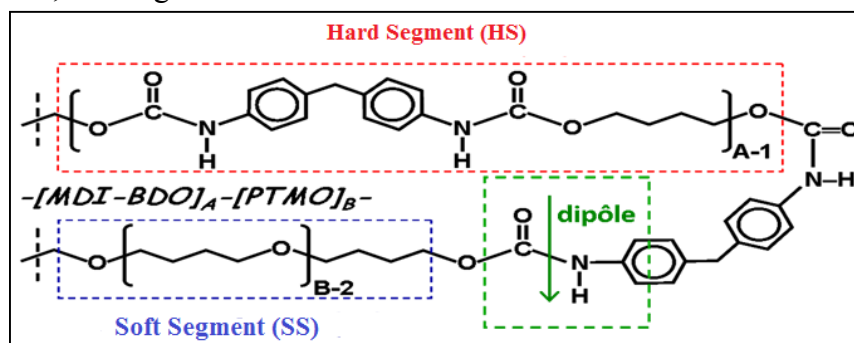


Fig. 2 Structure of the polyurethane consisting of MDI-BDO hard segments and PTMO soft segments [8].

Three polyurethanes with different weight fractions of hard segments (HS) have been provided by the same company, Lubrizol: Estane 58888 NAT 021 (PU88), Estane X-4977 NAT 039 (PU75) and Estane ETE60DT3 NAT 022 (PU60). They are synthesized by the same industrial process from the same initial chemical components. Table. 1 shows the weight fraction of HS and SS for each PU.

This range of polyether-based aromatic thermoplastic polyurethane shows good electromechanical performance [9, 10]. They have also been tested for energy harvesting applications [11].

1.1.3 Main physical properties of the 3 PU studied

Table. 1 presents the density and the HS content from the materials data sheet [12], as well as the glass transition temperature and the Young modulus measured using DSC and DMA, respectively.

Table. 1 Density, glass transition temperature and Young modulus of the 3 PU versus HS content.

	Composition	HS	Density	T_{gSD}	Y (MPa)
	MDI/BDO-PTMO	%. wt	(g/cm³)	(K)	0.1 Hz, 300 K
PU75	PTMO2000	26	1.07	209	19
PU88	PTMO1000	45	1.13	228	33
PU60	PTMO1000	65	1.17	253	120

The density is slightly affected by the HS content. On the contrary, the glass transition temperature T_{gSD} of the SD (rich in SS) -which may indicate changes in the micro-phase separation- increases when increasing the weight fraction of HS, which confirms the partial miscibility of HS and SS [13]. The three Tg values are far below room temperature and consequently, for room temperature applications, the three PU will be in the rubbery state. The Young modulus (Y) increases with the fraction of HS, since HS can act as crosslink points [14].

1.2 Carbon nanotubes (CNT)

1.2.1 Characteristics of the raw CNTs

The CNTs used in this study are multi-walled CNT, provided by Cheap Tubes [15]. The main characteristics are presented in the Table. 2.

Table. 2 Main characteristics of the CNTs used

MWNTs Outer Diameter	30-50 nm
MWNTs Length	10-20 μ m
MWNTs Purity	>95 wt%
MWNTs Specific Surface Area	60 m ² /g

Before use, the CNT have been characterized using Transmission Electron Microscopy (TEM) in order to control their dimensions (length and diameter distributions), the presence of defect on their surface, and their dispersion.

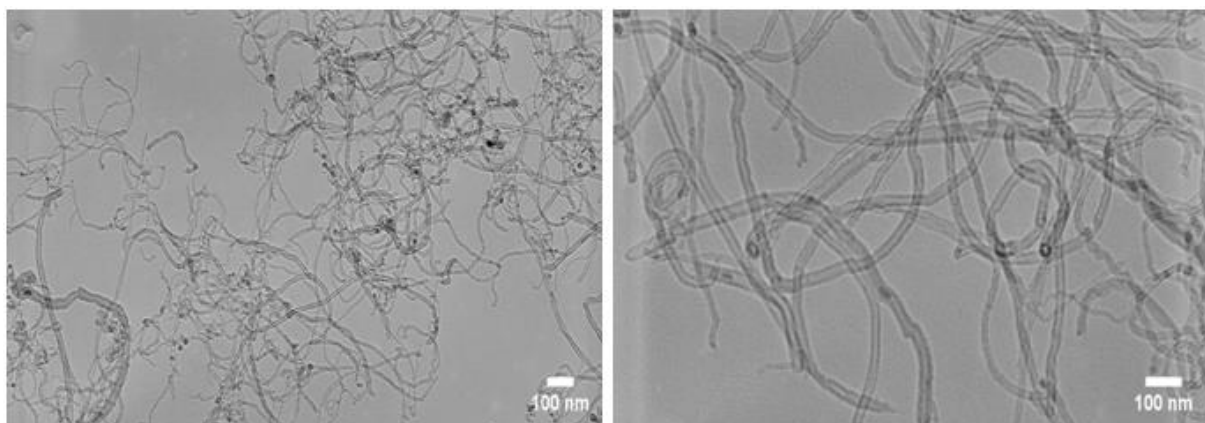


Fig. 3 Typical micrographs of the CNT

Measurements of carbon nanotubes diameters were performed on a Jeol 200CX (LaB6 filament, 200 kV). The samples were dispersed in ethanol using an ultrasonic bath for 5 minutes. A droplet of suspension was then deposited on a 200-mesh Copper grid covered with a uniform

carbon layer. Conventional bright field images were acquired at different places, see Fig. 3. An average diameter of 30 nm was measured manually on at least 60 CNTs. The diameter distribution is shown in Fig. 4.

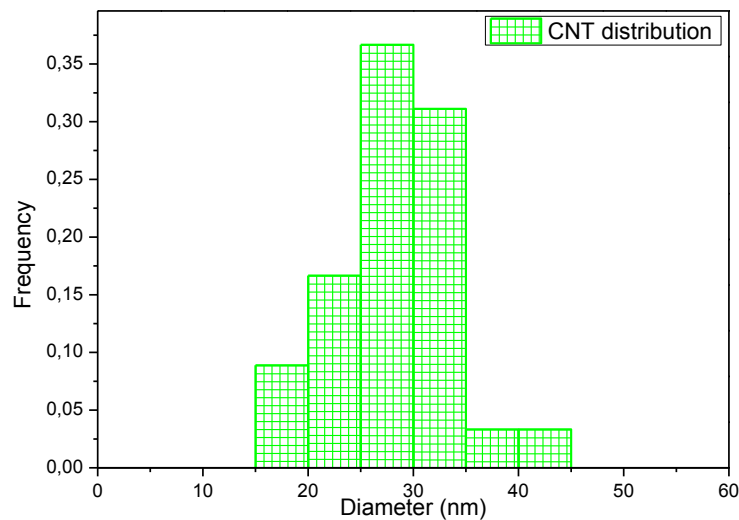


Fig. 4 distribution of the CNT diameters

1.2.2 Grafting of PU chains onto CNTs

The grafting step was performed at the Polymer Materials Engineering laboratory (IMP) within the frame of the ANR project NAPOLECO. *Marie Claire Dib Jawhar* was in charge of the development of the grafting procedure and the preparation of grafted CNTs. We were in charge of the control of grafting process step by step using microscopic observations.

The grafting reactions (see Fig. 5) were performed using a "grafting onto" technique to graft PU chains on the surface of CNT in order to have a good compatibility between the grafted chains on the surface of CNT and the PU matrix. The choice to graft the same polymer on the surface of CNT for goal to improve the dispersion state and interfacial adhesion, which is a key challenges for development of high performance CNT composites [16].

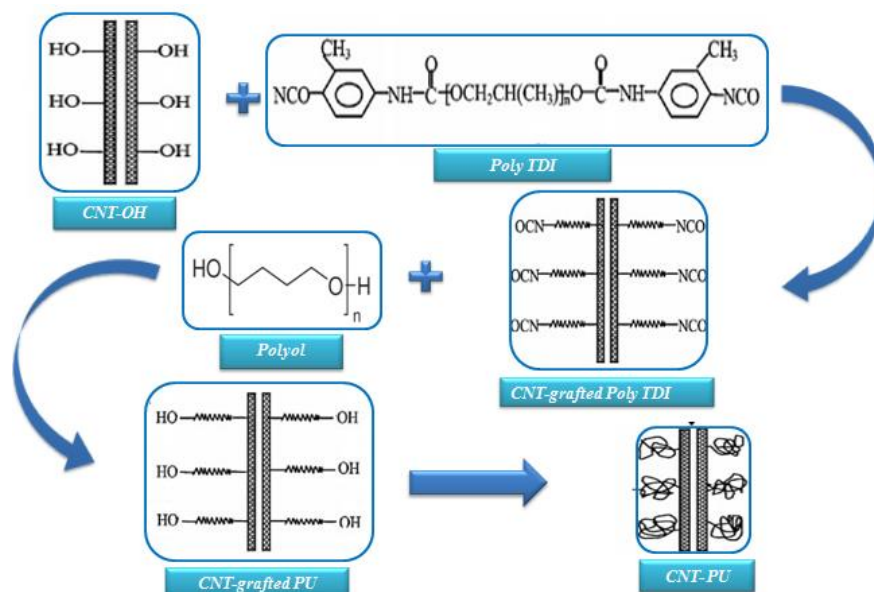


Fig. 5 Grafting process of CNT

i. CNT oxydation

In order to graft polyurethanes chains on the surface of CNTs, hydroxide-type anchors sites have first to be created. This is possible through an oxidation of the CNTs.

The following procedure was used: 10 grams of CNT and 350 mL of hydrogen peroxide (H_2O_2) were mixed in a 500 mL flask, and then the assembly was placed in an ultrasonic bath at 40 kHz for 2 hours to disperse the CNTs [17].

The flask was then heated to 395 K under reflux for 24 hours with stirring (Fig. 6 (a)). Then the solution was filtered using a polycarbonate filter (PCFE: $0.45\ \mu m$) - with a pressure column, the solution was adjusted to neutral pH (the filtrated solution was controlled via a pH-meter). To facilitate the drying step, CNT-OH were rinsed with acetone and then with Tetrahydrofuran (THF).

The oxydized CNTs (CNT-OH) were finally dried under vacuum oven for 24 hours at $T=335\ K$. After drying, the product was weighed to determine the efficiency of the reaction (The yield obtained is 95%).

ii. Grafting of polyTDI on CNT-OH

In a second step, the CNT-OH were mixed with 70 g of polyTDI (tolylene-2,4-diisocyanate terminated poly(propylene glycol) (Aldrich) – $M_n = 2300\ g.mol^{-1}$ – isocyanate = 3.6 wt%), 0.30 g of Dabco 33-LV (1,4-Diazabicyclo(2,2,2) octane) and 500 mL of DMF (dimethylformamide, solvent) in a flask. The solution was placed in the ultrasonic bath at 40 kHz for 30 minutes.

The flask was then refluxed over 24 hours at a temperature of 373 K and stirred. Afterwards, the solution was centrifuged to separate the CNT-PolyTDI of the organic phase. After centrifugation, the solution was filtered using a PCFE filter ($0.45\ \mu m$), and then washed with DMF with the help of a Soxhlet apparatus for 48 hours at 440 K (Fig. 6 (b)). Finally, the solid was placed under vacuum for 48 hours at 373 K.

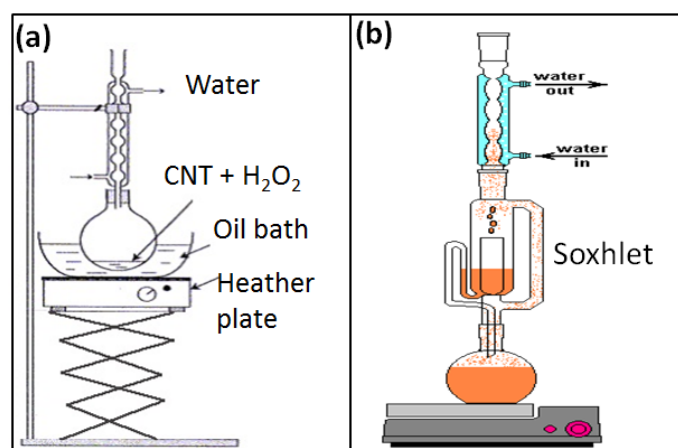


Fig. 6 (a) CNT oxidation under reflux, (b) system of purification / washing with a soxhlet apparatus

iii. Grafting of polyol on CNT grafted with poly-TDI

A mixture of 4.5 g of the CNT-polyTDI prepared in step 2, 22.5 g of polyol, 0.3 g of Dabco 33-LV and 265 ml of DMF was sonicated at 40 kHz for 30 minutes at room temperature, and then put under reflux at 373 K for 24 hours under stirring. The solution was then filtered with a PTFE filter (0.45 μm) and washed with DMF.

The product was then purified and washed in a Soxhlet apparatus with DMF for 60 hours to remove the polyol in excess. The CNTs grafted with PU were then dried under vacuum at 345 K for 48 hours.

1.2.3 Control of the grafting process

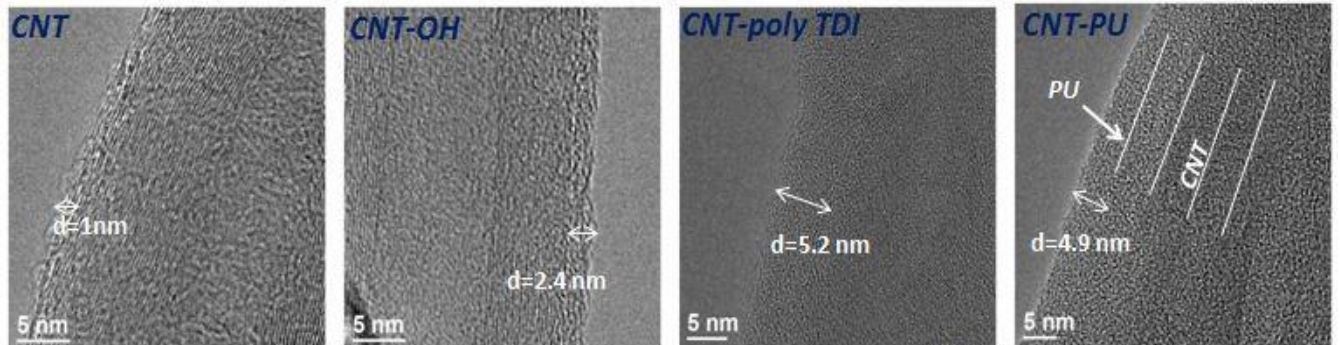


Fig. 7 TEM observation of CNT during grafted process.

Fig. 7 shows the CNT wall structure after each step of the grafting process. An amorphous layer can be observed on the CNT outer surface. This layer covers the entire surface of the CNT but its thickness varies during the grafting process. At the end a homogenous and uniform thickness of around 5 nm is measured on the CNT-PU. Thermo Gravimetric Analysis (TGA) on the CNT-PU showed a mass loss - equal to 4.2%-at a temperature similar to that of the degradation of PU, and quite dissimilar to the degradation temperatures of amorphous carbon. It is thus suggested that the final grafted layer is made of PU. It is observed from Fig. 8 that throughout the grafting process, the stability of the CNT in DMF solvent is improved.

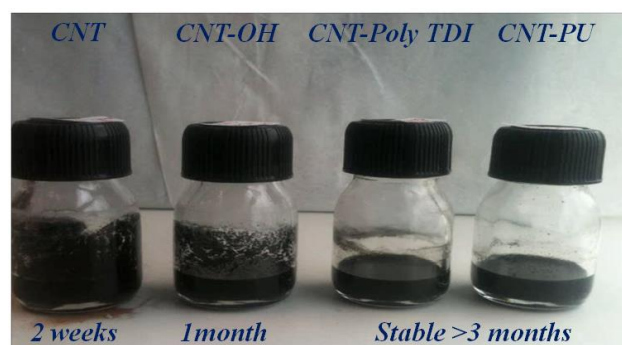


Fig. 8 stability of CNT in DMF solvent

2 Film elaboration:

2.1 Elaboration protocole of pure PU

2.1.1 Elaboration protocol using existing system « open system »

First films elaborations were performed using an open system - the same system used by K. Wongtimnoi for his PhD - (Fig. 9) with the following main steps:

The polymer films were prepared by solution casting. N, N-dimethylformamide pure 99.3% (DMF D158550 Sigma-Aldrich, 99%) was used as the organic polar solvent to dissolve PU [18]. It has a density of 0.949 g / cm³ at 293 K and a boiling point of 425 K. Because of its relative toxicity, experiences with this product are performed under a fume cupboard and in some cases with a suitable breathing mask. PU granules were previously put in an oven at T = 350 K for at least 3 hours according to the supplier's recommendations.

➤ Dissolution of the PU granules

The second step was to dissolve the PU granules and mix the polymer solution. To do this, the PU granules were dissolved in DMF in a crucible covered with parafilm at a temperature of about 350 K. The solution containing DMF and partially dissolved PU was stirred with a half-moon-type blade. Stirring and heating (T=350 K) was ensured until complete dissolution of the pellets. The process time varies according to the desired quantity (approximately 2 hours for a quantity of 25 wt% of PU in DMF). It was experimentally adjusted so that the solution was homogeneous, with an average viscosity.

After complete dissolution of the PU granules, the solution was transferred to a bottle and left standing for 24 h in order to remove air bubbles. A degassing step was sometimes necessary, for instance when the solution was very viscous and / or when it was containing a lot of bubbles. In such cases, degassing was carried out on a vacuum bell for 10 to 15 minutes.

➤ Films deposition

For the last step, the films were deposited on plates by film-casting, with an Elcometer 3700 film applicator (Fig. 9). This technique of casting-solution allows the control of the film thickness through the use of an adjustable stainless steel blade.

After deposition, the liquid film prepared from the viscous solution was dried in air in an oven at a temperature of T = 335 k during about 20 hours, to evaporate the DMF. This long step was delicate because the liquid film must be applied on a perfectly horizontal surface. A non-horizontal surface would indeed lead to non-uniform thicknesses. After having unsticked the film from the glass plate, an additional annealing was performed at T = 400 k for 3 hours in a ventilated oven to remove any remaining DMF solvent.

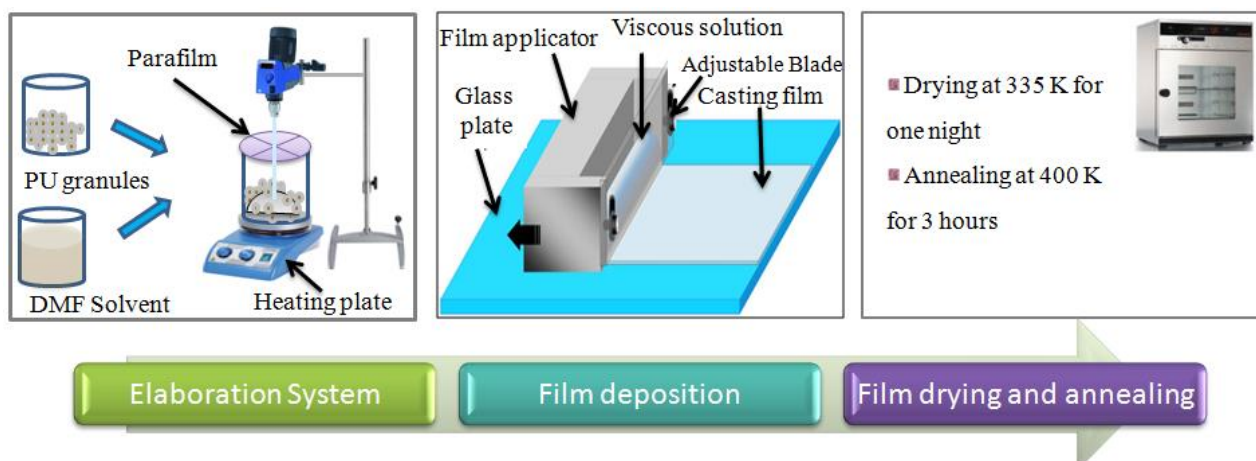


Fig. 9 Elaboration protocol of pure polyurethanes films using an “Open system”.

This method of preparation, called "open system", has several drawbacks. First, it implies a large evaporation of DMF and therefore the use of large initial quantities, which is harmful for the environment and for health. Furthermore there is a poor control of the viscosity of the solution, because the amount of evaporated solvent is not easily controllable. In addition an appearance of micro-gels or poorly dissolved gels (which are clearly visible with the naked eye (Fig. 10 (a)) could be noticed in the first films. Furthermore, a skin layer was previously observed by K. Wongtimnoi, see Fig. 10 (b). This may be due to the conditions used to dry the films.

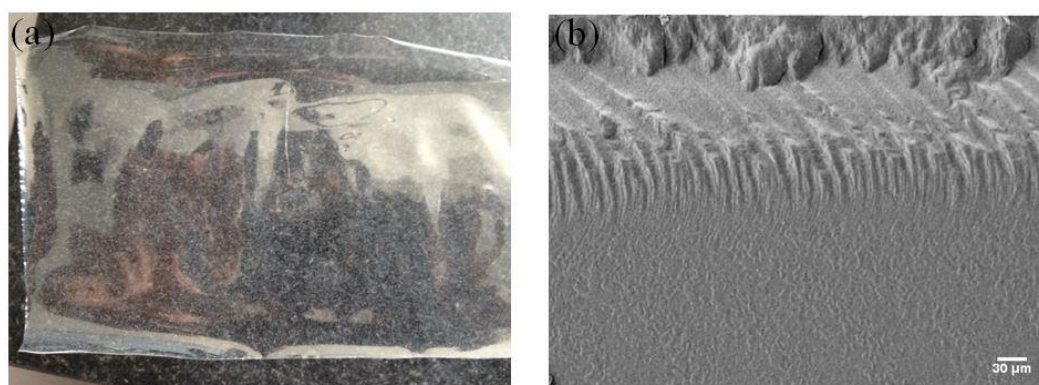


Fig. 10 (a) PU film with microgel, (b) air dried layer

In order to decrease the amount of solvent, a new preparation system, called “closed system”, has been developed. Moreover, it should be more environmentally friendly and is expected to provide films with more reproducible morphologies.

2.1.2 Elaboration protocol using « closed system »

The beaker used in the open system was replaced by a spherical flask with 3 inputs (Fig. 11): the first one was used to introduce the PU granules and DMF, the second one to condense the evaporated solvent (using cooled water), and the third one was used for mechanical stirring. During the dissolution of PU in DMF, these three inputs were closed with appropriate plugs (use of the grease). In order to ensure a homogenous distribution of temperature, the flask containing the PU+ DMF was placed in an oil bath equipped with a magnetic bar (Fig. 11). The same preparation conditions as with the “open system” were used to prepare the solutions

(dissolution for 2 h and stirring for 2 h at $T = 350 \text{ K}$). Similarly, the deposition of films and the drying conditions were not changed.

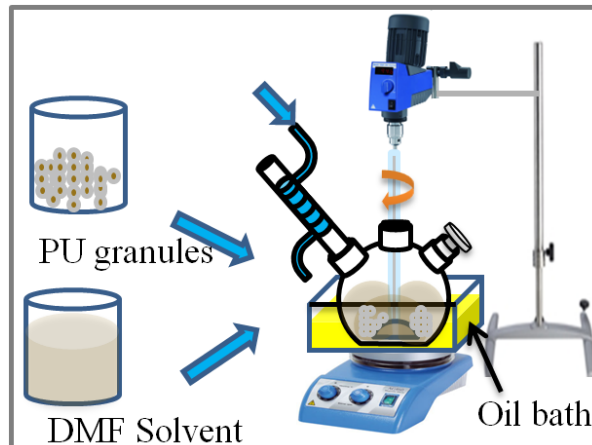


Fig. 11 "closed system"

With this new preparation protocol, the DMF vaporized is then re-condensed, which ensures no uncontrolled loss of DMF and therefore a constant amount of DMF until the end of the elaboration. This allows us to work with lower amounts of solvent than those used with the open system. In addition, the closed system ensures a homogenous distribution of the temperature during the whole process.

Nevertheless, whatever the protocol used, it appeared that the polyurethane solutions were sometimes a little turbid, which probably suggests the presence of micro-gels. In the following, we will investigate whether the amount of micro-gel can be reduced by optimizing the elaboration conditions.

2.1.3 Optimization of the elaboration process

i. Filtration

A first attempt was to filter the polymer solution. Using a system equipped with a filter made of glass microfibers and a pump (Fig. 12 (a)), the 3 solutions (PU88, PU75 and PU60) were filtered out. For these tests, the 3 PU were prepared with the open system, using 25% of PU in DMF.

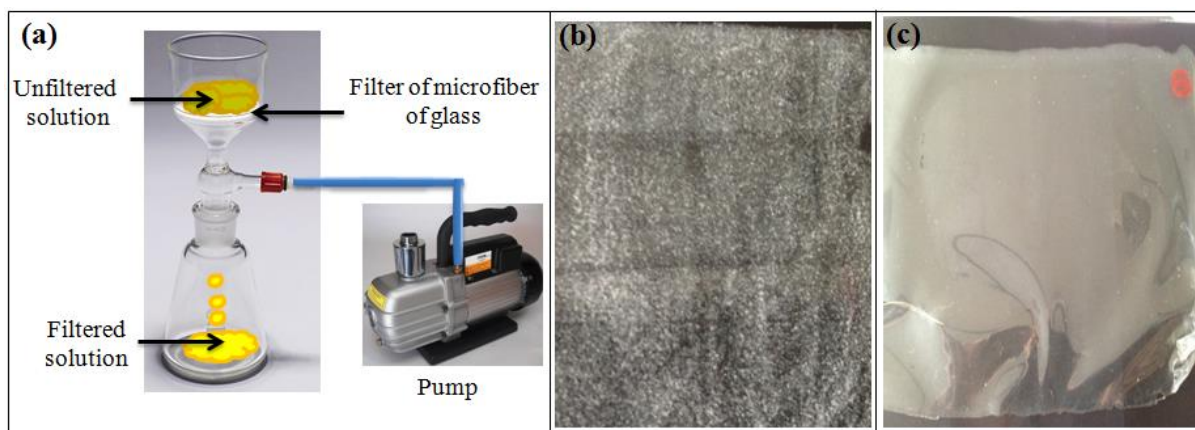


Fig. 12 Filtration system (a), Film prepared from unfiltered solution (b), filtered solution (c).

The difference between the films prepared with a filtered solution and those prepared with an unfiltered solution can be clearly seen with the naked eye (Fig. 12(b & c)). Using these filtration conditions, it was possible to eliminate the micro-gels. However, as the PU chemical composition may have changed, it is necessary to quantify the influence of the filtration step on the electrical, mechanical and electrostrictive properties of films. To answer this, a complete characterization (DSC, mechanical, electrical, electrostrictive) was performed on films from the unfiltered and filtered solutions (for 3 PU). It can be concluded from all the measurements that filtration does not affect or does not change significantly the electrical, mechanical and morphological characteristics of the films.

Even if the filtration step allows us to eliminate the micro-gel without changing the morphological properties of films, it was decided to not filter solutions because the filtration process is slow (about 4 hours) and results in DMF evaporation.

ii. Modification of the elaboration conditions

Tests have been carried out to increase the stirring time while decreasing the amount of PU in the solvent. 15 wt% PU in DMF were used instead of 25 wt%, with a preparation protocol slightly changed: the solution was stirred, the stirring speed was increased. In addition the elaboration time was doubled (from 2 to 4 hours).

With these new conditions of preparation, we managed to avoid micro-gels. As a consequence, these conditions were kept for all film elaborations.

2.2 Elaboration Protocol of PU nanocomposites

2.2.1 Optimization of the grafted CNT dispersion state of in DMF solvent

The elaboration process of the PU-CNT nanocomposites –with different volume fractions of grafted CNTs- is a crucial issue. The first step concerns the grafted CNT dispersion state in DMF solvent, prior to the addition of the PU –containing solution. The grafted CNT have to be separated from each other in the solution, without damaging the grafted layer. Indeed, it has been shown that depending on the kind of nanotubes and on the process involved in the fabrication of nanocomposites, the percolation threshold could dramatically change [19].

Furthermore, it was found that the dispersion state depends on the nanofiller functionalization [20], type, solvent, sonication time [21], and volume fraction of nanoparticles [22]. Here, four tests were performed using two different methods of sonication: sonication in an ultrasonic bath (UB) and /or sonication using an ultrasonic processor (UP). The ultrasonic processor used was a 7 mm sonotrode from Hielscher UP400S 400W, working at 24 kHz. The amplitude was set between 10 and 30% and cycle 0.5. Each time, the CNT individualization was characterized using TEM observations, with the investigation of the wall integrity preservation (see Fig. 13).

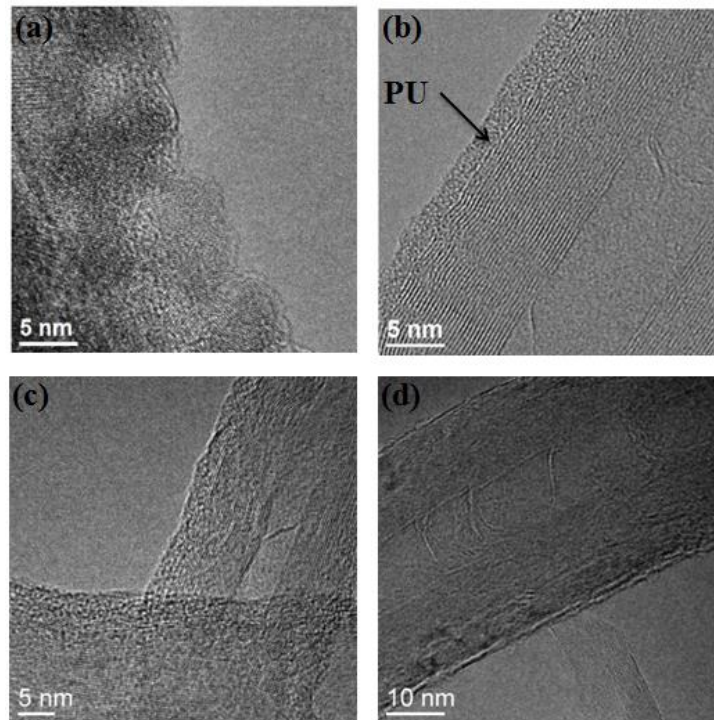


Fig. 13 Optimization of the dispersion conditions in DMF using ultrasonic bath (UB) and ultrasonic processor (UP): (a) UP-30 min, (b) UB-1h30, (c) UB-1h30 + UP-5 min, (d) UB-1h30 + UP-15 min.

Fig. 13 (a) shows that the grafted CNTs were heavily damaged after 30 min of UP even with low amplitude and pulse conditions. After 1h30 of UB sonication, the grafted CNTs were relatively well dispersed and the grafted layer was not damaged: it was still uniform and covered the whole CNT surface (Fig. 13 (b)). By adding an additional sonication using the UP during 5min with the most gentle conditions, the dispersion seemed to be further improved and negligible damage could be observed on the grafted layer (Fig. 13 (c)). Fig. 13 (d) indicates that an increase of the UP time up to 15 min induces damage in the grafted layer.

To conclude, two dispersion conditions led to the best compromise, with a good dispersion and negligible damage in the grafted layer: (i) UB-1h30 (used for films with 1 and 2 Vol. % CNT), (ii) UB-1h30 + UP-5 min (used for films with 3, 4 and 5 Vol. %, when the CNT dispersion was not good enough with the UB-1h30 only).

2.2.2 Elaboration protocol of PU nanocomposites

As for the films with pure PU, the nanocomposite films were prepared using a solution casting method. Before use, PU granules were heated at 350 K for 3 hours. The grafted CNTs were

first dispersed in DMF using the conditions detailed above. Then, PU granules were added to the solution with a ratio of 15 wt.% of PU into DMF. The solution was heated at 350 K for 4 hours under mechanical agitation, until a homogeneous solution was obtained. As for the films prepared from pure PU, this operation was carried out in the closed device, to avoid evaporation of the DMF solvent and to ensure good reproducibility. Then, the solution was then kept overnight to remove air bubbles. Afterwards, this solution was cast on glass plates with an Elcometer 3700 doctor blade film applicator, put in an oven at 335 K for one day, and then removed from the glass. A second heating treatment at a temperature below the HS melting temperature was performed at 400 K for 3 h in order to eliminate the residual solvent. The thickness of the films was about 100 μm after drying.

3 Characterization techniques

3.1 Microstructural

3.1.1 Thermal properties characterization

The thermal analysis comprises a series of methods, which detect the changes in the physical and mechanical properties of a substance and/or its reaction products by the application of heat or thermal energy. The physical properties include mass, temperature, enthalpy, dimension, dynamic characteristics and others.

Thermal properties characterizations are used to determine the purity, cristallinity and thermal stability of the chemical substances under study. Sometimes it is used in the determination of the composition of complex mixtures and/or material inspection [23].

In this thesis, the selected techniques to the study of pure PU, grafted CNT and PU grafted CNT nanocomposites were Thermogravimetric Analysis (TGA)-not presented here because it is used just to control grafting process- and Differential Scanning Calorimetry (DSC).

Differential Scanning Calorimetry (DSC)

Differential Scanning Calorimetry is the dominant technique for the thermal analysis of polymeric materials. Thus, in this work, DSC was used to determine microstructural changes of polymer matrices and carbon nanotube composites. Glass transition (T_g), melting (T_m) and crystallization temperatures (T_c) were determined at several filler concentrations.

Experimental Technique

When a sample undergoes a physical transformation (such as melting, crystallization and glass transition), heat will be needed to maintain both a reference and the sample at the same temperature, depending on the type of process (exothermic or endothermic). The measurement of the required heat to increase or decrease the temperature of a sample is performed as a function of temperature. By observing the difference in heat flow between the sample and reference, DS calorimeters are able to measure the amount of energy absorbed or released during such transitions.

A typical DS calorimeter (Fig. 14) consists in two sealed pans (reference and sample pan). These pans are often covered by or composed of aluminum, which acts as a radiation shield. The two pans are heated, or cooled, uniformly while the heat flow is monitored. This can be done isothermally or by changing the temperature at constant rate. The result is a plot of the differential heat flow as a function of temperature: a DSC thermogram. Generally, the

differential heat flow is calculated by subtracting the sample heat flow from the reference heat flow. Thus in this case, exothermic processes will show up as positive peaks, while peaks resulting from endothermic processes are negative.

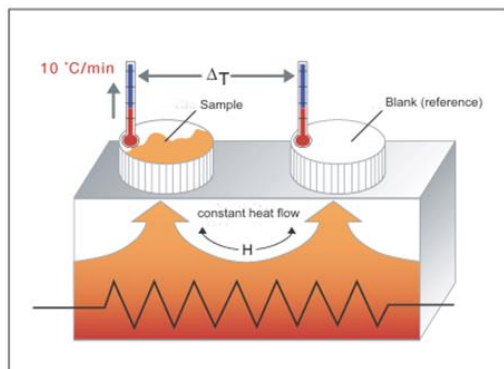


Fig. 14 Schematic principle of DSC measurement

Applications to nanocomposites

A DSC thermogram may be interpreted to obtain information about the previous thermal and mechanical history of a polymer sample. DSC is often used to study the effects of thermal pretreatment on polymer morphology. DSC is widely used to investigate the properties of polymer blends. It is especially useful for distinguishing compatible and incompatible polymers. DSC studies of composite materials help in the interpretation of the interactions among polymers and additives. As the vitreous transition T_g is sensitive to quite a series of factors, it is suited to be used in microstructural and phase-behavioral studies in polymer blends and composites. In polymer blends, T_g has been used as a parameter to determine thermodynamic component miscibility. In composite materials, T_g has been proved useful in the study of the effects related to the polymer adhesion at the interface. Thus, the shift in the T_g value is commonly associated to a difference in the polymer chain mobility due to the presence of filler. Above the glass transition, the polymer chains possess a notable mobility. At higher temperature it is observed an endothermic peak corresponding to the melting of the crystalline phases of the polymer. This peak enables to estimate melting temperature and heat. An evolution of this peak with the addition of nanofillers can be used to investigate the influence of nanofillers on the polymer crystallinity. The melting is a first order transition since when the melting temperature is reached; the polymer temperature does not rise until all the crystals have completely melted. Semi-crystalline polymers exhibit a particularly broad melting peak.

Experimental conditions

Differential Scanning Calorimetry was performed using an apparatus from Setaram, DSC 131 Evo Instruments under nitrogen flow ($P = 1.5$ bar). Samples of 20 mg were cooled to 140 K under liquid nitrogen and then heated to 480 K before being cooled to room temperature. The heating and cooling rates were set at 10 K / min.

3.1.2 Microscopic

Scanning electron microscopy: SEM

Principles

The scanning electron microscope (SEM) enables the investigation of specimens with a resolution down to the nanometer scale. An electron beam is generated by an electron gun, accelerated at the desired energy. The electromagnetic lenses of the column permit to control the electron probe size, to focus it on the sample surface. The electron probe scans the sample surface using deflection coils (Fig. 15 (a)). As a consequence the magnification is simply defined as the ratio of the image width with the width of the scanned area.

The signals are generated by the interaction of the primary electrons (PE) of the electron beam and the specimen. The most common signals come from secondary electrons (SE) and backscattered electrons (BSE). They come from an interaction volume (Fig. 15 (b)) in the specimen which diameter depends on the energy of the primary electrons (typically between 200 eV and 30 keV) and the sample composition and density. The SEs come from a small layer on the surface and yield the best resolution. The contrast in SE images is due to the topography of the sample.

BSEs come from deeper regions and thus give images with lower resolutions. On flat samples, the contrast in BSE images arise from composition variations in the sample. In the case of polymer materials and polymer/CNT nanocomposites, the differences in the atomic number of the polymer phase(s) and the CNTs is too small to give rise to a significant contrast in BSE images. As a consequence, this mode will not be used in our case [24].

In conventional scanning electron microscopes, which operate under vacuum, the specimen has to be electrically conductive. For insulators such as polymer-based materials, images may be distorted because of charge accumulation on the sample surface. The most classical solution is to coat the sample with a conductive layer (e.g. Carbon, Gold etc.). It is also possible to work on uncoated materials at low acceleration voltages – typically 1 kV – where there is naturally no charging effect. On specific SEMs, it is also possible to use low vacuum conditions to eliminate the charges in excess. In that case, the gas molecules are ionized by the electron beams (the PEs, the SEs, or the BSEs) and compensate the charges at the sample surface [25].

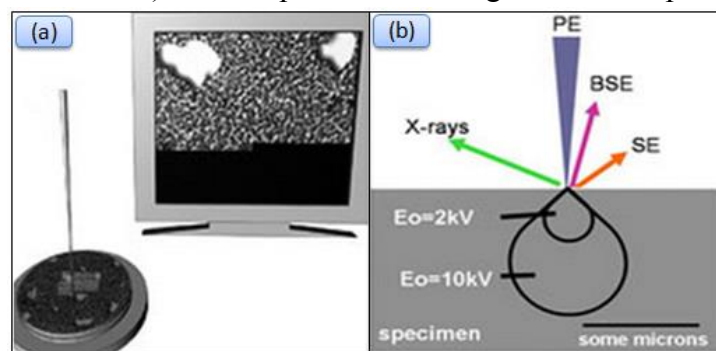


Fig. 15 SEM principles

Experimental conditions

Microstructural observations on cryofractured samples - using liquid nitrogen - were carried out in order to control the dispersion state as well as the interfacial adhesion strength between the matrix and CNTs. The observations were performed on uncoated samples using a Zeiss Supra 55VP Scanning Electron Microscope operating under high vacuum, at low accelerating voltage (typically 1000 V). Images were acquired with the Everhart-Thornley secondary electron detector.

□ Transmission Electron Microscopy

Principles

Transmission electron microscopes are designed to investigate the materials' inner structure at large magnifications. They are capable of probing atomic structures, identifying defects and measuring chemical composition - all features that control the materials' behaviour. For these reasons, electron microscopy is indispensable in materials science, especially for the study of nanostructured materials. Transmission electron microscopy uses high energy electrons (up to 300 kV accelerating voltage for usual TEMs). The electron beam can be considered as waves with wavelengths about a million times shorter than lightwaves. When an electron beam passes through a thin specimen, electrons can be scattered either elastically or inelastically. Electromagnetic lenses allow the formation of an image or a diffraction pattern, depending on the mode of operation. On amorphous materials like polymers, the contrast in the images is due to absorption. Thus, on polymer blends, it may be necessary to use staining agents (OsO₄, RuO₄ being the most common stains), which will preferentially react with one of the phases.

Experimental conditions

Studies of phase separation into SDs and HDs were performed on stained samples-more information related to staining protocol will be detailed in Part III- using a TEM microscope JEOL 2010F microscope, operating at 200kV. Bright field images were recorded with a Gatan Orius 200 camera. Measurements were performed manually using ImageJ on at least 90 objects. As staining may introduce artifacts, morphological observations of the HDs and SDs were also performed by Atomic Force Microscopy (AFM) on a Nanoscope 5 from VEECO. Thin polymer films of each PU were deposited on a glass plate and dried overnight prior to imaging. Tapping mode phase images of sample surfaces were made using NanoProbe tips PPP-NCL (Nanosensor) for PU88 with a frequency of 153.2 kHz. PU75 and PU60 were analyzed with a NanoProbe tip SSS-NCH (Nanosensor) at a frequency of 272 kHz.

□ 3D tomography

In the case of polymer/CNT nanocomposites, it may be necessary to have a 3D representation of the material to quantify the CNT dispersion state. Among the tomography techniques available, electron tomography can provide the appropriate resolution.

Electron tomography was first proposed in TEM microscopes and now, many tomography techniques allowing a nanometer resolution are available. One can cite electron tomography in TEM [26] or in SEM (in the transmission mode) [27], where the sample is tilted and images are acquired at different tilt angles. Then, the images have to be aligned and the volume reconstructed. Several algorithms are available or under development to compensate the presence of images at large tilt angles ("missing wedge"). Electron tomography can also be performed using slice-and-view methods. In this case, images of the sample surface are acquired, followed by successive removals of thin sections of the sample, using a Focused Ion Beam (FIB) [28'29], or with an ultramicrotome inside an SEM (serial-block face SEM) [30]. In that case, the images have to be aligned but no volume reconstruction is needed.

As far as polymer-based materials are concerned, Y. Liu [31] compared different tomography techniques, among which TEM tomography (in the STEM-HAADF mode or using Energy Filtered TEM), tilted tomography in SEM and FIB/SEM. He was faced with some issues related

to contraction (shrinking) of the polymer matrix. Two solutions were proposed (i) correction of images (which needs a heavy digital numerical processing), or (ii) optimization of the acquisition conditions (by working at lower temperatures or reducing the acceleration voltage of electrons, for example 80 kv). On polymer/CNT nanocomposites, a poor contrast between CNT and the polymer matrix was obtained in FIB/SEM. The quantification of the CNT dispersion state was difficult using tomography in TEM, because the segmentation step was hindered by the fact that the CNT wall structure was resolved. Tilted SEM tomography was found to be a good compromise. Indeed, by combining low-voltage SEM and STEM performances, 3D characterizations of material structures can be realized with a resolution level estimated to about few nm. Because of the low-vacuum mode, it is well suited for the study of non-conductive samples; it further offers a good contrast for low-atomic number materials, which can then be observed in relatively ‘thick’ states, up to several hundreds of nanometers. In the case of grid supported samples, the range of tilt angles (up to $\pm 90^\circ$) is only limited by the geometry of the grid. As a consequence in this work, we used tilted tomography in SEM to characterize the CNT dispersion state in the nanocomposites.

Tilted tomography in an Environmental SEM (ESEM) was named ‘tomo-STEM®’ [32]. The tomo-STEM developments took benefits from a previous work undertaken to observe liquids in the SEM, using the transmission imaging mode (so-called ‘wet-STEM’ [33]). With the home-made device shown in Fig. 16, a TEM grid supporting thin sample sections can be mounted and cooled by the Peltier stage, and projection images are acquired with an annular dark field (ADF) detector placed under the grid. This imaging mode allows the observation of wet samples or objects in a liquid phase in the transmission mode, in parallel with classical imaging with the usual SE and BSE detectors.

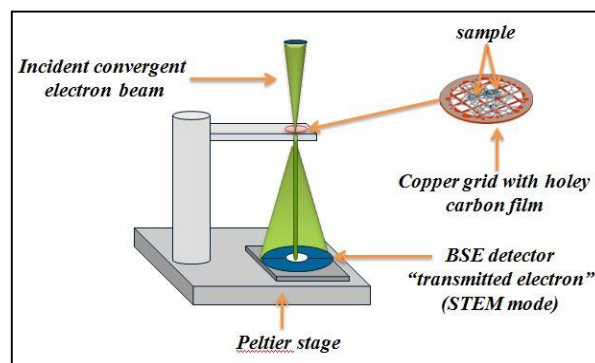


Fig. 16 Principles of the ‘wet-STEM’ device.

For tomography experiments, not only the transmission mode is needed but also the ability to tilt the sample in order to acquire projections at different angles. A dedicated device has thus been developed [32] and has been further developed [34]. It consists in 3 principal parts: a rotation generator; two translation generators to position the sample at the eucentric position; a detection system. The rotation system permits tilting the sample around a horizontal axis up to 360° with an accuracy of 0.001° . A TEM grid is maintained at the tip of the eucentric positioner, which allows the tilt axis to be adjusted in order to pass through the grid mean plane in order to keep the area of interest in the field of view while tilting (typical eucentric positioning). The detection of transmitted electrons is ensured as for the ‘wet-STEM’ imaging, an ADF detector being placed under the sample grid. The distance between the grid and the detector may be varied, which will modify the collection angles of the transmitted signals ($14\text{-}40^\circ$ in our case).

According to the similitude in geometry, this ‘tomo-STEM®’ technique can be considered as the low-voltage version of the STEM-HAADF mode in TEM.

However, it is significantly more complicated in terms of nature of collected electrons, since the wavelength of the primary beam, as well as the value of collection angles are very different from the case of STEM-HAADF in the TEM: thus, all types of electrons (elastic and inelastic) can be collected contrarily to the case of STEM-HAADF [35]. Because various types of electrons can be detected, contrasts can be exploited even for surprisingly large thicknesses (up to the micrometer range in favorable cases). This explains why conventional thin foils or ultramicrotomic sections adequate for TEM observations can easily be observed in this tomo-STEM technique. In our case, thin sections of a few hundreds of nm were prepared by cryo-ultramicrotomy, with a Ultracut Reichert S apparatus, equipped with a 35° diamond knife at 1 mm/s speed. The temperature of the sample was set to 200K. The thin sections were deposited onto 200-mesh TEM copper grids previously covered with holey carbon films. For an accurate alignment, gold nanoparticles of 15 nm in diameter were deposited onto the thin sections and used as fiducial markers. The acquisition of the tilt series was performed on a FEI XL-30 FEG ESEM microscope, operating at 30 kV. A water environment (3 Torr) was used to neutralize the charges in excess. The sample was cleaned with an Evactron system at the beginning of the experiment to avoid contamination, and the region of interest was irradiated during 10 minutes prior to the acquisition to stabilize its morphology and reduce shrinking due to irradiation damage during the acquisition of the tilt series. Images were then recorded in transmission from 66° to -66°, with a constant tilt step of 2°. After the tilt series acquisition an accurate alignment of the projections was performed using the Etomo software with Au nanoparticles as fiducial markers [36,37]. The volume reconstruction was performed with algebraic reconstruction technique (ART) [38] implemented in the Tomoj [39] plugin of ImageJ software, using 15 iterations. The volumes could be qualitatively analyzed slide by slide through visualizations at different depths and orientations. However, segmentation was necessary to get quantitative information. Segmentation was initially carried out combining Trainable Weka Segmentation, a plug-in in Fiji and 3D Slicer software (<http://www.slicer.org/>) [40] further used for advanced segmentation. It was necessary to confirm the artifacts were minimized as far as possible during the advanced segmentation, in order to sure a reliable quantification.

3.2 Electrical measurement

Dielectric spectroscopy (sometimes called impedance spectroscopy) consists in studying the frequency dependent complex dielectric permittivity of insulator materials. It is based on the interaction of an external electrical field with the dipole moment of the sample. In this thesis, dielectric spectroscopy has been used (i) to determine the dependence of the electrical behavior at room temperature of pure PU (with different weight fractions of HSs), (ii) to study their different relaxation phenomena (γ, β, α and conductivity relaxations) in a wide temperature-frequency range, and (iii) to optimize the copolymer composition in view of their best efficiency as actuators or energy harvesting devices. For nanocomposites, dielectric measurements were performed in order to highlight the effect of incorporation of CNT on the electrical permittivity and the effect of functionalization of CNT on the final conductivity of the nanocomposites. Further measurements were also performed in a wide range of frequencies and temperatures in

order to study the effect of the CNT volume fraction and the presence of the grafted layer on dielectric relaxation process.

Principles

The conductivity of a material is measured by the application of a sinusoidal tension of the form:

$$U = U_0 \sin(\omega t) \quad (1)$$

Resulting in a sinusoidal current I with a phase shift ϕ ,

$$I = I_0 \sin(\omega t + \phi) \quad (2)$$

Using low electrical fields (in the order of Volt/cm), the polarization and conductivities are proportional to the electrical field. The conductivity σ^* could be defined as the ratio between the current and the voltage in the sample and is a complex number,

$$\sigma^* = \frac{I}{U} \quad (3)$$

Thus, the real and imaginary parts of the conductivity are $\sigma' = |\sigma| \cos(\phi)$ and $\sigma'' = |\sigma| \sin(\phi)$. The ratio between the real and the imaginary parts of the conductivity, $\tan \delta = \frac{\sigma''}{\sigma'}$, represents the energy dissipated by Joule effect.

Dielectric spectroscopy in a homogeneous medium could permit the study of relaxations in the polymer. Furthermore, the evolution of the real and imaginary parts of the conductivity a low frequency in a blend insulant-conductor could be followed [41]. Three main domains could be defined, see Fig.17 :

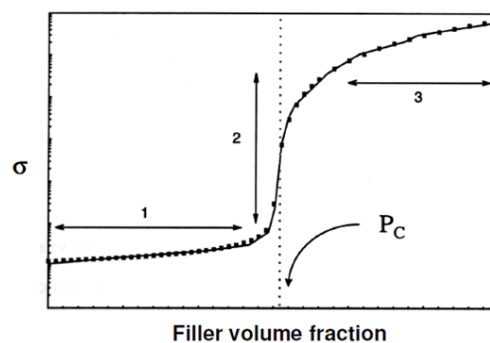


Fig. 17 shows the conductivity zones of a material

- (1) *Dielectric zone*. The composite behavior corresponds to an insulating material. The measured phase is near from 90° and the conductivity is almost the same as that of the matrix.
- (2) *Transition zone*. The conductivity suffers considerable variations due to the formation of a percolating network.
- (3) *Conductive zone*. This zone corresponds to the increment of the density of the conductor network.

Experimental Technique

In dielectric spectroscopy or AC impedance spectroscopy, the sample is placed between two parallel electrodes, constituting, hence, a capacitor. The sample is subjected to a sinusoidal

voltage V , at a variable frequency. The analyzer measures the current (intensity and phase) through the sample at each frequency. The complex impedance is calculated as a function of frequency. The impedance can then be separated into the frequency dependent conductivity and relative permittivity [42].

From the AC impedance spectroscopy performed at room temperature, the real and imaginary parts of the impedance (Z^*) can be obtained as a function of the frequency. The complex admittance ($Y^* = 1/Z^*$) of the nanocomposites can be modeled as a parallel resistor (R) and capacitor (C) and written as a function of angular frequency (ω)

$$Y^*(\omega) = Y' + jY'' = \frac{1}{R} + j\omega C \quad (4)$$

The specific AC conductivity of the nanocomposites as a function of frequency $\sigma(\omega)$ is calculated from the modulus of the complex admittance, and was used as a means of comparing the frequency behavior

$$Y(\omega) = |Y^*| \frac{d}{A} \quad (5)$$

where d is the sample length or distance between the electrodes, and A is the contact area. Values of AC conductivity can be determined from the real part of the complex admittance

$$\sigma = Y' \frac{d}{A} \quad (6)$$

A pure insulating behavior is indicated by a frequency-dependent increase in conductivity with a slope of unity on the log-log plot of specific conductivity against frequency. This behavior is typical of a dielectric material, which, for frequencies

$$f > \frac{\sigma_0}{2\pi \epsilon_0 \epsilon'} \quad (7)$$

gives a conductivity of

$$\sigma = 2\pi f \epsilon' \epsilon_0 \quad (8)$$

Where ϵ_0 is the permittivity of the vacuum and ϵ' is the real part of the dielectric constant.

A material permittivity is usually normalized to the permittivity of vacuum. The real part of permittivity, ϵ' , is a measure of the energy stored and is called the dielectric constant. The imaginary part of permittivity, ϵ'' , is a measure of the energy loss and called the loss factor. In addition, loss tangent is the imaginary part divided by the real part for a given frequency.

Many materials are a mixture of different sized molecules. The permittivity of these blends will depend on the interactions between these molecules, their masses, charges and charge distributions.

Experimental conditions

The dielectric properties of pure PU and PU filled with grafted or ungrafted CNTs were measured with a Modulab MTS at an AC voltage of 1 VRMS, over a frequency range of 10-1 to 106 Hz. Both surfaces of the film were coated with a gold electrode of 20 mm in diameter, deposited by sputtering (Cressington 208 HR). The real and imaginary parts of the dielectric permittivity ϵ^* and of the conductivity σ^* were obtained.. Isothermal measurements were

performed under liquid nitrogen using a cryostat (JANIS-STVP-200XG), in the temperature range 180 K to 380 K (for pure PU) and from 100 K to 400 K for nanocomposites. Dielectric relaxation, activation energy and characteristic relaxation time (τ) were determined for each relaxation process of each studied films.

3.3 Dynamic mechanical analysis

Principle

Dynamic Mechanical Analysis (DMA), also known as Dynamic Mechanical Spectroscopy, is a useful tool that permits the determination of the viscoelastic properties of the material. The test consists in applying a sine wave mechanical force to the sample in the linear domain (elastic or viscoelastic domain), and in measuring the response of the system in function of the temperature (isochronal measurements) or frequency (isothermal measurements). The sample undergoes a periodical stress,

$$\sigma = \sigma_0 \sin(\omega t) \quad (9)$$

Resulting in a sinusoidal deformation of the sample with a phase shift ϕ

$$\varepsilon = \varepsilon_0 \sin(\omega t + \phi) \quad (10)$$

The complex modulus G^* can be deduced from the ratio between the applied stress and the measured deformation ,

$$G^* = \sigma^*(i\omega) / \varepsilon^*(i\omega) = G' + iG'' \quad (11)$$

Where

$$G' = \frac{\sigma_0}{\varepsilon_0} \cos(\phi) \quad (12)$$

$$G'' = \frac{\sigma_0}{\varepsilon_0} \sin(\phi) \quad (13)$$

Furthermore, the loss factor between the stress and the deformation is defined as $\tan \delta = \frac{G''}{G'}$. This coefficient is also named internal friction coefficient and represents the proportion of the energy dissipated in the form of heat in the sample.

In homogeneous systems, the variations of the dynamic modulus as function of the temperature (or the frequency) corresponds to the relaxation phenomena characteristics of the polymer. These relaxations have their origin in the mobility of the polymer chains at the molecular scale and their molecular motions depend on the temperature and the characteristics of the polymer (as the molecular weight). In the case of polyphase systems, the mechanical behavior depends additionally of the domain sizes and the morphology [43].

Experimental conditions

The equipment used is a home-made device built, but also commercially available (Metravib SA). A schematic representation of the apparatus is given in Fig. 18. A magnet between two Helmholtz coils where an alternative current is injected creates the shear stress. The torque is transmitted to the sample by a metallic hard stick. The material strain is detected by a reflected laser diode and transmitted to the computer interface for calculation. The particularity of this

device lies in its ability to measure the complex mechanical modulus with a very high accuracy, for sample thicknesses ranging from 100 μm to few mm. All the measurements were carried out at 1Hz, using a heating rate of 3 K/min [44].

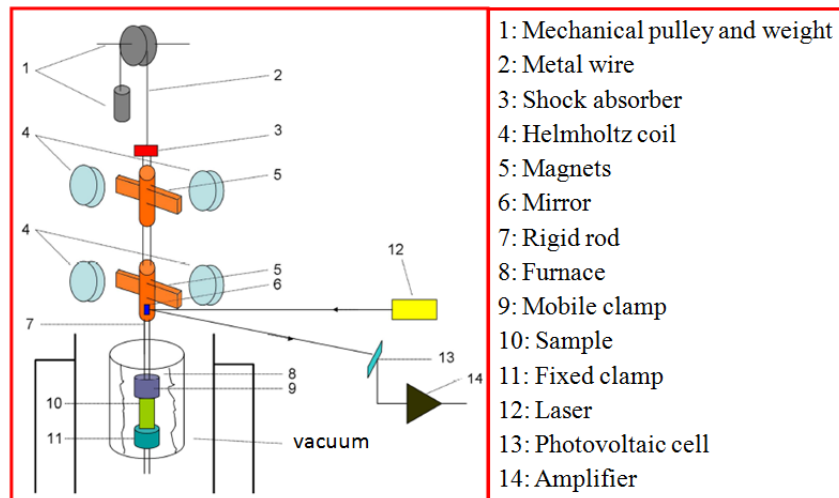


Fig. 18 Schematic representation of the Shear Dynamic Mechanical Analysis device used.

As the accuracy on the modulus measurement largely depends on the accuracy on the film thickness, additional mechanical characterizations were carried out. The Young modulus was measured at room temperature in tensile mode using a multifunctional dynamic mechanical analyzer, Eplexor from Gabo. The films of 100 μm of thickness were cut into 10 X 40 mm² rectangular specimens, which were fixed at both ends, thus leaving 20 mm long for the measurements. The tests were carried out with an elongation speed of 24 mm/min at room temperature under air.

3.4 Electromechanical

3.4.1 Electrostriction

The field-induced thickness strain S was measured on circular samples (25mm of diameter) with a homemade setup based on a double-beam laser interferometer measurement (Agilent 10889B) with a precision on the order of 10 nm [45]. Uncoated samples were placed between two circular electrodes of 20 mm in diameter (8.58 g). A mirror (0.75 g) was placed on the upper electrode to reflect the laser beam. A bipolar electric field was supplied by a function generator (Agilent 33250A) amplified by a factor of 1000 through a high-voltage lock-in amplifier (Trek10/10B) [10]. Measurements were made at room temperature on 100 μm -thick samples.

References

- [1] Legge, N. R, Holden, G. and Schroeder, H. E. Thermoplastic elastomers: A comprehensive review; Carl Hanser Verlag. British Polymer Journal. 1987. Volume 21, p 1881, 1989.
- [2] D. Coleman. Block copolymers: Copolymerization of ethylene terephthalate and polyoxyethylene glycols. Journal of Polymer Science. 1954. Vol 14, p 15–28.
- [3] Bayer, O, Muller, E. Petersen, S. Piepenbrink, H.F. and Windemuth, E. Angew. Chem. 1950,62, 57
- [4] Ronny Mathieu Versteegen. Well-defined Thermoplastic Elastomers. PhD Thesis 2003.
- [5] <http://www.essentialchemicalindustry.org/polymers/polyurethane.html>.
- [6] Hepburn, C, Polyurethane Elastomers. Elsevier Science Publishing Co, Inc, New York, 1982. 402.
- [7] Helfand, E. and Wasserman, Z.R. Developments in Block Copolymers – I Applied Science Publishers, New York, NY, 1982. pp.99.
- [8] Pascal PICHON. Fatigue thermomecanique des elastomers polyurethane: Caracterisations experimentale de l'evolution des microstructures et modelisations des echanges thermiques. PhD Thesis INSA Lyon 2010.
- [9] C. Putson, L. Lebrun, D. Guyomar, N. Muensit, P-J. Cottinet, L. Seveyart, and B. Guiffard. J.Appl. Phys. 2011. 109,024104.
- [10] K.Wongtimnoi, B. Guiffard, A. Bogner-Van de Moortèle, L. Seveyart, C. Gauthier, J-Y. Cavallé. Improvement of electrostrictive properties of a polyether-based polyurethane elastomer filled with conductive carbon black: Composites Sciences and Technology. 2011: 885-892
- [11] B. Guiffard, D.Guyomar, L. Seveyart, Y Chowanek, M Bechelany, D Cornu and P Miele. J.Phys. D: Appl. Phys. 2009. 42. 055503
- [12] K. Wongtimnoi, 'Polyuréthanes électrostrictifs et Nanocomposites: Caractérisation et Analyse des mécanismes de couplages électromécaniques', PhD Thesis, 2011, INSA-Lyon.
- [13] Koberstein J T, Russell T P. Simultaneous SAXS-DSC Study of Multiple Endothermic Behavior in Polyether-based Polyurethane Block Copolymers. Macromolecules. 1986; 19: 714-720.
- [14] K Kojio, S Nakashima, M Furukawa. Micorphase-separated structure and mechanical properties of norbornane diisocanate-based polyurethanes. J.polymer.2007;48: 997–1004
- [15] <http://www.cheaptubes.com/MWNTs.htm#multi>
- [16] Nanda Gopal Sahoo, Sravendra Rana, Jae Whan Cho, Lin Li, Siew . Polymer nanocomposites based on functionalized carbon nanotubes: Progress in Polymer Science. 2010. 35: 837–867
- [17] Jong-Hwan Jeon, Seung-Hwa Lee, Jung-Hyurk Lim and Kyung-Min Kim. Fabrication and characterization of homogeneous composites of polypropylene and multiwalled carbon nanotubes. Journal of Applied Polymer Science, 2012. Vol.124, 3064-3073
- [18]Jingwen WANG1,Tao CHEN1, Nan WEI1,Congcong WU,Shuqin..Enhanced Dielectric Response in Polyurethane Based All-organic Nanocomposite. Advanced Materials Research.2011,73-80
- [19] J. K. W. Sandler, J. E. Kirk, I. A. Kinloch, M. S. P. Shaffer and A. H. Windle Ultra-low electrical percolation threshold in carbon-nanotube-epoxy composites, Polymer. 2003 vol. 44: p. 5893-5899.
- [20] So Hyang Hwa, Cho Jae Whan, Sahoo Nanda Gopal. Effect of carbon nanotubes on mechanical and electrical properties of polyimide/carbon nanotubes nanocomposites. Eur Polym J 2007;43,3750–6
- [21] Yun Sungryul, Kim Jaehwan. Sonication time effect on MWNTs/PANI-EB composite for hybrid electro-active paper actuator. Synth Met 2007;157: 523–8.
- [22] Kabir Md E, Saha MC, Jeelani S. Effect of ultrasound sonication in carbon nanofibers/polyurethane foam composite. Mater Sci Eng A 2007;459: 111–6.
- [23] Kroschwitz, J.I., Polymers: Polymer characterization and analysis. Encyclopedia Reprint Series. 1990, New York: Wiley Intersciences. 957.
- [24]Goldstein, J., Newbury, D.E., Joy, D.C., Lyman, C.E., Echlin, P., Lifshin, E., Sawyer, L., Michael, J.R. Scanning Electron Microscopy and X-ray Microanalysis.2003.eBook ISBN 978-1-4615-0215-9
- [25] Ludwig Reimer. Scanning Electron Microscopy: Physics of Image Formation and Microanalysis. Springer Science & Business Media, 1998. ISBN 3540639764, 9783540639763
- [26] Koster A.J., Ziese U., Verkleij A.J., Janssen A.H., and de Jong K.P. Three-Dimensional Transmission Electron Microscopy: A Novel Imaging and Characterization Technique with Nanometer Scale Resolution for Materials Science. J. Phys. Chem. B. 2000, vol.104, pp: 9368–9370.

- [27] Friedrich H., McCartney M.R., and Buseck P.R. Comparison of intensity distributions in tomograms from BF TEM, ADF STEM, HAADF STEM, and calculated tilt series. *Ultramicroscopy*. 2005, vol.106, pp: 18–27.
- [28] Holzer L., Muench B., Wegmann M., Gasser P., and Flatt R.J. FIB-Nanotomography of Particulate Systems—Part I: Particle Shape and Topology of Interfaces. *Journal of the American Ceramic Society*. 2006, vol.89, pp: 2577–2585.
- [29] Kato M., Ito T., Aoyama Y., Sawa K., Kaneko T., Kawase N., and Jinnai H. Three-dimensional structural analysis of a block copolymer by scanning electron microscopy combined with a focused ion beam. *Journal of Polymer Science Part B: Polymer Physics*. 2007, vol.45, pp: 677–683.
- [30] Holzer L., Indutnyi F., Gasser P.H., Münch B., and Wegmann M. Three-dimensional analysis of porous BaTiO₃ ceramics using FIB nanotomography. *J Microsc*. 2004, vol.216, pp: 84–95.
- [31] Yang LIU. ‘Tri-3D’ electron microscopy tomography by FIB, SEM and TEM: Application to polymer nanocomposites. PhD Thesis INSA Lyon. 2013.
- [32] JORNANO, P., THOLLET, G., FERREIRA, J., MASENELLI-VARLOT, K., GAUTHIER, C. & BOGNER, A.. Electron tomography combining ESEM and STEM: A new 3D imaging technique. *Ultramicroscopy*. 2011 111, 1247–1254.
- [33] A. Bogner, G. Thollet, D. Basset, P.-H. Jouneau, C. Gauthier. Wet STEM: A new development in environmental SEM for imaging nano-objects included in a liquid phase. *Ultramicroscopy*. 2005, 104, 290-301
- [34] Karine Masenelli-Varlota¹, Annie Malchère, José Ferreira, Hamed Heidari Mezerji, Sara Bals, Cédric Messaoudi and Sergio Marco Garrido. Wet-STEM Tomography: Principles, Potentialities and Limitations. *Microscopy and Microanalysis*. 2014; Vol 20, pp 366-375.
- [35] BOGNER, A., THOLLET, G., BASSET, D., JOUNEAU, P.H. & GAUTHIER, C. Wet-STEM: A new development in environmental SEM for imaging nano-objects included in a liquid phase.
- [36] Kremer, J.R., Mastrorade, D.N., Mc Intosh, J.R. Computer visualization of three-dimensional image data using IMOD. *J Struct Biol*. 1996; 116, 71–76.
- [37] Maiorca M, Hanssen E, Kazmierczak E, Maco B, Kudryashev M, Hall R, Quiney H, Tilley L. Improving the quality of electron tomography image volumes using pre-reconstruction filtering. *J Struct Biol*. 2012 180 :132-42.
- [38] Gordon, R., Bender, R. & Herman, G.T. Algebraic Reconstruction Techniques (ART) for three-dimensional electron microscopy and X-ray photography *J Theor Biol A*. 1970, 29, 471–481.
- [39] Messaoudi, C., Boudier, T., Sorzano C.O.S. & Marco, S. TomoJ: tomography software for three-dimensional reconstruction in transmission electron microscopy. *CBMC Bioinformatics*. 2007. 8, 288.
- [40] Fedorov, A., Beichel, R., Kalpathy-Cramer, J., Finet, J., Fillion-Robin, J.-C., Pujol, S., Bauer, C., Jennings, D., Fennessy, F., Sonka, M., Buatti, J., Aylward, S.R., Miller, J.V., Pieper, S., Kikinis, R. *Magn Reson Imaging*. 2012. 30, 1323-41.
- [41] Flandin, L., Etude expérimentale et modélisation microstructurale de l'évolution des propriétés électriques d'un matériau composite en cours de déformation PhD Thesis. 1998.
- [42] Allaoui, A., S. Bai, H.M. Cheng, and J.B. Bai, Mechanical and electrical properties of a MWNT/epoxy composite. *Composites Science and Technology*, 2002. 62: p. 1993-1998.
- [43] Mariamne DEHONOR GOMEZ. Polystyrene grafting of CN_x nanotubes for the elaboration of polystyrene-based nanocomposites. PhD Thesis 2007. INSA Lyon.
- [44] Benjamin FRAGNEAUD. Synthesis and characterization of polymer/carbon nanotubes composites: Impact of polymer grafting on the surface of CN_x MWNTs on the electrical and mechanical properties of the nanocomposites. PhD Thesis 2006. INSA Lyon.
- [45] B. Guiffard, L.S., G. Sebald and D. Guyomar. Enhanced electric field induced strain in non speculative carbon nanopowder/ polyurethane nanocomposites. *J. of Phys. D: Appl. Phys.* 2006.39, 3053
- [46] P.-J. Cottinet, D. Guyomar, B. Guiffard, C. Putson, and L. Lebrun, *IEEE Trans. Ultrason. Ferroelectr. Freq. Control*. 2010, 57, 774.
- [47] F. Belhora, P.-J. Cottinet, A. Hajjaji, D. Guyomar, M. Mazroui, L. Lebrun, Y. Boughaleb. Mechano-electrical conversion for harvesting energy with hybridization of electrostrictive polymers and electrets *Sensors and Actuators A*. 2013, 201, 58-65

Part III: study of pure Polyurethanes

Introduction

This part is dedicated to the study of pure PU. We will investigate the relationships between its microstructure and electrical, mechanical and electrostrictive properties. For that purpose, three pure segmented PUs were chosen, with different weight fractions of hard segments.

The first paper [1] deals with the dielectric properties of the 3 PUs. Three relaxation phenomena (β , α and conduction) will be investigated for each PU in the temperature-frequency range studied here. In the second paper [2], we will present the viscoelastic response (as measured through mechanical spectrometry) of the same polyurethanes and their respective time dependence electrostriction response. The objective of this work will be to study the response to a step function and/or the frequency dependence of electrical to mechanical energy conversion.

Moreover, it is well documented that the properties and the performances of pure polyurethanes are strongly dependent on the degree of microphase separation and on the ensuing morphologies. As a consequence in the third paper [3], a model taking account the PU nanostructure will be presented. In order to validate this model, three PUs of similar compositions but different soft segment fractions will be characterized by DSC, TEM, AFM and SAXS and their electrostriction properties will be measured. The purpose of this work will be to investigate how the recent model can explain the electrostriction properties of segmented pure PUs.

At the end of this part, the choice of the more suitable PU for actuation properties will be discussed on the basis of specific requirements for actuation, and in terms of large stability of electrostriction, electrical and mechanical behaviour temperatures.

[1] M.H. Jomaa *et al.*, Polymer 63 (2015), 214-221.

[2] manuscript to be submitted

[3] M.H. Jomaa *et al.*, Polymer 62 (2015), 139-147.

Chapter 3: Dielectric properties of segmented polyurethanes for electromechanical applications

M. H. Jomaa^{1,2*}, L. Seveyrat², L. Lebrun², K. Masenelli-Varlot¹, J.Y. Cavaille¹.

¹ Université de Lyon, INSA-Lyon, CNRS, MATEIS, 69621 Villeurbanne Cedex

² Laboratory of Electrical Engineering and Ferroelectricity, LGEF INSA Lyon EA682, Université de Lyon, F-69621 Villeurbanne Cedex, France

*Author to whom all correspondence should be addressed

Abstract

The paper deals with electromechanical and dielectric properties of polyurethanes (PU) block-copolymers. Most of the works published in the literature only consider electrostriction at room temperature at a given frequency. In this work, it is shown that electrostrictive coefficient M_E is divided by 3 to 10 at increasing frequency over 3 decades of frequency, depending on the ratio of hard to soft segments in PU. Thus it is important to analyze the energy conversion efficiency by investigating the dielectric and viscoelastic properties. This work deals with the study of dielectric properties of 3 PU with different fractions of hard segments. Three relaxation phenomena (β , α and conduction) were investigated for each PU in the temperature-frequency range studied here, in order to optimize the copolymer composition in view of their best efficiency as actuators or mechanical energy harvesting devices.

Keywords: EAP, Electrostriction, Hard and soft segment, Dielectric relaxation

1 Introduction

Electroactive polymers are one of the most promising technologies. Compared to inorganic materials, these versatile polymers have various attractive properties, such as being lightweight, inexpensive and easy to manufacture into any desirable shape. Tremendous amounts of research and development have led to Electroactive Polymers (EAP) that can change in size or shape when stimulated by an external electrical field, meaning they can convert electrical energy into mechanical energy [1]. Among the various EAPs, polyurethane (PU) elastomers are of great interest due to the significant electrical-field strains [2, 3, 4], and due to their attractive and useful properties, such as abrasion resistance, high mechanical strength and biocompatibility with blood and tissues [5]. The PU elastomers studied here are block copolymers of soft and hard segments (SS and HS). In this study, the hard segments (HS) are composed of 4,4' methylene bis (phenyl isocyanate) (MDI) and 1,4-butanediol (BDO), whereas poly(tetramethylene oxide) is employed as soft segments (SS). It is worthy to notice that HS

and SS are not miscible, and during the process, a partial phase separation occurs leading to the formation of soft domains (SD) rich in SS and hard domains (HD) poor in SS. This phase separation is limited because of the relatively low molecular weight of SS and HS blocks which prevents the entropy of mixing to decrease too much [6,7]. Furthermore, a slight crystallization can grow inside SD and HD. All of these parameters, namely the crystallinity ratio, the SD and HD topology, composition and concentration influence properties such as hardness, stiffness, and tensile strength [8]. It is well documented that the properties and the performances of polyurethanes are strongly dependent on the degree of microphase separation and on the ensuing morphologies [9, 10, 11, 12]. The objective of this present study is to highlight the strain thickness frequency dependence and to investigate the effect of the chemical composition through the HS content on the dielectric behavior of three different pure segmented PU, where the weight fraction of HS is varied. In order to achieve our goal, dielectric spectroscopy measurements were performed in a wide range of temperature and frequencies.

2 Materials and methods

The studied polymers are polyether-based thermoplastic polyurethanes. They are co-block polymers with two major blocks: HS and SS. HS are composed of 4,4' methylene bis (phenyl isocyanate) (MDI) and 1,4-butanediol (BDO). Poly (tetramethylene oxide) (PTMO) is used as SS. The structure of PU is presented in Fig 1.

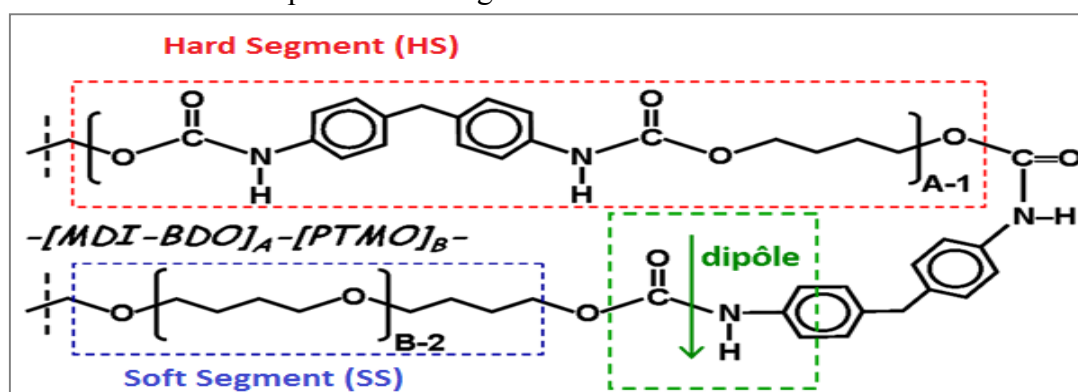


Fig 1 Structure Structure of the polyurethane consisting of MDI-BDO hard segments and PTMO soft segments [13].

The three different types of PU are commercially available and provided by the same company Lubrizol. They are synthesized by the same industrial process from the same initial chemical components. They differ in their weight fractions of HS: 26% for PU 75 (Estane X-4977), 45% for PU88 (Estane 58888 NAT021) and 65% for PU60 (Estane ETE60DT3 NAT022), and in different molecular weights of PTMO SS; 1000 g/mol for PU88, PU60 and 2000 g/mol for PU75.

The SS originate from the polyol and are responsible for the elastomeric behaviour of the polymeric material; the HS contain highly polar urethane linkages and it is thought [14, 15, 16,17] that due to phase separation they form highly polar and stiff microdomains embedded in a soft poorly polar matrix. Essentially, the morphology of the segmented polyurethanes depends on the relative amount of the soft and hard segments and on other physical phenomena such as crystallization and hydrogen bonds formation between the two types of segments.

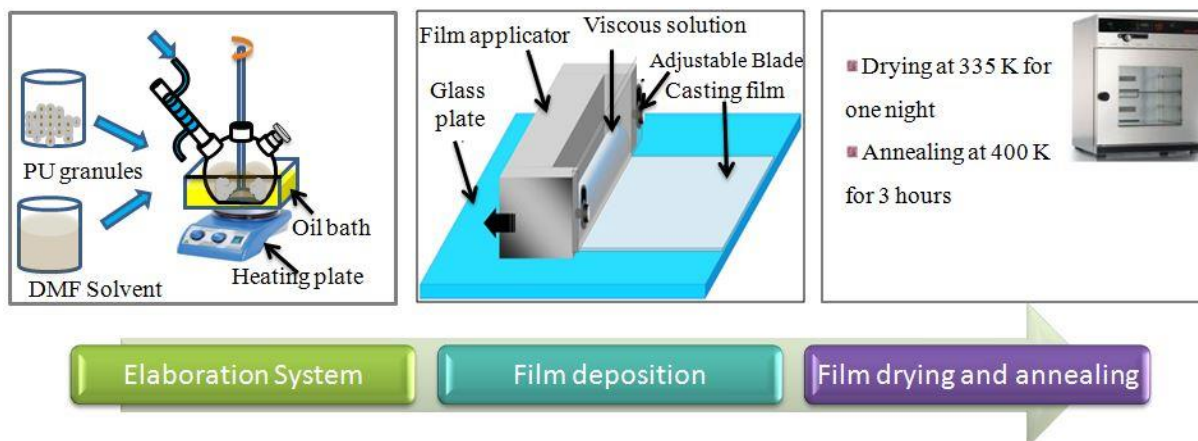


Fig 2 Elaboration protocol of polyurethanes polymers..

The polymer films were prepared by solution casting. The elaboration process steps are described in the Fig 2. Before use, PU granules were heated at 350 K for 3 hours. Then they were dissolved in N,N-dimethylformamide (DMF, Sigma-Aldrich D158550, 99%) with a ratio of 25% weight of PU into DMF. The solution was heated at 350 K for 4 hours under mechanical agitation, until a homogeneous solution was obtained. This operation was carried out in a closed device, to avoid evaporation of the DMF solvent and ensure good reproducibility of films.

The solution was then kept overnight to remove air bubbles. Afterwards, this solution was cast on glass plates with an Elcometer 3700 doctor blade film applicator Fig 2, put in an oven at 335 K for one day, and then removed from the glass. A second heating treatment at a temperature below the HS melting temperature was performed in order to eliminate the residual solvent. The thickness of the films was 100 μm after drying.

Glass transition and melting temperatures were determined with Differential Scanning Calorimetry (Setaram, DSC 131 Evo) under nitrogen flow ($P = 1.5$ bar). Samples of 20 mg were cooled by liquid nitrogen to 140 K and then heated to 480 K before being cooled to room temperature. The heating and cooling rates were set at 10 K / min.

The field-induced thickness strain S was measured on circular samples (25mm of diameter) with a homemade setup based on a double-beam laser interferometer measurement (Agilent 10889B) [4]. Samples were placed between two cylindrical brass mass acting as conductive electrodes. A mirror was placed on the upper electrode to reflect the laser beam. A bipolar electric field was supplied by a high voltage amplifier (Trek10/10B) driven with a function generator (Agilent 33250A). Measurements were made at room temperature on samples of 100 μm of thickness.

The dielectric properties of these films were measured with a Modulab MTS at an AC voltage of 1 VRMS, over a frequency range of 10^{-1} to 10^5 Hz. Both surfaces of the film -of 100 μm of thickness- were coated with a gold electrode of 20 mm in diameter, deposited by sputtering (Cressington 208 HR). The real and imaginary parts of the dielectric permittivity ϵ^* and of the conductivity σ^* were obtained. The complex dielectric modulus, $M^* = \frac{1}{\epsilon^*}$ was also determined as explained below. Isothermal measurements were performed under liquid nitrogen using a cryostat (JANIS-STVP-200XG), in the temperature range 180 K to 380 K. Dielectric relaxation, activation energy and characteristic relaxation time (τ) were determined for each relaxation process of each PU.

3 Results and discussion

3.1 Main physical properties of 3 PU

The properties of the three types of PU are summarized in Table. 1. The glass transition temperature T_{gSD} of the SD - microphase - increases by increasing the weight fraction of HS, which confirms the partial miscibility of HS and SS. The melting temperatures T_m of HD are almost the same for the three PU. From the literature, they are related to the micro-mixing of non-crystalline semi-crystalline hard and soft phases followed by the fusion of crystalline HS [18,19]. The enthalpy related to these endothermal phenomena increases with the HS amount, which indicates an enhanced crystallinity. Indeed, Liff *et al.* [20] confirm that the crystallinity and crystallite perfection increases with HS content due to the perfection of microphase separation between HS and SS. Furthermore Nakamae *et al.* [21] show that an increase of ΔH_m of HS must amplify a crystalline morphology within the HS microdomains, which accounts for the HS strengthening and the enhancement in melting endotherm intensity [21].

Table. 1 Main physical properties of three studied polyurethanes.

	Composition	HS	Density	T_{gSD}	T_m	ΔH_m
	MDI/BDO-PTMO	%wt	(g/cm ³)	(K)	(K)	(J/g)
PU75	PTMO2000	26	1.07	209	430-452	5.13
PU88	PTMO1000	45	1.13	228	420-444	10.13
PU60	PTMO1000	65	1.17	253	422-455	16.11

3.2 Electrostriction properties

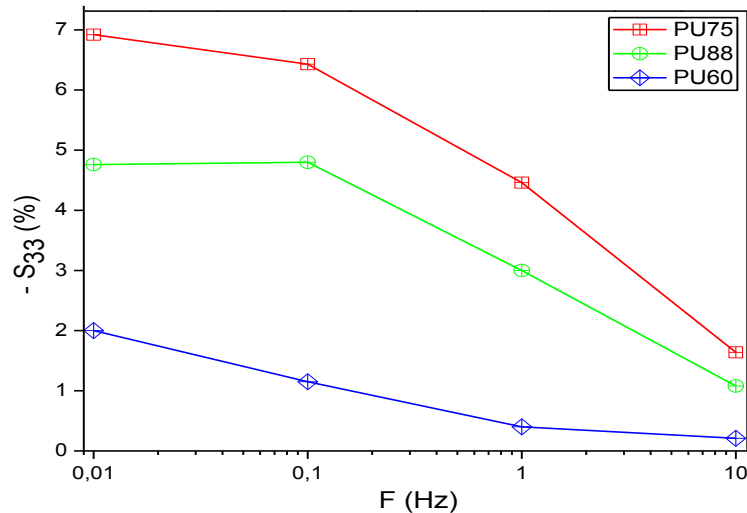


Fig 3 Variation of the strain thickness at 2 V/ μ m of 3 PU versus frequency.

Fig 3 depicts the variations of the strain thickness at 2 V/ μ m of the 3 PU versus frequency. Experimental S_{33} values decreases when the frequency is increased. Diaconu *et al.* reported that the thickness strain decreases when the relaxation time is decreased. Moreover the relaxation time also influences on the electrostrictive polymers behavior [22]. Guillot *et al.* [11] have demonstrated that the electrostriction coefficient of PU should decrease when the frequency is increased. Furthermore, Putson *et al.* confirmed that an increase of frequency- for

example from 0.1 Hz to 1 KHz- induces a decrease by a factor of 100 the electrostrictive coefficient [23]. The dielectric constant ϵ of polyurethane is known to decrease when the frequency is increased because of the decrease of the interfacial Wagner polarization contribution, which exists in all heterogeneous dielectric materials, including multiphase polyurethane [24]. On the contrary, the Young's modulus is known to increase as a function of frequency because large translational motions are restricted and because relaxation processes can occur when the frequency is increased.

The latter result confirms that the applied frequencies play an interesting role on the electromechanical properties of PU. In addition the frequency can limit the application range of PU polymer as an actuator. On one hand, by decreasing the frequency, the ionic conductivity increases, which can be attributed to charge displacements (which corresponds to dielectric losses). On the other hand by increasing the applied frequency, the Young modulus and the mechanical loss increase as a result of viscoelastic relaxation of PU. Thus, studying the dielectric and viscoelastic properties including relaxation phenomena in a wide range of frequencies and temperatures is necessary to optimize the conditions- applied frequency and temperature- for the use of PU as actuator.

3.3 Dielectric properties of 3PU

3.3.1 Isochronal study

Fig 4 presents the real and imaginary parts of dielectric permittivity and the real and imaginary parts of dielectric modulus M^* at 0.1 Hz and at 1 kHz versus temperature from 180 K to 380 K. As $M^* = \frac{1}{\epsilon^*}$, the real dielectric modulus M' and the dielectric loss modulus M'' can be deduced by the following relations

$$\begin{aligned} M' &= \frac{\epsilon'}{(\epsilon'^2 + \epsilon''^2)} \\ M'' &= \frac{\epsilon''}{(\epsilon'^2 + \epsilon''^2)} \end{aligned} \quad (1)$$

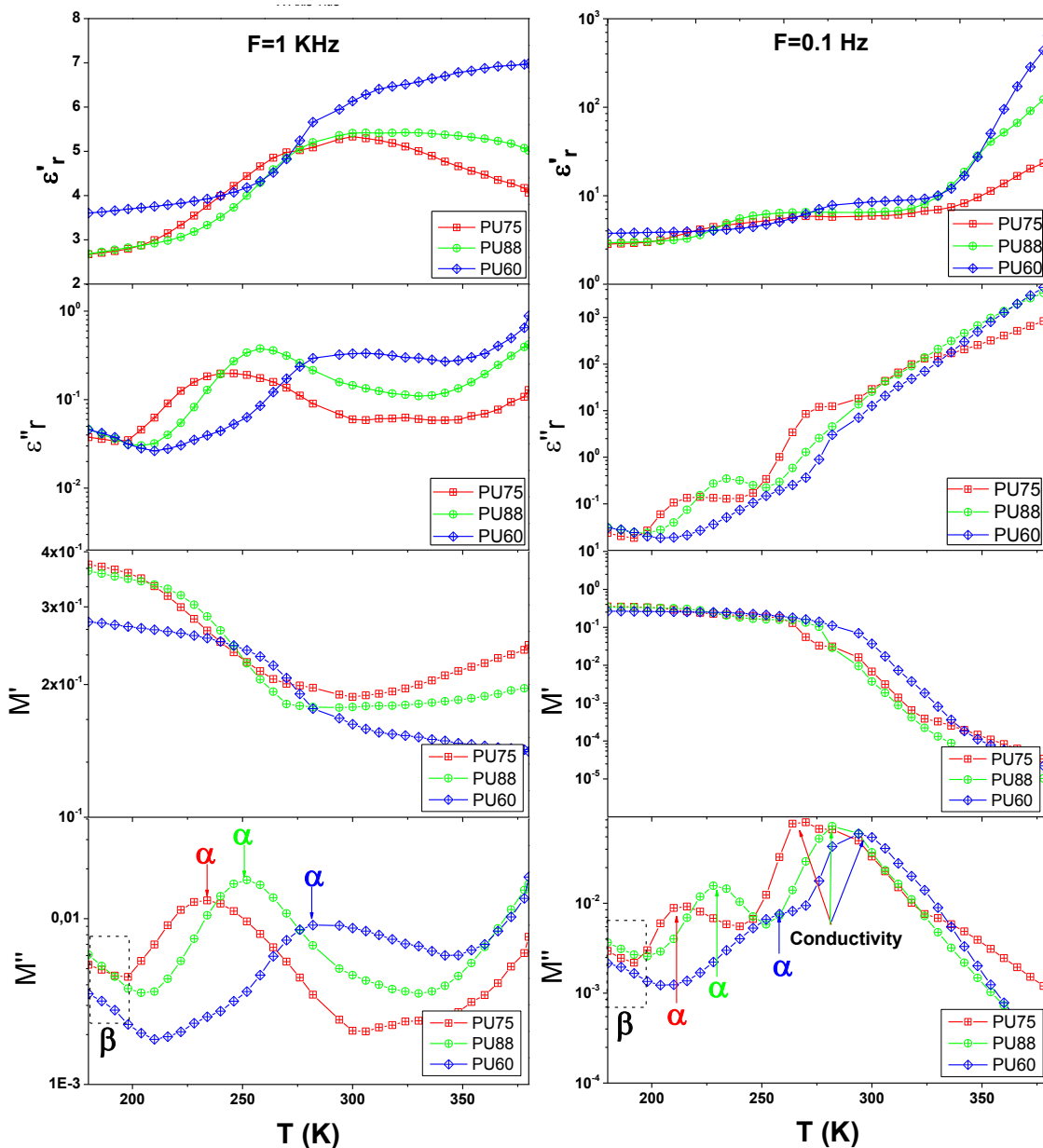


Fig 4 Evolution of the real and imaginary parts of the dielectric permittivity and the real and imaginary parts of dielectric modulus versus temperature for the 3 PU at 1 kHz (left) and 0.1 Hz (right).

As frequently observed on polymers [25], the dielectric permittivity starts to increase just above T_g (see Fig 4). Indeed as the temperature increases, the intermolecular forces between polymer chains are easier to break and the polar groups are freer to move. This behavior corresponds to the α -relaxation. At temperatures higher than 330 K and depending on the type of polyurethane, the real component of the permittivity ϵ' remains constant or starts to decrease due to strong thermal motion which disturbs the dipole orientation [25]. Such permittivity decrease is mainly observed on PU75. The evolution of ϵ' between 300 and 350 K shows that PU88 is the most stable upon the 3 types of PU.

The evolution of ϵ'' versus temperature shows the dielectric relaxations which are highlighted by ϵ'' maxima. One important relaxation seen in Fig 4 is the α relaxation associated with the

motion of the SD microphase [26, 27]. Moreover, a slight increase of ε'' can be observed slightly above 190 K, which is probably related to β -relaxation, as it will be shown in the next section. For the temperature range used here, these relaxations need to be observed at much lower frequencies. These relaxations could be related to the local motion of polymer segments [25, 28, 29, 30]. At higher temperatures, the strong increase of the imaginary dielectric permittivity is related to the Maxwell Wagner Sillars (MWS) interfacial polarization due to accumulation of charges at the interfaces [29, 31]. It corresponds to the ionic conductivity which appears at high temperature - low frequency and which will be discussed later. At 1 kHz, the real part of the dielectric modulus M' decreases in the range of temperatures where it is observed a maximum of M'' , after M' is almost constant. At 0.1 Hz there is an abrupt decrease of M' showing that the conductivity is the predominant phenomenon.

The examination of loss modulus M'' presented in Fig 4 allowed the observation of three relaxation mechanisms especially at high temperature and high frequency range. The main advantage of using the complex modulus, M^* , rather than ε^* is that the electrode polarization effect can be better separated from the α -relaxation and it is a very important and convenient way to analyze and interpret the dielectric relaxation of polymeric materials [32].

3.3.2 Isothermal Study

In order to analyze the relaxation processes of the 3 PU, additional measurements were performed over a wide range of temperatures and frequencies. Relaxation spectra are presented as isothermal curves, which display the variation of the imaginary part of M'' in function of the frequency. Fig 5, 6 and 7 shows the logarithm of the dielectric loss modulus M'' in the function of the frequency and the temperature for PU75, PU88 and PU60, respectively. For sake of clarity, isothermal M'' data of the 3 PU are presented each time in two different figures: one for high temperatures (270 K to 380 K) and the other one for low temperatures (180 K to 264 K). In the high temperature range, M'' reaches very high values which makes difficult the analysis of the relaxation phenomena around and below T_g .

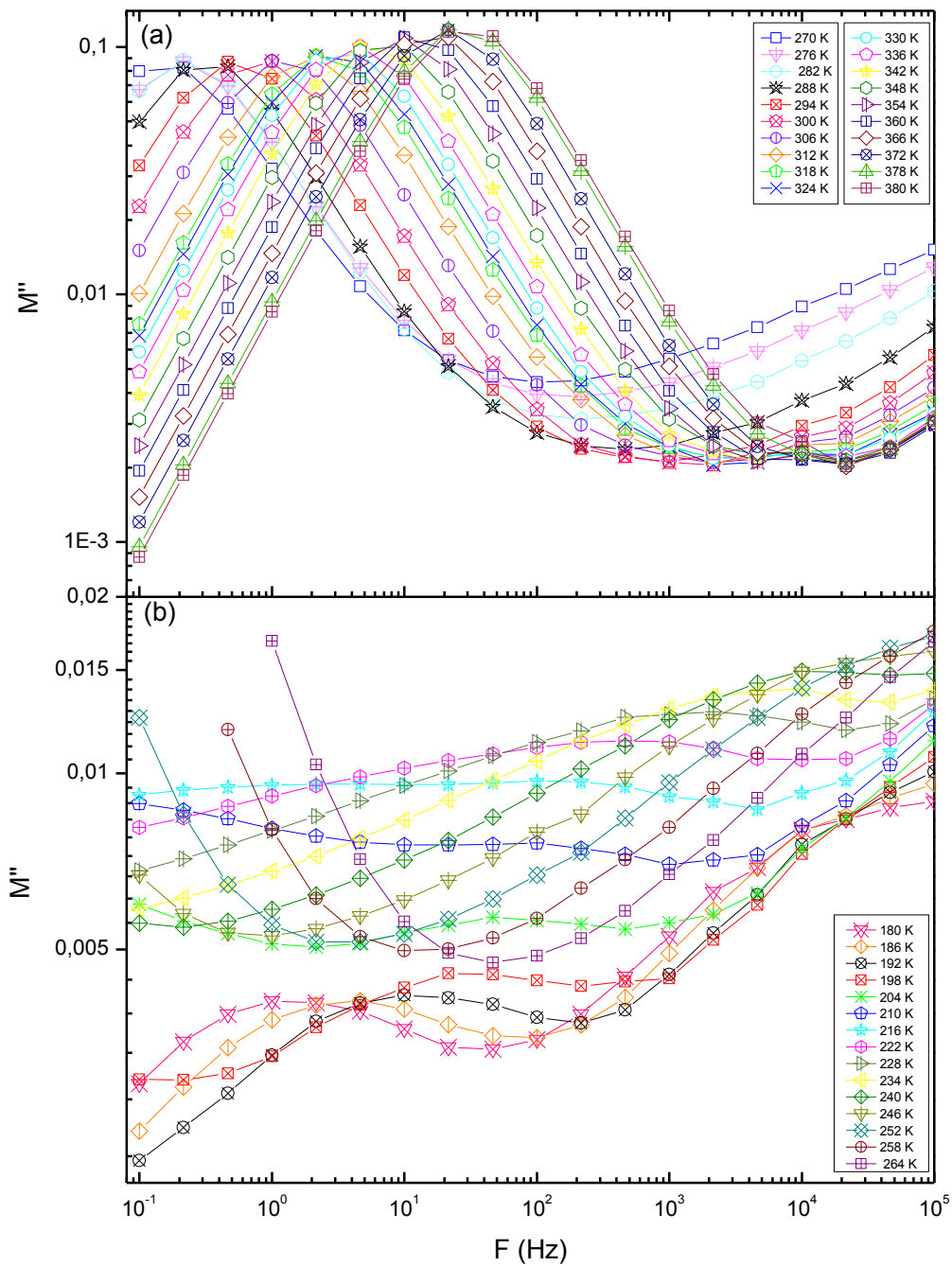


Fig 5 Electric loss modulus M'' of PU75 versus frequency and temperature; (a) from 270 K to 380 K, (b) from 180 K to 264 K.

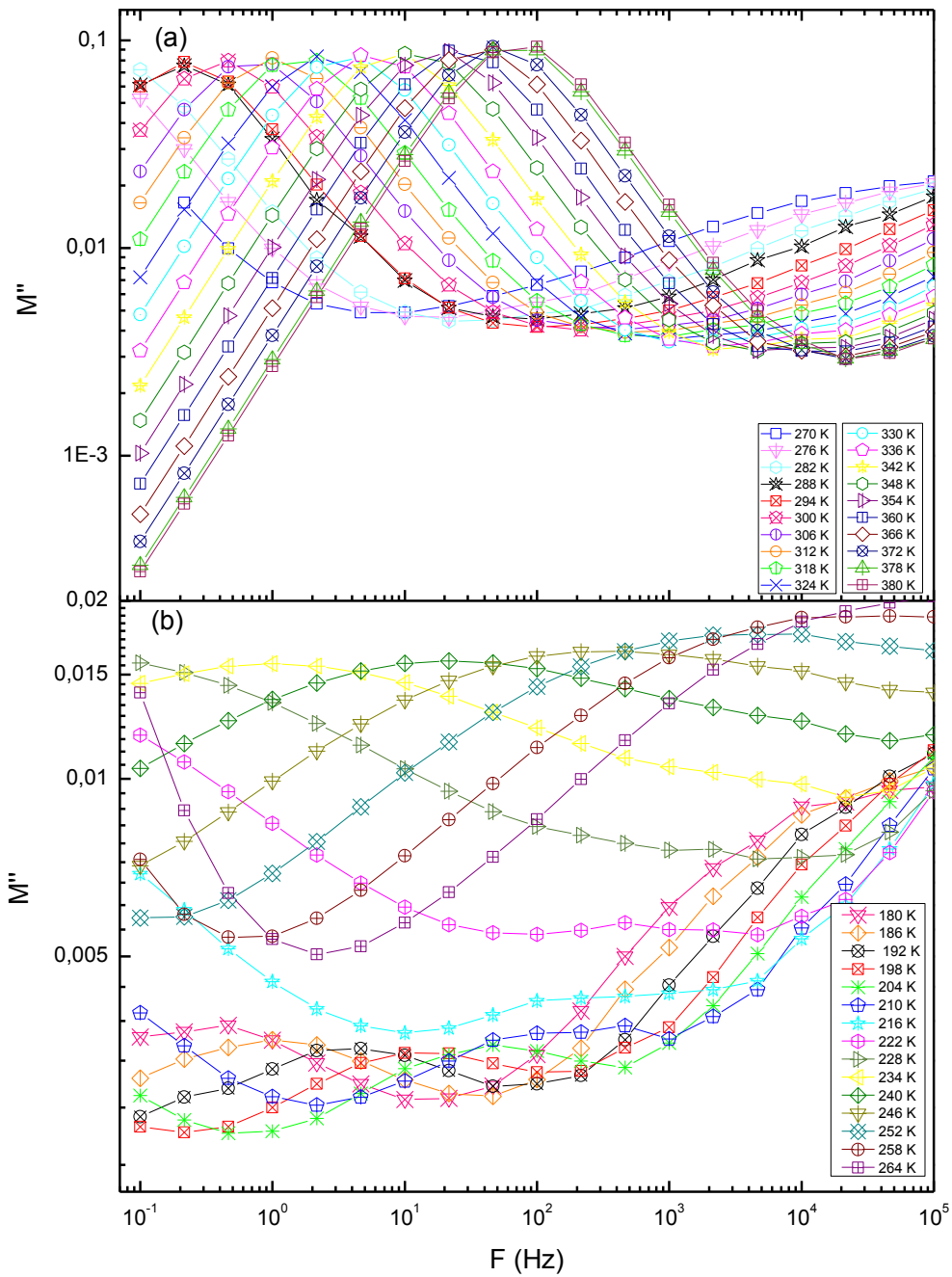


Fig 6 Electric loss modulus M'' of PU88 versus frequency and temperature; (a) from 270 K to 380 K, (b) from 180 K to 264 K.

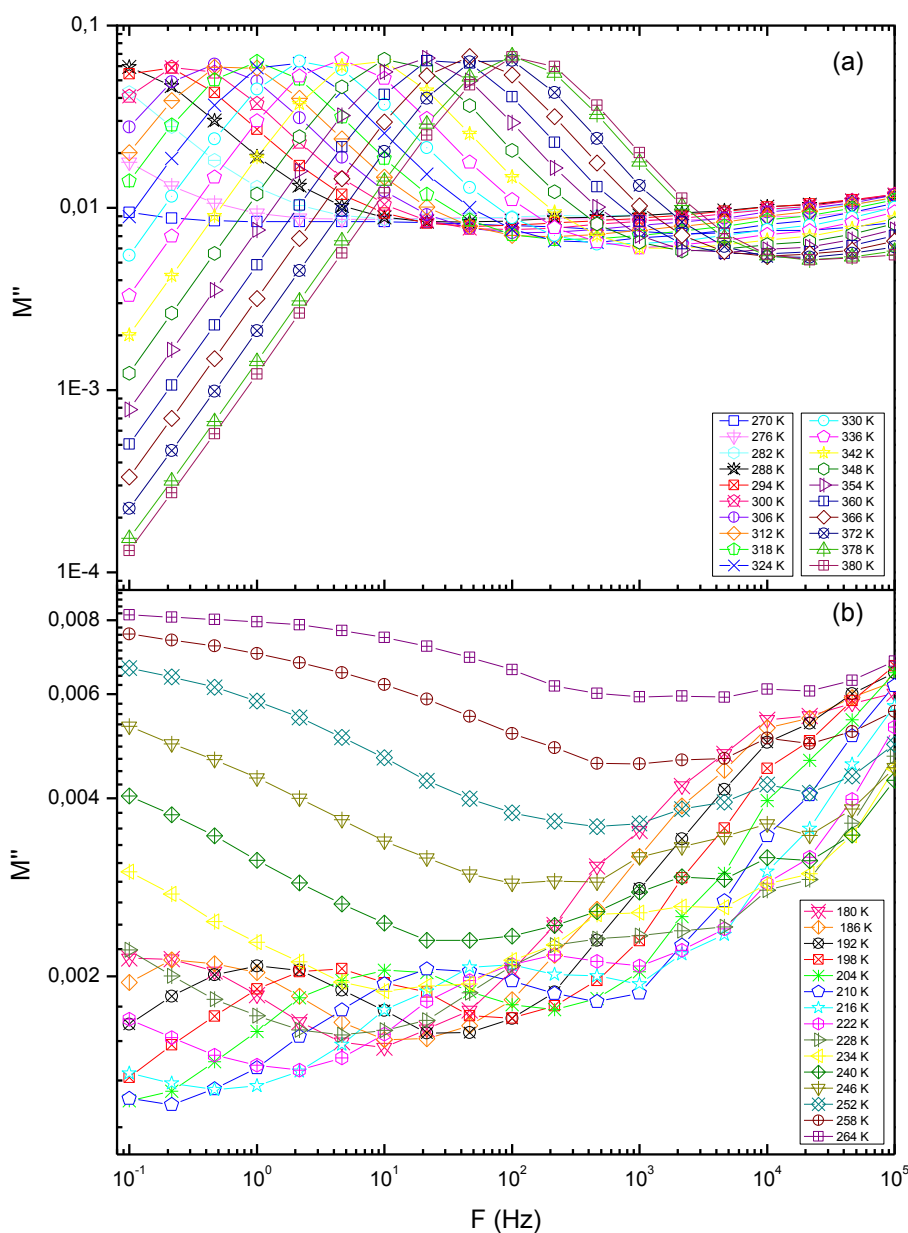


Fig 7 Electric loss modulus M'' of PU60 versus frequency and temperature; (a) from 270 K to 380 K, (b) from 180 K to 264 K.

Again, three relaxation processes can be observed for the three investigated polymers. At low temperature and/or low frequency, a β -relaxation with very small amplitude can be seen (Fig 5, 6, 7 (b)). In the temperature-frequency range used here, the γ -relaxation is not visible. It is related to the local motion of $(CH_2)_n$ [25, 29], and occurs at temperatures lower than the β -relaxation. Figures 5, 6 and 7 highlight the β -relaxation. The β -relaxation has been attributed in the literature to the motion of the polymer chain segments with attached water molecules [28, 29, 30]. It is present in many water-containing systems, and even if the PU are dried before

measurements, some residual water may remain because of strong interactions between HS segments or SS segments and water [32]. The β relaxations are similar for the three PU. At higher temperatures (or lower frequencies) the β -relaxation mechanism is hidden by the beginning of the α -relaxation of SD [32], and further by the high electrical conductivity.

The α -relaxation appears in the temperature range of 204 to 264 K only at high frequencies (1 to 10^5 Hz) for the 3PU, and has a larger amplitude than the β -relaxation as seen in Fig 5 b, 6b, 7b. This relaxation corresponds to a longer scale segmental motion, and is associated with the glass transition [26, 27]. As for T_g , the α -relaxation shifts to higher temperatures with increasing HS amounts. For PU60 the α -relaxation cannot be easily analyzed because it is superimposed to the conductivity effect, which is especially large in that case, as discussed below.

A third very strong relaxation process starts at 270 K at low frequency Fig 5a, 6a, and 7a. This phenomenon is very sensitive to frequency and shifts to higher frequencies when increasing the temperature. It corresponds to high values of the DC conductivity. Karabanova *et al* discussed such high values of the dielectric loss M'' at low frequencies and high temperatures [26, 33]. This relaxation phenomenon is attributed to the existence of ionic polarization in polyurethane network due to "free" charge motion within the material.

For the different relaxation processes, using $M''(T,f)$ data, and more precisely the frequencies f_M at which M'' passes through a maximum, it is easy to determine the so-called relaxation time $\tau = 1/2\pi f_M$ and to get a set of $\tau(T)$. It is usual to plot $\log(\tau)$ versus $1/T$ (in a so-called Arrhenius plot), and to determine the equation of the corresponding curve. If the curve is a straight line, then the relaxation time follows the Arrhenius equation:

$$\tau = \tau_0 \cdot \exp \frac{E}{k_B T} \quad (2)$$

Where τ_0 is the pre-exponential time, k_B the Boltzmann constant and E the activation energy. For the cooperative α -relaxation, the temperature dependence of τ is often described by the Vogel-Tammann-Fulcher (VTF) equation

$$\tau = \tau_0 \cdot \exp \frac{B}{(T-T_0)} \quad (3)$$

Where τ_0 is the pre-exponential time, B is an activation parameter and T_0 is the ideal glass transition temperature (or the Vogel temperature) [26, 33], (T_0 being 40 K lower than T_g) [33].

Fig. 8 shows semi-logarithmic plot of τ against reciprocal temperature, $1/T$, for the 3 PU. The curves are the fits of equations (2) and (3) for the β and α relaxations respectively. The experimental points are also included in the plots.

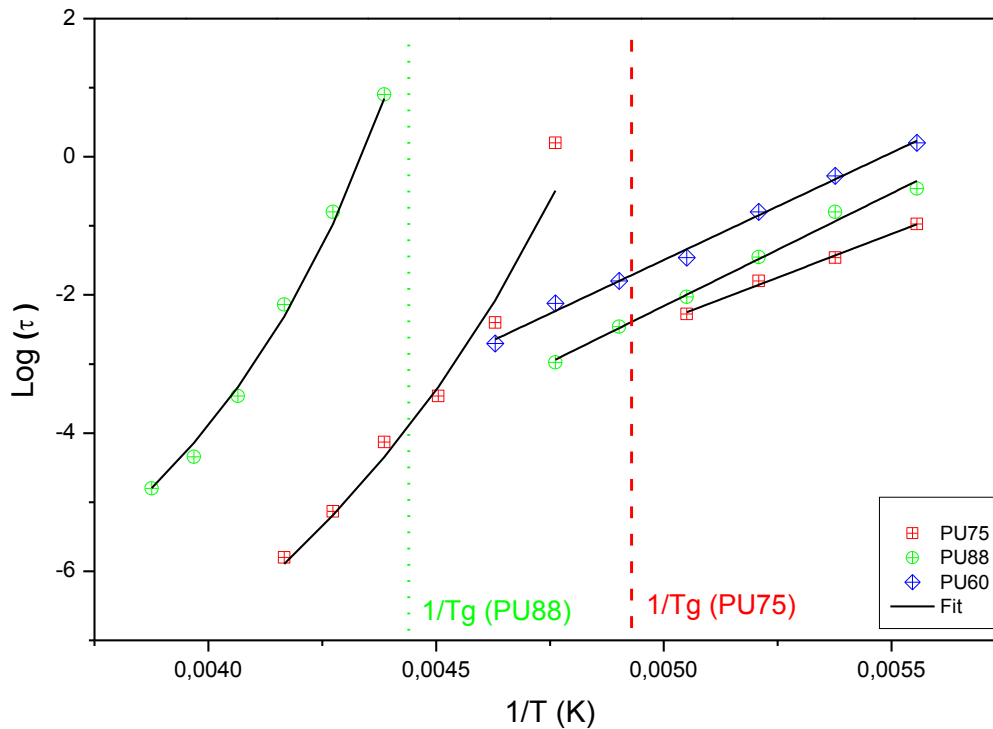


Fig 8 $\log(\tau)$ versus $1/T$ for α and β relaxations for the 3 PU.

The results of the fitting procedure are listed in Table. 2.

Table. 2 Parameters of Arrhenius equation (equation (2)) for the β -relaxation, and of VTF equation for the α -relaxation (VTF equation, equation (3)). The parameters related to the α -relaxation could not be measured on PU60 because of the large conductivity.

		PU75	PU88	PU60
β-relaxation	E (kJ/mol)	49	63	60
	τ_0 (S)	10^{-15}	10^{-18}	10^{-17}
α-relaxation	B (K)	1400	900	N.D.
	T_0 (K)	165	195	N.D.
	τ_0 (s)	10^{-15}	10^{-12}	N.D.

The β relaxation is described by practically the same parameters E and τ_0 for the three materials. The relaxation times of the β -processes are not significantly affected by the HS content and the values of the activation energies are similar to other reported values [34].

For the α -relaxation, it is striking that the VTF parameters are different for sample PU75 compared with PU88. The results indicate that the cooperative primary α process is more sensitive to morphology changes than the local secondary β process [26].

The fitting parameters have reasonable values for all three samples, e.g. for T_0 is 165 K for PU75 and 195 K for PU88 Table 2, in reasonable agreement with T_0 being about 40 K lower than T_g [26, 34].

T_g can be estimated from the segmental relaxation by extrapolation of the VTF fit to $\tau = 100$ s. T_g equals to 207 K and 226 K for PU75 and PU88 respectively. These values are in good agreement with experimental data obtained by DSC measurement (see Table 1).

3.3.3 Conductivity

Fig. 9 displays the evolution of the real part of conductivity of the 3PU in function of the frequency, for temperature ranging from 270 K to 378 K.

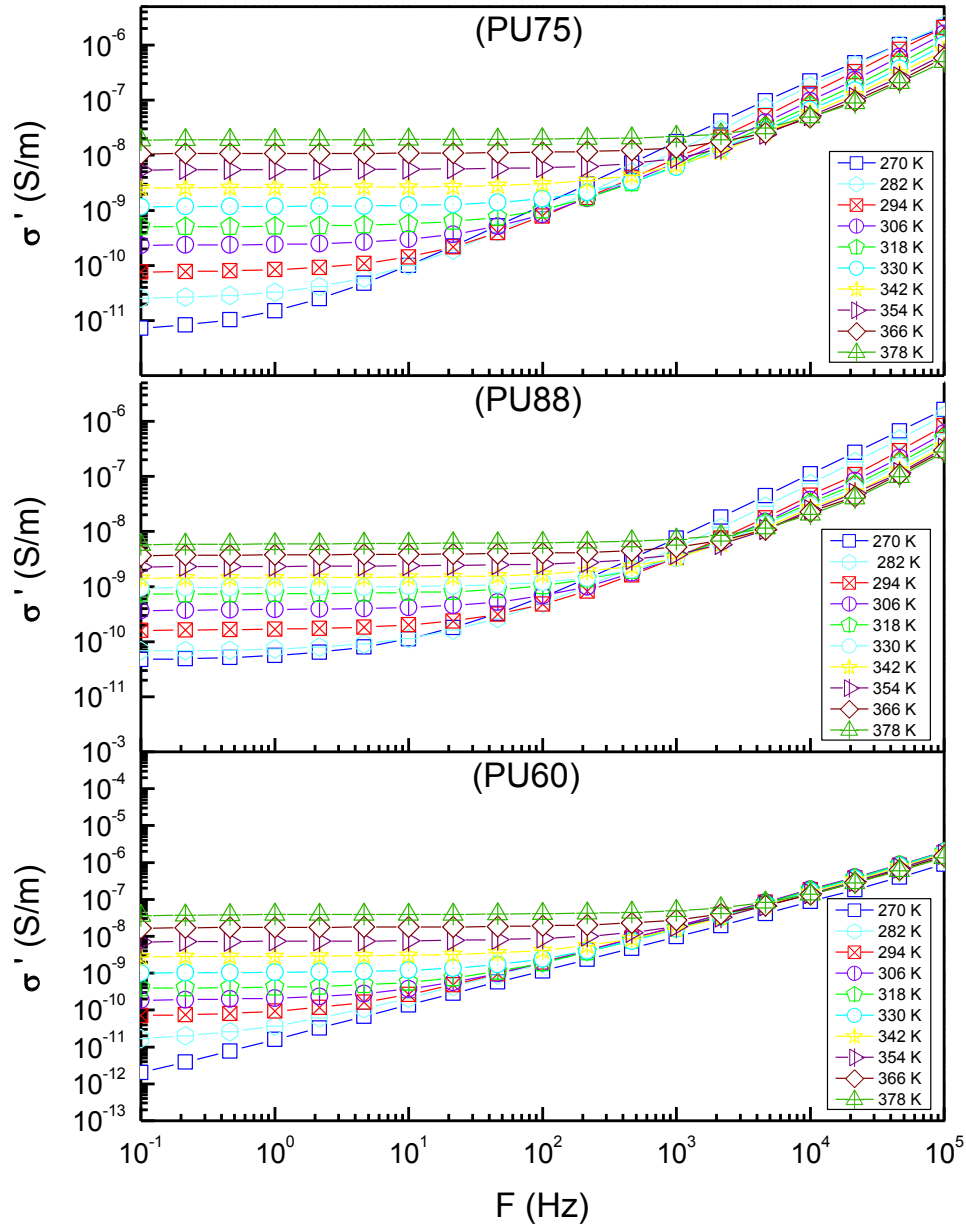


Fig 9 Real part of conductivity versus frequency measured at different temperatures.

Two regions can be observed from the curves: one for which the conductivity is almost independent on the frequency in the low frequency range. This corresponds to a resistive behavior and is attributed to charge displacements (which corresponds to dielectric losses), and another one for which the conductivity increases with the frequency and corresponds to almost purely capacitive behavior. The dc conductivity σ_{dc} -for each sample- is considered to be equal to the value of $\sigma(f)$, at the lowest measured frequency $f=10^{-1}$ Hz in the present case, in the

temperature range where the low-frequency plateau occurs. If this electrical conductivity σ_{dc} comes from ions flow, the corresponding current is driven by diffusion process, and as expected, the σ_{dc} increases with increasing temperatures. Such ions are probably impurities introduced during the polymerization process of polyurethane. In Fig 10 both Arrhenius plots drawn either from the maxima of the M'' peak or from $\log(\sigma_{dc})$ –at $f=10^{-1}$ Hz and for all temperatures- versus reciprocal temperature are displayed for the three PU. Curves of Fig 5a, 6a, and 7a were used for the calculation of the activation energy of ionic conductivity E_c , and τ_{0c} [33, 34] and curves of Fig 10 were used for the determination of E_{dc} . As it can be seen in Fig 10, both curves have very similar slopes. Thus, as expected, the apparent activation energies measured from these two set of curves lead to the same values.

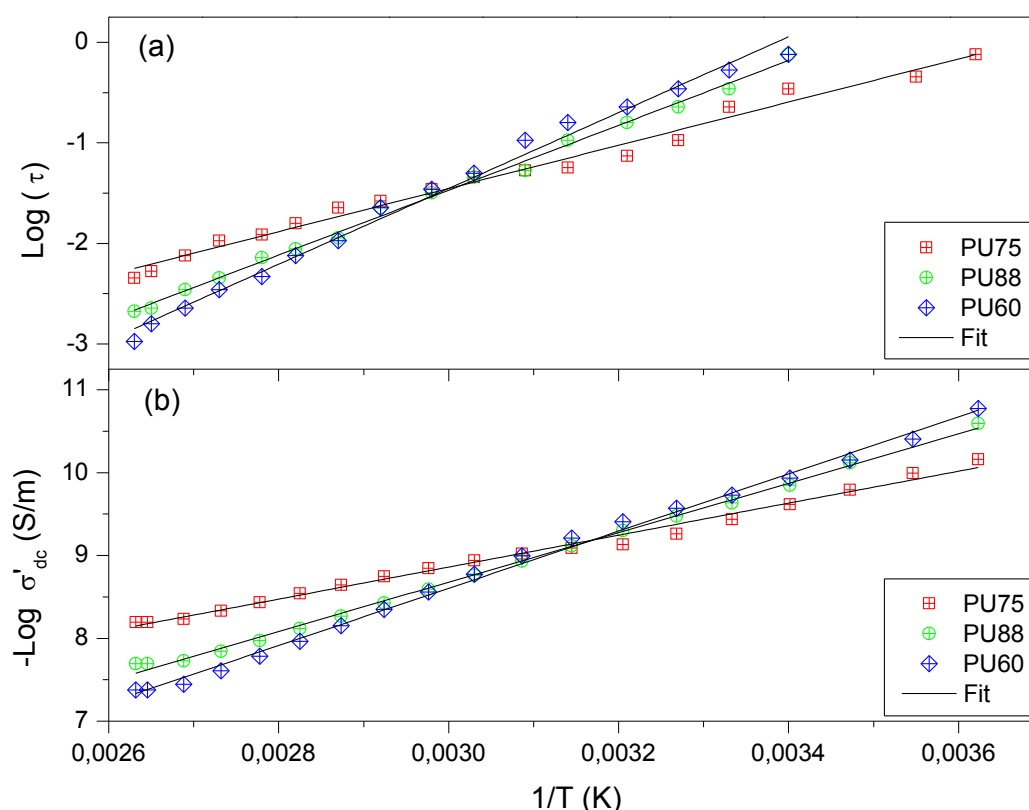


Fig 10 Arrhenius plot of conductivity relaxation, obtained from M'' maxima (a) and from σ_{dc} conduction measurements (b).

The results of the fitting procedure are listed in Table. 3.

Table. 3 Parameters of Arrhenius equation (equation (2)) for the conductivity relaxation, E_c activation energy and τ_{0c} pre-exponential relaxation time obtained from M'' maxima (a) and E_{dc} activation energy from σ_{dc} conduction measurements (b) (see Fig 9).

		PU75	PU88	PU60
Conductivity relaxation	E_c (kJ/mol)	41	62	75
	τ_{0c} (S)	10^{-7}	10^{-11}	10^{-12}
	E_{dc} (kJ/mol)	39	57	67

It is worthy to notice that in the temperature-frequency window, the curves appear as straight lines and their slopes lead to the apparent activation energy of the conduction mechanism. As expected for each PU, the data lead to the same activation energy within the measurement uncertainty (see Table. 3). It seems to be related in these polyurethanes to a conductivity of ionic type only. Furthermore this activation energy increases by increasing the weight fraction of HS Fig 10. Two remarks have to be done. First of all, very long pre-exponential times such as τ_{0c} for PU75 are incompatible with a two wells relaxation model which are known to follow the Arrhenius law: their order of magnitude should be around the Debye time, i.e. 10^{-13} s. On the other hand, if the conductivity is governed by diffusion processes of the macromolecules, thus a VTF type behavior is expected. In the high temperature range and narrow frequency range, the VTF equation leads to almost linear curves. If this is the case, the extrapolation of such function to infinite temperatures has thus no meaning, and neither the pre-exponential time. This may explain the very high value for τ_{0c} in Table 3 for PU75.

Moreover, it is noteworthy that the conductivity temperature dependence is almost the same for the 3 PU and relatively small. The 3 PU exhibits the same conductivity around room temperature. It is probable that the conductivity occurs mostly in the soft phase, and strongly depends on the presence of impurities which in turn should depend on the polymerization step. The diffusion processes are slower in PU60 because of its higher T_{gSD} , which is consistent with a higher DC conductivity activation energy. However, this weak temperature dependence leads to the fact that for PU60, the DC conductivity strongly overlaps with the α -process.

4 Conclusions

The purpose of this study was to provide as many pieces of information as possible on the dielectric behaviour of polyurethane frequently used for their rather strong electrostrictive properties.

In order to determine in which temperature - frequency domain they have their maximum efficiency, and minimum electrical loss, the relaxation maps have been determined for 3 polyurethanes of similar chemical compositions but containing different fraction of hard and soft segments. A particular attention has been paid (i) on one of their secondary relaxations (just below T_g of the soft phase) so-called β -relaxation, (ii) on their α -relaxation corresponding to T_g of the soft phase and (iii) on a relaxation which results from the conductivity. It is worthy to notice that the β -relaxations behave in a very similar way for the 3 PU, and is probably associated to interactions of polar chain segments with residual water. On the contrary, the α -relaxation is very sensitive on the composition and shifts towards high temperature with increasing content of hard segments. Finally, the DC conductivity analysis through the study of the complex dielectric modulus shows that it is comparable for the 3 PU, and that probably most of its contribution comes from the soft phase, as it disappears for temperatures lower than T_g . For PU60, the overlap of the soft phase α process with the conductivity relaxation made impossible to determine with precision the characteristics of the α -relaxation. The consequence is that losses come from both the α and the DC processes for PU60, which in turn would decrease its efficiency in energy conversion (both for actuation or energy harvesting applications). PU88 and PU75 show a better stability of the dielectric properties at temperatures

above the ambient temperature, making them more suitable for energy conversion applications.

In order to optimize the composition of such materials, not only the dielectric behaviour must be analysed, but also their mechanical properties, as both behaviours are involved for energy conversion. Such mechanical analysis, performed on the 3 same PU is under study. The relations between the dielectric, mechanical and electrostrictive properties in PU will also be discussed.

Acknowledgments

The author acknowledges the financial support of the French Agence Nationale de la Recherche (ANR), under grant NAPOLECO (ANR- 2010-INTB-910-01).

References

- [1] Bar-Cohen Y. *Electroactive Polymer (EAP) Actuators as Artificial Muscles (Reality, Potential and Challenges)*. SPIE Press. Bellingham. 2004.
- [2] Watanabe M, Hirai T, Suzuki M, Yoichi M. Electric conduction in bending electrostriction of polyurethanes. *Appl. Phys. Lett* 1999; 18: 2717–2719.
- [3] Su J, Zhang Q M, Kim C H, Ting R Y, Capps R J. Effects of transitional phenomena on the electric field induced strain–electrostrictive response of a segmented polyurethane elastomer. *Appl. Polym. Sci.* 1997; 65: 1363–1370.
- [4] Guiffard B, Seveyrat L, Sebald G, Guyomar D. Enhanced electric field induced strain in non percolative carbon nanopowder / polyurethane composites. *J. Phys. D: Appl. Phys.* 2006; 14:3053- 3057.
- [5] Guelcher S A, Gallagher K M, Didier J E, Klindinst D B, Doctor J S, Goldstein A S, Wilkes G L, Beckman E J, Hollinger J O. Synthesis of biocompatible segmented polyurethanes from aliphatic diisocyanates and diurea diol chain extenders. *Acta Biomater.* 2005; 4: 471-484.
- [6] Petrović Z S, Javni I. The effect of soft-segment length and concentration on phase separation in segmented polyurethanes. *J. Polym.Sci. B Polym. Phys.* 1989; 27: 545–560. doi: 10.1002/polb.1989.090270305.
- [7] Lin J R, Chen L W. Study on shape-memory behaviour of polyether-based polyurethanes. II. Influence of soft-segment molecular weight. *Appl. Polym. Sci.* 1998; 69: 1575–1586. DOI: 10.1002/(SICI)1097-4628(19980822)69:8<1575:AID-APP12>3.0.CO;2-U.
- [8] Chattopadhyay D K, Raju K V S N. Structural engineering of polyurethane coatings for high performance applications. *Prog. Polym. Sci.* 2007; 32: 352–418. DOI : 10.1016/j.progpolymermsci.2006.05.003
- [9] Byung K K, Sang Y L. Polyurethanes having shape memory effects. *Polymer.* 1996; 37:5781-5793. DOI: 10.1016/S0032-3861(96)00442-9
- [10] Sudipto D, Iskender Y, Emel Y, Bora I, Ozgul T, Frederick L B, Garth LW. Structure property relationships and melt rheology of segmented, non-chain extended polyureas: Effect of soft segment molecular weight. *Polymer.* 2007; 48:2 90-301. DOI:10.1016/j.polymer.2006.10.029.
- [11] Guillot F M , Balizer E. Electrostrictive effect in polyurethanes. *Journal of Applied Polymer Sci.* 2003; 89: 399-404. DOI: 10.1002/app.12096.
- [12] Korley LT J, Pate B D, Thomas E L, Hammond P T. Effect of the degree of soft and hard segment ordering on the morphology and mechanical behavior of semicrystalline segmented polyurethanes. *Polymer.* 2006; 47: 3073-3082. DOI: 10.1016/j.polymer.2006.02.093.

- [13] Pichon P G, David L, Mechin F, Sautereau H. Morphologies of Cross-Linked Segmented Polyurethanes. Evolution during Maturation and Consequences on Elastic Properties and Thermal Compressive Fatigue. *Macromolecules*. 2010; 43: 1888–1900. DOI: 10.1021/ma901602y
- [14] Petrovic Z S, Ferguson J. Polyurethane elastomers. *Prog. Polym. Sci.* 1991; 16: 695-836.
- [15] Laity P R, Taylor J E, Wong S S, Khunkamchoo P, Norris K, Cable M, Andrews G T, Johnson A F, Cameron R E. A review of small-angle scattering models of random segmented poly(ether-urethane) copolymers. *Polymer*. 2004; 45: 7273-7091. DOI: 10.1016/j.polymer.2004.08.033.
- [16] Eun A K, Han S L. Effect of molecular shape of diisocyanate units on the microscopic/macrosopic phase separation structure of polyurethanes. *J. Polym. Sci. Polym. Phys.* 2011; 49: 890–897. DOI: 10.1002/polb.22264.
- [17] Yang C Z, Grasel TG, Bell J L, Register R A, Cooper S L. Carboxylate containing chain-extended polyurethanes. *J. Polym. Sci. B Polym. Phys.* 1991; 28: 581–588. DOI: 10.1002/polb.1991.090290507.
- [18] Koberstein J T, Russell T P. Simultaneous SAXS-DSC Study of Multiple Endothermic Behavior in Polyether-based Polyurethane Block Copolymers. *Macromolecules*. 1986; 19: 714-720. DOI: 10.1021/ma00157a039.
- [19] Lapprand A, Mechin F, Pascault J P. Synthesis and properties of self-crosslinkable thermoplastic polyurethanes. *J. Appl. Polym. Sci* 2007; 105: 99-113. DOI: 10.1002/app.26086.
- [20] Liff SM, Kumar N, McKinley G. High- performance elastomeric nanocomposites via solvent - exchange processing. *Nature Materials*. 2007; 6: 76-83.
- [21] Nakamae K, Nishino T, Asaoka S, Sudaryanto. Microphase separation and surface properties of segmented polyurethane - Effect of hard segment content. *Int. Journal of Adhesion and Adhesives*. 1996; 16: 233-239.
- [22] Diaconu I, Dorohoi D. Properties of polyurethane thin films, *J. Optoelectron. Adv. Mater.* 2005; 7:921-924.
- [23] Putson C. Energy conversion from electroactive materials and modeling of behaviour on these materials. PhD Thesis, 2010, INSA Lyon, France.
- [24] Guyomar D, Cottinet P J, Lebrun L, Putson C, Yuse K, Kanda M, Nishi Y. The compressive electrical field electrostrictive coefficient M33 of electroactive polymer composites and its saturation versus electrical field, polymer thickness, frequency, and fillers. *Polym. Adv. Technol.* 2012; 23:946-950
- [25] Ahmad Z. *Polymer Dielectric Materials, Dielectric Material*, Dr. Marius Alexandru Silaghi (Ed.), 2012, ISBN: 978-953-51-0764-4, InTech, DOI: 10.5772/50638.
- [26] Pissis P, Kanapitsas A, Savelyev Y V, Akhranovich E R, Privalko E G, Privlako V P. Influence of chain extenders and chain end groups on properties of segmented polyurethanes, II. Dielectric study. *Polymer*. 1998; 39: 3431-3435. DOI:10.1016/S0032-3861(97)10100-8.
- [257] Boiteux G, Seytre G, Cuve L, Pascault J P. Dielectric studies of segmented polyurethanes based on polyolefine: relations between structure and dielectric behavior. *J. Non-Cryst. Solids*. 1991; 133: 1131-1135. DOI: 10.1016/0022-3093(91)90739-S.
- [28] Zhang Q M, Su J, Kim C H. An experimental investigation of electromechanical responses in a polyurethane elastomer. *J. Appl. Phys.* 1997; 81:2770-2776. DOI: 10.1063/1.363981.
- [29] Kanapitsas A, Pissis P. Dielectric relaxation spectroscopy in crosslinked polyurethanes based on polymer polyols. *Eur. Polym. J.* 2000; 36: 1241–1250. DOI: 10.1016/S0014-3057(99)00167-6.
- [30] Castagna A M, Fragiadakis D, Hyungki L, Choi T, Runt J. The Role of Hard Segment Content on the Molecular Dynamics of Poly(tetramethylene oxide)-Based Polyurethane Copolymers. *Macromolecules*. 2011; 44 : 7831-7836. DOI: 10.1021/ma2017138.
- [31] Hanafy T A. Dielectric and Electric Modulus Behavior of Chlorinated Poly(Vinyl Chloride) Stabilized with Phenyl Maleimide. *Adv. Mater. Phys. Chem.* 2012; 2: 255-266. DOI: 10.4236/ampc.2012.24038.

- [302] Pissis P, Apekis L, Christodoulides C, Niaounakis M, Kyritsis A, Nedbal J. Water effects in polyurethane block copolymers. *J. Polym. Sci Part B: Polym. Phys.* 1996; 34:1529-1539. DOI:10.1002/(SICI)1099-0488(19960715)34:9<1529::AID-POLB1>3.0.CO;2-G.
- [33] Karabanova L V, Boiteux G, Seytre G, Stevenson I, Gain O, Hakme C, Lutsyk E D, Svyatyna A. Semi-interpenetrating polymer networks based on polyurethane and poly(2-hydroxyethyl methacrylate): Dielectric study of relaxation behavior. *J. Non-Cryst. Solids.* 2009; 355:1453-1460. DOI:10.1002/app.12592.
- [34] Georgoussis G, Kyritsis A, Pissis P, Savelyev Y V, Akharonovich E R, Privalko E G, Privalko V P. Dielectric studies of molecular mobility and microphase separation in segmented polyurethane. *Eur. Polym. J.* 1999; 35: 2007- 2017. DOI : 10.1016/S0014-3057(98)00288-2.

Chapter 4: Time and frequency dependence of the electromechanical response of segmented polyurethane-based actuators.

M. H. Jomaa^{1,2*}, L. Seveyrat², V. Perrin², L. Lebrun², K. Masenelli-Varlot¹, J.Y. Cavaille¹.

¹ Université de Lyon, INSA-Lyon, CNRS, MATEIS, 69621 Villeurbanne Cedex, France

² Laboratory of Electrical Engineering and Ferroelectricity, LGEF INSA Lyon EA682, Université de Lyon, F-69621 Villeurbanne Cedex, France

*Author to whom all correspondence should be addressed

Abstract

Among the key parameters which must be taken into account for the choice of actuators used as electrical to mechanical energy converters, the response to a step function and/or the frequency dependence of this response is extremely important. For polymeric actuators, 3 mechanisms can be at the origin of energy losses, namely dielectric relaxations, viscoelastic relaxations and electrical conductivity. In a previous paper (Jomaa et al., *Polymer* 63 (2015) 214-221) we studied the dielectric behaviour of segmented polyurethanes with different weight fractions of hard (MDI-BDO) and soft (PTMO) segments. They were shown to exhibit 3 mains mechanisms, namely, from the fastest to the slowest, a secondary or β -relaxation, the main or α -relaxation associated to the glass-rubber transition of the soft phase and their electrical conductivity. In the present work, we present the general viscoelastic response (as measured through mechanical spectrometry) of the same polyurethanes and their respective time dependent electrostriction response. It appears that their response is limited by the ionic or space charges mobility, which limits their use to frequency lower than 0.1 Hz at room temperature. Thus it is clear that any improvement should have as a target a large decrease of this conductivity.

Finally the choice of the more suitable PU for actuation properties is discussed on the basis of specific requirements for actuation, and in terms of large stability of electrostriction, electrical and mechanical behaviour in a wide range of frequencies and temperatures.

Keywords: electroactive polymer, Polyurethane, Viscoelastic relaxation, electrical losses, Electrostriction

1 Introduction

Electroactive polymers or EAPs, are part of the broad group of smart materials. The use of polymers with electroactive response has emerged since the early 1990's with the introduction of new materials which exhibit significant deformations, up to few percent. These materials are highly attractive for their low density, large strain capability, and small response time. In general, the biggest advantages over conventionally used systems in most application fields are the large displacement they can provide, an adaptable stiffness combined with various form factors and sizes from micrometers to meters. Especially, for actuation, vast R&D activity can be seen for specialized applications such as medical devices and biomimetic-robotics. Here the features of electroactive polymers are used to enable movements and generate forces as well as electrically control surface properties. Haptics for consumer portable touch screen devices and peripherals is going to be the next big application and potentially the first large-scale implementation of EAPs in general with an expected penetration of 60% for haptic feedback in mobile phones for 2018 [1]. Among the various EAPs, polyurethane (PU) elastomers are of great interest due to the significant electrical-field strains [2, 3, 4], and due to their attractive and useful properties - such as flexibility, light weight, abrasion resistance, easy processing to large area films and ability to be molded into various shapes as well as their biocompatibility with blood and tissues [5, 6].

In the particular case of electrostrictive polymers, the strain is a quadratic function of the applied electric field. Even if the electromechanical coupling is relatively weak for polymers, they can generate high strains. The total strain is a combination of electrostriction $S_{electrostriction}$ and Maxwell strains $S_{Maxwell}$, as shown in Equation (1) [7]:

$$S = S_{electrostriction} + S_{Maxwell} = M_{33}^* E^2 \quad (1)$$

Where M_{33}^* is the apparent electromechanical coefficient, and E the applied electrical field. The Maxwell stress effect comes from electrostatic attractions between the electrodes and can be expressed as:

$$S_{Maxwell} = -\frac{\epsilon_r' \epsilon_0}{Y} E^2 \quad (2)$$

Where ϵ_r' , ϵ_0 , and Y refer to the real part of the relative permittivity, to the vacuum permittivity and to the Young modulus of the polymer, respectively.

The electrostriction is the direct coupling between the polarization and mechanical response in the material:

$$S_{electrostriction} = Q P^2 \quad (3)$$

By assuming a linear relationship between the polarization P and the electrical field E ,

$$P = \epsilon_0 (\epsilon_r' - 1) E \quad (4)$$

$S_{electrostriction}$ can be expressed by Equation (3):

$$S_{electrostriction} = Q P^2 = Q \epsilon_0^2 (\epsilon_r' - 1)^2 E^2 = M_{33} E^2 \quad (5)$$

Where Q is the charge-related electrostrictive coefficient and M_{33} the electrical field-related electrostrictive coefficient.

It has been previously published [8] that the M_{33} coefficient of electrostriction varies like

$$(\epsilon_0 (\epsilon_r' - 1)^2) / (\epsilon_r' Y) \quad (6)$$

As seen in these equations, actuation capabilities depend on the dielectric and mechanical properties of the polymer. A compressive effect is always reported.

Polyurethanes are segmented polymers composed of alternating sequences of soft segments (SS) and of hard segments (HS). The structural differences/incompatibility between the SS and the HS lead to a separation into microphases or domains formed from the respective HS and SS. Hard domains (HD) -domains rich in HS- play the role of physical crosslinks and act as high modulus fillers, whereas the soft domains (SD) -domains rich in SS- provide extensibility [9, 10, 11]. In addition, HDs exhibit a permittivity larger than soft domains. It has been recently pointed out that the large electric field induced strain in PU results mainly from heterogeneities in contrast to both elastic constants and dielectric constants and to electric field gradients, which make the soft domains shrink and the whole material compress [12].

To better understand the relations between the PU dielectric, mechanical and electrostrictive properties, we previously showed that it was important to study the different relaxation processes and we investigated the dielectric properties of PU with 3 different fractions of HS [13]. In this paper, we focus on the viscoelastic and electrostriction properties of the same PU, again as functions of the temperature and the frequency. The relations between the HS fraction and the dielectric, mechanical and electrostrictive properties will be discussed. Finally, the best-suited PU composition for actuation applications will be discussed, as well as the limits in use of pure polyurethanes.

2 Materials and experiment

The polymers studied are polyether-based thermoplastic polyurethanes. They are co-block polymers with two major blocks; namely the hard and soft segments. The hard segment (HS) is composed of 4,4' methylene bis (phenyl isocyanate) (MDI) and 1,4-butanediol (BDO). Poly (tetramethylene oxide) (PTMO) is used as soft segments (SS).

The three different types of PU are commercially available and were provided by the company Lubrizol. They were synthesized from the same initial chemical components. They differ in their weight fractions of HS: 26% for PU 75 (Estane X-4977), 45% for PU88 (Estane 58888 NAT021) and 65% for PU60 (Estane ETE60DT3 NAT022), and in different molecular weights of PTMO SS; 1000 g/mol for PU88, PU60 and 2000 g/mol for PU75.

The SSs originate from the polyol and are responsible for the elastomeric behaviour of the polymeric material; the HSs contain highly polar urethane linkages and it is thought [14,15,16,17] that due to phase separation they form highly polar and stiff microdomains embedded in a soft poorly polar matrix. Essentially, the morphology of segmented polyurethanes depends on the relative amount of soft and hard segments and on other physical phenomena such as crystallization and hydrogen bonds formation between both types of segments.

The polymer films were prepared by solution casting. Before use, PU granules were heated at 350 K for 3 hours. Then they were dissolved in N,N-dimethylformamide (DMF, Sigma-Aldrich D158550, 99%) with a ratio of 25% weight of PU into DMF. The solution was heated at 350 K for 4 hours under mechanical agitation, until a homogeneous solution was obtained. This operation was carried out in a closed device, to avoid evaporation of the DMF solvent and ensure good reproducibility of films. The solution was then kept overnight to remove air

bubbles. Afterwards, this solution was cast on glass plates with an Elcometer 3700 doctor blade film applicator, put in an oven at 335 K for one day, and then removed from the glass. A second heating treatment at a temperature below the HS melting temperature at 400 K was performed in order to eliminate the residual solvent. The thickness of the films was about 100 μm after drying.

Glass transition and melting temperatures were determined with Differential Scanning Calorimetry (Setaram, DSC 131 Evo)). Samples of 20 mg were cooled to 140 K and then heated to 480 K before being cooled to room temperature. The heating and cooling rates were set at 10 K / min.

The dynamic shear measurements were measured by mechanical spectroscopy (also called dynamic mechanical analysis or DMA) [18]. The dimensions of the samples were equal to 12 mm in length, 3 mm in width and 0.1 mm in thickness. A sinusoidal shear stress was applied and the corresponding strain can be obtained. Thus, the complex shear modulus ($G^* = G' + iG''$) was measured and then storage (G') and loss (G'') dynamic shear modulus were calculated. Loss factor $\tan \delta_m = G''/G'$ was also determined. Experiments were performed both on isochronal mode (0.1 Hz, temperatures 150-350 K, with a heating rate of 1 K/min) and isothermal mode (frequencies from $2 \cdot 10^{-3}$ to 1 Hz, temperatures from 180- 350 K, with a heating rate of 3K/min). All experimental tests were carried out under helium.

The field-induced thickness strain S (electrostriction) was measured on circular samples (25mm of diameter) with a homemade setup based on a double-beam laser interferometer measurement (Agilent 10889B) [4]. Samples were placed between two cylindrical brass masses acting as conductive electrodes. A mirror was placed on the upper electrode to reflect the laser beam. A bipolar electric field was supplied by a high voltage amplifier (Trek10/10B) driven with a function generator (Agilent 33250A). Measurements were made at room temperature.

3 Results and discussion

3.1 Density, glass transition temperature and Young modulus of the 3 PU versus HS content

Table 1 presents the HS content from the materials data sheet [19], as well as the glass transition temperature and the Young modulus – $Y = 2 G' (1 + \nu)$, where G' and ν , shear modulus and Poisson's ratio, respectively- measured using DSC and DMA, respectively.

Table 1 Glass transition temperature and Young modulus of the 3 PU versus HS content.

	HS %wt	T_{gSD} (K)	Y (MPa) 0.2 Hz 300 K
PU75	26	209	19
PU88	45	228	33
PU60	65	253	120

The glass transition temperature T_{gSD} of the SD -which may indicate changes in the micro-phase separation- increases by increasing the weight fraction of HS, which confirms the partial miscibility of HS and SS [20, 21]. The three T_{gSD} values are far below room temperature and consequently at room temperature applications the three PU will be in the rubbery state. For

use at very low temperatures, for example -220 K, the PU75 might be the best suited PU since it exhibits the lowest T_g .

The Young modulus (Y) increases with the fraction of HS, because HS can act as crosslink points [22, 23]. As the electrostrictive coefficient is inversely proportional to the Young modulus, a complete study of the variations of Y over a wide range of frequencies and temperatures will be conducted in order to determine the limits of use of the 3 PU.

3.2 Viscoelastic properties:

3.2.1 Isochronal study

The measurements were performed at 0.1 Hz, in the temperature range 150-350 K. Fig. 1 shows the evolution of the storage modulus (G') and the mechanical losses $\tan \delta_m$ of the 3 PUs in function of the temperature.

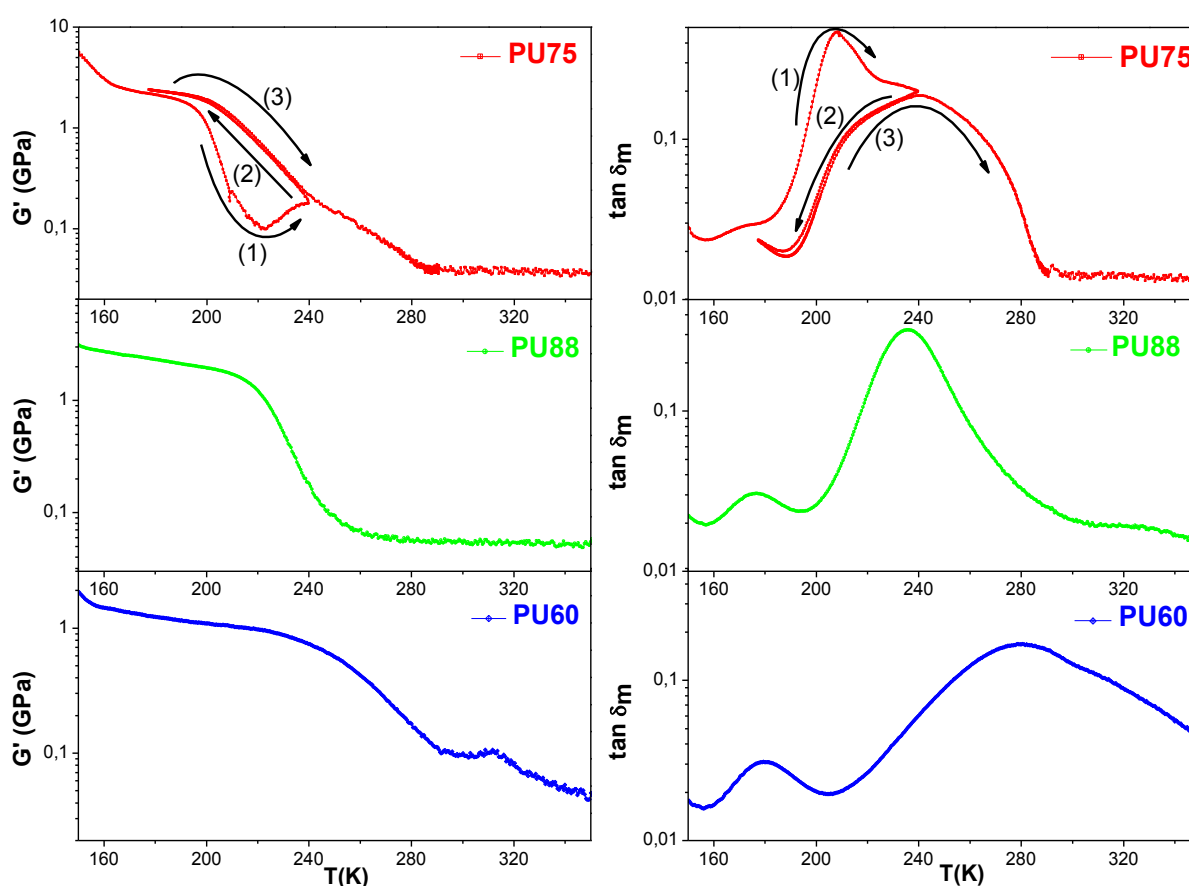


Fig. 1 Evolution of the storage modulus (G') and the mechanical losses $\tan \delta_m$ of the 3 PU versus temperature at a frequency of 0.1Hz

The glass transition temperatures (T_{gSD}) roughly estimated from (G'') curves –figure not shown- (200 K, 226 K and 254 K for PU75, PU88 and PU60, respectively) are very close to the ones measured by DSC (Differential Scanning Calorimetry) (see Table 1).

PU88 exhibits an almost constant storage modulus and low mechanical losses around room temperature (280-330K), which corresponds to a large temperature range of use. On the contrary, PU60 undergoes high mechanical losses. Its storage modulus is greatly dependent on the temperature around room temperature, which could be associated to a higher content of HS.

The case of PU75 is more complex. Indeed, the loss factor of PU75 exhibits one abrupt decrease around 200 K followed a small peak around 240 K. The abrupt decrease is undoubtedly related to the glass transition relaxation since its temperature is close to T_g . The peak at 240 K is associated to an increase of (G'). In natural rubber, such increase can be attributed to crystallization [24]. To check that the shoulder at 240 K is due to a partial crystallization of PU75 during the experiment, a temperature cycle was applied during the DMA analysis. In step (1), the temperature was increased until the peak maximum ($T= 240$ K) -where crystallisation is supposed to occur, then during step (2), the sample was cooled down (from 240 K to 180 K) and finally in step (3), the sample was heated again. Clearly, there is a good superposition of G' during steps (2) and (3), which confirms the reproducibility of our results. Furthermore the value of G' increases from step (1) to step (3) and the shoulder disappears. This seems to confirm that the shoulder corresponds to a partial crystallization of PU75.

Isochronal measurements of $\tan \delta_m$ show the observation of two relaxations (characterized by maxima). The α -relaxation, observed above the glass transition temperature, is a universal feature of all amorphous materials and it is attributed to the cooperative motion of molecules. The α -relaxation is characterized by a decrease in storage modulus of 1 to 2 orders of magnitude. The β -relaxation is detected at lower temperature (or high frequencies domains). It is often much weaker than the α -process. It is not always obvious to detect the β -relaxation in all amorphous materials, although it is considered as a universal feature of amorphous polymers. The nature of β -relaxation in polymers is attributed to local almost non-cooperative motions of the polymers segments [25]. Moreover it may be connected to ductility below T_g in amorphous polymers. From the measurements on PU75, PU88 and PU60, it can be noticed that the α -relaxation is shifted to higher temperatures when increasing the HS fraction. On the contrary, the β -relaxation is found to be less sensitive to the amount of HS, as it occurs around 175 K for the three PU. Because the β process is not significantly dependent on the HS fraction, the isothermal study will be focused on the α -relaxation only.

3.2.2 Isothermal study

The measurements were performed in the frequency range $2 \cdot 10^{-3} - 1$ Hz. Fig. 2 shows the evolution of the storage modulus (G') and loss modulus (G'') of the 3 PU in function of the frequency, at different temperatures.

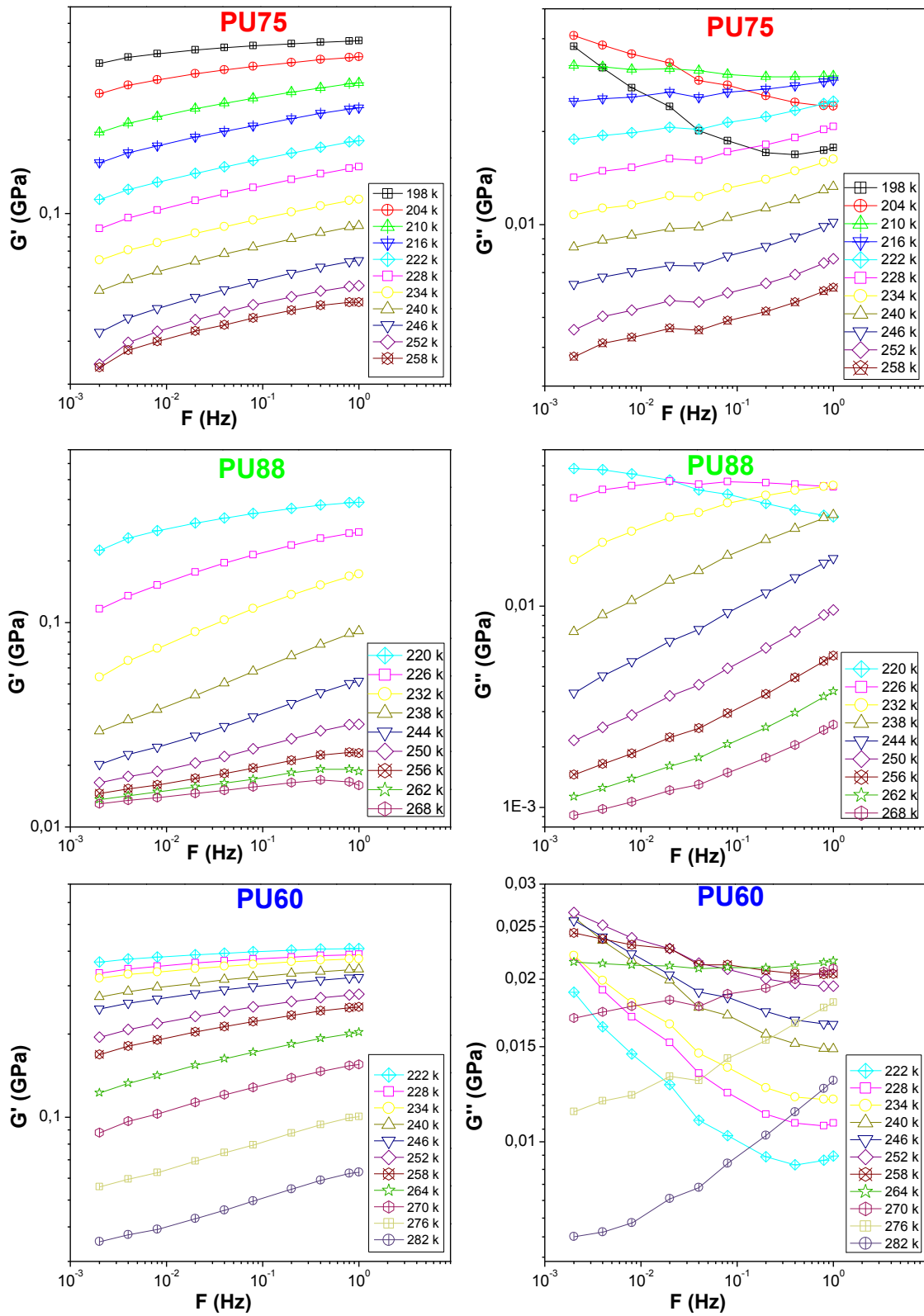


Fig. 2 Frequency dependence of the storage modulus and loss factor of 3 PU in isothermal mode at different temperatures

From a general point of view, at a given temperature, an increase in G' is observed when increasing the frequency. Meanwhile for temperatures below T_{gSD} , G'' decreases. Moreover, at a given frequency, G' decreases and G'' increases when the temperature increases, as already observed on Fig. 1. These evolutions simply correspond to facilitated molecular mobility when the temperature increases or when the driving frequency is reduced [26]. These tendencies have been already reported for other polyurethanes [27].

Based on the isothermal tests, master curves of G' and $\tan \delta_m$ can be obtained by shifting the modulus-versus-time curves toward a reference temperature until perfect superposition [28, 29]. Such master curves give the viscoelastic behaviour over a wider range of frequencies. Fig. 3 shows the obtained master curves for the 3 PUs at room temperature.

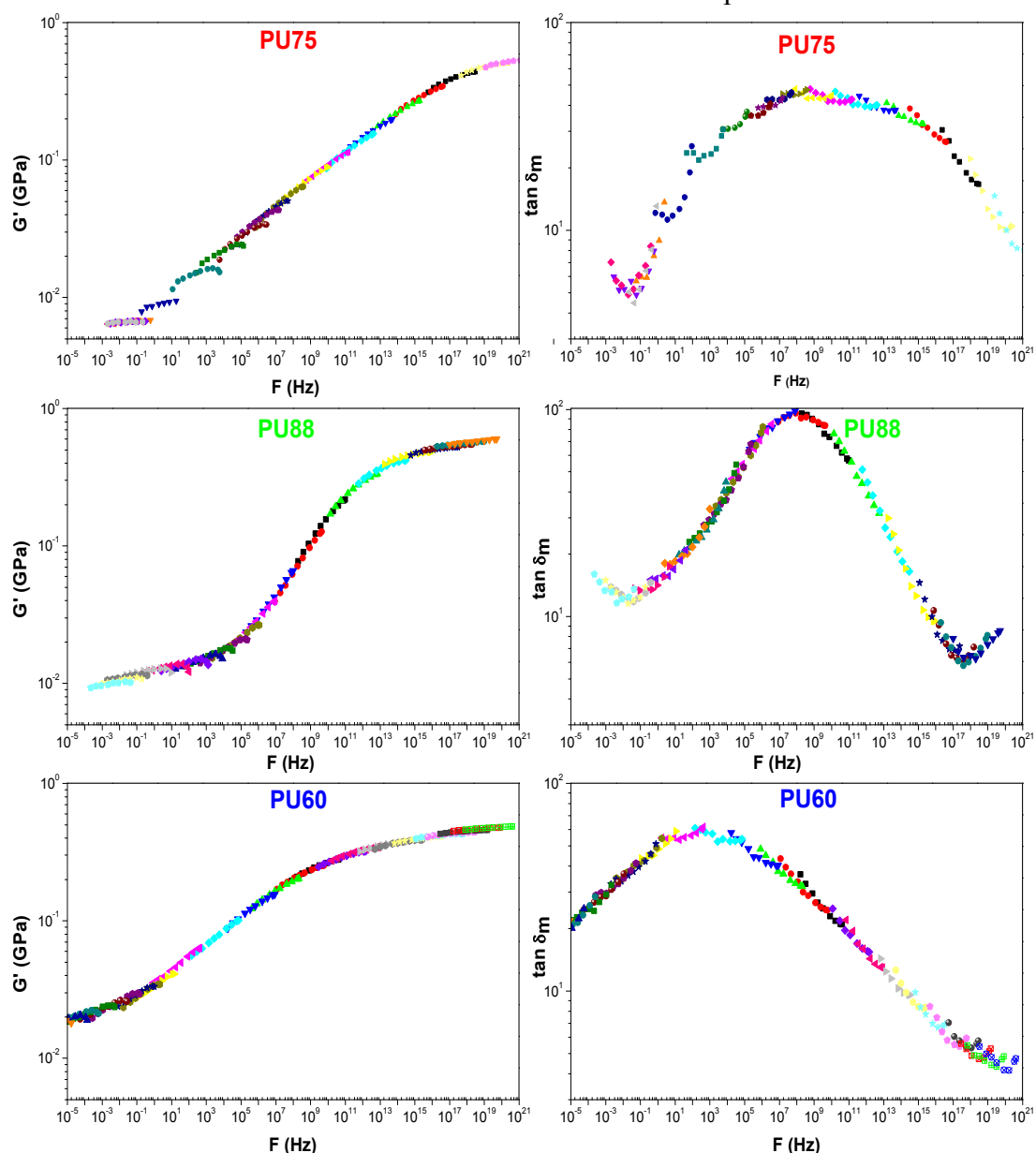


Fig.3 Master curves for the storage modulus and the loss factor of the 3 PU at room temperature.

As for many other polymers, unique curves are obtained, which confirms the validity of the time- temperature superposition principle. As analysed above, it can be noticed that G' and

$\tan \delta_m$ are very sensitive to frequency for the 3 PUs. PU88 exhibits low variations of G' and reasonable $\tan \delta_m$ values for frequencies ranging from 10^{-3} to 10^5 Hz. PU60 presents high mechanical losses at low frequencies and G' increases rapidly with frequency. Finally, PU75 has high mechanical losses for a wide range of frequencies and G' increases linearly with frequency.

The maximum of $\tan \delta_m$ observed for the 3 polymers could be attributed to the α -relaxation [30]. For the highest frequency values, the very beginning of the β -relaxation is evidenced for PU88 and PU75. From the master curves, the experimental relaxation times can be calculated for both relaxations using the following relation

$$\tau = 1/2\pi f_{peak} \quad (7)$$

where f_{peak} is the frequency read at the maximum value of G'' .

For the cooperative α -relaxation, it is common to use the Vogel-Tammann-Fulcher (VTF) equation instead of the Arrhenius law to describe the temperature dependence of the relaxation time:

$$\tau = \tau_0 \cdot \exp \frac{B}{(T-T_0)} \quad (8)$$

where τ_0 is the pre-exponential time, B is an activation parameter and T_0 is the ideal glass transition temperature (or the Vogel temperature) [31, 32].

Figure 4 presents the experimental values of $\log \tau$ versus $1/T$ deduced from the viscoelastic master curves, with the fits using the VTF law. The fitting parameters values are listed in table 2. The values obtained from the dielectric measurements (see Chapter 4) are also shown for comparison.

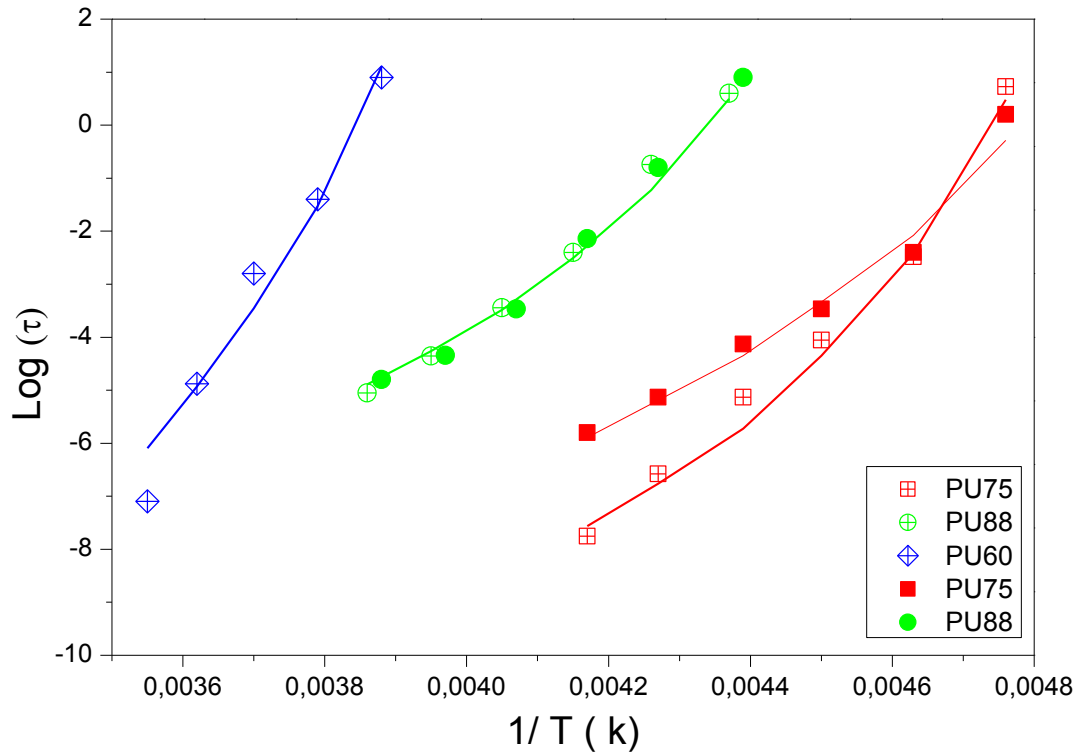


Fig. 4 Experimental and VTF fitted values of $\log \tau$ versus $1/T$ from viscoelastic curves (open symbols) and from dielectric measurements (full symbols).

Table 2 Parameters of VTF equation for the viscoelastic and dielectric α -relaxation.

		PU75	PU88	PU60
Viscoelastic α-relaxation	$B(K)$	1100	900	1300
	$T_0(K)$	181	195	225
	$\tau_0(s)$	10^{-17}	10^{-12}	10^{-17}
Dielectric α-relaxation	$B(K)$	1400	900	N.D.
	$T_0(K)$	165	195	N.D.
	$\tau_0(s)$	10^{-15}	10^{-12}	N.D.

It is noteworthy that the α -process has been successfully evidenced for PU60 from its viscoelastic properties, which was not the case from the dielectric ones, due to high conductivity effect [13]. This result highlights the fact that the mechanical measurements are not sensitive to ionic conductivity, which makes DMA more efficient to study the α -relaxation in high conductive polymers.

The VTF parameters are different for the 3 samples. In fact, as the α -process refers to the soft phase of each PU, and, as recalled above, this phase results from the phase separation of HS and SS during the sample preparation. Thus parameter T_0 is expected to vary as T_g . Roughly speaking, T_0 is often related to T_g by $T_0 \sim 0.7 T_g$ which leads here to $T_0 \sim T_g - 30 K$.

The changes of B may indicate that the cooperative primary α process is sensitive to morphology changes [30]. For PU88 a very good correlation is obtained between viscoelastic and dielectric α -relaxation (see Fig. 4 & Table 2). For PU 75 the dielectric and mechanical

relaxation times exhibit different temperature dependences for temperatures above 222 K. This can be explained by the starting of crystallization of SS at this temperature (see Fig. 1), which is known to strongly impact the mechanical behaviour.

3.3 Electrostriction

The electromechanical performances were first performed at a fixed voltage of $2\text{V}/\mu\text{m}$ applied for 300 s. Fig. 5 presents the time dependence of induced thickness strain S during the contraction process of the 3 PUs, at room temperature.

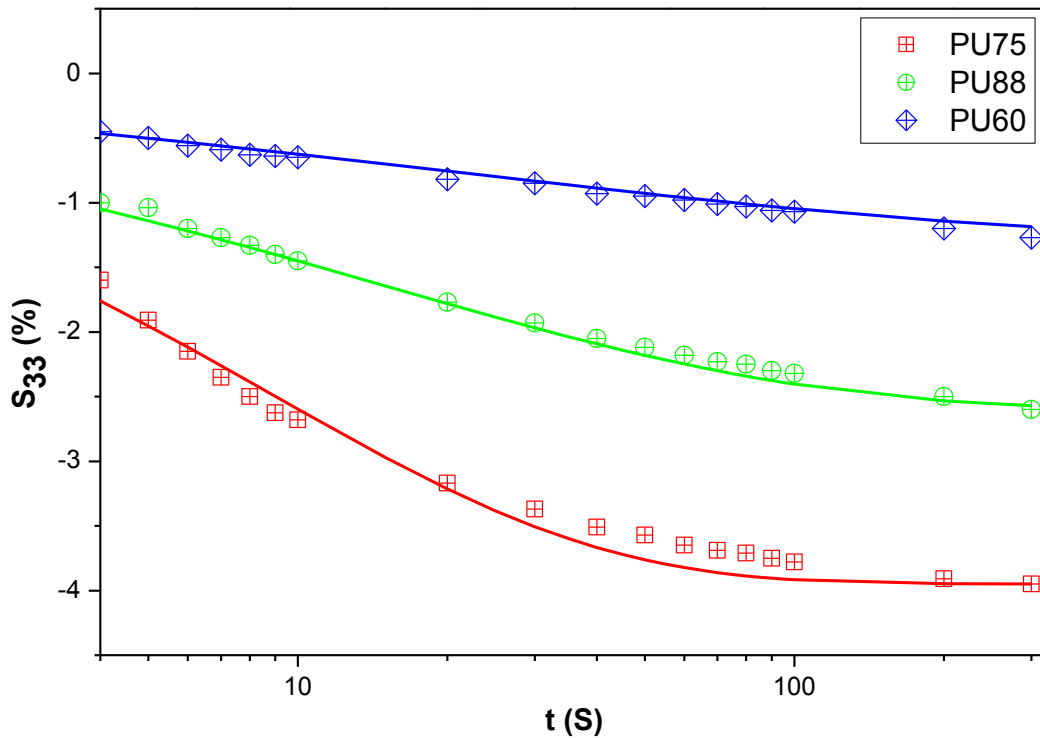


Fig. 5 Time response of contraction deformation processes of 3 PU at $2\text{ (V}/\mu\text{m})$ at room temperature.

The dots refer to experimental results and the solid lines are the results of fits using the following stretched exponential equation:

$$S(t) = S_{max} \left(1 - e^{-(t/\tau)^b} \right) \quad (9)$$

Where τ is the characteristic relaxation time, b is the extent of deviation from a single exponential behaviour ($0 < b \leq 1$).

It is worth noticing that the thickness strain is negative, which indicates a compression of the film. Depending on the time t , three strain behaviours can be defined: (i) a rapid increase during the first 10 s, (ii) a linear behaviour in the low response time region, where S increases linearly with t , and (iii) an asymptotic behaviour after 100 s, where S remains about constant in the high response time. For the 3 PUs, the strain presents a steady state after 100s.

Table 3 summarizes the parameters of the fits for the 3 PUs using equation (6).

		PU75	PU88	PU60
Electrostriction relaxation	τ (s)	9	15	25
	b	0.65	0.5	0.4

It is clear that the weight fraction of HS has an effect on the relaxation time. The 3 PUs exhibit increasing relaxation times, as their HS content increases. However, these relaxation times (in the order of tens of seconds) are interestingly much longer than the α -process relaxation times at room temperature. Surprisingly, they are in fact comparable to the conductivity relaxation times as determined in our previous work and as seen in Fig. 10 in ref [13]. Parameter b in eqn. 9 refers to the width of the relaxation time distribution, $b=1$ corresponding to a Debye relaxation. The broadness of the relaxation as determined from Fig.5 increases at increasing HS content, which may be due to a more complex microstructure for PU60 compared to PU75: at low HS content, we may expect a simple system made of a soft matrix embedding hard spheres, while at higher HS content, hard domains may start to connect with each other leading to co-continuous phases. If the electrostriction process involves the conductivity (which occurs mainly in the soft matrix), more complex mechanisms are expected for such co-continuous microstructure. Fig. 6 reveals the electrical field induced thickness strain of the 3 PUs as a function of square of applied electric field (E^2) at 0.1 Hz. At this step, it is worthy to notice that there is a certain discrepancy from a sample to another, maybe due to the fact that we do not use any coating on the sample surface. This choice was made to avoid any constraints on the sample surface which could limit planar strain, and thus thickness strain (Poisson's effect). The consequence is probably that no perfect contact is obtained between the sample and the electrodes which may induce a certain uncertainty on the local electron field. But for each sample, a quadratic behaviour is observed in the low electrical field region, where S increases linearly with E^2 . An apparent electrostrictive coefficient can be deduced from the slope of the curves, leading to values in the order of 10^{-14} (V/ μm)².

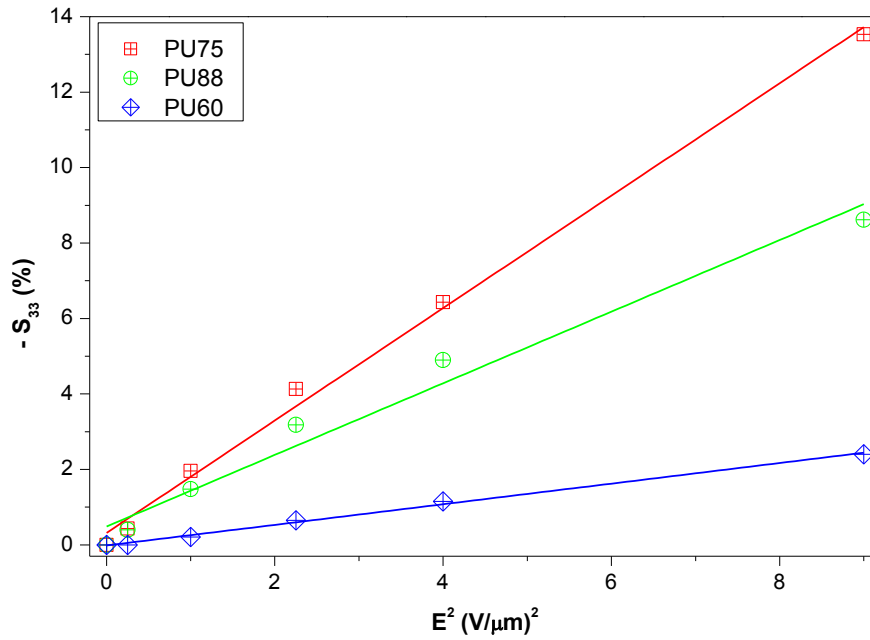


Fig. 6 Evolution of the electrical field induced thickness strain of the 3 PUs as a function of square of applied electric field (E^2) at 0.1 Hz

These results are in good agreement with the electrostriction contribution to the strain as previously reported [33, 34, 35]. They are however very large compared to the calculated Maxwell strain coefficient (see equation 2) of about 10^{-18} ($V/\mu m$)².

3.4 Comparison between PU75, PU88 and PU60

Fig. 7 presents the variation of the dielectric M'' and viscoelastic properties G'' of the three PU samples as a function of frequency and temperature.

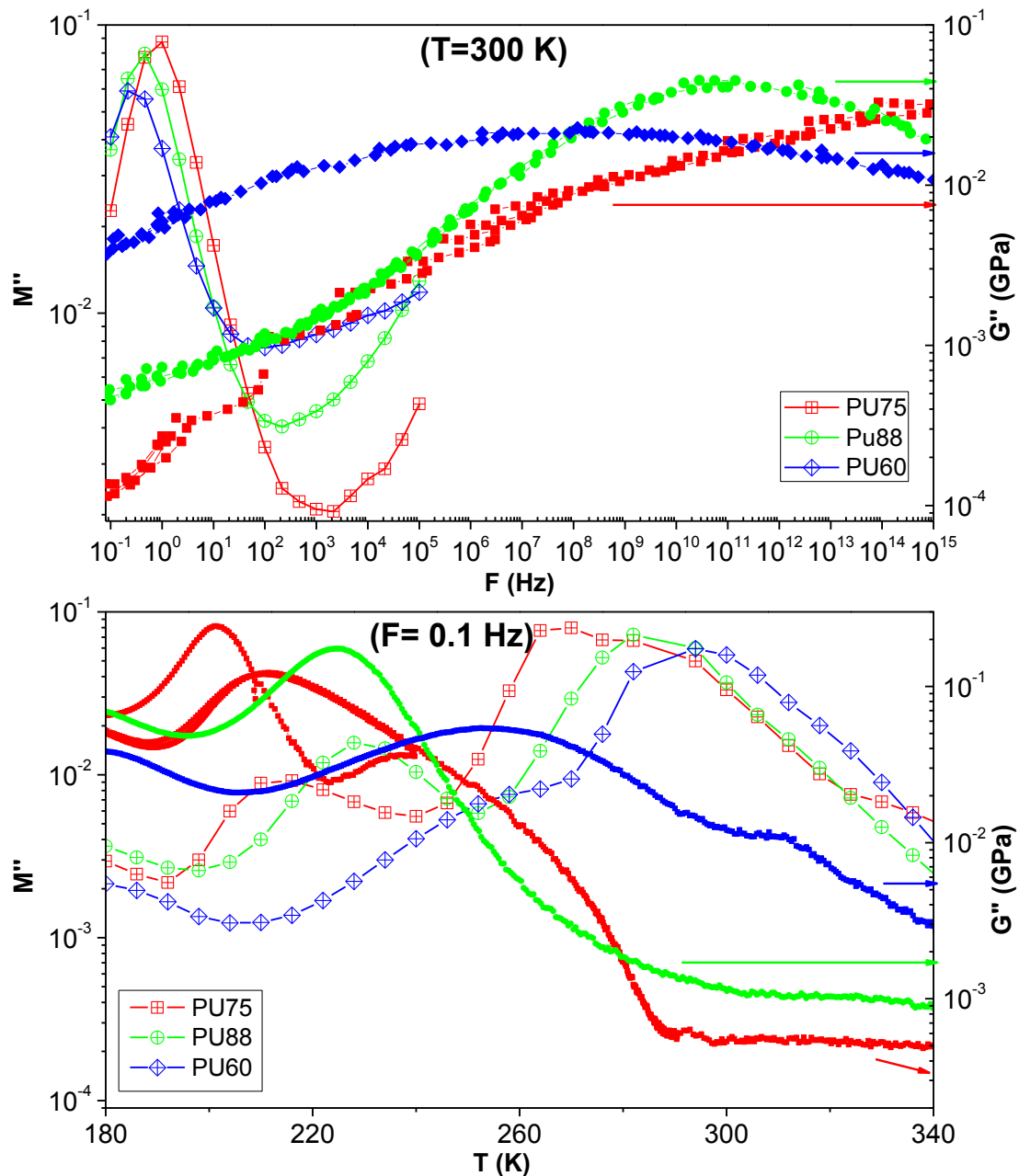


Fig. 7 Variations of the dielectric modulus M'' (open symbols) and the viscoelastic modulus G'' (filled symbols) of the 3 PUs in a wide range of frequencies and temperatures.

For the 3 PUs, the dielectric losses are preponderant in the low frequency regime with a maximum around 1 Hz, whereas the mechanical losses are preponderant at much higher frequency. At low frequency, dielectric losses are mainly due to ionic conductivity or space charges displacements and at high frequency mechanical losses are the consequences of the viscoelastic relaxation. These results show the limitations of the use of PU versus frequency. Below 280 K both M'' and G'' exhibit large changes whereas they behave more smoothly at higher temperatures where it is observed a slight variation of G'' and a linear decrease of M'' .

From Fig 6, it has been observed that the electrostriction coefficients of PU88 and PU75 are very close to each other. Taking into account the fact that PU88 exhibits low mechanical and dielectric losses in the largest range of frequencies and of temperature, this polymer is the best candidate for actuation applications.

4 Conclusions

In this work, viscoelastic and electrostriction properties of three PUs with different fractions of hard segments were investigated on a wide range of temperatures and frequencies. Mechanical measurements highlight the main relaxations in the same manner as dielectric measurements (except for conduction relaxation). The temperature dependence of the relaxation times for α -relaxation is similar with one obtained with dielectric measurements. It has been found that DMA seems to be more efficient to study the α -relaxation of high conductive polymers. For example it was not possible to obtain the dielectric α -relaxation parameters for PU60 because of its overlapping with conductive effects. In addition it was found that PU88 has an almost constant shear modulus and low mechanical losses around room temperature.

Interestingly, the response time does not depend on mechanical or dielectric α relaxations as expected. It seems to be directly linked to the space charge diffusion (leading to the Maxwell-Wagner-Sillars or MWS phenomenon). This requires further experimental data and theoretical analyses, which will be performed later on.

Larger M_{33} coefficients have been obtained for PU88 and PU75 compared to PU60 ones. This may be due to the fact that at increasing HS content, the microstructure may no more be of matrix-inclusions type, but starts to become co-continuous, which in turn leads to a higher Young modulus and thus to a smaller strain.

For actuation applications, an intense electrostriction is sought, but the device has to be stable over the frequency and the temperature of operative range, have a quick response time, and low mechanical and electrical losses. The coefficients M_{33} of PU88 and PU75 are very close to each other. Taking into account the fact that PU88 exhibits low mechanical and dielectric losses in the largest range of frequencies and of temperature around room temperature, this polymer is the best candidate for actuation applications.

Acknowledgments

The author acknowledges the financial support of the French Agence Nationale de la Recherche (ANR), under grant NAPOLECO (ANR- 2010-INTB-910-01).

References

- [1] Cathleen Thiele, Raghu DAS, Electroactive Polymers and Devices 2013-2018: Forecasts, Technologies, Players, Dielectric elastomers, electronic & ionic EAPs and their applications
- [2] Bar-Cohen Y. Electroactive Polymer (EAP) Actuators as Artificial Muscles (Reality, Potential and Challenges). SPIE Press. Bellingham. 2004.
- [3] Watanabe M, Hirai T, Suzuki M, Yoichi M. Electric conduction in bending electrostriction of polyurethanes. Applied physics letters, 1999, 74, 2717
- [4] Guiffard B, Seveyrat L, Sebald G, Guyomar D. Enhanced electric field induced strain in non percolative carbon nanopowder /polyurethane composites. J. of Phys. D: Appl. Phys. 2006; 3039- 3053.

- [5] Irusta L, Fernandez-Berridi; M J. Photooxidative behaviour of segmented aliphatic polyurethanes. *Polym. Deg. & Stab.*1999; 63: 113-119.
- [6] Putson C, Lebrun. L, Guyomar D, Muensit N, Cottinet P-J, Seveyrat L, Guiffard B. Effects of copper filler sizes on the dielectric properties and the energy harvesting capability of nonpercolated polyurethane composites. *J. Appl. Phys.* 2011; 109:024104.
- [7] Zhang Q M, Su J, Kim C H. An experimental investigation of electromechanical responses in a polyurethane elastomer. *J. Appl. Phys.* 1997; 81: 2770-2776. DOI: 10.1063/1.363981.
- [8] Guillot F M, Balizer E. Electrostrictive effect in polyurethanes. *J. Appl. Polym. Sci.* 2003; 89: 399-404. DOI: 10.1002/app.12096.
- [9] Pichon P G, David L, Mechin F, Sautereau H. Morphologies of Cross-Linked Segmented Polyurethanes. Evolution during Maturation and Consequences on Elastic Properties and Thermal Compressive Fatigue. *Macromolecules.*2010; 43: 1888–1900. DOI: 10.1021/ma901602y
- [10] Elwell. M. J, Mortimer. S, Ryan. A. J. A synchrotron SAXS study of structure development kinetics during the reactive processing of flexible polyurethane foam. *Macromolecules*, 1994; 27: 5428-5439. DOI: 10.1021/ma00097a024.
- [11] Li. Y, Ren. Z, Zhao. M, Yang. H, Chu. B. Multiphase structure of segmented polyurethanes: effects of hard-segment flexibility. *Macromolecules.* 1993; 26: 612-622. DOI:10.1021/ma00056a010
- [12] Diguët. G, Bogner. A, Chenal. J-M, Cavaillé. J-Y. Physical modeling of the electromechanical behavior of polar heterogeneous polymers. *J. Appl. Phys.* 2012, 112 :114905-1-8.
- [13] M. H. Jomaa, L. Seveyrat, L. Lebrun, K. Masenelli-Varlot, J.Y. Cavaillé. Dielectric properties of segmented polyurethanes for electromechanical applications. 2015, *Polymer*, 2015, 63, 214-221, doi:10.1016/j.polymer.2015.03.008.
- [14] Petrovic Z S, Ferguson J. Polyurethane elastomers. *Prog. Polym. Sci.* 1991;16: 695-836.
- [15] Laity P R, Taylor J E, Wong S S, Khunkamchoo P, Norris K, Cable M, Andrews G T, Johnson A F, Cameron R E. A review of small-angle scattering models of random segmented poly(ether-urethane) copolymers. *Polymer.* 2004; 45: 7273-7091. DOI: 10.1016/j.polymer.2004.08.033.
- [16] Eun A K, Han S L. Effect of molecular shape of diisocyanate units on the microscopic/macrosopic phase separation structure of polyurethanes. *J. Polym Sci, Polym Phys.* 2011; 49: 890–897. DOI: 10.1002/polb.22264.
- [17] Yang C Z, Grasel TG, Bell J L, Register R A, Cooper S L. Carboxylate containing chain-extended polyurethanes. *J. Polym. Sci. Part B Polym. Phys.* 1991; 28: 581–588. DOI: 10.1002/polb.1991.090290507.
- [18] Etienne S, Cavaillé. J-Y, Perez. J, Point. R, Salvia. M. Automatic system for analysis of micromechanical properties. *Rev. Sci. Instrum.* 1982 ; 53: 1261. DOI : 10.1063/1.1137153
- [19] Wongtimnoi. K, "Polyuréthanes électrostrictifs et Nanocomposites: Caractérisation et Analyse des mécanismes de couplages électromécaniques", PhD thesis, 2011, INSA-Lyon, France.
- [20] Koberstein J T, Russell T P. Simultaneous SAXS-DSC Study of Multiple Endothermic Behavior in Polyether-based Polyurethane Block Copolymers. *Macromolecules.* 1986; 19: 714-720. DOI: 10.1021/ma00157a039.
- [21] Lapprand A, Mechin F, Pascault J P. Synthesis and properties of self-crosslinkable thermoplastic polyurethanes. *J. Appl. Polym. Sci* 2007; 105: 99-113. DOI: 10.1002/app.26086.
- [22] Sigamani. N. S. Characterization of Polyurethane at Multiple Scales for Erosion Mechanisms Under Sand Particle Impact. PhD thesis, 2010, Texas A&M University.
- [23] Kojio. K, Nakashima. K, Furukawa. M. Microphase-separated structure and mechanical properties of norbornane diisocyanate-based polyurethanes. *Polymer.* 2007; 48: 997–1004. DOI: 10.1016/j.polymer.2006.12.057
- [24] Joseph D. Menczel (Ed), R. Bruce Prime (Ed). *Thermal Analysis of Polymers: Fundamentals and Applications.* John Wiley & Sons. 2009.

- [25] Volynskii A L, Bakeev N F. Structural Aspects of Inelastic Strain in Glassy Polymers. *Polym. Sci. C.* 2005; 47: 1332-1367.
- [26] Cavaille, J.Y., J. Perez, and G.P. Johari, Molecular Theory for the Rheology of Glasses and Polymers. *Physical Review B*, 1989. 39(4): p. 2411-2422.
- [27] MacAloney. N, Bujanda. A, Jensen. R, Goulbourne. N. Viscoelastic Characterization of Aliphatic Polyurethane Interlayers. U.S. Army Research Laboratory. ATTN: AMSRD-ARL-WM-MA.2007
- [28] Ali E. Akinay, Witold B, Victor M. Castana, Robert M, Przemylaw O. Time-temperature correspondence prediction of stress relaxation of polymeric materials from a minimum of data. *Polymer*, 2002; 3593-3600
- [29] Giovanni P, Otakar J-V, Dario B, Jiri S, Ludovit Z. Dynamic Master Curves of Polymer Modified Asphalt from Three Different Geometries. *Appl. Rheol.* 2003; 13: 118-124
- [30] Lunkenheimer. P, Sehneider. V, Brand. R, Loid. A. Glassy dynamics. *Contemporary Physics.* 2000;41:15-36.
- [31] Vatalis. A.S, Delides. C.G, Georgoussis G, Kyritsis. A, Grigorieva. O.P, Sergeeva. L.M., Brovko. A.A, Zimich. O.N, Shtompel. V.I, Neagud. E, Pissis. P. Characterization of thermoplastic interpenetration polymer networks by various thermal analysis techniques. *Thermochimica Acta.* 2001; 371: 87±93
- [32] Haibao Lu, Wei Min Huang. On the origin of the Vogel–Fulcher–Tammann law in the thermo-responsive shape memory effect of amorphous polymers. *Smart Mater. Struct.* 2013; 22: 105021.
- [33] Wongtimnoi K , Guiffard B , Bogner-Van de Moortèle A , Seveyrat L, Cavaille J-Y. Electrostrictive thermoplastic polyurethane-based nanocomposites filled with carboxyl-functionalized multi-walled carbon nanotubes (MWCNT-COOH): Properties and improvement of electromechanical activity. *Composites Science and Technology* 2013; 85: 23–28.
- [34] Diaconu I, Dorohoi D. Properties of polyurethane thin films, *journal of optoelectronics and advanced Materials.* 2005; 7: 921-924.
- [35] Guyomar. D, Cottinet. P-J, Lebrun. L, Putson. C, Yuse. K, Kanda. M, Nishi. Y. The compressive electrical field electrostrictive coefficient M_{33} of electroactive polymer composites and its saturation versus electrical field, polymer thickness, frequency, and fillers. *Polym. Adv. Technol.* 2012; 23: 946-950.

Chapter 5: Modeling of segmented pure polyurethane electrostriction behaviors based on their nanostructural properties

M. H. Jomaa^{1,2*}, K. Masenelli-Varlot¹, G. Diguët³, L. Seveyrat², L. Lebrun², K. Wongtimnoi¹, C. Vechambre¹, J. M. Chenal¹, J.Y. Cavailé¹.

¹ Université de Lyon, INSA-Lyon, CNRS, MATEIS, F-69621 Villeurbanne Cedex, France

² Université de Lyon, INSA-Lyon, LGEF, F-69621 Villeurbanne Cedex, France

³ Institut Néel (CNRS & UJF) - Building 25 rue des Martyrs BP166 - 38042 Grenoble France

* Author to whom all correspondence should be addressed

Abstract

Polyurethane (PU) exhibit very high electromechanical activity, and has a great interest for a wide range of transducer and actuator applications. It has been recently pointed out that this strong electrostriction may result from the phase separation. In the present work, a model taking into account the PU nanostructure is presented. In order to validate this model, three PUs of similar compositions but different soft segment fractions have been characterized by DSC, TEM, AFM and SAXS and their electrostriction properties have been measured. When taking into account the diameter of the hard domains (HD) and the HD-HD distance, it is found that the model proposed well reproduces the experimental electrostriction properties of these phase-separated PUs.

Keywords: Polyurethane, electrostriction, modeling, microstructure.

Nomenclature section for parameter used in the model:

a : radius of sphere (HD as sphere)	A : dielectric contrast
D : half-distance between two spheres	f_v : body force
V : volume	F : total force
A_S : surface	σ : stress
E : electric field	S : deformation
E_0 : applied electric field	S_{outer} : outer deformation
E_{loc} : local effective field	S_{inner} : inner deformation
P : material electric polarization	S_{SD} : soft domain deformation
χ : electric susceptibility	S_{theo} : global deformation
ϵ_{HD} : permittivity of hard domains	Y_{SD} : Young modulus of SD
ϵ_{SD} : permittivity of soft domains	Φ_{SD} : fraction of soft domains
ϵ_0 : vacuum permittivity	Φ_{HD} : fraction of hard domains

1 Introduction

Electroactive Polymers (EAP) are a relatively new class of "smart material" that deform in the presence of an applied electric field [1], meaning they can convert electrical energy into mechanical energy [2]. EAPs can be used in various applications including actuators and sensors, biomimetics, robotics, energy harvesting and storage devices, among others [2, 3]. Polyurethanes have demonstrated their ability to convert electrical energy into mechanical energy and vice versa. Furthermore, these materials are lightweight, very flexible, biocompatible and tissue compatible, highly resistant to abrasion; they present low manufacturing costs, and can be readily molded into any desirable shape [4]. Segmented polyurethane elastomers are block copolymers with alternating soft and hard blocks. In the present study the hard segments (HS) are composed of 4,4'-methylene-bis-(phenyl-isocyanate) (MDI) and 1,4-butanediol (BDO)-and Poly(tetramethylene-oxide) is used as soft segments (SSs). The soft segments originate from the polyol and impart elastomeric characteristics to the polymeric material; the hard segments contain the highly polar urethane linkages and act as high modulus "fillers". Due to structural differences/incompatibility, microphases or domains can be formed from the respective hard and soft segments. Hard domains (HDs) - domains rich in HSs - play the role of physical crosslinks and act as high modulus fillers, whereas soft domains (SDs) - domains rich in SSs - provides extensibility [5,6]. The morphology of segmented PUs depends on the structure and relative amounts of these soft and hard domains and their ordering [7] (as well as from the form and the size distribution of HDs).

It is well documented that the properties and the performances of polyurethanes are strongly dependent on the degree of microphase separation and on the ensuing morphologies [6, 8]. It has been recently pointed out that the strong electrostriction properties of pure segmented PU can be explained by the phase separation into HDs and SDs with high and weak dielectric constants, respectively. Indeed, phase separation leads to heterogeneities of both elastic and dielectric constants and to electric field gradients, which makes the SDs shrink and induces a compression of the whole material [9]. Nevertheless, this model is based on several microstructural parameters, such as the HD diameter, the HD-SD distance and the weight fractions of HDs and SDs. To our knowledge, the values of these parameters are still missing in the literature.

The purpose of this work is to investigate how the recent model can explain the electrostriction properties of segmented pure PUs. Since microstructural parameters are entry parameters of this model, an extensive microstructural characterization will be carried out. Three PUs with different weight fractions of HSs and SSs will be studied to check the robustness of the model.

2 Material and methods

Three different types of aromatic polyether-based thermoplastic PU are commercially available and were provided by the same company, Lubrizol, with different weight fractions of HSs and SSs. In the following, PU60, PU75 and PU88 respectively refer to Estane® ETE 60DT3 NAT022, Estane® X4977 NAT 039 and Estane® 58888 NAT021. From the supplier data sheet, it is mentioned that these PUs were synthesized by the same industrial process from the same initial chemical components. In addition to the different weight fractions of HSs and SSs, they

also exhibit different molecular weights of SSs: 1000 (g/mol) for PU88 and PU60, and 2000 (g/mol) for PU75.

The polymer films were prepared by following a solution casting method. Before use, the PU granules were heated at 350 K for 3 hours. Then they were dissolved in N,N-dimethylformamide (DMF, Sigma-Aldrich D158550, 99%) with a ratio of 25 wt.% of PU into DMF. The solution was heated at 350 K for 4 hours under mechanical agitation, until a homogeneous and viscous solution was obtained. Afterwards, this solution was casted on glass plates with an Elcometer 3700 doctor blade film applicator, put in an oven at 335 K for one day. A second heating treatment at $T = 400$ K for 3 hours was then performed to eliminate any residual solvent.

The microstructural morphology of segmented pure PU was studied by Differential Scanning Calorimetry (Setaram, DSC 131 Evo) under nitrogen flow ($P = 1.5$ bar). Samples of 20 mg were cooled to 140 K under liquid nitrogen and then heated to 480 K before being cooled to room temperature. The heating and cooling rates were set at 10 K / min.

Transmission Electron Microscopy (TEM) was used to investigate the phase separation into HDs and SDs but for that purpose, the samples had to be stained prior to the observation. The choice of the staining agent used in a given polymer system is guided largely by empirical success [10]. OsO_4 and RuO_4 are probably among the best known staining agents and are routinely used to stain polymers. OsO_4 is believed to act as a covalent crosslinker between unsaturated carbon double bonds [11]. RuO_4 is mainly used to differentially label aromatic moieties from aliphatic ones [12, 13]. However due to similar chemical structures between HSs and SSs in the PUs studied here, a significant differential staining could not be obtained with OsO_4 or RuO_4 alone. Indeed for each PU type, a piece of film was stained in a 4% aqueous solution of OsO_4 for 24 hours. After rinsing with ethanol, the films of PU60 and PU75 turned to colors which clearly indicates incomplete staining see Fig. 1. RuO_4 led to similar colors on the PUs studied here (not shown). Thus, a protocol similar to that of Janina Foks [14] was used, since they demonstrated that it was possible to localize the HDs of pure PU by using a double staining technique based on OsO_4 and formaldehyde. By adding OsO_4 , Os stained double bonds on both segments as a first step. As a second step by adding formaldehyde and OsO_4 , formaldehyde opened the N-H bonds and made it accessible for osmium (the N-H bond exists only in the HS).

For each PU type, a piece of film was stained in a 4% aqueous solution of OsO_4 for 24 hours. After rinsing with ethanol, the films were stained in a 50:50 aqueous solution of OsO_4 and HCHO_4 (initial concentrations of 4% and 37% in water, respectively) for 24 hours [14]. After a second rinsing with ethanol, the films appeared to be completely black, which is an indication of a successful staining step (see Fig.1). Thus, the films were embedded in an Epofix® resin and ultrathin sections were obtained by cryoultramicrotomy with a Reichert Ultracut S. The sample temperature was set to 200 K and the 35° diamond knife speed to 1 mm/s.

TEM observations were carried out at acceleration voltage of 200 KV with a JEOL 2010F microscope, operating at 200kV. Bright field images were recorded with a Gatan Orius 200 camera. Measurements were performed manually using ImageJ on at least 90 objects.

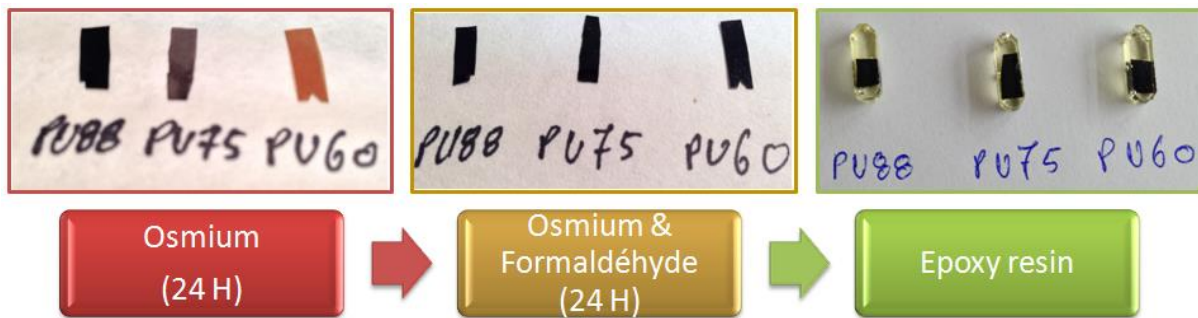


Fig. 1 Double staining protocol of segmented pure polyurethane.

Morphological observations of the HDs and SDs were performed by Atomic Force Microscopy (AFM) Nanoscope 5 (VEECO). Thin polymer films of each PU were deposited on a glass plate and dried for one night prior to imaging. Tapping mode phase images of sample surfaces were made using NanoProbe tips PPP-NCL (Nanosensor) for PU88 with a frequency of 153.2 kHz. PU75 and PU60 were analyzed with a NanoProbe tip SSS-NCH (Nanosensor) at a frequency of 272 kHz.

Small Angle X-ray Scattering (SAXS) was used to investigate the HD distribution. For that purpose, stacks composed of several layers of films were analyzed in transmission mode in two different directions, see Fig. 2. Patterns were acquired using a RU-300 generator equipped with a copper anode ($\lambda_{\text{Cu-K}\alpha} = 1.54 \text{ \AA}$). The 1-2 mm thick stack was placed at a distance of 60 cm from the 2D CCD detector.

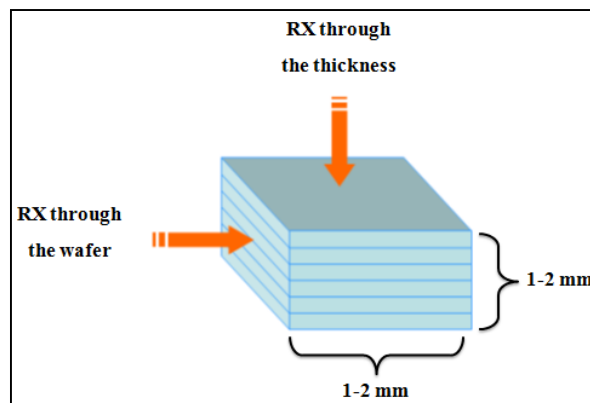


Fig. 2 Set-up used for SAXS characterisations. The samples are stacks composed of several layers of the films. Two different analysis directions are indicated.

The field-induced thickness strain S_{exp} was measured on circular sample (25mm of diameter) with a homemade setup based on a double-beam laser interferometer measurement (Agilent 10889B) [15, 16, 17]. Samples were placed between two cylindrical brass masses acting as conductive electrodes. A mirror was placed on the upper electrode to reflect the laser beam. A bipolar electric field was supplied by a high voltage amplifier (Trek10/10B) driven with a function generator (Agilent 33250A). Measurements were made at room temperature .

3 Results and discussion

3.1 Modeling

Guillot *et al.* explained from macroscopic level, that there was an empirical relationship between the electrostrictive coefficient, the dielectric constant and the compliance coefficient [18]. Recently, Diguët *et al.* pointed out that the phase separation into HDs with high dielectric constant and SDs with weak dielectric constant can result into the strong electrostriction properties of pure segmented PU. This, in turn, leads to heterogeneities of both elastic and dielectric constants and to electric field gradients, which makes the SDs shrink and the whole material compress [9]. In this work, Diguët's model is extended to take into account morphological parameters such as the HD diameter, the HD-SD distance and the HS weight fraction.

The strain is calculated from the Z-component of electric body force, created by HD taken as a sphere with radius a into the surrounding SD. For a linear polarized dielectric medium in presence of an electric field E , the Z-component of electric body force is:

$$\vec{f}_{v_z} = \left[-\frac{d}{dz} \left(-\vec{P} \cdot \vec{E} \right) \right] \vec{u}_z = \left[\frac{d}{dz} \left(\varepsilon_0 \chi \vec{E} \cdot \vec{E} \right) \right] \vec{u}_z = (\varepsilon_{SD} - \varepsilon_0) \frac{dE^2}{dz} \vec{u}_z \quad (1)$$

Where ε_{SD} and χ are the dielectric constant and the electric susceptibility of the material respectively, ε_0 is vacuum permittivity and P is the material electric polarization.

Within a volume V delimited by a surface A_S , the total force F , the body force f_v and the stress σ are related as:

$$\vec{F} = \int_V \vec{f}_v dV = \int_{A_S} \vec{\sigma} \cdot \vec{n} dA_S \quad (2)$$

So, the force created at the distance $z \geq a$ from the centre of the sphere is obtained by summing contributions from the edge of a HD sphere:

$$\int_{A_S} \int_a^z (\varepsilon_{SD} - \varepsilon_0) \frac{dE^2}{dz} \vec{u}_z dz dA_S = \int_{A_S} (\varepsilon_{SD} - \varepsilon_0) (E^2(z) - E^2(a)) dA_S \quad (3)$$

Identifying with (2), the stress is extracted from (3) and the deformation S of the soft domain at the distance $z \geq a$ from the centre of the HD sphere is then obtained by dividing the stress by the SD Young modulus Y_{SD} :

$$S(z) = \frac{(\varepsilon_{SD} - \varepsilon_0) (E^2(z) - E^2(a))}{Y_{SD}} \quad (4)$$

It can be seen that the strain is proportional to the difference of the square of the fields at the edge of the sphere and at the considered point. Consequently, the electric field inside the material has to be calculated. The applied electric field E_0 is considered to be directed along the

u_z direction. Using boundaries conditions and considering only the Z-component (1D), the electric field created out ($z \geq a$) of the dielectric sphere, can be expressed as:

$$\vec{E}(z) = E_0 \left[1 - 2A \left(\frac{a}{|z|} \right)^3 \right] \vec{u}_z \quad (5)$$

With A the so-called dielectric contrast defined by:

$$A = \frac{\epsilon_{SD} - \epsilon_{HD}}{2\epsilon_{SD} + \epsilon_{HD}} \quad (6)$$

The constant A varies, depending on the HD sphere and its SD surrounding dielectric constants, between -1 and 0.5 for $\epsilon_{SD}/\epsilon_{HD} \rightarrow 0$ and $\epsilon_{HD}/\epsilon_{SD} \rightarrow 0$ respectively.

Considering two spheres weakly interacting spaced by a distance 2D, i.e. one placed at $z=-D$ and the second one placed at $z=+D$, the electric field is expressed as the superposition of the fields created by each of the sphere:

$$\vec{E}(z) = \left[E_0 - 2AE_0 \left(\frac{a}{|z-D|} \right)^3 - 2AE_0 \left(\frac{a}{|z+D|} \right)^3 \right] \vec{u}_z \quad (7)$$

At the middle of the gap ($z=0$), the electric field is:

$$\vec{E}(z=0) = E_0 \left[1 - 4A \left(\frac{a}{|D|} \right)^3 \right] \vec{u}_z \quad (8)$$

And far away from both spheres ($z=\pm\infty$), the electric field is:

$$\vec{E}(z = \pm\infty) = \vec{E}_0 \quad (9)$$

At the sphere interfaces ($|z|=D \pm a$), the electric field is:

$$\vec{E}(|z|=D \pm a) = E_0 \left[1 - 2A \left(1 + \left(\frac{1}{2\frac{D}{a} \pm 1} \right)^3 \right) \right] \vec{u}_z \quad (10)$$

As a quick estimation, with $A=-3/4$ and $D \gg a$, equations (8) and (10) give $E(0)=E_0$ and $E(|z|=D \pm a)=2.5E_0$ which can be seen in Fig. 3; or to be more precise, with $A=-3/4$ and $D=4a$, $E(0)=1.04E_0$ which can be seen in the inset of the figure below.

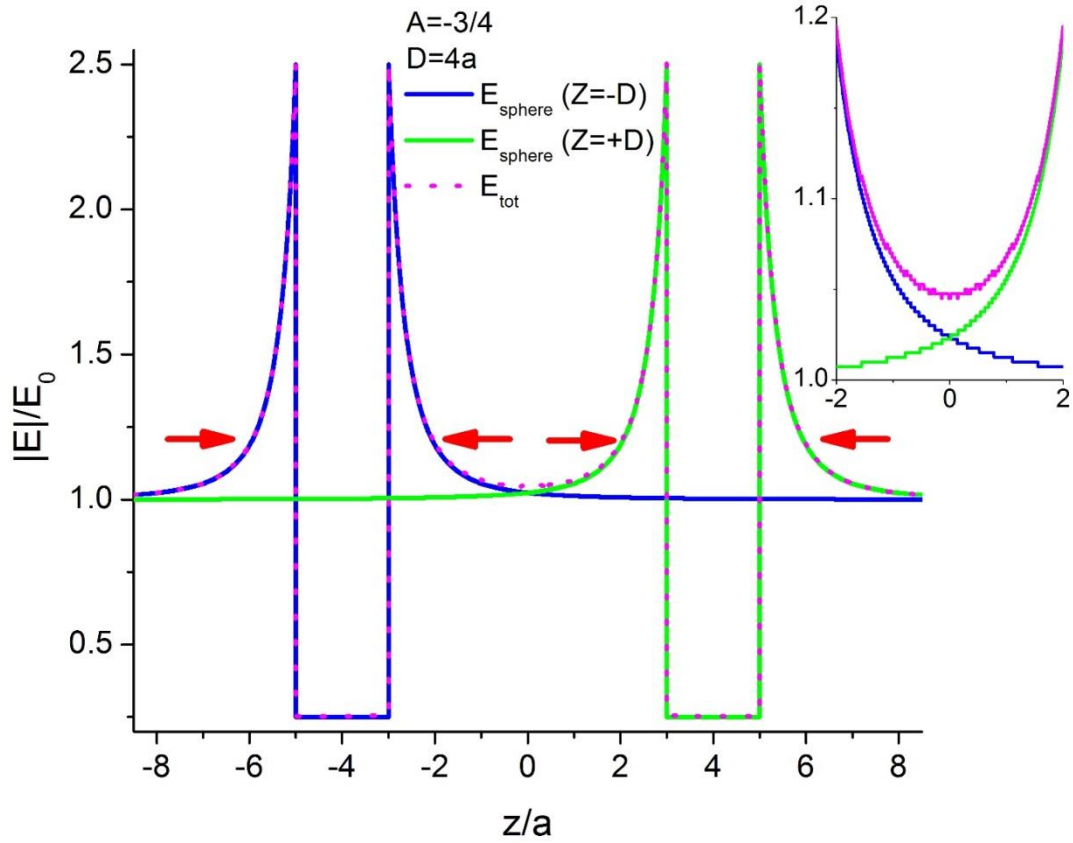


Fig. 3 : Value of the electric field calculated from equations (6) to (9), with a the sphere radius, the half distance between both spheres D equal to $4a$ and the dielectric contrast A equal to $-3/4$. The inset shows a magnified view of the electric field variations in the gap between both spheres.

As seen in Fig.3, there are 4 regions of SD deformation which can be reduced to 2 regions because of the symmetry; the region named below as ‘inner’ corresponded to the two deformations between the spheres whereas the region named below as ‘outer’ corresponded to the two deformations in the region apart the spheres.

The outer deformation can then be expressed from (4) with (9) and (10) as:

$$S_{outer} = 2 \frac{(\varepsilon_{SD} - \varepsilon_0)}{Y_{SD}} (E^2(|z| = \infty) - E^2(|z| = D + a)) \quad (11)$$

$$S_{outer} = K \left[1 - \left[1 - 2A \left(1 + \left(\frac{1}{2\frac{D}{a} + 1} \right)^3 \right) \right]^2 \right] \vec{u}_z \quad (12)$$

where $K = 2 \frac{(\varepsilon_{SD} - \varepsilon_0)}{Y_{SD}} E_{loc}^2$,

And the inner deformation is expressed from (4) with (8) and (10) as:

$$S_{inner} = 2 \frac{(\varepsilon_{SD} - \varepsilon_0)}{Y_{SD}} (E^2(z=0) - E^2(|z|=D-a)) \quad (13)$$

$$S_{inner} = K \left[\left[1 - 4A \left(\frac{a}{|D|} \right)^3 \right]^2 - \left[1 - 2A \left(1 + \left(\frac{1}{2 \frac{D}{a} - 1} \right)^3 \right) \right]^2 \right] \vec{u}_z \quad (14)$$

For a long chain of spheres, the outer contribution acts only at the ends of the chain while the inner one acts at every gap between spheres. Hence, for long chain of spheres, the most contributive component is expected to be the inner contribution and outer contribution will be neglected below; i.e. the SD deformation $S_{SD} = S_{inner}$. In Fig.4, the curve of S_{SD} versus a/D is plotted.

The final strain, S_{theo} , is extrapolated as follow; adding more HD in the SD will increase the amount of deformation due to the SD, and setting a 1D fraction of HD ($\phi_{HD}=a/D$) then we can express the global deformation by:

$$S_{theo} = S_{SD} \phi_{HD} = S_{inner} \frac{a}{D} \quad (15)$$

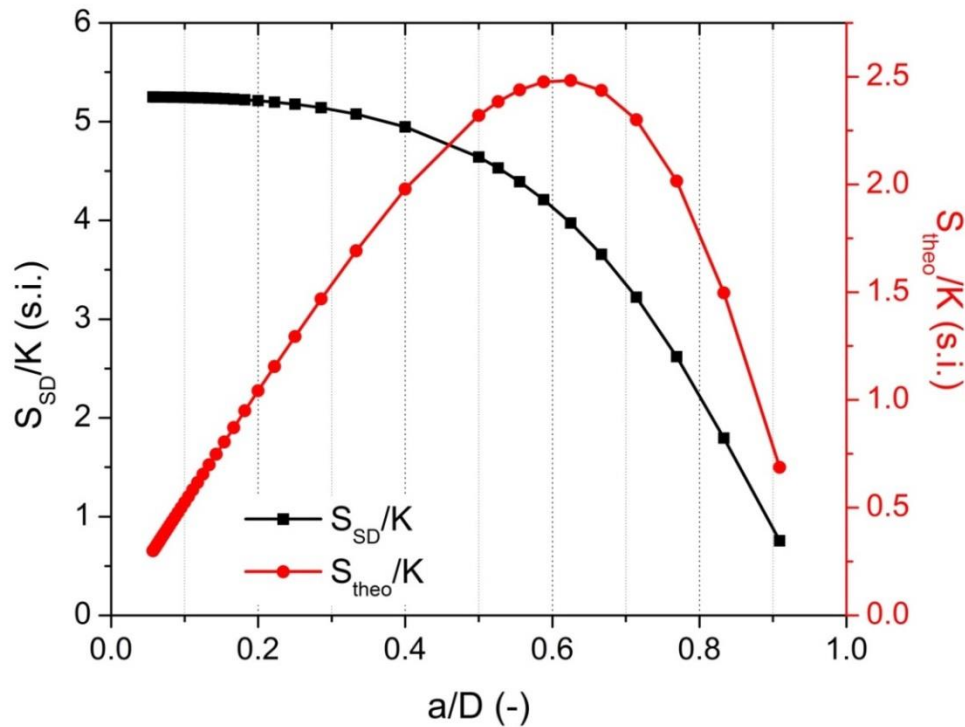


Fig. 4: calculated variations of the total strain -1D system- for different values of a (sphere diameter) and D (half-distance between two spheres). The dielectric contrast A was fixed to - $3/4$.

The variations of the total strain as a function of the morphological parameters a and D are shown in Fig. 4. It is noteworthy that the total strain is highly dependent on a/D . Thus, the

experimental measurement of such parameters – as well as the shape of the HD – is crucial to validate the model.

3.2 Experimental determination of the morphological parameters

3.2.1 Phase separation

The DSC thermograms presented in Fig. 5 and Fig. 6 were recorded in order to study the influence of the HS weight fraction as well as that of the phase separation on the crystalline morphology of the polyurethane host. The glass transition temperature for the soft segments (T_{gSD}), melting temperatures (T_{mIIHD} and T_{mIIIHD}), heat of fusion (ΔH_m), crystallization temperature (T_c) and heat of crystallization (ΔH_c) are summarized in Table 1.

Two temperature cycles were run in order to decouple the effects of the chemical structure and those due to the elaboration conditions. The first run reflects PU microstructures partly due to their thermal history whereas before the second run, the thermal history was erased through cooling from the viscous melt. It can be noticed that the thermal events observed during the first run are always more visible than during the second one, especially around the melting endotherms, (not shown). A thermal pretreatment is often used for polymers before DSC analysis. This pretreatment must be done at a temperature greater than 443-453 K and it is a problem because it can imply a possible degradation of PUs [19]. For this reason the results given are based on the analysis of the first run.

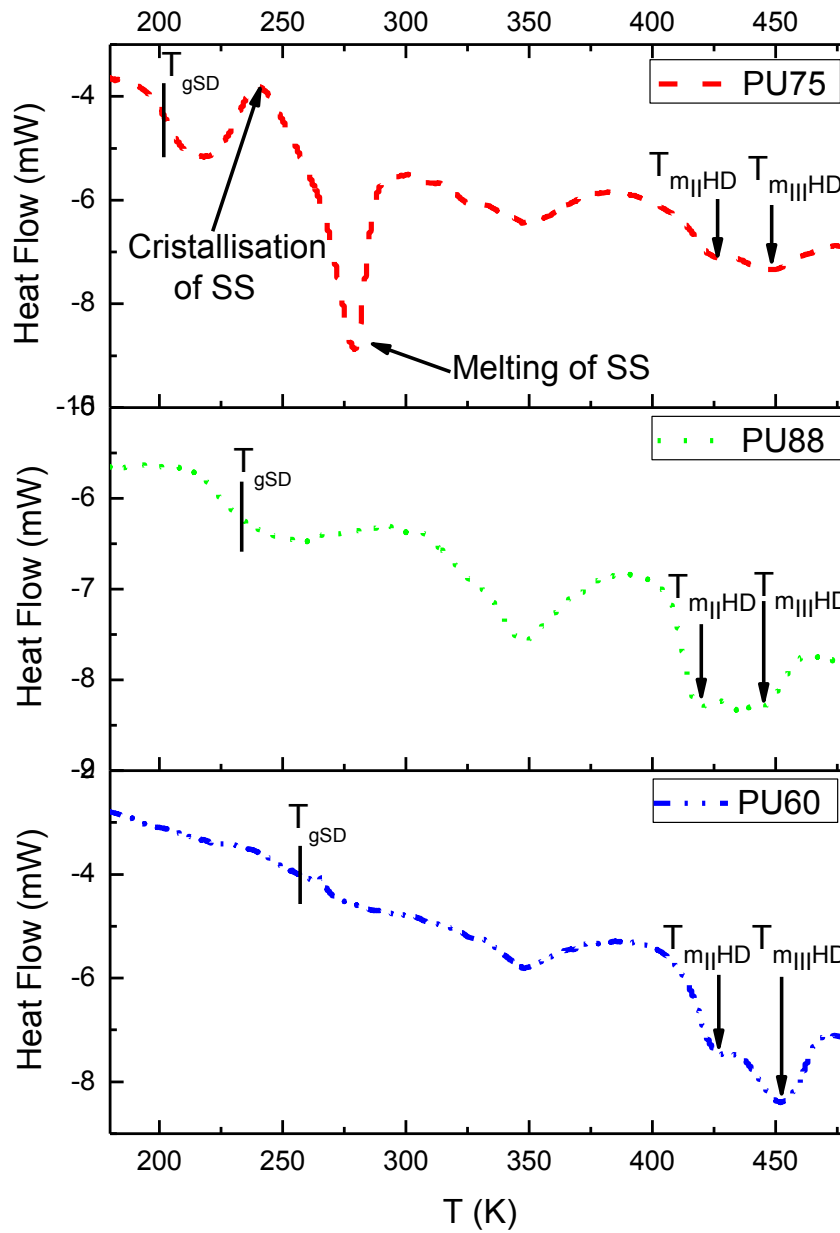


Fig. 5: DSC thermograms of the 3 pristine PUs upon heating (1st run)

Table 1. Parameters extracted from the DSC thermograms for the 3 PUs. T_{gSD} , $T_{m_{II}HD}$, $T_{m_{III}HD}$ are the glass transition temperatures related to the soft domains, and melting temperatures of hard domains, respectively. T_c is the crystallization temperature. ΔH_m and ΔH_c and the enthalpies of fusion and crystallization, respectively.

	T_{gSD} (K)	$T_{m_{II}HD}$ (K)	$T_{m_{III}HD}$ (K)	ΔH_m (J/g)	T_c (K)	ΔH_c (J/g)
PU75	205	425	447	11	285	-17
PU88	234	418	443	12	361	-8
PU60	259	427	451	16	423	-15

The glass transition temperature T_{gSD} and the two melting temperatures suggest that each one of the 3 studied PUs has two "mixed" phases, one rich in SSs (the SDs), the other one rich in HSs (the HDs). This is in agreement with the results found by Saiani *et al.* [20]. The elaboration conditions (thermal history, evaporation of DMF, etc...) are important factors that influence the overall morphology of PUs.

The first thermal phenomena - near 204 K, 228 K and 254 K for PU75, PU88 and PU60 respectively- can be related to the glass transition of soft domains (T_{gSD}). This value can give an estimation of the amount of hard segments (HS) dissolved in the SDs and as a consequence an indication of the "purity" of the soft phase [21, 22]. Indeed, an increase of the HS weight fraction led to a significant decrease of the T_{gSD} [23]. This suggests an increase of the SS fraction in the HS when increasing the SS fraction.

For PU75 a characteristic peak around 240 K seems to correspond to the crystallization of SSs then followed by melting around 280 K (see Fig. 5), which is confirmed by dynamic mechanical measurement on the same sample (not shown). This indicates that during elaboration, the cooling was rapid enough to prevent crystallisation of the SSs.

Moreover, a bimodal endothermic transition can be observed for the 3 PUs on the DSC thermograms around 425 and 450 K. From the literature, the existence of a bimodal peak could correspond to the fusion of crystalline hard segments with two different chain lengths [21, 24]. Alternatively, it can be related to rearrangements within the HDs and SDs, followed by the fusion of crystalline HDs [25, 19]. In the two cases an increase of these temperatures values or an increase of the bimodal endotherm enthalpy indicates a higher crystallinity. PU60 presents the highest ΔH_m value in agreement with the highest fraction of HD.

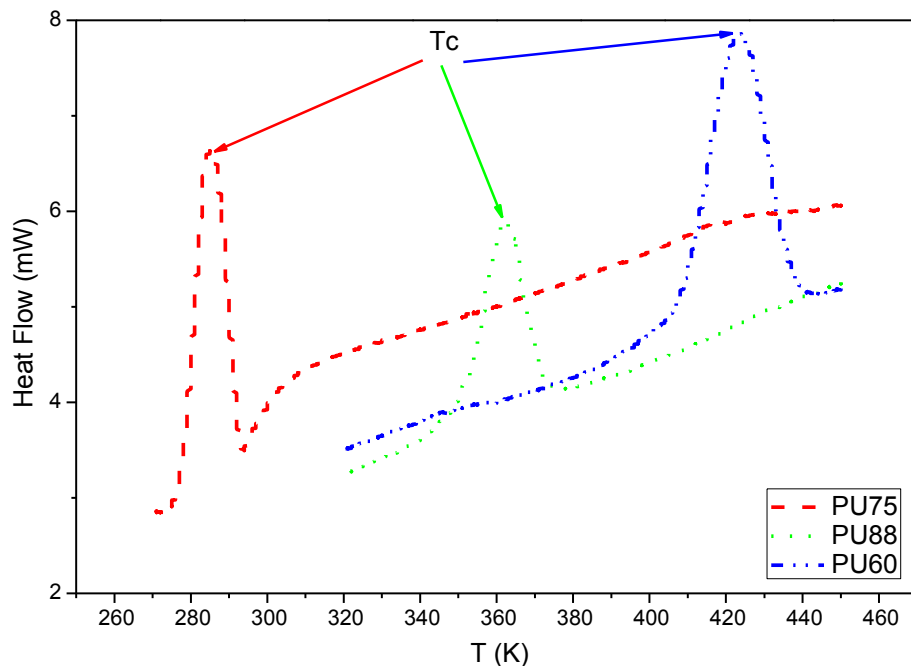


Fig. 6: DSC thermograms of the 3 pristine PUs upon cooling.

During cooling from the molten state to lower temperature (see Fig. 6), the 3 PUs exhibit a single exothermal crystallization event. This peak can be attributed to the crystallization of the HDs. Interestingly, the presence of one crystallization peak only does not seem to be compatible with 2 different HS lengths. This suggests that the bimodal peak observed upon heating was rather due to rearrangements of the HSs and SSs inside the HDs and SDs followed by melting of the HDs. The crystallization temperatures are highly dependent on the HS fraction (see Table 1). Indeed, they are equal to 285 K, 361 K and 423K for PU75, PU88 and PU60, respectively. It is thought that an increase of the HS fraction leads to an enrichment of the HS fraction within the HDs, which facilitates their crystallization.

3.2.2 Diameter distribution of HDs

AFM exhibits a very high resolution for imaging morphologies at the surfaces of segmented copolymers [26, 27]. In the tapping mode, the crystalline or hard domains in segmented copolymers can be imaged even at low hard-segment contents [28, 29]. Fig. 7 presents typical phase images obtained on PU75, PU88 and PU60 by AFM.

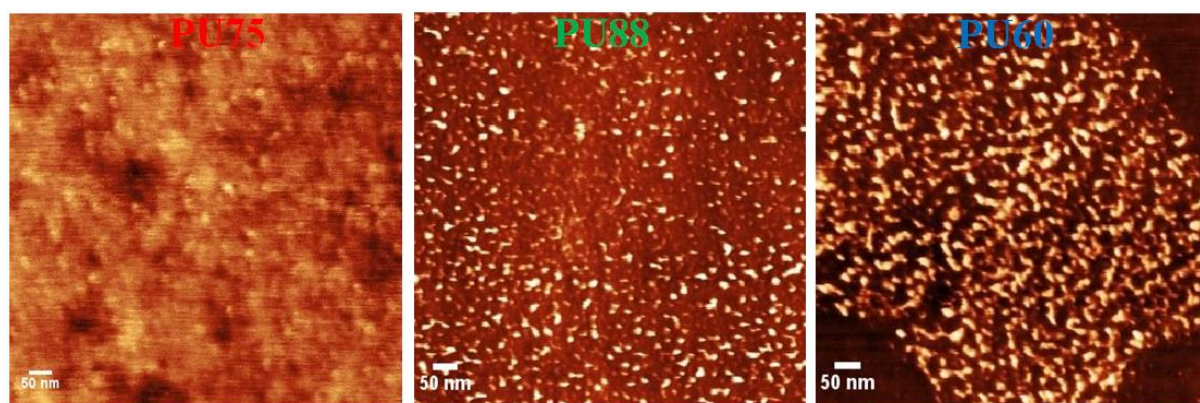


Fig. 7 AFM micrographs for PU75, PU88 and PU60 (phase images). The bright regions correspond to stiffer domains, i.e. the HDs.

These three segmented pure PUs exhibit two-phase morphologies, with bright stiff domains embedded in dark soft matrices [30, 31, 32]. This confirms the phase separation deduced from the DSC thermograms, the bright domains and the dark matrices being the HDs and the SDs, respectively. The HDs are found to be irregular in shape but mostly globular. A globular morphology is not always observed on polyurethane systems. Indeed, Elwell et al. evidenced percolated co-continuous microstructures [33]. Here, it is thought that the AFM images do not reveal co-continuous system. Indeed, the AFM images correspond to a planar section of the materials and in the case of co-continuity, elongated should lead to some elongated HDs. On the contrary, Schrader et al. [11] and Prici et al. [34] found a globular microstructure with a PU similar to the ones studied here, although with a different weight fraction of HS. This irregular shape and quite diffuse domain boundaries is thought to originate from polymer phase mixing in the form of hydrogen bonding between hard and soft regions of the polymer, which is commonly seen in polyether polyurethanes [30, 31].

The HD diameter distributions, measured from the AFM images, are presented in Fig. 9. The HD diameters mostly lie in the 6-14 nm range. It is noteworthy that the 3 PUs exhibit very

similar HD diameter distributions. It can thus be concluded that the HS fraction has a negligible effect on the HD diameter but rather influences the HS content within each phase (HD and SD). The distribution of HD diameters can result on the one hand from an aggregation of different numbers of HSs and on the other hand from the existence of HSs of different sequence lengths [11].

A similar study was conducted by TEM on stained samples, to confirm the phase separation and the HD diameter distribution. Fig. 8 displays a representative micrograph obtained on PU75.

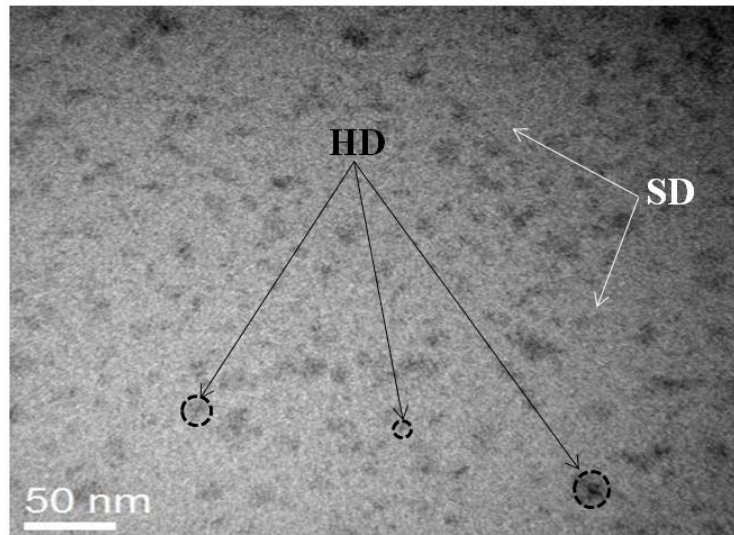


Fig. 8 TEM micrograph obtained on a stained sample of PU75.

Again, two phases can be distinguished, with dark domains embedded in a bright matrix. As the double-staining method is expected to stain preferentially the hard segments, the dark domains can be attributed to the HDs and the bright matrix to the SDs. At this point, it is important to recall that TEM provides a 2D projected view of a 3D volume. Thus, the HDs may appear in contact with each other in the TEM image whereas they are disconnected and at different heights in the volume. Nevertheless, the microstructure observed by TEM is consistent with a globular morphology, in agreement with the results from AFM and from the literature [34].

The HD diameter distributions measured on TEM micrographs for each PU are presented in Fig. 9. For PU75 and PU88, the distributions are very similar to those derived from AFM, whereas the distribution is shifted towards smaller values for PU60. This shift is thought to be non-significant, since the distances measured on TEM bright field images are known to depend on the defocus [35]. Thus, it can be concluded that AFM and TEM lead to similar HD diameter distributions, and that the average HD diameter does not depend on the HS weight fraction. For the electrostriction model, a value of 10 nm can reasonably be used.

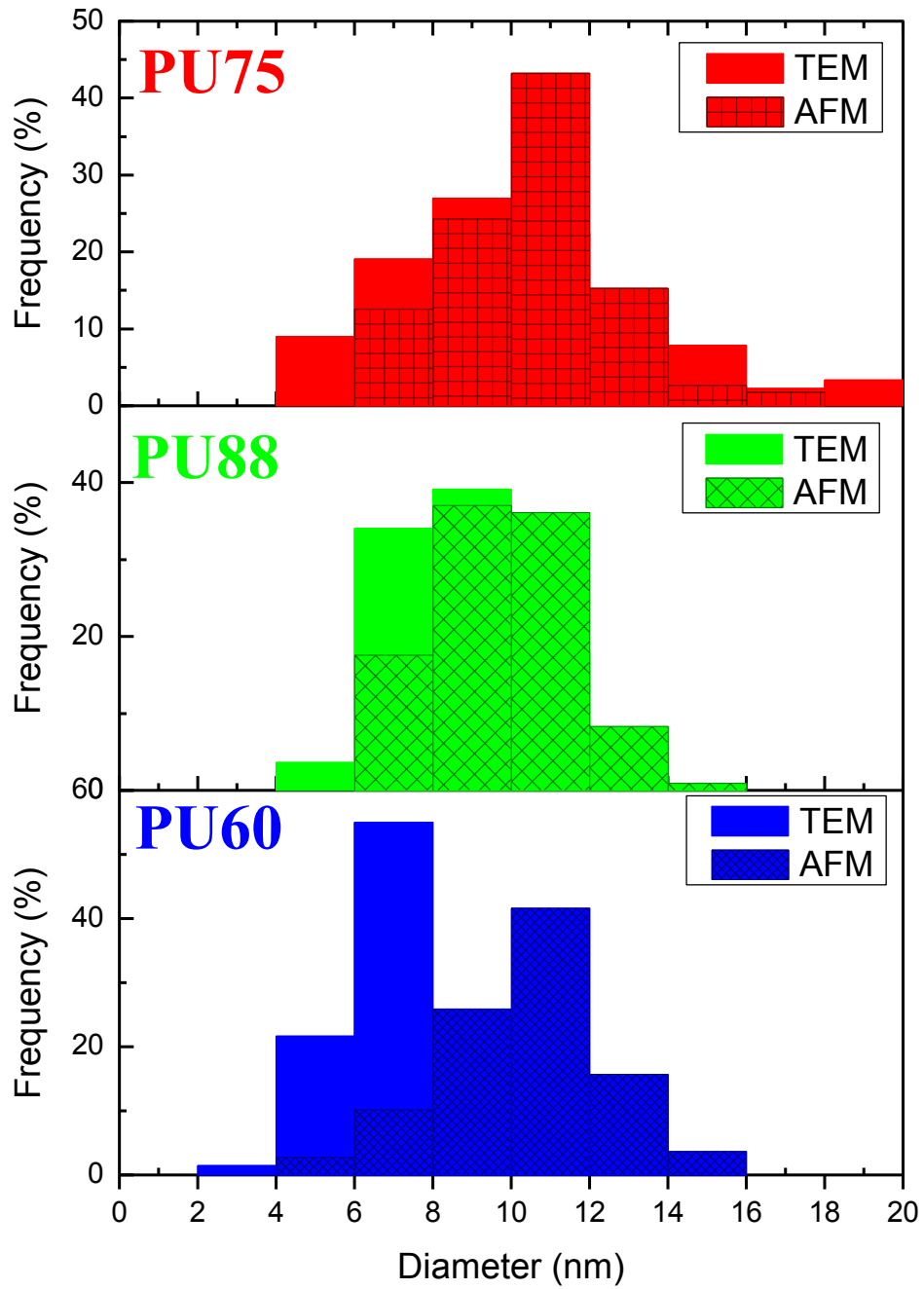


Fig. 9 Diameter distributions of hard domains of 3 PU using TEM and AFM microscopies.

3.2.3 Distance between HDs

SAXS measurements were performed on the 3 PUs in order to measure the mean distance between HDs. The 2D SAXS patterns are shown in Fig. 10. A diffuse ring can be seen for each PU in each configuration. As the samples are obviously isotropic, the intensities were plotted in function of the scattering vectors q by averaging the signals over the rings.

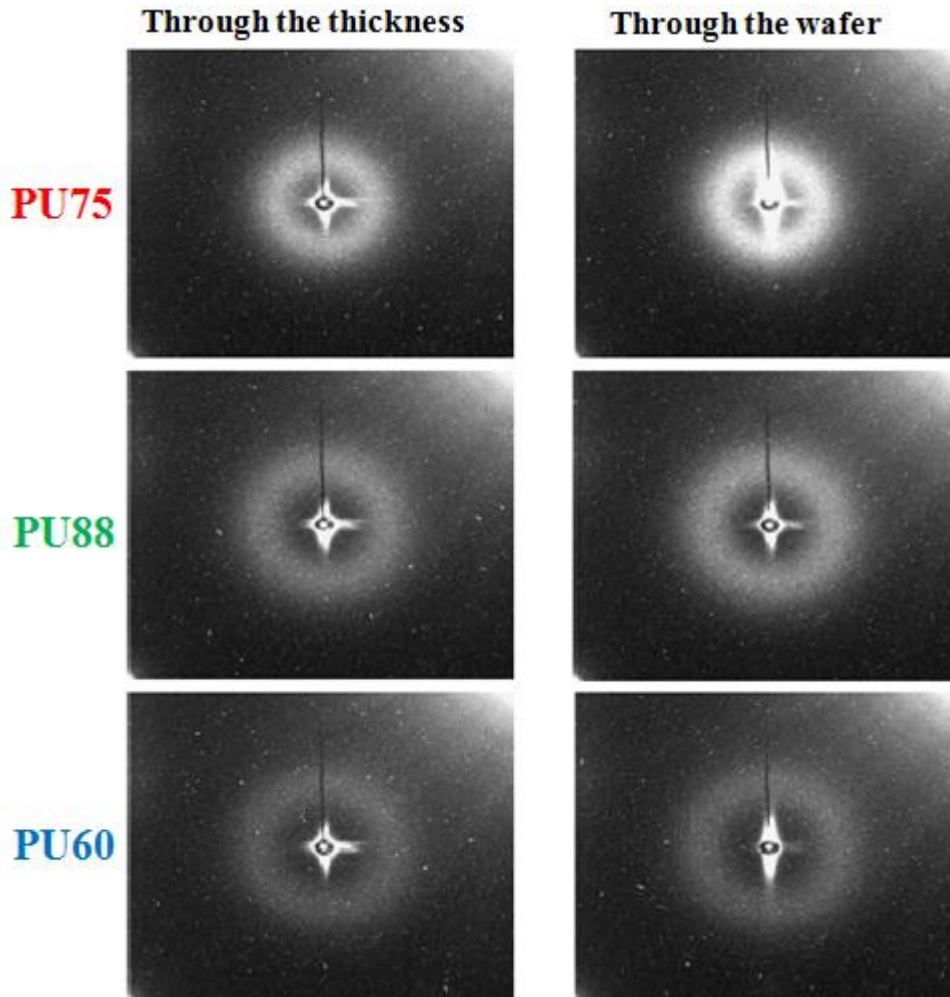


Fig. 10 SAXS 2D patterns obtained for the 3 PUs with two different orientations with respect to the X-ray beam.

The intensity variations in function of the scattering vector q are displayed in Fig. 11. The correlation bumps, corresponding to the rings observed on the 2D patterns, are clearly visible. From the previous analysis including DSC, AFM and TEM, the correlation bumps are expected to reflect the distribution of HDs in the film. The maxima of the correlation bumps can be used to determine a mean HD-HD distance, using Bragg relationship $d_i = \frac{2\pi}{q_{\max}}$ [36]. The values are reported in Table 2. Clearly, the average distances between HDs lie in the 10-20 nm. It decreases when increasing the HS fraction, as was qualitatively observed on the AFM images.

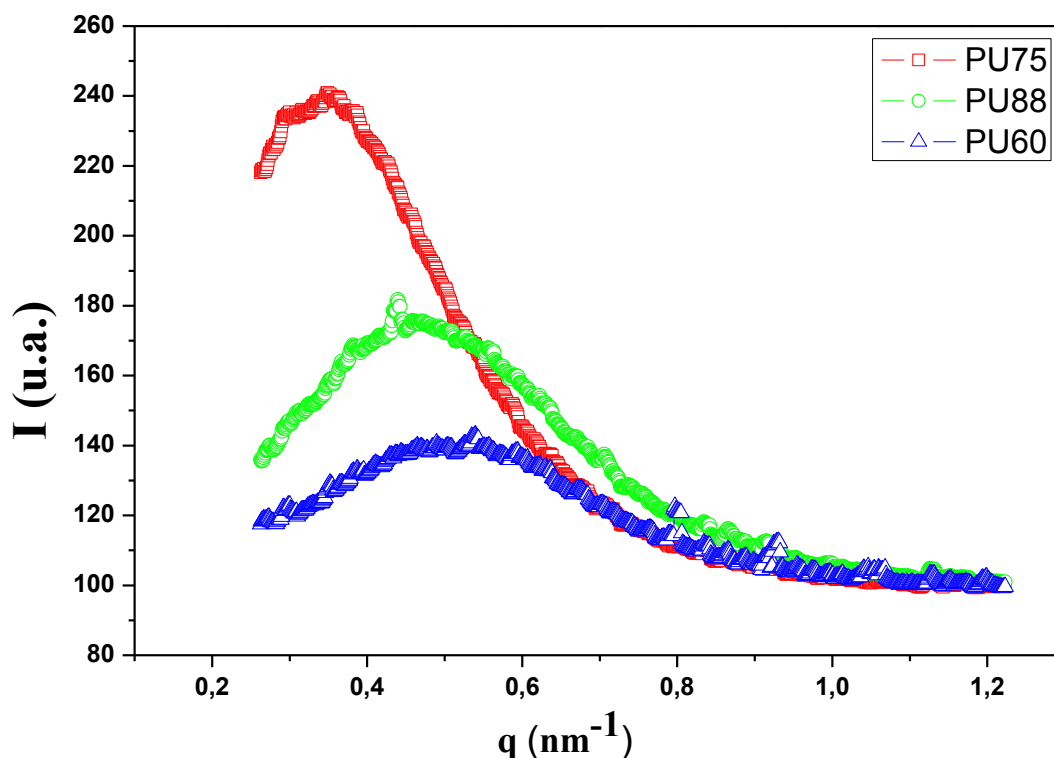


Fig. 11 Scattered intensity I in function of the norm of the scattering vector q , for the 3 PUs.

Table 2. Average distance between two HD domains for the 3 PUs [23].

	PU75	PU88	PU60
q_{\max} (nm⁻¹)	0.36	0.44	0.53
Average distance (nm)	17.5	14.3	11.8

3.3 Electrostriction

Based on the achieved parameters (diameter of HD -from TEM and AFM observation- and inter distance between HD and SD-from SAXS measurements) on the 3 pure segmented PUs, we calculated the inner and total deformations, either in 1D – considering only Z component, see equation (13)- or in 3D considering (X, Y, Z) components. The values are presented in Table 3. For each PU, the experimental value, S_{exp} , measured using a laser interferometer setup ($E_0=1(\text{V}/\mu\text{m})$), is given for comparison.

Table 3. Strain deformation of segmented PU; experimental & calculated values

	a	D	a/D	$S_{\text{theo}}/K(\text{S.I.})$	$S_{\text{exp}}(\%)$
PU60	10	12	0.83	1.50	0.5
PU88	10	14	0.72	2.30	1.19
PU75	10	17	0.59	2.48	1.73

S_{theo} results from our calculation based on the facts that i) the HD does not contribute to the deformation, ii) for a long chain of particles only the S_{inner} contribution should be taken into account (and not S_{outer}) and iii) because only S_{inner} is taken into account, it has to be weighted

by the fraction of HD to obtain S_{theo} . However, this model is suffering from the lack of knowledge on the intrinsic SD and HD properties, but we can assume that they have to be the same for the three PU. So, by dividing S_{theo} by K the deformation of each PU is divided by a constant. Thus, S_{theo}/K provides information solely due to the effect of "a/D". In Fig.4, it can be seen that PU75 has the a/D ratio the closest to the optimal around 0.62, allowing the maximal deformation according to our model. This shows the beneficence of our model in the comprehension of the polymer electrostriction. However, the experimental value of PU60 is relatively lower than expected; this can be explained by the fact that a 0.83 a/D ratio is high, which should increase interaction between HD spheres.

To determine the order of magnitude of S_{theo} , the value of K (eq.12) has to be evaluated. Using $\epsilon_0 = 8.8 \cdot 10^{-12}$, $\epsilon_{HD} \sim 4\epsilon_0$, $Y_{SD} \sim 10^6$ Pa, $E_0 = 10^6$ V/m, and estimating the local effective field of $E_{loc} = E_0(\epsilon_r + 2)/3$, (see ref. [9]) with the PUs permittivity $\epsilon_r \sim 8\epsilon_0$, we have $K \sim 5.9 \cdot 10^{-4}$, and as an example, the deformation of PU75 is then $S_{theo} \sim 0.14\%$ to be compare to the 1.7% measured. It is worthy to notice that this value strongly depends on Y_{SD} which is difficult to determine, and in the other hand the linear model is far from the reality. However, the general tendency is correctly predicted, as shown in Fig. 12.

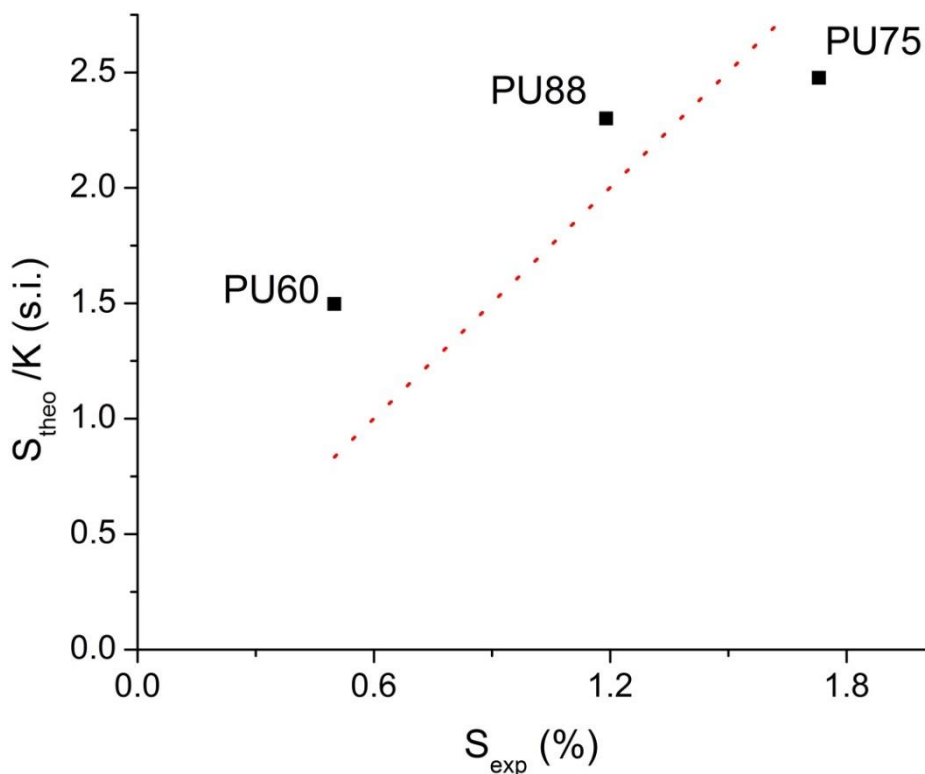


Fig. 12 variation of S_{exp} as a function of S_{theo}/K

This also suggests that the electrostriction properties of polyurethanes polymers can be tuned by controlling the polymer morphology, in terms of phase separation, HD diameter and HD-HD distance. Among the further discussions to be conducted, the effect of the distribution of inter-particles distance is an important point, as it is clear than HD aggregates should lead to

lower efficiency than regularly repartition of HD. Within the aggregates, almost no deformation should occur, and between the aggregates, long distances should lead to weak deformations.

4 Conclusions

The purpose of this work was to provide a model of the segmented PU electrostriction properties, based on their microstructures and taking into account morphological parameters such as the HD diameter, the HD-HD distance and the HS weight fractions. Such model has been presented in a first part of the paper.

To validate the model, a complete analysis was performed by coupling DSC, TEM, AFM and SAXS experiments on three PUs with similar compositions but different weight fractions of HSs. It has been found that the 3 PUs exhibit segmented morphologies with spherical HDs embedded in soft matrices. The average HD diameter estimated from TEM and AFM observations has been found to be independent on the HS fraction since it was found to be equal to 10 nm in the three PUs. On the contrary, the HS fraction influences the distance between two adjacent HDs and may also play a role on the HS content inside the HDs and SDs. The distance was found to vary from 17 nm for the PU with the lowest fraction of HS to 12 nm for the PU with the highest fraction.

With the introduction of these microstructural parameters values into the model such as average HD diameter and HD-HD distance, the model reproduces –with a reasonable correlation- the experimental values of the electrostriction deformation. This opens the route to the design of materials with improved electrostrictive properties, by optimizing the diameter of HD and inter-distance HD-HD in order to get the best electrostrictive properties of two phase polymer based materials with globular morphologies. The next step will be to develop the model in 3D, to mimic as well as possible true polymeric nanocomposites, accounting with the particle spatial distribution.

Acknowledgments

The author acknowledges the French Agence Nationale de la Recherche (ANR) for financial support, under grant NAPOLECO (ANR- 2010-INTB-910-01), and the Centre Lyonnais de Microscopie (CLYM) for the access to the JEOL 2010F and Nanoscope 5 (VEECO) microscopes and the Centre Technologique des Microstructures for the access to the cryo-ultramicrotome. KMV would also like to thank B. Vastenhout and F. Gilleron for fruitful discussions regarding staining methods.

References

- [1] Bar-Cohen Y. *Electroactive Polymer (EAP) Actuators as Artificial Muscles (Reality, Potential and Challenges)*. SPIE Press. Bellingham. 2004.
- [2] Cathleen T ,Raghu DAS, *Electroactive Polymers and Devices 2013-2018: Forecasts, Technologies, Players, Dielectric elastomers, electronic & ionic EAPs and their applications*
- [3] Cottinet. P-J, Guyomar. D, Guiffard. B, Lebrun. L, Putson. C. *Electrostrictive polymers as high-performance electroactive polymers for energy harvesting*. INTEC. 2010. DOI: 10.5772/9946
- [4] Zokay S-P, Fergusont. J. *Polyurethane elastomers*. Prog. Polym. Sci.1991; 16: 695-836.
- [5] Hepburn C. *Polyurethane elastomers*. 2nd ed. London: Elsevier; 1991.

- [6] Petrović Z-S, Javni I. The effect of soft-segment length and concentration on phase separation in segmented polyurethanes. *J. Polym.Sci. B Polym. Phys.* 1989; 27: 545–560. DOI: 10.1002/polb.1989.090270305.
- [7] Xu. Y, Petrovic. Z, Das. S, Garth. L-W. Morphology and properties of thermoplastic polyurethanes with dangling chains in ricinoleate-based soft segments. *Polymer.* 2008; 49: 4248–4258. DOI: 10.1016/j.polymer.2008.07.027
- [8] Yang. C_Z., Grasel. T-G., Bell. J-L, Register. R-A, Cooper. S-L. Carboxylatecontaining chain-extended polyurethanes. *J. Polym. Sci. Part B Polym. Phys.* 1991; 28: 581–588.
- [9] Diguët. G, Bogner. A, Chenal. J-M, Cavaillé. J-Y. Physical modeling of the electromechanical behavior of polar heterogeneous polymers, *Journal of Applied Physics.*2012; 112: 0000. DOI: 10.1063/1.4766280.
- [10] Chou. T-M, Prayoonthong. P, Aitouchen. A, Libera. M. Nanoscale artifacts in RuO4-stained poly(styrene). *Polymer.* 2002; 43: 2085-2088. DOI: 10.1016/S0032-3861(01)00767-4.
- [11] Schrader. S, Li. X, Guo. F, Liu. Y, Luo. J, Xu. D. Electron microscopy investigation of polyester-polyurethane elastomers stained with ruthenium tetroxide. *Die Makromolekulare Chemie, Rapid Communications.*1998.; 9 : 597-601. DOI: 10.1002/marc.1988.030090901
- [12] Haubruge. H-G, Jonas. A-M. Staining of poly(ethylene terephthalate) by ruthenium tetroxide. *Polymer.* 2003; 44: 3229-3234. DOI:10.1016/S0032-3861(03)00255-6
- [13] Jeny I-S, Couchman. P-R. Ruthenium tetroxide staining of polymers for electronmicroscopy. *Macromolecules*, 1983; 16: 589-598. DOI:10.1021/ma00238a021.
- [14] Foks. J, Naumannz. I, Michler. G-H. Beitrag zur aufklärung der morphologie von segmentierten polyurethanen/ contribution to the reconnaissance of the morphology of segmented polyurethanes. *Die Angewandte Makromolekulare Chemie.* 1991; 189: 63- 76
- [15] Guiffard B, Seveyrat L, Sebald G, Guyomar D. Enhanced electric field induced strain in non percolative carbon nanopowder / polyurethane composites. *J. of Phys. D: Appl. Phys.* 2006; 3039- 3053.
- [16] Guyomar D, Cottinet. P-J, Lebrun. L, Putson. C, Yuse. K, Kanda. M, Nishi. Y. The compressive electrical field electrostrictive coefficient M33 of electroactive polymer composites and its saturation versus electrical field, polymer thickness, frequency, and fillers. *Polymers for Advanced Technologies.* 2012; 23, 946–950. DOI: 10.1002/pat.1993
- [17] Seveyrat. L, Guyomar. D, Lebrun. L. Preparation of graphene nanoflakes/polymer composites and their performances for actuation and energy harvesting applications. 2012; 111. DOI: 10.1063/1.4718577.
- [18] Guillot F M , Balizer E. Electrostrictive effect in polyurethanes. *Journal of Applied Polymer Science.* 2003; 89: 399-404. DOI: 10.1002/app.12096.
- [19] Lapprand A, Mechin F, Pascault J-P. Synthesis and properties of self-crosslinkable thermoplastic polyurethanes. *J. Appl. Polym. Sci.* 2007; 105: 99-113. DOI: 10.1002/app.26086.
- [20] Saiani. A, Daunch. W-A, Verbeke. H, Leenslag. J-W, Higgins. J-S. Origin of Multiple Melting Endotherms in a High Hard Block Content Polyurethane. 1. Thermodynamic Investigation. *Macromolecules.* 2001; 34: 9059-9068
- [21] Martin. D-J, Meijs. G-F, Gunatillake. P-A, McCarthy. S-J, Renwick. G-M. The effect of average soft segment length on morphology and properties of a series of polyurethane elastomers. II. SAXS-DSC annealing study. *Journal of Applied Polymer Science.* 1997; 64: 803. DOI: 10.1002/(SICI)1097-4628(19970425)64:4<803::AID-APP20>3.0.CO;2-T
- [22] Chen. K-S, Leon. T-Y, Chen. Y-S, Lin. T-L, Liu. W-J. Soft- and hard-segment phase segregation of polyester-based polyurethane. *Journal of Polymer Research.* 2001; 8: 99. DOI: 0.1007/s10965-006-0139-3.
- [23] Wongtimnoi. K, "Polyuréthanes électrostrictifs et Nanocomposites: Caractérisation et Analyse des mécanismes de couplages électromécaniques", PhD thesis, 2011, INSA-Lyon, France.

- [24] Król. P, Pilch. B-P. Phase structure and thermal stability of crosslinked polyurethane elastomers based on well-defined prepolymers. *Journal of Applied Polymer Science*. 2007; 104: 1464. DOI: 10.1002/app.25011
- [25] Koberstein J-T, Russell T-P. Simultaneous SAXS-DSC Study of Multiple Endothermic Behavior in Polyether-based Polyurethane Block Copolymers. *Macromolecules*. 1986; 19: 714-720. DOI: 10.1021/ma00157a039.
- [26] McLean. S, Sauer. B-B. Nano-deformation of crystalline domains during tensile stretching studied by atomic force microscopy. *J Polym Sci Part B: Polym Phys*. 1999; 37: 859–866. DOI: 10.1002/(SICI)1099-0488(19990415)37:8<859::AID-POLB11>3.0.CO;2-U.
- [27] McLean. S, Sauer. B-B. Tapping-mode AFM studies using phase detection for resolution of nanophases in segmented polyurethanes and other block copolymers. *Macromolecules*. 1997; 30: 8314–8317. DOI: 10.1021/ma970350e.
- [28] Brayan. B-S, Scott Maclean. R, Reinoud. J-G, Meike. C, Nilesten. J-E. Crystalline Morphologies in Segmented Copolymers with Hard Segments of Uniform Length. *Journal of Polymer Science: Part B: Polymer Physics*. 2004; 42: 1783–1792. DOI: 10.1002/polb.20060.
- [29] Sauer. B-B, McLean. R-S, Brill. D-J, Londono. D-J. Morphology and orientation during the deformation of segmented elastomers studied with small-angle X-ray scattering and atomic force microscopy. *J Polym Sci Part B: Polym Phys*. 2002; 40: 1727–1740. DOI: 10.1002/polb.10234
- [30] Matthew. J-O, Bruce. D-L, Garth. L-W. Structure–Property Relationships of Poly(urethane urea)s with Ultra-low Monol Content Poly(propylene glycol) Soft Segments. I. Influence of Soft Segment Molecular Weight and Hard Segment Content. *Journal of Applied Polymer Science*. 2002; 84: 229–243. DOI: 10.1002/app.10168.
- [31] Waletzko. R-S, LaShanda T. Korley. J, Brian D-P, Edwin L-T, Hammond. P-T. Role of Increased Crystallinity in Deformation-Induced Structure of Segmented Thermoplastic Polyurethane Elastomers with PEO and PEO-PPO-PEO Soft Segments and HDI Hard Segments. *Macromolecules*. 2009; 42: 2041-2053. DOI: 10.1021/ma8022052.
- [32] Gogolewski, S. Selected Topics in Biomedical Polyurethanes- a Review. *Colloid Polym. Sci*. 1989; 267: 757–785.
- [33] Michael J. Elwell, Anthony J. Ryan, Henri J. M. Grunbauer and Henry C. Van Lieshout. In-Situ Studies of Structure Development during the Reactive Processing of Model Flexible Polyurethane Foam Systems Using FT-IR Spectroscopy, Synchrotron SAXS, and Rheology. *Macromolecules*. 1996; 29: 2960-2968. DOI: 10.1021/ma9511208.
- [34] Princi. E, Vicini. S, Stagnaro. P, Conzatti. L. The nanostructured morphology of linear polyurethanes observed by transmission electron microscopy. *Micron*. 2011; 42: 3-7. DOI: 10.1016/j.micron.2010.09.007
- [35] Yao. B, Edwards. D-J, Kurtz. R-J, Odette. G-R, Yamamoto. T. Multislice simulation of transmission electron microscopy imaging of helium bubbles in Fe. *J. Electron Microsc.* 2012; 61: 393-400. Doi: 10.1093/jmicro/dfs065
- [36] Saiani. A, Rochas. C, Eeckhaut. G, Daunch. W-A, Leenslag. J-W, Higgins. J-S. Origin of Multiple Melting Endotherms in a High Hard Block Content Polyurethane. 2. Structure Investigation. *Macromolecules*, vol. 37, p. 1411-1421, 2004. DOI: 10.1021/ma0105993.

Conclusion

In this study many pieces of information on segmented PUs could be obtained, regarding their microstructures (in particular the phase separation), as well as their dielectric and viscoelastic behaviours in a wide range of temperatures and frequencies.

The relations between the dielectric, mechanical and electrostrictive properties in PU have been discussed and it appears that the mechanical measurements highlight the main relaxations in the same manner as dielectric measurements (except for the conduction relaxation). The temperature dependence of the relaxations times for α -relaxation is similar with one obtained with dielectric measurements. It is also found that DMA seems to be more efficient to study the α -relaxation of high conductive polymers. Interestingly, the electrostriction response time does not depend on mechanical or dielectric α relaxations as expected. It seems to be directly linked to the space charge diffusion (leading to the Maxwell-Wagner-Sillars or MWS phenomenon). This requires further experimental data and theoretical analyses, which will be performed later on.

Then, a model of the segmented PU electrostriction properties, based on their microstructures and taking into account morphological parameters reproduces –with a reasonable correlation- the experimental values of the electrostriction deformation. This means that segmented PUs should not be considered as homogeneous materials, since their electrostrictive properties are driven by phase separation. The HD diameter remaining almost constant in the PUs studied here, the most important parameter was found to be the HD-HD distance.

When comparing the 3 different PUs, PU88 exhibit low mechanical and dielectric losses in a largest range of frequencies and of temperature, and a good mechanical stability at room temperature, making it the most suitable PU for actuation and energy conversion applications.

In the next part, we will elaborate nanocomposites with PU88 and grafted CNTs. In particular, we will study how the presence of a grafted layer can improve the dispersion state as well the interfacial adhesion. We will couple microstructural characterisations with dielectric, mechanical and actuation measurements. The model based on the PU microstructure will be adapted to take into account the presence of the grafted CNTs. This will be used to discuss the benefit of using grafted CNTs on the electromechanical properties of PU.

Part IV: PU/ CNT Nanocomposites

Introduction

The previous part dealt with a study on the microstructural, electrical, mechanical and electromechanical properties of 3 pure segmented PU with different weight fractions of HS. PU88 was found to be the most suitable PU for actuation properties. In this part, PU88 will be filled with grafted or oxidized CNTs.

It has been recently pointed out that incorporation of CNTs can improve the electromechanical properties of PU nanocomposites [1,2]. In this study, we will present how the grafting process can improve the physical properties of PU nanocomposites. As for pure PU, we will focus on the microstructural, mechanical, electrical and accordingly the electromechanical properties of the PU/ grafted CNTs nanocomposites – with various CNT fractions. The results will be compared with those on PU / ungrafted CNTs and on pure PU.

In a first paper (chapter 6), a multi-scale characterization approach will be carried out to control the grafting process step-by-step. The monitoring of the grafted layer thickness and its compatibility with the PU matrix using TEM observations will be presented. Thermal analysis will be conducted to study the effect of the CNT on the microstructure. As for pure PU, mechanical and dielectric measurements will be performed in function of frequency and the temperature in order to study the influence of the grafted CNTs on the different polymer relaxations processes. Finally, the electromechanical performances of such nanocomposites films will be evaluated.

In a second step (chapter 7), the effect of CNTs and their grafting onto the actuation properties of PU will be analyzed and modeled. The effect of the grafting process onto the CNT dispersion state will be quantified using electron tomography. The CNT orientation, the local CNT fraction, the CNT tortuosity, the CNT-CNT distance and the number of contacts will be determined experimentally from the tomograms. Then, the model taking account the experimental microstructural parameters will be adapted to account for the actuation properties of the polymer/CNT nanocomposites. The results will be used to evaluate the real impact of CNTs.

[1] Zhang, Q. M., Li, H., Poh, M., Xia, F., Cheng, Z.Y., Xu, H. & Huang, C. An all-organic composite actuator material with a high dielectric constant. *Nature* 419, 284-287 (2002).

[2] Huang, C. & Zhang, Q. M. Fully functionalized high-dielectric-constant nanophase polymers with high electromechanical response. *Adv. Mater* 17, 1153-1158 (2005).

Chapter 6: Investigation of elastic, electrical and electromechanical properties of polyurethane/grafted carbon nanotubes nanocomposites

M. H. Jomaa^{1,2*}, K. Masenelli-Varlot¹, L. Seveyrat², L. Lebrun², M.C. Dib Jawhar³, E. Beyou³, J. Y. Cavaille¹.

¹ Université de Lyon, INSA-Lyon, CNRS, MATEIS, 69621 Villeurbanne Cedex, France

² Laboratory of Electrical Engineering and Ferroelectricity (LGEF), INSA Lyon, Université de Lyon, F-69621 Villeurbanne Cedex, France

³ Polymer Materials Engineering Lab (IMP) UCBL & CNRS, Université de Lyon, 69622 Villeurbanne Cedex, France

* Author to whom all correspondence should be addressed

Abstract

Polyurethanes (PU) have demonstrated their ability to convert electrical energy into mechanical energy and vice versa. In addition, it has been shown that the incorporation into a PU matrix of nanofillers, such as carbon nanotubes (CNT), can enhance the actuation and the harvested energy performances. However, it is well known that CNTs are hardly dispersed in a polymeric matrix, and that the interfacial adhesion strength is generally poor. Moreover, the improvement of electromechanical properties is limited by the low volume fraction of CNT that can be dispersed because of their low percolation threshold. Above the percolation threshold, losses due to Joule effect become predominant. It was recently pointed out that functionalizing CNTs by grafting polymer chains onto their surfaces may improve; their dispersion, their interfacial adhesion and frustrate the electrical conductivity. In this study, we present how the grafting process can improve the physical properties of PU nanocomposites, including microstructural, mechanical, electrical and accordingly the electromechanical properties of the PU/ grafted CNT nanocomposites, compared to those of pristine PU. The dielectric permittivity was largely increased with the introduction of grafted CNT and the percolation threshold was found around 5 vol. %. Measurements of the thickness strain under an applied electrical field demonstrated a twofold increase of the electrostriction coefficient. The energy harvesting properties investigated by monitoring the evolution of the current under a DC electric field were also enhanced.

Keywords: Grafting of CNT; Microstructural, electrical, properties, electrostriction.

1 Introduction

In the field of smart materials, a tremendous amount of research and development has led to Electroactive Polymers (EAP) that can also change in size or shape when stimulated by the right external electrical activation mechanism, meaning they can convert electrical energy into mechanical energy. Especially in the actuators segment, vast R&D activity can be seen for specialized applications such as medical devices and biomimetic-robotics [1]. These materials are highly attractive for their large strain capability, and resilience. Polyurethane (PU) elastomers are EAPs of great interest due to their significant electrical-field strains [2], and due to their attractive and useful properties such as flexibility, light weight, easy processing to large area films as well as their ability to be moulded into various shapes and biocompatibility with blood and tissues. In addition, it has recently been shown that the incorporation of nanofillers into a PU matrix, such as carbon nanotubes (CNTs) [3,4, 5], can greatly enhance the expected strain, or the harvested energy [6]. This outstanding result seems to be related to the increase of the permittivity when nanofillers are incorporated within the polymers, hence requiring a lower bias electric field for the same effect. To develop high-efficiency polymer nanocomposites for energy harvesting and actuation applications, it is thus important to obtain large values of the dielectric permittivity while maintaining adequate mechanical properties [7].

However, it is well known that CNTs are hardly dispersed in a polymeric matrix and that the interfacial adhesion strength is generally poor [8]. An effective method to improve both dispersion and interfacial adhesion consists in functionalizing CNTs by grafting polymer chains onto their surfaces [9,10]. S. Li et al [11] reported that grafting chains with different molecular weights on the surface of MWCNTs increases the solubility of MWCNTs and as a consequence the conductivity of the nanocomposites decrease.

This study reports the effect of the incorporation of grafted CNTs on the physical properties of PU nanocomposites, namely microstructural, mechanical, electrical and electromechanical properties. A multi-scale characterization approach using TEM observations is performed to control the grafting process step-by-step, including the monitoring of the grafted layer thickness and its compatibility with the PU matrix. Optimization of nanocomposite film elaboration avoiding damage of the grafted layer is monitored with the help of TEM observations. Thermal analysis was carried out to study the effect of the CNTs on the nanocomposites microstructure. Isochronal mechanical measurements are performed, as well as dielectric measurements over a wide range of frequencies and temperatures in order to study the influence of the grafted CNTs on the different relaxations processes of the polymer. Finally, the electromechanical performances of such nanocomposites films are evaluated.

2 Materials and methods

Multi-walled CNTs were provided by Cheap Tubes and had average diameters of 30 nm and lengths of 10 to 20 μm . The grafting reactions were performed using a "grafting onto" technique [12] to form a PU thin layer on the surface of the CNTs. First, functional groups such as $-\text{COOH}$ or $-\text{OH}$ were created on the sidewalls of CNTs, by oxidation of the CNTs. Then as a second step, polyTDI-tolylene-2,4-diisocyanate terminated poly(propylene glycol)- was grafted on the functionalized CNTs. Finally, polyol was also grafted on CNT-PolyTDI [13], see Fig: 1(a).

The matrix was a polyether-based thermoplastic polyurethane (Estane 58888 NAT021 – Lubrizol). It is a co-block polymers with two major blocks, made of hard and of soft segments. Hard segment (HS) are composed of 4,4' methylene bis (phenyl isocyanate) (MDI) and 1,4-butanediol (BDO). Poly(tetramethylene oxide) (PTMO) is used as soft segments (SSs).

The polymer films were prepared by a solution casting method. Before use, PU granules were heated at 350 K for 3 hours. The grafted CNTs were first dispersed in N,N-dimethylformamide (DMF, Sigma-Aldrich D158550, 99%) using sonication in an ultrasonic bath (UB) (Bioblock Scientific TS540 (power 10 %)) and /or using an ultrasonic processor (UP) with a 7 mm sonotrode (Hielscher UP400S 400W, 24 kHz, (power 30%)). PU granules were added to this solution with a ratio of 15 wt.% of PU into DMF. The solution was heated at 350 K for 4 hours under mechanical agitation, until a homogeneous solution was obtained. This operation was carried out in a closed device, to avoid evaporation of DMF and to ensure good reproducibility of films. Then, the solution was kept overnight to remove air bubbles. Afterwards, this solution was cast on glass plates with an Elcometer 3700 Doctor Blade ® film applicator, put in an oven at 335 K for one day, and then removed from the glass. A second heating treatment at a temperature below the HS melting temperature was performed at 400 K for 3 h in order to eliminate any residual solvent. The thickness of the films was about 100 µm after drying.

The control of the grafting process as well as the control of the CNT dispersion state in DMF was performed step by step using Transmission Electron Microscopy (TEM). Observations were carried out in the bright field mode with a JEOL 2010F operating at 200 kV.

The microstructural observations on the cryofractured surfaces - in order to control the CNT dispersion state and interfacial adhesion strength - were performed using a Zeiss Supra 55VP Scanning Electron Microscope operating under high vacuum, at low accelerating voltage (typically 1000 V) and without any gold coating. Images were acquired with the Everhart-Thornley secondary electron detector.

The microstructural characterization of PU nanocomposites was also performed by Differential Scanning Calorimetry (Setaram, DSC 131 Evo)) under nitrogen flow (P = 1.5 bar). Samples of 20 mg were cooled to 140 K under liquid nitrogen and then heated to 480 K before being cooled to room temperature. The heating and cooling rates were set at 10 K / min.

The dielectric properties of these films were measured with a Modulab MTS at an AC voltage of 1 V RMS, over a frequency range of 10⁻¹ to 10⁶ Hz. Both surfaces of the film were coated with a gold electrode of 20 mm in diameter, deposited by sputtering (Cressington 208 HR). Isothermal measurements were performed under liquid nitrogen using a cryostat (JANIS-STVP-200XG), in the temperature range 100-400 K, and the activation energy and characteristic relaxation time (τ) were determined for all the relaxation processes. Dielectric data were fitted with the Havriliak Negami (HN) function with of the help of WINFIT software (Novocontrol):

$$\varepsilon(\omega) = \varepsilon_{\infty} + \frac{\Delta\varepsilon}{[1+(i\omega\tau_0)^a]^b} \quad (1)$$

With Δε the dielectric strength, τ the relaxation time and a, b the parameters giving respectively the width and the skewness of the distribution of the relaxation function.

As the contribution due to the Ohmic conduction was not visible in ε', the following relation was beforehand used to estimate the conduction free loss ε_D'' [14]:

$$\varepsilon_D'' = -\frac{\pi}{2} \frac{\partial \varepsilon'(\omega)}{\partial \ln(\omega)} \quad (2)$$

The dynamic shear measurements were measured by Dynamic Mechanical Analysis (DMA) on samples of 12 mm in length and 3 mm in width. A sinusoidal shear stress was applied, the complex shear modulus ($G^* = G' + iG''$) was measured and then storage (G') and loss (G'') dynamic shear modulus were calculated. The loss factor $\tan \delta_m = G''/G'$ was also determined. Experiments were performed in the isochronal mode (0.1 Hz, temperatures 100-400 K, with a heating rate of 1 K/min) under helium, to insure a better thermal conductivity. The mechanical behaviours of the PU and PU/grafted CNT films were measured with a multifunctional dynamic mechanical analyzer, Eplexor from Gabo, in the simple tensile mode. The tests were carried out on 10 x 40 mm² rectangular specimens fixed at both ends thus leaving 20 mm long for the measurements, with an elongation speed of 24 mm/min.

The field-induced thickness strain was measured on circular samples (25mm of diameter) with a homemade setup based on a double-beam laser interferometer measurement (Agilent 10889B) [2]. Samples were placed between two cylindrical brass masses acting as conductive electrodes. A mirror was placed on the upper electrode to reflect the laser beam. A bipolar electric field was supplied by a high voltage amplifier (Trek10/10B) driven with a function generator (Agilent 33250A).

For energy harvesting capabilities, 10 x 40 mm² samples were subjected to a DC bias electric field to induce the electrical polarization - using a function generator and amplified by the Trek Model 10/10 high-voltage power amplifier, and under mechanical strain [6].

3 Results and discussion

3.1 Optimization of elaboration process

3.1.1 Control of grafting process

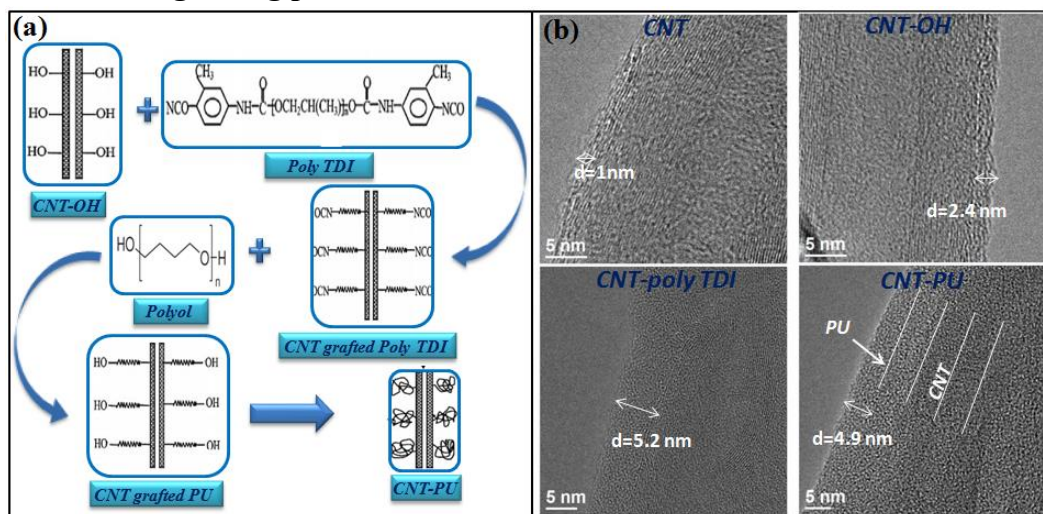


Fig: 1 (a) Schematic illustration of the grafting process of polyurethane on the multi-walled CNTs, (b) TEM observation of the CNTs during the grafting process.

Fig: 1 presents the different steps of the grafting process, and the corresponding TEM observations. As shown in Fig: 1(b), the raw nanotubes are well crystallized and their outer surfaces rarely exhibit amorphous layers. During the grafting process, an amorphous layer appears and its thickness changes. At the end of the grafting process, this layer obviously covers the entire CNT surface. It is rather homogenous and uniform with an average thickness of 5 nm. Thermogravimetric Analysis (TGA) on grafted CNT shows a degradation of the grafted layer at a temperature similar to that of the pure PU degradation (not shown). Furthermore Differential Scanning Calorimetry (DSC) confirms that the grafted CNTs contain PU, which indicates a successful grafting. Furthermore, the grafting leads to an impressive improvement of the CNT suspension stability in DMF (not shown).

3.1.2 Optimization of elaboration process

In order to have a good dispersion of grafted CNTs in DMF without damaging the grafted layer, four tests were performed using the two ways of sonication described above, ultrasonic processing (UP) or ultrasonic bath (UB). A control of the CNT surface and entanglement was carried out for the 4 tests using TEM observations.

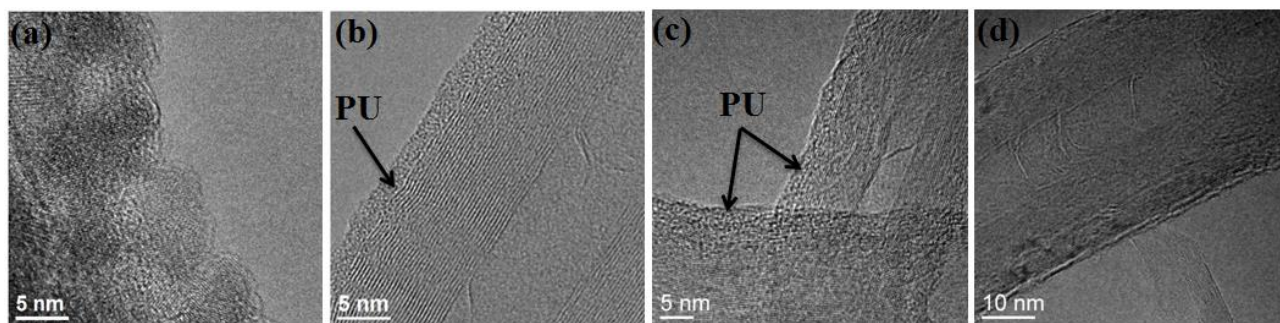


Fig: 2 Optimization of the dispersion conditions in DMF using ultrasonic bath (UB) and ultrasonic processor (UP): (a) UP-30 min, (b) UB-1h30, (c) UB-1h30 + UP-5 min, (d) UB-1h30 + UP-15 min.

Fig: 2(a) shows that the grafted CNT are heavily damaged after 30 min of UP even with low amplitude and pulse conditions. On the contrary, within the ultrasonic bath (UB) during 1h30, CNT are relatively well dispersed and the grafted layer does not seem to be damaged and still covers the whole CNT surface (Fig 2.b). By adding a further treatment with the ultrasonic probe during 5 min, the dispersion is further improved with negligible damage within the grafted layer (Fig: 2(c)). Finally in Fig: 2(d) with UB-1h30 + UP-15 min conditions, the grafted layer is damaged. To conclude, two dispersion conditions lead to the best compromise, with good dispersion and negligible damage in the grafted layer; (i) UB-1h30 (used for films with 1 and 2 vol. % CNT) , (ii) UB-1h30 + UP-5 min (used for films with higher volume contents, namely 3, 4 and 5 Vol. %, when the CNT dispersion was not good enough with the UB-1h30 only).

3.1.3 Control of dispersion and interfacial adhesion

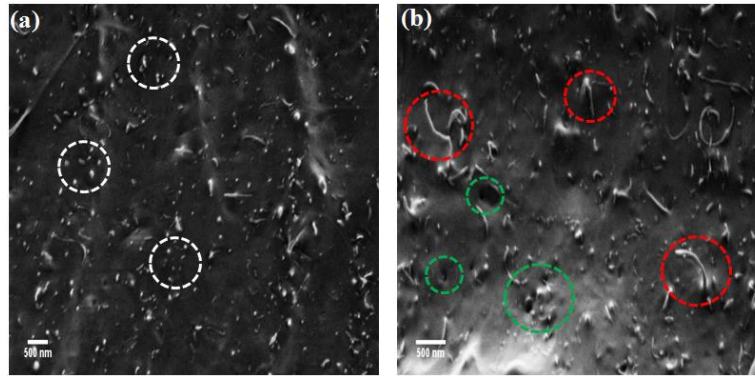


Fig: 3 SEM photomicrographs of (a) PU/ 4 vol. % grafted CNT and, (b) PU/ 4 vol. % ungrafted CNT cryofractured surfaces.

Fig: 3 displays SEM photomicrographs of the PU nanocomposites filled with either grafted or ungrafted CNTs. Observations were performed on cryofractured samples at low temperature using liquid nitrogen. Although it is quite difficult to extract quantitative data, grafting seems to lead to a better dispersion of the nanotubes within the PU matrix as the proportion of CNT aggregates seems to decrease upon grafting. This good dispersion may be associated to the initial good dispersion of nanotubes in the organic solvent after sonication.

It is noteworthy that CNTs were cut (see white circles in Fig: 3(a)) meaning that the adhesion at the grafted CNT/ PU interface is strong enough to propagate the fracture through the nanotube and not along the interface. A better interfacial adhesion was expected since the same chemical component is present in both sides of the interface (PU in the grafted layer and in the matrix). On the contrary, with ungrafted CNTs, the presence of pulled-out tubes (red circles) and holes (green circles) indicate a poor adhesion between ungrafted CNTs and PU. Indeed, they indicate that the matrix released the stress during the fracture by nanotubes sliding.

3.2 Thermal analysis

The DSC thermograms presented in Fig: 4 were recorded in order to study the influence of grafted layer and the volume fraction of grafted CNT on the crystalline morphology of the polyurethane host. The glass transition temperature for the soft domains –rich in SS- (T_{gSD}), melting temperatures of hard domains -rich in HS- (T_{mII} and T_{mIII}), enthalpies of melting (ΔH_m), crystallization temperature (T_c) and enthalpies of crystallization (ΔH_c) are summarized in Table 1.

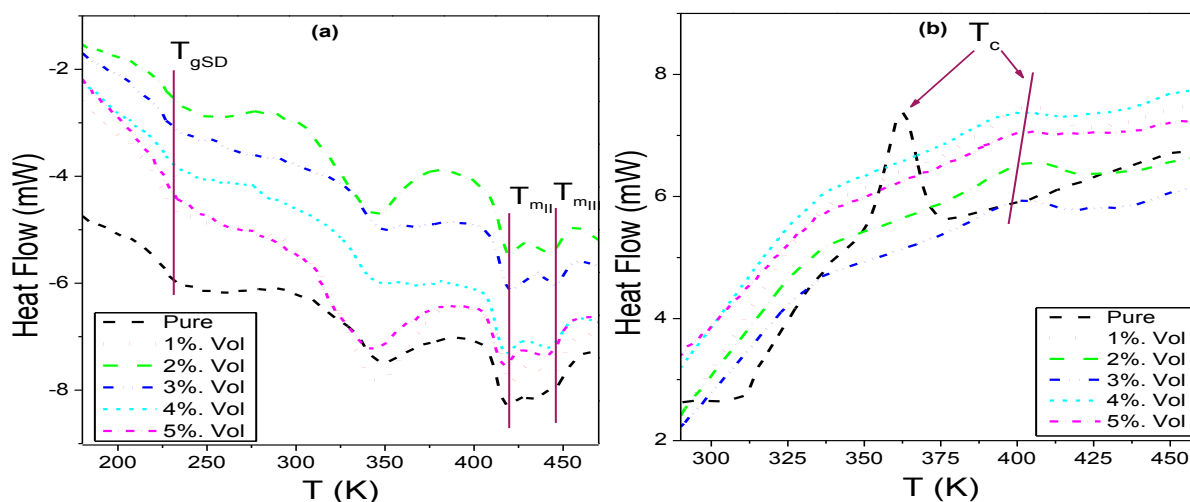


Fig: 4 DSC thermograms of pristine PU and PU/grafted CNT nanocomposites: (a) upon heating, (b) upon cooling.

Table 1 Parameters extracted from the DSC thermograms for PU grafted CNT nanocomposites.

	T_{gSD} (K)	ΔC_p (J/g.K)	T_{mII} (K)	T_{mIII} (K)	ΔH_m (J/g)	T_c (K)	ΔH_c (J/g)
Pure	228	0.23	419	442	10.9	362	-8.6
1 vol.%	227	0.24	421	444	10.5	401	-4.8
2 vol.%	227	0.24	419	443	9.2	406	-4.1
3 vol.%	226	0.25	420	445	8.5	399	-4.3
4 vol.%	226	0.22	418	441	8.6	393	-3.6
5 vol.%	226	0.22	418	441	8.7	399	-4.0

The first thermal phenomena near 228 K can be related to the glass transition of soft domains (T_{gSD}), in agreement with values reported in the literature [15]. This value can give an estimation of the amount of hard segments (HS) dissolved in the SDs and as a consequence an indication of the “purity” of the soft phase. Indeed, when the fraction of grafted CNTs is increased, no significant change of T_{gSD} is observed. Several authors found no effect of carbon nanotubes on the T_{gSD} of PU-based nanocomposites, even at filler concentrations higher than 10 wt.% [16]. It can thus be concluded that the composition and morphology of HD and SD are not significantly modified by the incorporation of grafted CNTs.

Moreover, a bimodal endothermic transition can be observed for all PU nanocomposites on the DSC thermograms around 425 and 450 K. From the literature, the existence of a bimodal peak could correspond to the fusion of crystalline hard segments with two different chain lengths [17]. Alternatively, it can be related to rearrangements within the HDs and SDs, followed by the fusion of crystalline HDs [13]. Furthermore, an increase of the samples’ crystallinity would be accompanied by an increase of these temperatures (with increasing crystal sizes) and/or an increase of the total enthalpy of the 2 phenomena. With the incorporation of grafted CNTs, both endothermic peaks remain almost the same and a slight decrease of the corresponding enthalpy

by a factor of 20% of the polymer can be observed. As a consequence the CNT incorporation leads to a little decrease of ΔH_m which reveals a decrease of the crystallinity.

During the cooling experiments, a more important influence of the grafted CNTs on the crystallization behaviour is observed, as shown in Fig: 4 (b). When the amount of grafted CNT is increased, the crystallization temperature is raised to ~ 400 K which shows that the grafted CNTs act as nucleating agents. However, a significant decrease of the enthalpy is observed, in agreement with the reduction in crystallinity.

3.3 Viscoelastic and mechanical properties of PU grafted CNT

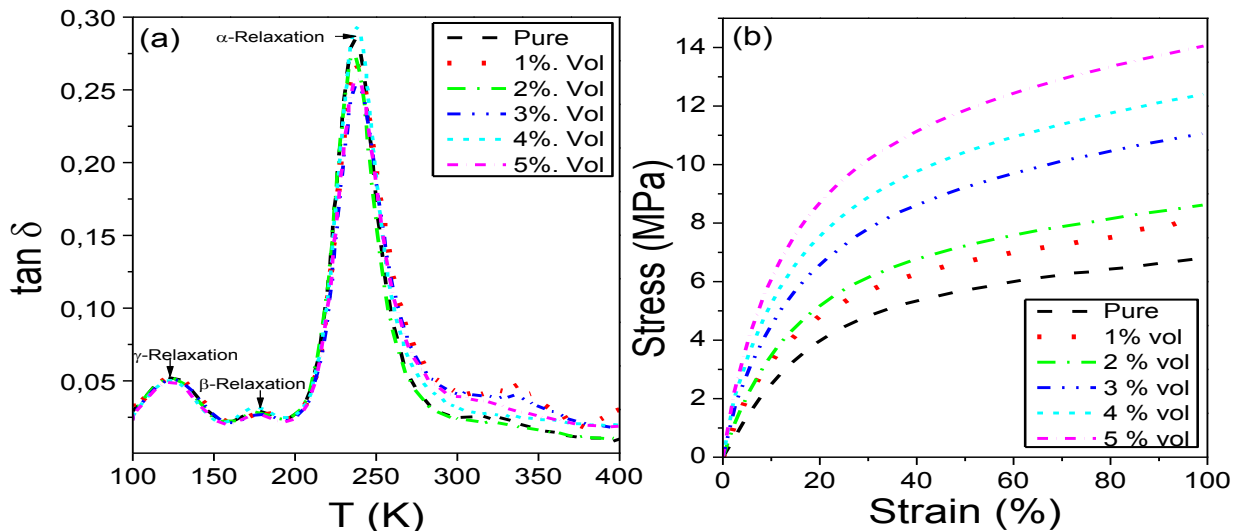


Fig: 5 Loss factors of pure PU and PU / grafted CNT nanocomposites, versus temperature at 0.1 Hz, (b) stress-strain profiles of PU composites at different CNT volume contents. Loss factors of pure PU and PU / grafted CNT nanocomposites were obtained at constant frequency as a function of the temperature (see Fig: 5(a)). According to the curves, there are typically three relaxations, characterized by maxima of the mechanical losses. They correspond to the so-called γ -, β -, and α -relaxations, at increasing temperatures. The first process known as “ γ -process” is related to the local intermolecular relaxation at a temperature below $T_{g(SD)}$ [18]. The second one, β -relaxation, seems to be related to the motions of side group chains or branches occurring in the amorphous phase, according to ref. [19]. The third one is the “ α -relaxation” or main relaxation, and is related to the intermolecular cooperative motions of chain segments and is observed around the glass-rubber transition temperature. These different viscoelastic relaxations are almost similar for all compositions. This behaviour reveals that the viscoelastic relaxations and so the macromolecular mobility is almost not affected by the presence of CNTs. Nevertheless, the incorporation of grafted CNTs into PU increases the tensile strength and modulus, as shown in Fig: 5(b) and Table 2.

Table 2 Young modulus of pure PU and PU/ graftedCNT nanocomposites from strain/stress curves in the linear part

	Pure PU	1 vol.%	2 vol.%	3 vol.%	4 vol.%	5 vol.%
Y (MPa)	29	40	47	55	65	75

The Young modulus increases from 29 MPa in pure PU to 75 MPa when the grafted CNT content reaches 5 vol.%. Strengthening the overall mechanical performance of the composites, it may be a result of strong interactions between the functionalized CNT and the PU matrix due to a great enhancement of the dispersion state and the interfacial adhesion.

3.4 Dielectric permittivity, electrical conductivity, percolation threshold

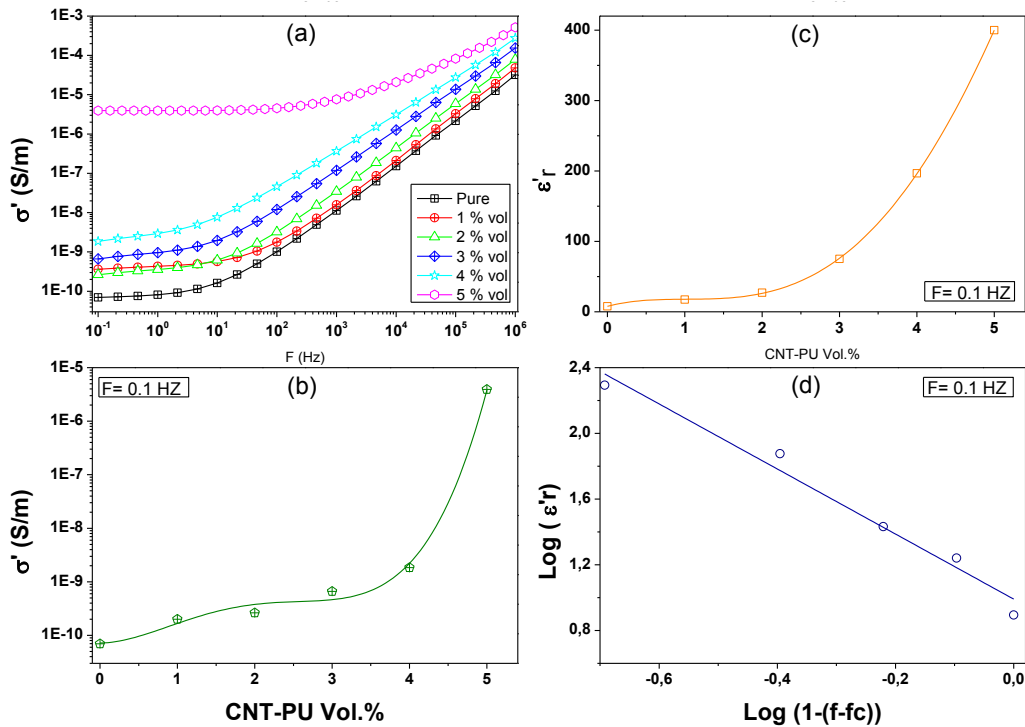


Fig: 6 Electrical conductivity of PU / grafted CNT nanocomposites (a) versus frequency for various CNT contents, (b) versus grafted CNT content at 0.1 Hz. (c) dielectric permittivity versus grafted CNT content at 0.1 Hz, (d) log-log plot of the dielectric permittivity versus $(1-f/f_c)$ at 0.1 Hz.

The real parts of the electrical conductivities (σ') of pure PU and PU / grafted CNT nanocomposites are plotted as functions of the frequency, see Fig: 6(a). Two regions can be observed: (i) one at low frequencies, where the conductivity is almost independent of the frequency and (ii) the other at higher frequencies, where the conductivity increases linearly with the frequency. For dielectric materials, the frequency-independent conductivity (thus mainly resistive) is generally attributed to electric charge displacements whereas the frequency-dependent part corresponds to a capacitive behaviour [20].

In Fig: 6(b), σ' first increases gradually up to 4 vol.% of grafted CNTs. But for higher contents, it jumps rapidly. This behaviour corresponds to the insulating-conductive transition behaviour (or percolation). The percolation threshold (f_c) is the volume fraction of CNT necessary to form a continuous conductive network through the matrix. Composites with PU-grafted CNTs present a higher f_c compared to those with ungrafted CNTs [21]. This is mainly due to the fact that grafted CNTs are electrically isolated from each other by the PU layer, and it is worthy to notice that the appearance of the percolation threshold suggests that the layer was damaged during the film fabrication process, for contents around 5 vol.%. At this content, the viscosity

becomes high and during the film casting, it is probable that friction between neighbouring CNTs removes the grafted layer inducing conductivity between the nanotubes.

Fig: 6(c) shows an abrupt increase of the relative permittivity just around 5 vol.%, which is characteristic of the percolation phenomenon. For a volume content of grafted CNTs lower than 5%, the increase in dielectric permittivity versus the filler content can be explained by space charges induced by the conductive fillers, which is in good agreement with the Maxwell Wagner mechanism [22]. Near the percolation threshold, the fillers behave like microcapacitor networks [23]. Each of these capacitors is formed by the neighbouring conductive grafted CNTs with a very thin layer of insulating PU in between and on the surface of each CNT. Close to the percolation threshold, the composite presents a high dielectric constant $\epsilon'_r=460$ at 0.1 Hz, i.e. about 60 times higher than that of pure PU (for which $\epsilon'_r=7$), see Fig: 6(d). The variation of the relative permittivity for $f < f_c$ can be described by the following relation [24], when the embedded particles are dispersed:

$$\epsilon'_r = \epsilon'_{rm} \left(1 - \frac{f}{f_c}\right)^{-q} \quad (3)$$

where ϵ'_{rm} is the relative permittivity of pure PU, f the volume fraction of grafted CNTs, f_c the percolation threshold and q the critical exponent.

The percolation theory for the insulating behaviour under f_c gives a linear logarithmic relation between $\log(\epsilon'_r)$ and $\log(1 - (f/f_c))$, as shown in Fig: 6 (b). The best fit is obtained with $f_c = 5$ vol.% and $q = 2$. The value q is higher than the so-called universal value, $q=1$, as shown by Stauffer [25]. This may reflect a non-random CNT dispersion, which is the main requirement for the applicability of Eq.3.

3.5 Dielectric relaxation of PU nanocomposites

Fig: 7 presents the imaginary part of dielectric modulus M^* at 0.1 Hz versus temperature. Calculated from ϵ' and ϵ'' with the following

$$M'' = \frac{\epsilon''}{(\epsilon'^2 + \epsilon''^2)} \quad (4)$$

The main advantage of this expression is that the space charge effects often do not mask the features of the spectra, owing to suppression of high capacitance phenomena in the plot $M''(f)$ [26].

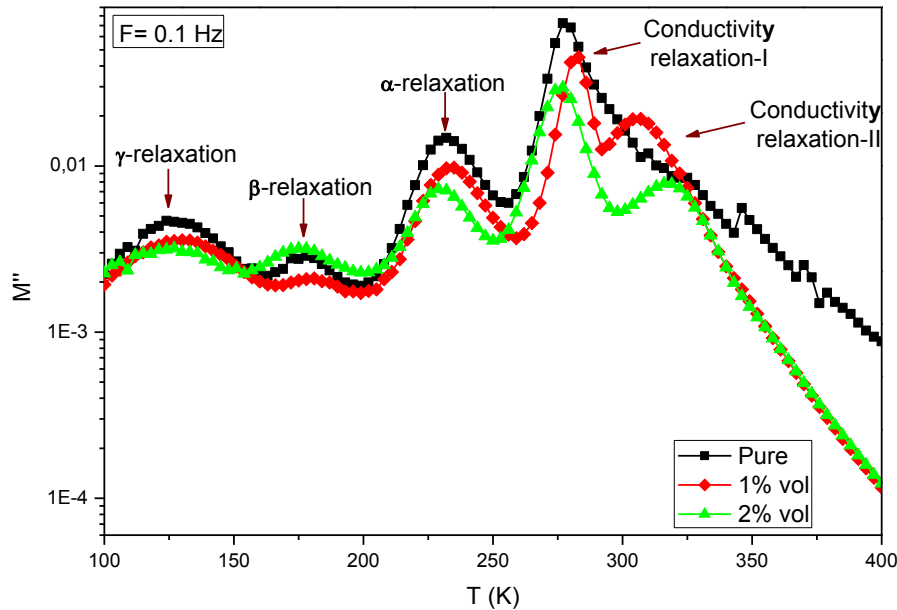


Fig: 7 Evolution of the loss modulus versus temperature for pure PU and nanocomposites (1 & 2 vol.% of grafted CNTs) at 0.1 Hz.

Based on isochronal measurements, four relaxation processes can be observed for the three investigated samples (pure PU, composites containing 1 and 2 vol.% of grafted CNTs). Fig: 7, exhibits their dielectric behaviours at 0.1 Hz. At low temperature, around 125 K, the γ -relaxation corresponds fairly well with the mechanical γ -relaxation which was previously attributed to local motion of $(\text{CH}_2)_n$ segments [27]. Around 175 K, the β -relaxation appears with a smaller amplitude compared to that of the γ -relaxation. It has been attributed in the literature to the motion of the polymer chain segments with attached water molecules [28]. The α -relaxation appears around 230 K, and has a larger amplitude than the two secondary γ - and β -relaxations. This relaxation corresponds to a longer scale segmental motions, and is associated to the glass transition [29]. A fourth process starts at 280 K at low frequency. This phenomenon is very sensitive to frequency and shifts to higher frequencies at increasing temperatures (not shown). It corresponds to high values of the DC conductivity. This phenomenon can be attributed to the existence of ionic polarization in the polyurethane network due to "free" charge motion within the material. Upon incorporation of CNTs, an additional relaxation appears, which can also be attributed to conductivity. A study performed by Gorgeoussis et al [30] on PU with metal chelates in the main chain reported that two mechanisms associated to conductivity can be observed, identified as conductivity (i) occurring in the bulk material, and (ii) more localized at the interface, respectively.

The three dielectric γ -, β - and α - relaxations are similar to the viscoelastic relaxations reported above. This confirms that incorporating CNT does not affect the relaxation processes of these PU nanocomposites. Furthermore, the cross-analysis of DMA and dielectric data leads to more complete information as interactions between molecules and (i) mechanical stress or (ii) electrical field are completely different. For the different relaxation processes, using $M''(T, f)$ data, and more precisely the frequencies f_M at which M'' passes through a maximum, it is easy to determine the so-called relaxation time $\tau = 1/2\pi f_M$ and to get a set of $\tau(T)$. For the

cooperative α -relaxation, the temperature dependence of τ is often described by the Vogel-Tammann-Fulcher (VTF) equation.

$$\tau = \tau_0 \cdot \exp \frac{B}{(T-T_0)} \quad (5)$$

where τ_0 is the pre-exponential time, B is an activation parameter and T_0 is so-called the ideal glass transition temperature (or the Vogel temperature) [31]. For the other relaxations it is usual to plot $\log(\tau)$ versus $1/T$ (in a so-called Arrhenius plot), and to determine the equation of the corresponding curve. If the curve is a straight line, then the relaxation time follows the Arrhenius equation:

$$\tau = \tau_0 \cdot \exp \frac{E}{k_B T} \quad (6)$$

Where τ_0 is the pre-exponential time, k_B the Boltzmann constant and E the activation energy. Fig: 8 shows a semi-logarithmic plot of τ in a function of the reciprocal temperature, $1/T$, for pure PU and the nanocomposites. The curves are the fits and the experimental points are also included in the plots.

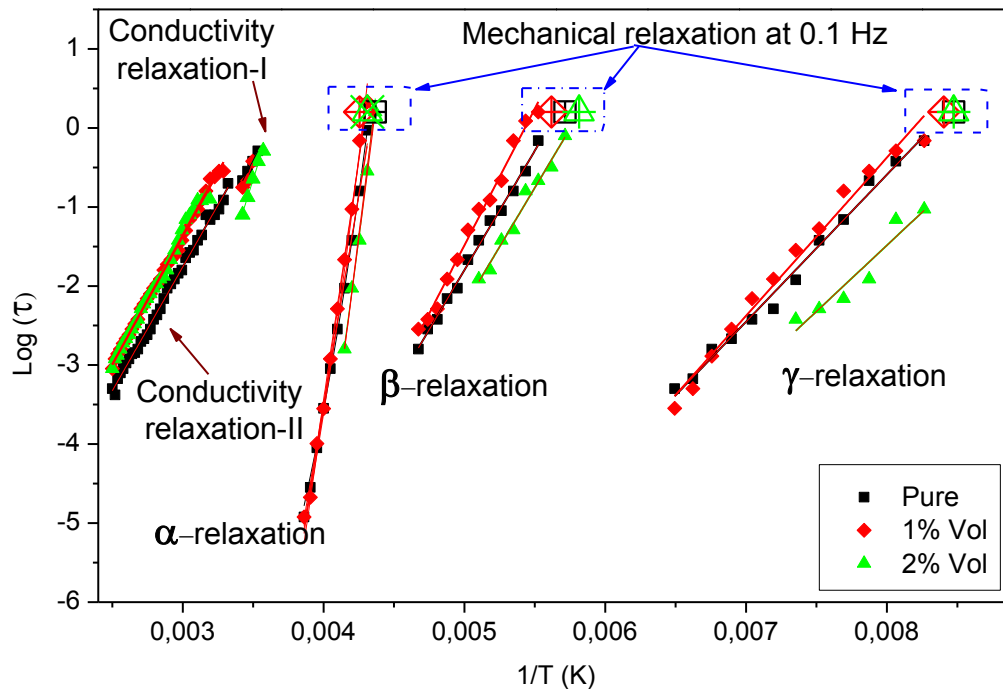


Fig: 8 $\log(\tau)$ versus $1/T$ for γ -, β -, α -relaxations and the two conductivity processes for pure PU and PU nanocomposites (1 & 2 vol.%) from dielectric measurements (full symbols) and from mechanical measurements at 0.1 Hz (open symbols).

Table 3 Parameters of the α , β , γ and conduction relaxations, obtained from the fits of the dielectric spectra

		PU	PU-1 vol.% CNT	PU-2 vol.% CNT
α-relaxation	$B(K)$	2000	2500	2200
	$T_0(K)$	174	174	174
	$\tau_0(s)$	10^{-16}	10^{-18}	10^{-17}
	$\Delta\epsilon$	0.28	0.46	0.76
	ϵ_∞	3.21	4.48	5.84
γ-relaxation	E (KJ/mol)	36	39	33
	τ_0 (s)	10^{-16}	10^{-16}	10^{-14}
	$\Delta\epsilon$	0.43	0.73	1.80
	ϵ_∞	2.43	3.63	4.68
β-relaxation	E (KJ/mol)	58	67	58
	τ_0 (s)	10^{-16}	10^{-18}	10^{-17}
	$\Delta\epsilon$	0.30	0.49	1.37
	ϵ_∞	2.66	3.96	5.11
Conductivity relaxation-I	E (KJ/mol)	57	62	63
	τ_0 (s)	10^{-10}	10^{-11}	10^{-11}
Conductivity relaxation-II	E (KJ/mol)	N.D.	89	110
	τ_0 (s)	N.D.	10^{-16}	10^{-20}

The γ - and β -relaxations are described by almost the same parameters E and τ_0 for the three materials. The relaxation times of the β -processes are not significantly affected by the grafted CNTs and the values of the activation energies are similar to those of pure PU as it is the case for other reported values [29]. For the α -relaxation, it is striking that the VTF parameters are quite similar for pure PU and for the nanocomposites. It is worthy to notice that the two conductivity processes are different, the first conductivity process-I seems to be related to a conductivity of ionic type only, with almost the same activation energy and only a slight dependence to the volume fraction of grafted CNTs. However the second one is more related to the volume fraction of grafted CNTs.

The $\Delta\epsilon$ dielectric strength and the ϵ_∞ value increase with the CNT amount for the 3 relaxations, as already reported on other conductive nanofillers based composites [32]. This increase may reflect a reduction in crystallinity, in agreement with DSC analysis. For secondary relaxations, the high values of $\Delta\epsilon$ for composites cannot be explained by the molecular origin but rather by the increase of the internal field due to the conductive nanotubes.

3.6 Electrostriction properties

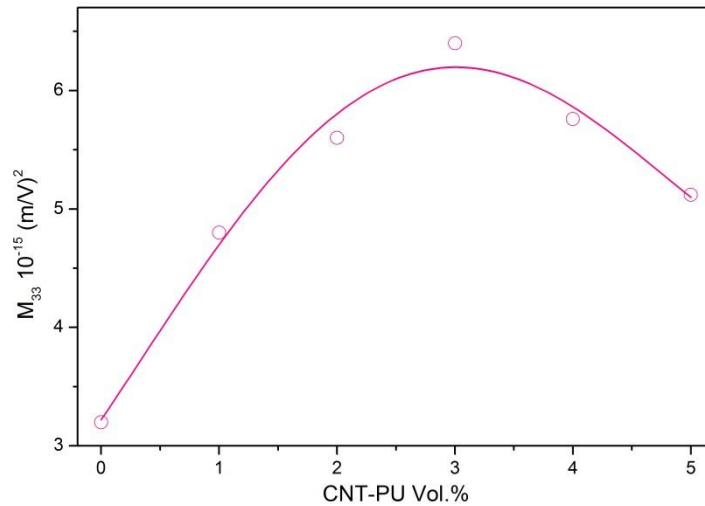


Fig: 9 M_{33} electrostrictive coefficient in function of the grafted CNT volume fraction at $E=2.5 \text{ V}/\mu\text{m}$ and 0.1 Hz.

Fig: 9 depicts the variations of the apparent electrostrictive coefficient M_{33} as a function of the grafted CNT volume content at 0.1 Hz. Below the percolation threshold, M_{33} increases effectively with grafting CNT contents up to 3 vol.%. M_{33} exhibits a maximum value for a filler content around 3% not far from the percolation threshold (around 5 vol.%). At the maximum, the value of M_{33} is twice larger than that for pure PU. These data show the advantage of the addition of nano-filler for increasing the coupling within the polymers with a significant decrease in driving voltage of the films, which is currently the major technological barrier to electroactive polymer films for application development. Indeed, the same level of deformation is obtained in the case of composites for an electric field 1.5 times lower. Furthermore, for a grafted CNT content above 3 vol.% and near f_c , M_{33} starts to decrease. This is consistent with the appearance of electric losses due to the Joule effect through the conducting filler network (resistive behaviour exhibited in Fig: 6)

Increasing the electromechanical response of the composite seems to indicate an effect of the space charges at its origin resulting in an increase in the permittivity. As the M_{33} coefficient does depend on the ratio of the permittivity on the Young modulus [33], one should expect a 4-fold increase of the electrostrictive coefficient at a filler content of 3%. The moderate 2-fold increase could be partially explained by a decrease of permittivity under electrical field, some measurement showed indeed a decrease of 25% of the ϵ value. Another explanation could be the local field or field gradient which decreases due to the increased incorporation of conductive nanotubes.

Despite strong permittivity values and the grafting of the nanotubes with the PU, it was not possible to obtain a strong improvement electromechanical performance. The results are similar to those obtained with CNT grafted COOH groups [5].

Recently, a theoretical model was developed to quantitatively understand the high electrostriction coefficient of polymers like such PU used in this study [34]. Such a model should be adapted to account for electrically conducting fillers contribution.

3.7 Harvesting energy

Fig 10 shows the variation of the measured short-circuit current on a polyurethane film and composites with 1 and 2 vol.% of grafted CNTs. These measurements were performed by applying a mechanical deformation of 5% on each film, at a frequency of 5 Hz, for different values of the DC applied electric field to the sample to maintain its polarization.

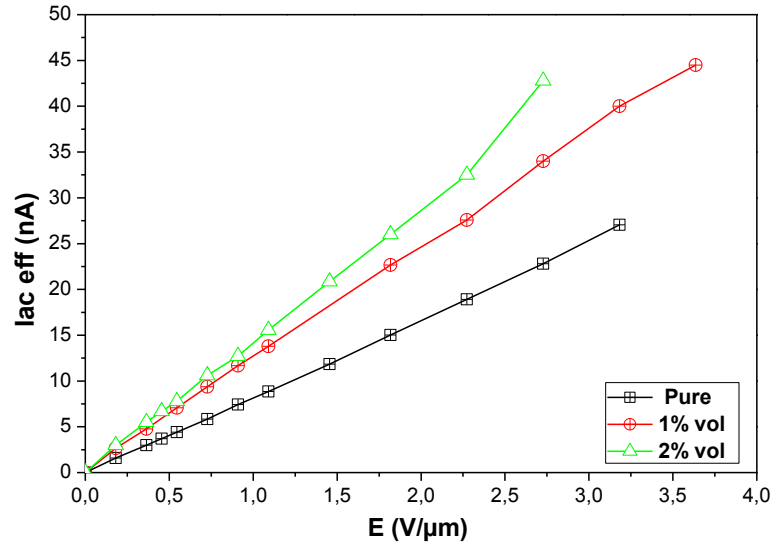


Fig: 10 Evolution of the current of pure PU and PU / grafted CNTs nanocomposites as a function of the applied DC electric field (mechanical strain: 5%, $f = 5$ Hz).

Fig 10 presents the evolution of the current measured on pure polyurethane films and PU/grafted CNT nanocomposites and under AC mechanical strain as a function of the applied electric field. The DC electrical field induces electrical polarization within the polymer, needed for the mechanical electrical conversion, which is a pseudo piezoelectric behavior.

Regardless of the composite studied, the current value increases linearly with the DC field. There is a significant increase in the measured current for both filled samples which therefore reflects higher performance in recovering energy. The greatest gain is obtained for the sample with 2 vol.% of grafted CNTs, which is in good agreement with the 2-fold increase of the permittivity (see Fig 6 (b)). Indeed for energy harvesting the capabilities are directly related to the permittivity [6].

4 Conclusion

Grafting a thin layer of PU - 5 nm in thickness- on the surface of CNTs was performed using a “grafting onto” technique. The interfacial adhesion between grafted CNTs and the PU matrix was improved due to the compatibility between grafted layer (PU) and polymer matrix (PU). DSC analysis showed that the microstructure of polyurethane was fairly modified by the incorporation of grafted CNTs, and dielectric and viscoelastic measurements over a wide range of frequencies and temperatures showed similar relaxation times. Only the dielectric strength was increased for composites. An important change was found to lie in the coexistence of two conduction relaxations for composites instead one for pure PU. Grafting PU macromolecules on the CNT surface lowered the conductive properties by insulating the nanotubes. This led to the increase of the percolation threshold to around 5%. Thanks to the increase of the

permittivity and by maintaining adequate mechanical properties, the electromechanical performances have been increased by a factor of 2.

Acknowledgement

The author acknowledges the French Agence Nationale de la Recherche (ANR) for financial support, under grant NAPOLECO (ANR- 2010-INTB-910-01), and the Centre Lyonnais de Microscopie (CLYM) for the access to the JEOL 2010F and FEI ESEM XL30-FEG microscopes.

References

- [1] Cathleen Thiele, Raghu DAS, *Electroactive Polymers and Devices 2013-2018: Forecasts, Technologies, Players, Dielectric elastomers, electronic & ionic EAPs and their applications.*
- [2] B. Guiffard, L.S., G. Sebald and D. Guyomar . *Enhanced electric field induced strain in non specular carbon nanopowder/ polyurethane nanocomposites*. *J. of Phys. D: Appl. Phys.*, 2006.39, 3053.
- [3] Cho JW, Kim JW, Jung YC, Goo NS. *Electroactive shape-memory polyurethane composites incorporating carbon nanotubes.* *Macromol Rapid Commun* 2005;26(5):412–6.
- [4] H.-J. Song, Z.-Z. Zhang, and X.-H. Men, ‘Surface-modified carbon nanotubes and the effect of their addition on the tribological behavior of a polyurethane coating,’ *European Polymer Journal*, vol. 43, no. 10, pp. 4092–4102, 2007.
- [5] K. Wongtimnoi, B. Guiffard, A. Bogner-Van de Moortèle, L. Seveyrat, J.-Y. Cavallé. *Electrostrictive thermoplastic polyurethane-based nanocomposites filled with carboxyl-functionalized multi-walled carbon nanotubes (MWCNT-COOH): Properties and improvement of electromechanical activity.* *Composites Science and Technology* 85, 2013, 23–28
- [6] Huang, C. & Zhang, Q. M. *Fully functionalized high-dielectric-constant nanophase polymers with high electromechanical response.* *Adv. Mater* 17, 1153-1158 (2005).
- [7] Cottinet PJ, Guyomar D, Guiffard B, Putson C, Lebrun L. *Modeling and experimentation on an electrostrictive polymer composite for energy harvesting.* *IEEE Trans Ultrason Ferroelectr Freq Control.* 2010 Apr;57(4):774-84.
- [8] Kim KS, Park SJ. *Influence of enhanced dispersity of chemically treated MWNTs on physical properties of MWNTs/PVDF films.* *Macromol Res*, 18, 981 (2010).
- [9] B. Fragneaud, K. Masenelli-Varlot, A. Gonzalez-Montiel, M. Terrones, J.Y. Cavallé. *Mechanical behavior of polystyrene grafted carbon nanotubes/polystyrene Nanocomposites.* *Composites Science and Technology* 68 (2008) 3265–3271.
- [10] Peng Liu. *Modifications of carbon nanotubes with polymers.* *European Polymer Journal* 41 (2005) 2693–2703
- [11] Li S, Qin Y, Shi J, Guo ZX, Li Y, Zhu D. *Electrical properties of soluble carbon nanotube/polymer composite films.* *Chem Mater* 2005;17:130–5.
- [12] P. Liu *Modifications of carbon nanotubes with polymers,* *European Polymer Journal*, (2005) vol. 41: p. 2693-2703.
- [13] Hesheng Xia, Mo Song, Jie Jin, Lei Chen. *Poly(propylene glycol)-Grafted Multi-Walled Carbon Nanotube Polyurethane.* *Macromol. Chem. Phys.* (2006), 207, 1945–1952.

- [14] Wubbenhorst M., Van Turnhout J. Analysis of complex dielectric spectra. I. One-dimensional derivative techniques and three-dimensional modeling, *Journal of Non-Crystalline Solids*, 2002, 305, 40-49.
- [15] Lapprand A, Mechin F, Pascault J P. Synthesis and properties of self-crosslinkable thermoplastic polyurethanes. *J. Appl. Polym. Sci* 2007; 105: 99-113.
- [16] A. K. Barick and D. K. Tripathy, Preparation, characterization and properties of acid functionalized multi-walled carbon nanotube reinforced thermoplastic polyurethane nanocomposites, *Mate. Sci. & Eng. B*, vol. 176(18), p. 1435-1447, 2011.
- [17] P. Król & B. Pilch Pitera. Phase structure and thermal stability of crosslinked polyurethane elastomers based on well-defined prepolymers. *Journal of Applied Polymer Science*, 104, 1464 (2007). DOI: 10.1002/app.25011.
- [18] Alaa El-din El-kotp Abd El-kader Mohammed. Relaxation Phenomena studies on Some Polymers and polymer blends. PhD Thesis. 2002. Faculty of Science Mansoura University.
- [19] Madalena Dionísio, Natália M. Alves, João F. Mano. Molecular dynamics in polymeric systems. *e-Polymers* 2004, no. 044.
- [20] Jeppe C. Dyre and Thomas B. Schröder. Universality of ac conduction in disordered solids. *Reviews of Modern Physics*, 72, 873 (2000).
- [21] W. Bauhofer, J.Z. Kovacs / *Composites Science and Technology* 69 (2009) 1486–1498
- [22] Z.-M. Dang, L. Wang, Y. Yin, Q. Zhang, Q.-Q. Lei. Giant Dielectric Permittivities in Functionalized Carbon-Nanotube/ Electroactive-Polymer Nanocomposites. *Advanced Materials*, 19, 852-857 (2007).
- [23] D. J. Bergman, Y. Imry. Critical Behavior of the complex dielectric constant near the percolation threshold of a heterogeneous material. *Physical review Letters*. 1997. 39, 1222-1225.
- [24] J. P. Straley & S. W. Kenkel. Percolation theory for nonlinear conductors. *Physical Review B*, 29, 6299 (1984).
- [25] D. Stauffer and A. Aharony, *Introduction to Percolation Theory* (Taylor & Francis, 1992)
- [26] R. J. Sengwa, S. Choudhary, S. Sankhla. Low frequency dielectric relaxation processes and ionic conductivity of montmorillonite clay nanoparticles colloidal suspension in poly(vinyl pyrrolidone)-ethylene glycol blends. *eXPRESS Polymer Letters* Vol.2, No.11 (2008) 800–809
- [27] Kanapitsas A, Pissis P. Dielectric relaxation spectroscopy in crosslinked polyurethanes based on polymer polyols. *Eur. Polym. J.* 2000; 36: 1241–1250.
- [28] Castagna A M, Fragiadakis D, Hyungki L, Choi T, Runt J. The Role of Hard Segment Content on the Molecular Dynamics of Poly(tetramethylene oxide)-Based Polyurethane Copolymers. *Macromolecules*. 2011; 44 : 7831-7836. DOI: 10.1021/ma2017138.
- [29] Boiteux G, Seytre G, Cuve L, Pascault J P. Dielectric studies of segmented polyurethanes based on polyolefine: relations between structure and dielectric behavior. *J. Non-Cryst. Solids*. 1991; 133: 1131-1135. DOI: 10.1016/0022-3093(91)90739-S.
- [30] G. Georgoussis, A. Kanapitsas, P. Pissis, Yu.V. Savelyev, V.Ya. Veselov, E.G. Privalko. Structure-property relationships in segmented polyurethanes with metal chelates in the main chain. *European Polymer Journal* 36 (2000) 1113±1126.
- [31] Karabanova L V, Boiteux G, Seytre G, Stevenson I, Gain O, Hakme C, Lutsyk E D, Svyatyna A. Semi-interpenetrating polymer networks based on polyurethane and poly(2-hydroxyethyl methacrylate): Dielectric study of relaxation behavior. *J. Non-Cryst. Solids*. 2009; 355:1453-1460. DOI:10.1002/app.12592.
- [32] G. Kortaberria, P. Arruti, A. Jimeno, I. Mondragon and M. Sangermano. Local dynamics in epoxy coatings containing iron oxide nanoparticles by dielectric relaxation spectroscopy. *Journal of Applied Polymer Science*, Vol 109, 3224–3229, 2008.

- [33] Sylvie Eury, Rattikorn Yimmirun, V Sundar, Paul J Moses, Sei-Joo Jang, Robert E Newnham. Converse electrostriction in polymers and composites *Materials Chemistry and Physics - MATER CHEM PHYS* , 61, 18-23, 1999.
- [34] Diguët. G, Bogner. A, Chenal. J-M, Cavallé. J-Y. Physical modeling of the electromechanical behavior of polar heterogeneous polymers. *J. Appl. Phys.* 2012, 112 :114905-1-8.

Chapter 7: Benefit of carbon nanotubes for energy conversion using polymers

M. H. Jomaa^{1,2*}, L. Roiban¹, G. Diguët³, D.S. Dhungana¹, L. Seveyrat², L. Lebrun², J.Y. Cavaille¹, K. Masenelli-Varlot¹.

¹ Université de Lyon, INSA-Lyon, CNRS, MATEIS, F-69621 Villeurbanne Cedex, France

² Université de Lyon, INSA-Lyon, LGEF, F-69621 Villeurbanne Cedex, France

³ Institut Néel (CNRS & UJF) - Building 25 rue des Martyrs BP166 - 38042 Grenoble France

* Author to whom all correspondence should be addressed

Abstract

Electroactive devices are developed for energy conversion purposes. In particular, polyurethanes (PU) are lightweight and flexible materials which have demonstrated their ability to convert electrical energy into mechanical energy and vice versa. In addition, it has recently been shown that the harvested energy can be increased by incorporating carbon nanotubes (CNTs) into a PU matrix. However, the nanocomposites may not have been optimized, since it is well known that CNTs are hardly dispersed in a polymeric matrix, and that the interfacial adhesion strength is generally poor. One solution to improve both dispersion and adhesion may consist in grafting polymer chains onto the CNT surfaces.

Here we report a comprehensive study of the role of CNTs and their grafting onto the actuation properties of PU. The effect of the grafting process onto the CNT dispersion state is quantified from electron tomography through the measurement of the local CNT fraction, the CNT tortuosity, the CNT-CNT distance and the number of contacts. Then, a model taking into account the experimental microstructural parameters is used for the evaluation of the role of CNTs. The results, compared to experimental data, evidence the minor role of carbon nanotubes compared to that of the matrix heterogeneities.

Keywords: 3D tomography; CNT dispersion; Electromechanical properties

1 Introduction

The last developments show promising properties of electroactive polymers (EAP) especially for actuation and energy harvesting applications. The EAPs are part of the broad group of smart materials [1]. Compared to inorganic materials these versatile polymers have various attractive properties, such as being lightweight, inexpensive and easy to manufacture. A tremendous amount of research and development has proved that EAP can change their size or their shape

when stimulated by the right external electrical activation mechanism, meaning they can convert electrical energy into mechanical energy. Especially in the actuator segment, vast research can be seen for specialized applications such as medical devices and biomimetic-robotics [2]. Here the features of EAPs are used to enable movement and generate forces as well as electrically control surface properties. Among the various EAPs, polyurethane (PU) elastomers are of great interest due to their significant electrical-field strains [3,4], and due to their attractive and useful properties such as flexibility, high mechanical strength and biocompatibility with blood and tissues [5,6]. In addition, it has recently been shown that the incorporation into a polyurethane (PU) matrix of nanofillers, such as carbon nanotubes (CNTs), can greatly enhance their electromechanical properties [7]. However, it is well known that CNTs are hardly dispersed in a polymeric matrix and that the interfacial adhesion strength is generally poor [8]. Furthermore, in all nanocomposites cases, the improvement of the materials performance is generally related to the degree of dispersion, the interaction of nanotubes with the host polymer (interfacial adhesion strength), and the alignment and orientation of the nanotubes in the polymer matrix [9]. One solution to improve both dispersion and adhesion consists in functionalizing CNTs by grafting polymer chains onto their surfaces [10,11]. In order to highlight the effect of grafting on the dispersion of CNTs in polyurethanes, several parameters have to be precisely determined, among which the distance between CNTs, the number of the contacts between them, their orientation, their curvature as well as the distance between entanglements/contacts. Measuring such parameters requires a three dimension characterization. Electron tomography is undoubtedly the most pertinent technique to perform a three dimensional analysis of polymer/ CNT microstructures composite material. Until now this information is still missing in the literature. To our knowledge, all the published studies of electron tomography of polymer /CNT nanocomposites are focused on how to obtain a good contrast between polymer matrix and CNT [12].

The aim of this work is to analyze the effect of CNTs and their grafting onto the actuation properties of PU. The effect of grafting process onto the CNT dispersion state is quantified from electron tomography through the measurement of the local CNT fraction, the CNT tortuosity, the CNT-CNT distance and the number of contacts. In a second step a model taking into account the experimental microstructural parameter is used for the evaluation of the role of CNTs. At the end the real impact of carbon nanotubes on the improvement of the electroactive properties is evaluated.

2 Materials and methods

The matrix is polyether-based thermoplastic polyurethane (Estane 58888 NAT021 – Lubrizol). There are co-block polymers with two major blocks; namely the hard and soft segments. The hard segment (HS) is composed of 4,4' methylene bis (phenyl isocyanate) (MDI) and 1,4-butanediol (BDO). Poly(tetramethylene oxide) (PTMO) is used as soft segments (SSs).

Multi-walled Carbon Nanotubes (Cheap Tubes) exhibit a specific surface area of 60 m²/g. Their mean outer diameter is equal to 30 nm and their length ranges between 10 and 20 μm. Their purity is claimed to be equal to 95 wt.% and therefore they have been used without any further purification. The grafting reactions were performed using a "grafting onto technique" in order to have a good compatibility between the grafted chains and the PU matrix. First, functional groups such as –COOH –OH are created on the sidewalls of CNTs, by oxidation of the CNTs. Then as a second step, polyTDI-tolylene-2,4-diisocyanate terminated poly(propylene glycol) is

grafted on the functionalized CNTs. Finally polyol is also grafted on CNT-PolyTDI to create PU chains [13].

The polymer films were prepared by a solution casting method (see Figure 1(a)). Before use, PU granules were heated at 350 K for 3 hours. The grafted CNTs were dispersed in N, N-dimethylformamide (DMF, Sigma-Aldrich D158550, 99%) using an ultrasonic bath for 1h and 30 minutes. Then it was dissolved in DMF with a ratio of 15 wt.% of PU into DMF. The solution was heated at 350 K for 4 hours under mechanical agitation, until a homogeneous solution was obtained. This operation was carried out in a closed device, to avoid evaporation of the DMF solvent and ensure good reproducibility of films. Then, the solution was then kept overnight to remove air bubbles. Afterwards, the obtained solution was cast on glass plates with an Elcometer 3700 doctor blade film applicator, put in an oven at 335 K for one day, and then unsticked from the glass. A second heating treatment at a temperature below the HS melting temperature was performed in order to eliminate residual solvent. The thickness of the films is about 100 μm after drying.

2.1 Sample preparation

To study the effect of grafting on the CNT dispersion state in PU, two samples composed of PU with 2 wt.% of either grafted or ungrafted CNTs have been analyzed. The specimens were embedded in epoxy and microtomed at low temperature ($T = 200\text{ K}$) with a Reichert Ultracut S cryoultramicrotome. Ultrathin sections of approximately 100 nm thick were deposited on a copper grid covered with a holey carbon film. Gold nanoparticles were deposited on the surface of the thin sections. They have been used to enhance the contrast during acquisition and to facilitate the alignment of the projections after the tilt series acquisition.

2.2 Image acquisition

Tilt series were acquired with a FEI XL-30 FEG environmental scanning electron microscope (ESEM) operating at 30 kV under 3 Torr of water partial pressure. The environmental mode allows a gas flow having the capacity to drive out the charges facilitating the study of non-conductive samples. The experimental set-up used for the tilt series acquisition is showed in Figure 1 (b) [14]. The samples, composed of the ultrathin sections deposited on a TEM grid and covered by gold nanoparticles, can be placed on a holder. A system allowing the sample rotation is not shown in Figure 1 (b) but is detailed elsewhere [15]. A solid detector is placed 10 mm below the sample and electrons with scattering angles ranging between 14 and 40° are collected. The contrast in the images is mass-thickness dependent, which makes this observation mode relatively similar to High Angle Annular Dark Field in Transmission Electron Microscopy. The ESEM performances combined with the HAADF-STEM imaging mode push the resolution down to a few nm [16,17], including in three dimensions [15]. A Peltier stage, indicated in Figure 1 (b), may be used to control the sample temperature, which was not necessary here. The tilt series were acquired with tilt angles ranging from 66° to -66°, with a constant tilt step of 2°. Prior to the acquisition, the stage and the samples were cleaned *in situ* using an Evactron system to avoid contamination during the tilt series acquisition. Moreover, the region of interest was irradiated during 5 minutes with the electron beam to induce irradiation damage before acquisition and therefore avoid shrinking problems during acquisition. Although this is known

to induce chemical changes inside the polymer phase, it is thought not to affect the CNT distribution.

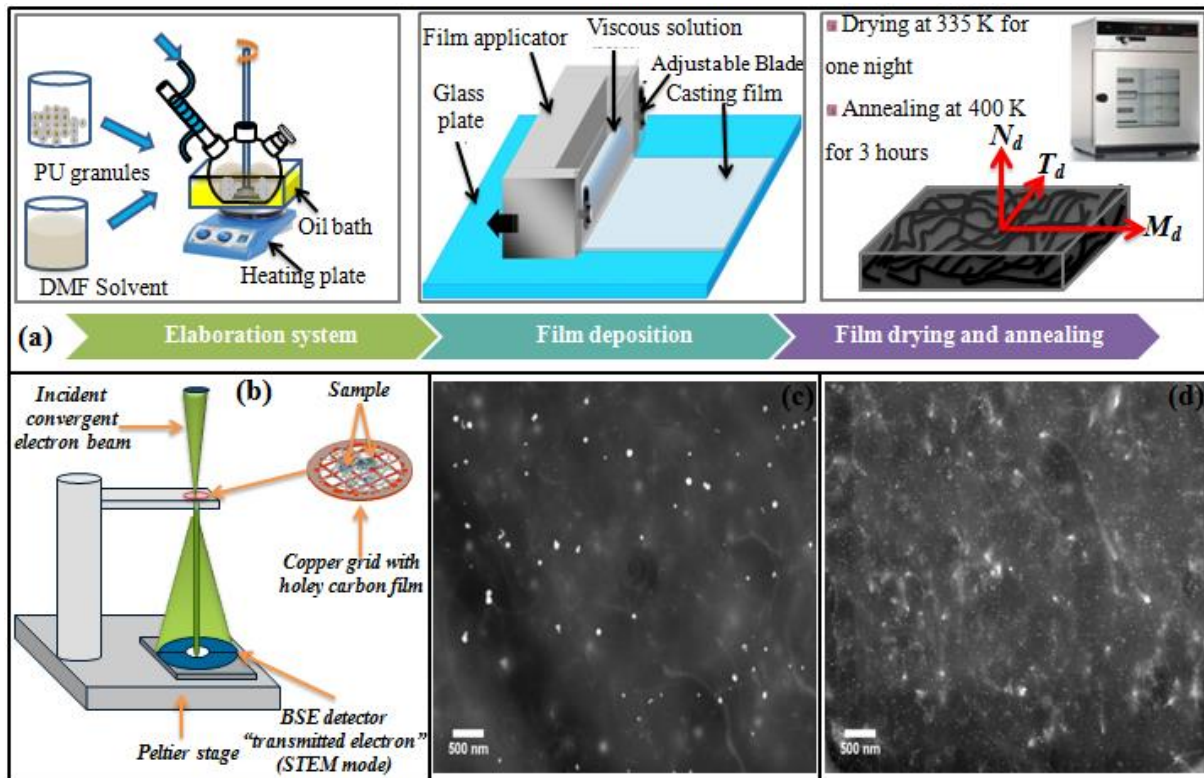


Figure 1 (a) Elaboration process, (b) Schematic diagram of the wet-STEM holder. HAADF-STEM projections recorded in an ESEM at zero tilt: (c) PU with grafted CNT; (d) PU with ungrafted CNT.

Figure 1 (c) and Figure 1 (d) display the images acquired at tilt 0° on the films containing grafted and ungrafted CNTs, respectively. A sufficient contrast can be obtained between the bright CNTs and the dark matrix, allowing the volume reconstruction and the 3D analysis of the CNT dispersion state. Gold nanoparticles are randomly dispersed on the sample surface and appear very bright.

2.3 Volume analysis

After the tilt series acquisition, an accurate alignment of the projections, *i.e.* the acquired images at different tilts, was performed in Etomo, with the gold nanoparticles as fiducial markers [18,19]. The volume reconstruction was performed using the Tomoj [20] plugin of ImageJ software, with the ART algorithm [21] (15 iterations). The volumes can be qualitatively analyzed slice by slice, through display at different depths and orientations. However, segmentation is necessary to extract quantitative information. Here, segmentation was initially carried out combining Trainable Weka Segmentation, a plug-in in Fiji and 3D Slicer software (<http://www.slicer.org/>) [22], further used for advanced segmentation.

3 Results and discussion

3.1 3D reconstruction

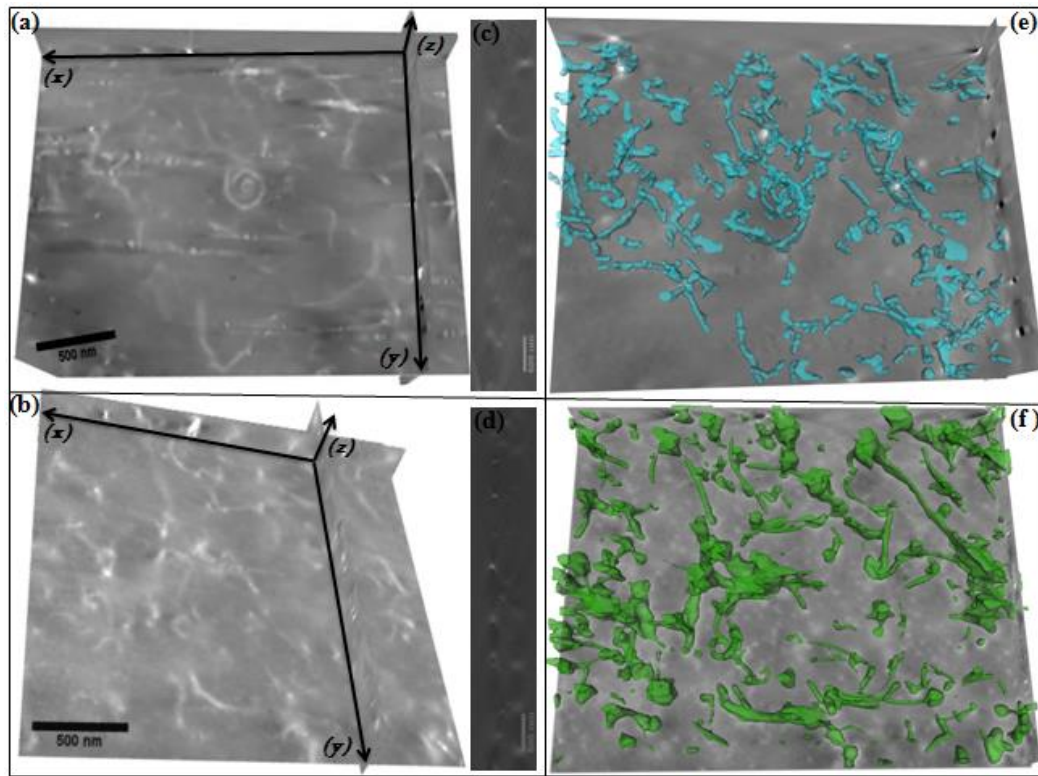


Figure 2 Orthogonal cross sections through the reconstructed volumes of the samples: (a) and (c) XY and XZ cross sections extracted from the volume of the sample with grafted CNTs, respectively; (b) and (d) XY and XZ cross sections extracted from the volume of the sample with ungrafted CNTs, respectively. (e) and (f) Three dimensional models obtained after segmentation, with grafted CNTs in blue (e) and ungrafted CNTs in green (f).

Figure 2 shows orthogonal cross sections extracted from the reconstructed volume. Figure 2 (a) and (c) represent two orthogonal sections extracted from the volume of the sample containing grafted CNTs, whereas Figure 2 (b) and (d) correspond to nanocomposites containing ungrafted CNTs. The contrast allows identifying the CNT distribution within the volume of the sample. From the analysis of the volumes at different depths and orientations, the thicknesses of the analyzed samples were measured to be around 350 nm and 450 nm for the nanocomposites containing grafted and ungrafted CNTs, respectively. The dispersion of grafted CNTs is rather uniform and only small heterogeneities can be seen, whereas in the sample containing ungrafted CNTs, regions with different densities of CNT can be observed. Grafting CNTs seems to improve the CNT dispersion within the PU matrix. This is consistent with the impressive improvement of the stability of the CNT suspension in DMF upon grafting. The interfacial adhesion strength is also expected to be excellent since the same chemical component is present in both sides of the interfaces (PU in the grafted layer and in the matrix).

3.2 Quantification and control of the CNT dispersion state

The quantification was carried out considering two main objectives: (i) characterization of the CNT dispersion state and (ii) measurement of the CNT orientation state. In order to facilitate these objectives, fiducial markers were numerically placed in the 3D model of the segmented volume generated by 3D Slicer. Their position is taken into account to get clear statistical information on possible contacts between the CNTs in the sample.

Each CNT was divided into small individual independent segments (see Figure 3 (a)). The 3D coordinates of endpoints as well as intermediate points were chosen based on the geometry of CNTs. The segments were characterized by the length of the segment r , the polar angle θ , representing the segment orientation in the plane YZ, and the azimuthal angle α expressing the segment orientation in the plane XY, see Figure 3(a). Analyzing the segments orientation give rise to a direct measurement of the CNT dispersion and orientation within the PU matrix.

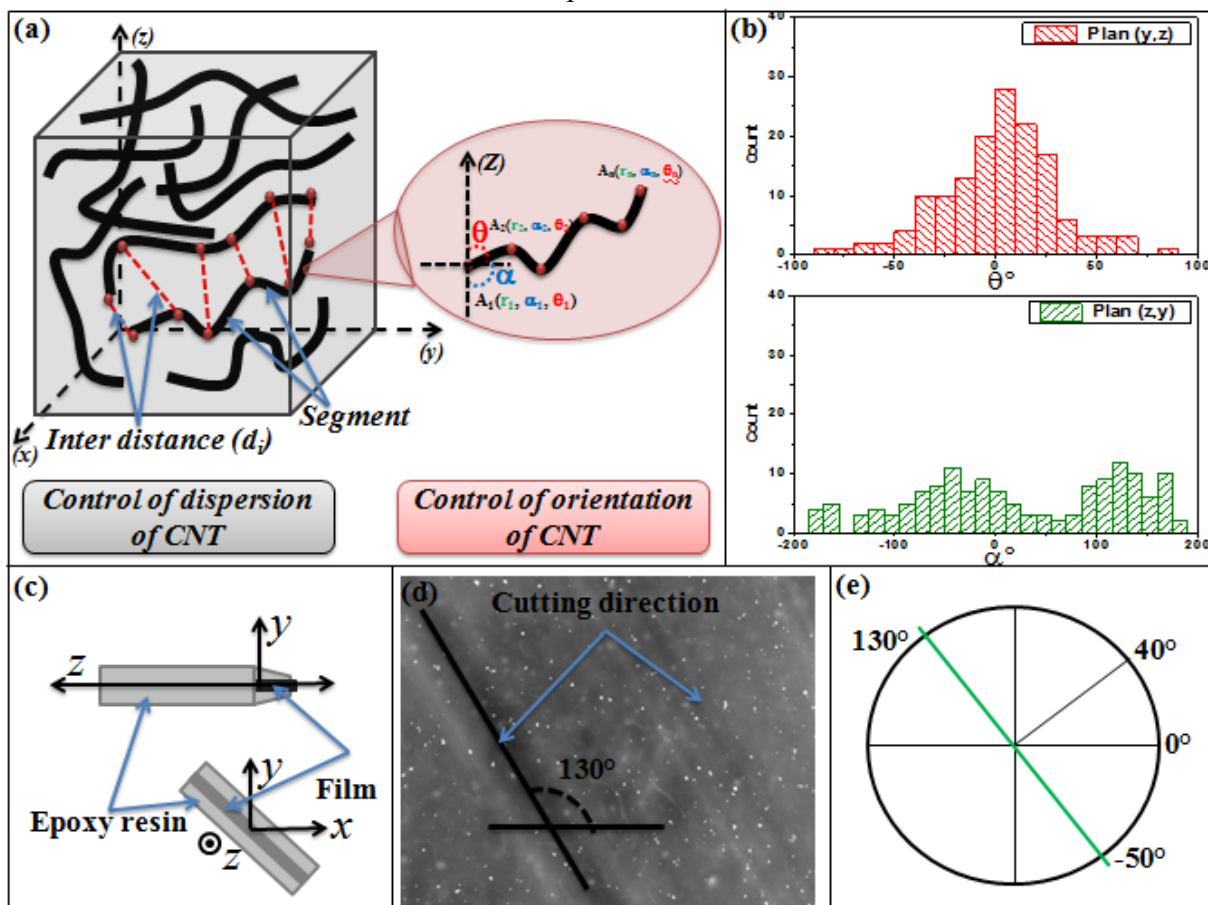


Figure 3 Characterization of the CNT dispersion and orientation: (a) method used for the analysis of the CNT orientation, (b) CNT orientation for the grafted sample: Polar angle θ represents the orientation of each segment in the YZ plane and the azimuthal angle α is the orientation of each segment in the XY plane, (c) schematic representation of the directions considered during the 3D analysis with respect to the film orientation during ultramicrotomy, determined from the image in (d); (d) image obtained at low magnification, the stripes show the cutting direction during ultramicrotomy; (e) Preferential orientation of the CNTs within the plane XY (derived from (b), following the direction $-50^\circ - 130^\circ$).

Table 3 CNT distribution within the volume of PU: number of contacts, minimum distance between CNTs and local CNT volume fraction.

Type of Composite	Number of Contacts	Minimum Distance	Volume Fraction
Ungrafted CNT (2vol.%)	11	-	10.5%
Grafted CNT (2 vol.%)	0	50 nm (approx)	7.5%
Grafted CNT (4 vol.%)	5	-	19.5%

The quantitative parameters describing the CNT dispersion state are showed in Table 3. The minimum distances between CNTs were measured using the segment method applied on the three dimensional model. The values obtained confirm that grafted CNTs are not in direct contact with each other in the nanocomposites containing 2 vol.% of grafted CNTs, since the minimum distance is equal to 50 nm. For ungrafted CNTs, 11 contacts between CNTs were found within the analyzed volume. The formation of a percolating path may reflect an overall conductive material. The local volume fractions of CNTs within the nanocomposites containing 2 vol.% of either grafted or ungrafted CNTs were also measured. Interestingly, the volume fractions measured for both samples are significantly higher than 2 vol.%: they are equal to 7.5 and 10.5 vol.%, respectively. This shows that the CNTs are not ideally dispersed within the PU matrix, which rather exhibits CNT-rich and CNT-poor regions. It is suggested that due to the limited contrast between CNTs and PU, a CNT-rich region was inadvertently chosen for the 3D characterization. Nevertheless, when considering that the CNT-rich regions exhibit the largest local CNT fraction within the sample, the measured values suggest that grafted CNTs are better dispersed, as expected.

As schematically displayed in Figure 3 (a), the angle θ shows the orientation of the CNT segments in the YZ plane and the azimuthal angle α represents the orientation of the segments in the XY plane, the origin of the frame being place at the center of the reconstructed volume. For grafted CNTs, the polar angles θ follow a Gaussian distribution centered near 0° , (see Figure 3 (b)). The azimuthal angle distribution is bimodal, with two preferential orientations at $\alpha \approx -50^\circ$ and $+130^\circ$. Both angles are complementary and actually represent one single orientation direction, as can be clearly seen on the circle in Figure 3 (e). The preferential orientations of θ and α depend on the cutting direction during ultramicrotomy, on the way the thin sections were deposited onto the TEM grids, and then the way the TEM grids were placed on the sample holder. Figure 3 (c) represents the orientation of the film embedded in the epoxy resin with the frame chosen for the 3D analysis. The z-axis corresponds to the casting direction and the x and y axes are in the transverse plane. As a consequence, a preferential orientation of the CNTs at $\theta \approx 0^\circ$ clearly indicates that the CNTs lay parallel to the film plane. Moreover, a low magnification image acquired before the acquisition of the tilt series is shown in Figure 3 (d). Scratches in the thin sections, oriented at 130° from the horizontal axis (x-axis) were unambiguously due to defects on the diamond knife edge used for cryoultramicrotomy. As a consequence, they correspond to the cutting direction, and Figure 3 (c) schematically shows the orientation of the film during the tilt series acquisition. The preferential orientation $\alpha \approx 130^\circ$

thus corresponds to a preferential orientation of the CNTs along the casting direction. The appearance of a preferential orientation has already been observed in the literature. For example, Ma et al. [23] obtained a significant enhancement in the dispersion quality and alignment upon functionalization of the nanotubes compared to pristine MWCNTs. Xie et al. [24] also observed aligned CNTs and showed that enhanced dispersion and alignment of CNTs in polymer matrices greatly improve the mechanical, electrical and thermal properties of CNT/polymer nanocomposites.

3.3 Electrostriction Modeling

Experimental data for electrostriction clearly show that adding conducting fillers like carbon black [25], or here CNTs, only slightly increase the electroactivity of pure PU (by a factor of only 2). In order to understand why the filler contribution is rather weak, we try to evaluate it from theoretical considerations. Recently, Cavallé [26] then Diguët *et al.* [27] pointed out that the phase separation into Hard Domains; HDs- domains rich in HS- with high dielectric constant and Soft Domains; SDs –domains rich in SS- with weak dielectric constant can result into the strong electrostriction properties of pure segmented PU. This, in turn, leads to heterogeneities of both elastic and dielectric constants and to electric field gradients, which makes the SDs shrink and the whole material compress [27]. In this work, we are mainly interested in evaluating the orders of magnitude of the contribution on electrostriction of, on one hand, the pure PU microstructure and, on the other hand, the presence of carbon nanotubes. Considering PU alone, i.e. without electrically conductive fillers, we studied recently [28] different compositions and the effect of both the domain size effect and their average distance in between. In order to give a rough evaluation of the CNT contribution, we used the following equation to relate the value of the electrostriction [27], such as: $S = M_E E^2$

$$M_E = -2 \frac{(\varepsilon_{SD} - \varepsilon_0)}{Y_{SD}} [A^2 - 0.8A] (\varepsilon_r + 2)^2 \quad (1)$$

where $A = \frac{\varepsilon_{SD} - \varepsilon_{HD}}{2\varepsilon_{SD} + \varepsilon_{HD}}$, where ε_{SD} and ε_{HD} are the permittivity of soft domains surrounding

hard domains, respectively and Y_{SD} is the elastic modulus of soft domain (within the approximation that it is possible to neglect the strain of HDs due to their much higher stiffness). The constant A varies, depending on the HD sphere and its SD surrounding dielectric constants, between -1 and 0.5 for $\varepsilon_{SD}/\varepsilon_{HD} \rightarrow 0$ and $\varepsilon_{HD}/\varepsilon_{SD} \rightarrow 0$ respectively. ε_0 and ε_r are the vacuum permittivity and matrix effective relative permittivity. As M_E is the electrostriction coefficient of a single HD sphere, the total electrostriction coefficient has to be multiply by the HD sphere content.

In this work, in order to evaluate the CNT contribution, we first point out the fact that two different scales might be considered: (i) the scale corresponding to heterogeneities of pure PU, induced by the phase separation between HD and SD, which is around 10 nm, and (ii) the scale of the nanotubes accounting for their flexibility, which can be evaluated as their gyration radius r_G . Although this parameter has not been evaluated, it should be around 1 μm , i.e. 100 times higher than for pure PU heterogeneities (for flexible fibers, $r_G \sim \sqrt{l}$, where l is the CNT length, which is in between 1 to 10 μm). Thus, as a first approximation, CNT can be considered as

embedded in a homogeneous matrix having the average properties measured by standard techniques (mechanical analysis, dielectric properties, etc.). Up to now, no physical model for electrostriction prediction can account for such a microstructure. However, it is interesting to evaluate, even very roughly, the effect of CNT within the hypothesis that the total electrostriction should be the addition of pure PU [29,30] contribution with the CNT contribution. According to equ.1, it is easy to evaluate the electrostriction induced by the fillers which play the role of heterogeneities in a continuous matrix in the case where fillers are spherical, which is far from the case for CNTs in this work. Nevertheless, as we consider the electrostrictive properties along the film thickness, aligned CNTs can fairly well be represented by their cross-section – disks - in the XY plane. At this point, we have to evaluate the apparent volume fraction V_{app} occupied by the sphere representing the CNT. One way to roughly evaluate this volume fraction consists in saying that at the percolation fraction of CNT, $V_{app} = 1$, and in calculating it using a simple linear relationship. Thus for a percolation threshold of 3%, $V_{app} \approx \text{CNT}\% \times 30$.

If we accept that the total electrostriction can be evaluated as the sum of (i) the PU electrostrictive behavior and of (ii) the CNT contribution, it becomes easy to calculate the electrostriction expected for such nanocomposites.

Using eqn.1 for the CNT contribution, ϵ_{SD} must be replaced by is the average permittivity of PU without filler (which is around $8\epsilon_0$), and Y_{SD} by the Young modulus of pure PU (i.e. 29 MPa). ϵ_r is the macroscopic relative permittivity of the composite which depends on the CNT content. On the other hand, for parameter A, which accounts for the contract of permittivity between CNT and matrix PU, ϵ_{HD} becomes the permittivity of CNT, which tends to infinity because of their excellent conductivity. Thus $A=-1$.

Table 4 gives, for each composition, the experimental electrostriction coefficient, the permittivity, the calculated contribution of the CNTs to the macroscopic electrostriction and the calculated total electrostriction. In this table, M_E is the total expected electrostriction coefficient which is the sum of experimental M_{exp} for pure PU (without fillers) and the calculated contribution of CNT, M_{CNT} (from eqn.1, and parameters as discussed just above).

Table 4: experimental electrostriction coefficient, relative permittivity, calculated contribution of the CNTs to the macroscopic electrostriction, calculated total electrostriction.

CNT (%)	M_{exp} CNT	ϵ_r	Contribution of CNT M_{CNT}	Total M_E
0.00	3.20E-15	8	0.00E+00	3.20E-15
1.00	4.80E-15	12	4.60E-17	3.25E-15
2.00	5.60E-15	18	1.88E-16	3.39E-15
3.00	6.40E-15	90	5.96E-15	9.16E-15
4.00	5.76E-15	190	3.46E-14	3.78E-14
5.00	5.12E-15	400	1.90E-13	1.93E-13

Figure 4 shows the experimental and the calculated data. Experimental data obtained on nanocomposites based on same PU with carbon black (CB) [25] are also plotted for comparison.

According to Table 4 and Figure 4, it appears that within the hypothesis of the model, the contribution from the CNTs to the total electrostriction remains negligible compared to that of pure PU, up to a CNT content of 3%. Their contribution is similar to that of CB fillers. On the contrary, the CNT contribution efficiency rapidly increases above this critical value. Experimental data indicates that above 3%, this efficiency decreases, which can be partially due to increasing losses at approaching the percolation threshold and/or to a decrease of the electric field gradient when fillers become to close each other, as discussed in a previous work [31].

The fact that the calculated CNT contribution, M_{CNT} remains small at low CNT content is probably due to the very simplified hypotheses used here. In fact we considered that CNT act as spheres, and due to the fact that the driving forces of electrostriction in this model come from electric field gradients, these forces should be much larger and distributed because not only the spherical surface are expected but a large variety of curvature gradients are present, radius of CNT, extremities, aggregates, etc. On the other hand, when decreasing the distance between two neighboring CNTs, the forces also decrease because of the electric field gradient decrease between these fillers. As a conclusion, we are far away from being able to accurately calculate the macroscopic strain of nanocomposites filled by aligned CNTs, but the interest of such a calculation is just to show that their contribution to the electrostriction would remain not much higher than the intrinsic contribution of pure PU, which finds its high activity in its own heterogeneous microstructure.

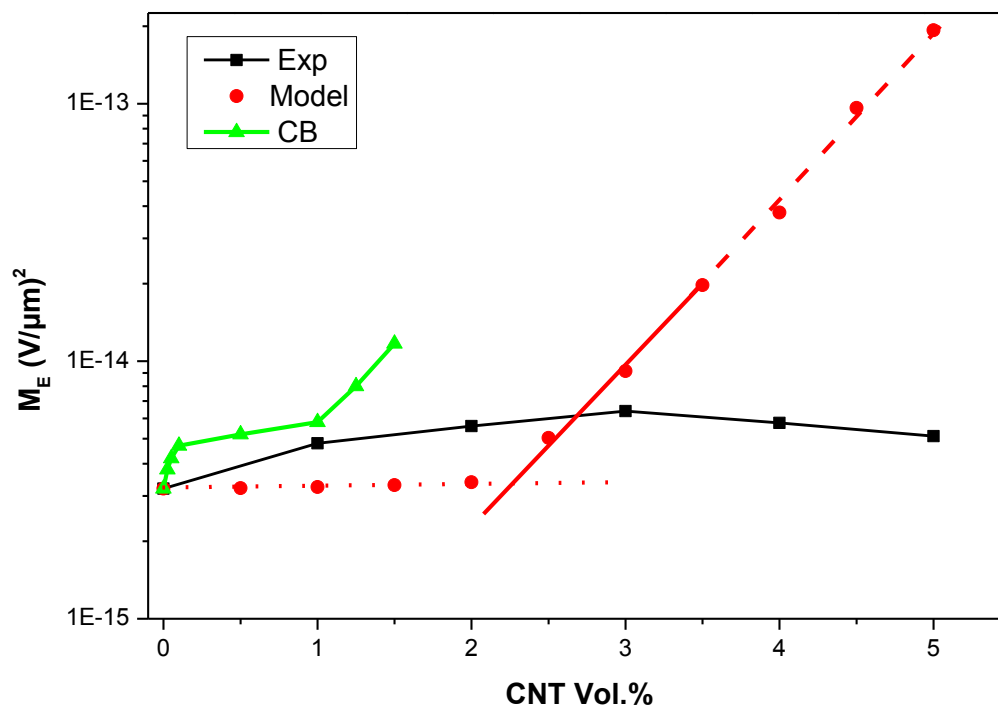


Figure 4 Experimental and calculated electrostriction coefficient of PU nanocomposites. Horizontal red dots represent the pure PU contribution (as experimentally measured). Full line represents the calculated data for the CNT contribution, M_{CNT} .

For comparison, data obtained for PU88 with carbon black [25] are also presented.

4 Conclusion

The aim of this paper was to evaluate the contribution of CNTs into the electrostrictive properties of PU/CNT nanocomposites. The first part of this work dealt with the quantification of the CNT dispersion and orientation states. For this purpose, electron tomography has been performed in an Environmental Scanning Electron Microscope. Electron tomograms have been reconstructed and segmented, and a quantification method has been proposed.

First, the local fractions of CNTs in the matrix have been determined. They are significantly higher than the macroscopic fraction, which indicates that the composites are composed of CNT-rich and CNT-poor regions. In this study, the tomograms corresponded to CNT-rich regions. With the above-mentioned limitations and from the measured CNT fractions, it seems that grafted CNTs are better dispersed than ungrafted CNTs confirmed by the measured distance between the CNT. For grafted CNT within the analyzed volume no contacts between the CNT were found (as observed with ungrafted CNTs). Moreover, samples containing either grafted or ungrafted CNTs exhibit similar CNT orientations: the CNTs were found to lie in the film plane and have a preferential orientation along the casting direction.

The second part concentrates to study the effect of adding conducting fillers on electrostriction properties as theoretical study of the contribution of conductive features for the improvement of electromechanical properties of PU nanocomposites. Though we are far away from being able to accurately calculate electrostrictive strain of nanocomposites filled by CNTs, using different approximations (such as the hypothesis that CNT are surrounded by a continuous and homogeneous medium having the average properties of pure PU, and they are considered as forming spherical coils), the contribution of CNT and more generally speaking, of randomly dispersed conductive fillers, appears to remain of the same order of magnitude as the pure PU activity which finds its origin in its own heterogeneous microstructure.

Acknowledgement

The author acknowledges the French Agence Nationale de la Recherche (ANR) for financial support, under grant NAPOLECO (ANR- 2010-INTB-910-01), the Centre Lyonnais de Microscopie (CLYM) for the access to the JEOL 2010F and FEI ESEM XL30-FEG microscopes, and the Centre Technologique des Microstructures for the access to the cryo-ultramicrotome.

References

- [1] <http://www.idtechex.com/research/articles/new-growth-opportunities-for-electroactive-polymers-00005413.asp>, New growth opportunities for electroactive polymers.
- [2] Cathleen Thiele, Raghu DAS, *Electroactive Polymers and Devices 2013-2018: Forecasts, Technologies, Players, Dielectric elastomers, electronic & ionic EAPs and their applications*
- [3] M. Watanabe, T.H., M. Suzuki & Y. Amaike Y, Electric conduction in bending electrostriction of polyurethanes. *Appl. Phys. Lett*, 74 (1999). 2717

- [4] B. Guiffard, L.S., G. Sebald and D. Guyomar, Enhanced electric field induced strain in non percolative carbon nanopowder / polyurethane composites. *J. of Phys. D: Appl. Phys.*, (2006). 39, 3053
- [5] L. Irusta and M. J. Fernandez-Berridi, Photooxidative behaviour of segmented aliphatic polyurethanes, *Polym. Deg. & Stab.*, vol. 63, p. 113-119, 1999.
- [6] C. Putson, L.L., D. Guyomar, N. Muensit, P.-J. Cottinet, L. Seveyart, and B. Guiffard. , Effects of copper filler sizes on the dielectric properties and the energy harvesting capability of nonpercolated polyurethane composites *J. Appl. Phys.*, 109 (2011). 024104.
- [7] D. Guyomar, L. Lebrun, C. Putson, P.-J. Cottinet, B. Guiffard, and S. Muensit. *J. Appl. Phys.* 106, (2009), 014910
- [8] Dang, Z. M., Wang, L., Yin, Y., Zhang, Q. & Lei, Q. Q. Giant Dielectric Permittivities in Functionalized Carbon-Nanotube/Electroactive-Polymer Nanocomposites. *Adv. Mater* 19, 852–857 (2007).
- [9] Zheng-Ming Huang, Y.-Z. Zhang, M. Kotakic, S. Ramakrishna, c,d. A review on polymer nanofibers by electrospinning and their applications in nanocomposites- *Composites Science and Technology* 63 (2003) 2223–2253
- [10] Zhu, J., Kim, J. D., Peng, H., Margrave, J. L., Khabashesku, V. N. & Barrera, E. V. Improving the dispersion and integration of single-walled carbon nanotubes in epoxy composites through functionalization. *Nano Lett* 3, 1107–1113 (2003).
- [11] Xia, H. & Song, M. Preparation and characterisation of polyurethane grafted single-walled carbon nanotubes and derived polyurethane nanocomposites. *J. Mater. Chem* 16, 1843–1851 (2006).
- [12] Masenelli-Varlot, K., C. Gauthier, L. Chazeau, F. Dalmas, T. Epicier and J.-Y. Cavallé (2014). "Advanced Microscopy Techniques for a Better Understanding of the Polymer/Nanotube Composite Properties" *Polymer Nanotube Nanocomposites: Synthesis, Properties, and Applications, Second Edition*: 365-404 (John Wiley & Sons)
- [13] Hesheng Xia, Mo Song, Jie Jin, Lei Chen. *Macromol. Chem. Phys.* (2006), 207, 1945–1952.
- [14] Jornsano P, Thollet G, Ferreira J, Masenelli-Varlot K, Gauthier C, Bogner A. Electron tomography combining ESEM and STEM: a new 3D imaging technique. *Ultramicroscopy*. 2011;111:1247-54.
- [15] K. Masenelli-Varlot, A. Malchère, J. Ferreira, H. Heidari Mezerji, S. Bals, C. Messaoudi, S. Marco, « Wet-stem tomography : principles, potentialities and limitations », *Microscopy and Microanalysis*, in press. DOI: <http://dx.doi.org/10.1017/S1431927614000105>
- [16] A. Bogner, G. Thollet, D. Basset, P. H. Jouneau, C. Gauthier, *Ultramicroscopy*, vol. 104, p. 290-301, 2005
- [17] A. Bogner, P. H. Jouneau, G. Thollet, D. Basset, C. Gauthier, *Micron*, vol. 38, p. 390-401, 2007
- [18] Kremer, J.R., Mastrorade, D.N., McIntosh, J.R. Computer visualization of three-dimensional image data using IMOD. *J Struct Biol* 116, 71–76 (1996)
- [19] Maiorca M, Hanssen E, Kazmierczak E, Maco B, Kudryashev M, Hall R, Quiney H, Tilley L. Improving the quality of electron tomography image volumes using pre-reconstruction filtering. *J Struct Biol*. 2012;180:132-42
- [20] Messaoudi, C., Boudier, T., Sorzano C.O.S. & Marco, S. TomoJ: tomography software for three-dimensional reconstruction in transmission electron microscopy. *CBMC Bioinformatics* 8, 288 (2007)
- [21] Gordon, R., Bender, R. & Herman, G.T. Algebraic Reconstruction Techniques (ART) for three-dimensional electron microscopy and X-ray photography *J Theor Biol A* 29, 471–481 (1970).
- [22] Fedorov, A., Beichel, R., Kalpathy-Cramer, J., Finet, J., Fillion-Robin, J.-C., Pujol, S., Bauer, C., Jennings, D., Fennessy, F., Sonka, M., Buatti, J., Aylward, S.R., Miller, J.V., Pieper, S., Kikinis, R. 3D Slicer as an Image Computing Platform for the Quantitative Imaging Network. *Magn Reson Imaging*. 30 (9), 1323-41 (2012)

- [23] Ma, C., Zhang, W., Zhu, Y., Ji, L., Zhang, R., Koratkar, N., & Liang J. (2006). Alignment and dispersion of functionalized carbon nanotubes in polymer composites induced by an electric field. *Carbon*, Vol. 46, pp. 706-720, ISSN 0008-6223
- [24] Xie, X.-L., Mai, Y.-W., & Zhou, X.-P. (2005). Dispersion and alignment of carbon nanotubes in polymer matrix: A review. *Mater. Sci. Eng., R*, Vol. R49, pp. 89-112, ISSN 0927-796X
- [25] K. Wongtimnoi, B. Guiffard, A. Bogner-Van de Moortèle, L. Seveyrat, C. Gauthier, J.-Y. Cavaille. Improvement of electrostrictive properties of a polyether-based polyurethane elastomer filled with conductive carbon black. *Composites Science and Technology* 71 (2011) 885–892
- [26] Physical Modeling of the Electromechanical Behavior of unfilled Polymers, Jean-Yves Cavaille, 8th International Conference on Flow Dynamics, Nov 9-11, 2011, Sendai, Japan
- [27] Diguët, G., Bogner, A., Chenal, J.-M., Cavaille, J.-Y. Physical modeling of the electromechanical behavior of polar heterogeneous polymers. *J. Appl. Phys.* 2012, 112 :114905-1-8.
- [28] M. H. Jomaa, K. Masenelli-Varlot, G. Diguët, L. Seveyrat, L. Lebrun, K. Wongtimnoi, C. Vechambre, J. M. Chenal, J.Y. Cavaille. Modeling of segmented pure polyurethane electrostriction behaviors based on their nanostructural properties. *Polymer*, 2015, 62, 139-147, doi:10.1016/j.polymer.2015.02.016.
- [29] H.-J. Song, Z.-Z. Zhang, and X.-H. Men, 'Surface-modified carbon nanotubes and the effect of their addition on the tribological behavior of a polyurethane coating,' *European Polymer Journal*, vol. 43, no. 10, pp. 4092–4102, 2007.
- [30] Huang, C. & Zhang, Q. M. Fully functionalized high-dielectric-constant nanophase polymers with high electromechanical response. *Adv. Mater* 17, 1153-1158 (2005).
- [31] M. H. Jomaa, K. Masenelli-Varlot, L. Seveyrat, L. Lebrun, M.C. Dib Jawhar, E. Beyou, J. Y. Cavaille. Investigation of elastic, electrical and electromechanical properties of polyurethane/grafted carbon nanotubes nanocomposites. To submit to *composites science and technology*.

Conclusion

Incorporation of grafted CNTs in the PU matrix was performed. The interfacial adhesion between grafted CNTs and the PU matrix was improved due to the compatibility between grafted layer (PU) and polymer matrix (PU). DSC measurements confirmed that the crystallinity of PU was not affected by the incorporation of CNTs. Furthermore the glass transition of SD remained unchanged, which was confirmed by viscoelastic characterizations. The viscoelastic and dielectric relaxation times were also not affected by the incorporation of grafted CNTs. On the contrary, grafting CNTs dramatically lowered the conductive properties of the nanocomposites by insulating the nanotubes. This allowed an increase of the percolation threshold up to 5 vol%.

The CNT dispersion and orientation states in the nanocomposites were quantified using electron tomography through the measurement of the local CNT fraction, the CNT tortuosity, the CNT-CNT distance and the number of contacts. It seemed that grafted CNTs were better dispersed than ungrafted CNTs. The distances between CNTs confirmed that they were better dispersed when grafted as it was difficult to find contacts (as observed with ungrafted CNTs). Furthermore, samples containing either grafted or ungrafted carbon nanotubes exhibited similar CNT orientations: the CNTs were found to lie in the film plane and have a preferential orientation along the casting direction.

The electrostriction properties of the films could be improved (twice larger than those of pristine PU) due to the direct improvement of the dielectric permittivity. In order to understand why the filler contribution is rather weak, the microstructural-based model proposed for pure PU in chapter 5 was extended to take into account the presence of the CNTs. This model was used to evaluate the contribution of CNTs into the electrostrictive properties of PU/CNT nanocomposites. By comparing the experimental electrostriction coefficient of PU nanocomposites with the calculation results, namely (i) the PU electrostrictive behavior and (ii) the CNT contribution, it seemed that the contribution of nanofiller to the electrostriction would remain not much higher than the intrinsic contribution of pure PU, which finds its high activity in its own heterogeneous microstructure.

Conclusion

The aim of this PhD was to study how the electromechanical properties of PU / CNT nanocomposite films can be improved by grafting polymer onto the CNT surface. For that purpose, a general study of the physical properties including microstructural, electrical & mechanical properties- in wide range of frequency and temperature- and their effect on electromechanical properties of pure segmented PU was essential especially since PU is a heterogeneous polymer and most of this information was still missing in the literature.

An optimization of the film elaboration conditions was first presented. A closed system was used to avoid solvent evaporation during the process and thus ensure a better control of the film properties. As far as CNTs are concerned, the grafting process was described and controlled step-by-step and the film elaboration conditions were optimized to achieve the best dispersion state with minimum damage in the tube structure and in the grafted layer.

Part III dealt with the study of three different pure PUs with similar compositions but different weight fractions of HSs.

A dielectric relaxation map has been determined for the 3 PUs in order to determine in which temperature - frequency domain they have their maximum efficiency, and minimum electrical and mechanical losses. The α -relaxation was found to be very sensitive to the composition and shifted towards high temperatures with increasing HS contents. Then, the study of the complex dielectric modulus showed that the DC conductivities of the 3 PUs were similar, and that probably most of its contribution came from the soft phase, as it disappeared for temperatures lower than T_g . For PU60, the overlap of the soft phase α process with the conductivity relaxation made impossible to determine accurately the characteristics of the α -relaxation. The consequence was that losses came from both the α and the DC processes for PU60, which in turn would have decreased its efficiency in energy conversion (both for actuation or energy harvesting applications). PU88 and PU75 showed better stabilities of the dielectric properties at temperatures above the ambient temperature, making them more suitable for energy conversion applications.

The mechanical behaviour of the 3 same PUs were analysed in order to optimize the composition of such materials. Mechanical measurements highlighted the main relaxations in the same manner as dielectric measurements did (except for conduction relaxation). The temperature dependence of the relaxations times for α -relaxation was similar with the one obtained with dielectric measurements. It was found that DMA seemed to be more efficient to study the α -relaxation of high conductive polymers. In addition it was found that PU88 has an

almost constant shear modulus and low mechanical losses around the room temperature. Interestingly, the electrostriction response time did not depend on mechanical or dielectric α relaxations as expected. It seemed to be directly link to space charge diffusion (leading to the Maxwell-Wagner-Sillars or MWS phenomenon). This requires further experimental data and theoretical analyses, which will be performed later on. PU88 exhibited low mechanical and dielectric losses in a largest range of frequencies and of temperature, an intense electrostriction properties and quick response time, which made him the best candidate for actuation applications.

From a microstructural point of view, it was found that the 3 PUs exhibited segmented morphologies with spherical HDs embedded in soft matrices. The average HD diameter estimated from TEM and AFM observations was found to be independent on the HS fraction since it was found to be equal to 10 nm in the three PUs. On the contrary, the HS fraction influenced the distance between two adjacent HDs and may also play a role on the HS content inside the HDs and SDs. The distance was found to vary from 17 nm for the PU with the lowest fraction of HS to 12 nm for the PU with the highest fraction. A model of the segmented PU electrostriction properties, based on their microstructures and taking into account morphological parameters such as the HD diameter, the HD-HD distance and the HS weight fractions reproduced –with a reasonable correlation- the experimental values of the electrostriction deformation.

Part IV addressed the question of the effect of the incorporation of grafted CNTs in the PU matrix. Grafting a thin layer of PU - 5 nm in thickness - on the surface of CNTs was performed at IMP lab using a “grafting onto” technique. The interfacial adhesion between grafted CNTs and PU matrix was improved due to the compatibility between grafted layer (PU) and polymer matrix (PU). DSC measurements confirmed that the crystallinity of PU was not affected upon incorporation of CNTs. Moreover, the glass transition of the SDs remained unchanged, which was confirmed by viscoelastic measurements. The viscoelastic and dielectric relaxation times were also not affected by the incorporation of grafted CNT. Only a double conductivity relaxation was detected - compared to pure PU- which is more related to the CNT- PU volume fraction. In addition the grafting process dramatically lowered the conductive properties by insulating the nanotubes. This allowed an increasing of percolation threshold up to 5%. Finally, the electrostriction properties of PU/grafted CNT nanocomposites were improved by a factor of 2 compared to those of pure PU. This increase was attributed to the direct improvement of the dielectric permittivity. The effect of the grafting process onto the CNT dispersion and orientation states was quantified from electron tomography through the measurement of the local CNT fraction, the CNT tortuosity, the CNT-CNT distance and the number of contacts. Then, the model based on the microstructure was extended to account for the presence of the CNTs. It was used to evaluate the role of the CNTs. The results, compared to experimental data, evidence the minor role of carbon nanotubes.

This pluridisciplinary project opens the route to the design of materials with improved electrostrictive properties. Indeed, this project helped to further understand the electrostrictive properties of pure PU for actuation and energy harvesting applications. Moreover, the real

benefit of incorporating grafted CNTs in PU was evaluated. Although an improvement of the electromechanical properties could be obtained, we found that the CNTs play a minor role. As a consequence, it may be more pertinent to optimize the microstructure of PU to further improve its electromechanical properties. For example, it may be interesting to optimize the diameter of the HDs and the HD-HD inter-distance.

Perspectives

This work was devoted to an extensively used class of polymers, segmented polyurethanes, empirically known to exhibit efficient electrostriction. The idea to introduce electrically conducting fillers came from the experience that such fillers are really efficient when dispersed in homogeneous elastomers.

Following a previous set of data and analysis performed by K. Wongtimoi, the present work allowed us to better understand the role of polymer microstructures, physical characteristics of their different phases and the effectiveness of their nanoheterogeneities through the use of an original model.

In order to progress, two main objectives arise from open question concluding this thesis:

- First, the widely used polyurethanes exhibit rather complex nanostructures, improper to nourish a systematic model-experiment comparison data-base. Thus, there is a need to synthesize tailor-made model materials with controlled architectures/gradients: The model materials should be designed so that the macroscopic electrostrictive behaviors will require the account for new effects. In particular, we aim to consider the interferences between close neighbors; such interferences are strongly linked to the order/disorder of the phases, and their intrinsic properties. Furthermore, the choice of the model materials components is also promising and innovating. For electroactive systems, we envision to synthesize materials based on conductive polymers (polyaniline, polypyrrole) with a high dielectric constant, enhancing the permittivity gradient inside the samples and consequently the electrostrictive behavior. Obviously, this work should also target energy harvesting applications.

- The second objective should be a direct consequence of our envy to design targeted nano-architectures: Indeed, with the incremental complexification of the microstructure, new numerical tools need to be developed to evaluate the macroscopic resulting strain. The use of tools like finite element calculations should provide a robust mean to obtain the macroscopic response from the local mechanical states induced by the interactions of dipoles and field gradients.

In parallel to such ambitious projects, several experimental questions should be revisited, such as the effect of electrodes and particularly in connections with their stiffness and the limits they can induce in the compressive strain. On a more theoretical level, the role of electrical charges diffusion (like ions, etc.) on the response characteristic time is still not clear.

FOLIO ADMINISTRATIF
THÈSE SOUTENUE DEVANT L'INSTITUT NATIONAL DES SCIENCES APPLIQUÉES DE
LYON

NOM : **JOMAA**

DATE de SOUTENANCE : 17/06/2015

Prénoms : **Mohamed Hedi**

TITRE : Elaboration, caractérisation et modélisation de matériaux électroactifs à base de polyuréthane et de nanotubes de carbone greffés

NATURE : Doctorat

Numéro d'ordre : 2015ISAL0053

Ecole doctorale : **Matériaux de Lyon**

Spécialité : **Sciences de Matériaux**

RESUME :

Le besoin de sources d'énergie autonomes connaît un regain d'intérêt de plus en plus important avec la multiplication des équipements portables et le développement des réseaux de capteurs. Au-delà de l'utilisation traditionnelle des batteries, il y a un intérêt évident à générer l'énergie électrique nécessaire au cœur du système lui-même en utilisant le gisement environnemental disponible : gradients thermiques, vibrations mécaniques... Ceci est également rendu possible par la réduction importante de la consommation des composants électroniques observés ces vingt dernières années. Parmi les dispositifs susceptibles d'exploiter le gisement vibratoire, les matériaux électro-actifs occupent une place de choix. Actuellement, on recherche des matériaux légers, pouvant se déposer sur des grandes surfaces et peu coûteux à la réalisation. Ceci ouvre des perspectives séduisantes à l'utilisation de polymères électro-actifs en lieu et place des matériaux céramiques piézoélectriques. Parmi les EAP disponibles, les polyuréthanes (PU) sont des élastomères thermoplastiques d'un grand intérêt pour une vaste gamme d'applications en tant que transducteurs ou actionneurs lorsque l'on considère leur importante déformation sous champ électrique, une énergie spécifique élevée, et leur réponse rapide. De plus, ces matériaux sont légers, très souples, présentent de faibles coûts de fabrication, et peuvent être facilement moulés dans n'importe quelle forme souhaitable. Des travaux récents ont en outre montré que l'énergie récoltée peut être augmentée en incorporant des nanotubes de carbone (NTC) dans une matrice de polyuréthane. Cependant, les nanocomposites peuvent ne pas avoir été optimisés, car il est bien connu que les NTC sont difficilement dispersés dans une matrice polymère et que la force d'adhésion interfaciale est généralement médiocre. Une solution pour améliorer à la fois la dispersion et l'adhésion peut résider dans le greffage de chaînes de polymère sur les surfaces des NTC.

L'objectif principal de cette thèse était de développer des polymères nanocomposites à haute efficacité pour la récupération d'énergie et l'actionnement. La motivation principale était d'utiliser des NTC greffés par un polymère pour améliorer la dispersion et l'adhésion interfaciale dans le PU, et de comprendre comment l'utilisation de tels NTC greffés peut changer les propriétés électroactives des matériaux. En d'autres termes, c'était un projet pluridisciplinaire, comprenant une optimisation du processus d'élaboration, des caractérisations physiques - notamment les comportements de microstructure, électriques et mécaniques dans une large gamme de fréquences et températures - et la détermination des propriétés électroactifs. Il s'agissait également de développer une modélisation des lois de comportements en s'aidant de l'analyse de la microstructure par imagerie. Afin de pouvoir identifier le rôle des NTC greffés, une grande partie de cette thèse a été dédiée à l'étude des PU purs, afin de mieux comprendre les relations entre leur microstructure et leurs propriétés électroactives.

MOTS-CLÉS : Polyuretanes, Polymers électroactive, Nanotube de Carbone fonctionnalisé, Actionnement et Récupération d'énergie, Matériaux intelligentes

Laboratoire (s) de recherche :

MATERIAUX Ingénierie et Science (MATEIS) INSA Lyon

Laboratoire de Génie Electrique et Ferroélectricité (LGEF) INSA Lyon

Directeur de thèse: **Prof. Karine MASENELLI-VARLOT**

Co-directeur de these: **Dr. Ing. Laurence SEVEYRAT**

Président de jury : **Prof. Jean-Yves CAVAILLE**

Composition du jury : **Prof. Jean-Yves CAVAILLE, Prof. Eric BEAUGNON, Prof. John Christopher PLUMMER, MCF. Jean-François CHATEAUX, MCF. Vincent SALLES, Dr. Ing. Laurence SEVEYRAT, Prof. Karine MASENELLI-VARLOT.**